Functional characterization of prenyltransferases involved in the biosynthesis of polycyclic polyprenylated acylphloroglucinols in the genus *Hypericum*

Von der Fakultät für Lebenswissenschaften

der Technischen Universität Carolo-Wilhelmina zu Braunschweig

zur Erlangung des Grades eines

Doktors der Naturwissenschaften

(Dr. rer. nat.)

genehmigte

D i s s e r t a t i o n

von Mohamed Mamdouh Sayed Nagia
aus Kalyobiya/ Ägypten

1. Referent:	Professor Dr. Ludger Beerhues
2. Referent:	Professor Dr. Alain Tissier
eingereicht am:	30.07.2018
mündliche Prüfung (Disputation) am:	15.10.2018

Druckjahr 2018

„Gedruckt mit Unterstützung des Deutschen Akademischen Austauschdienstes“

„Und sag: O mein Herr, mehre mein Wissen“

Der Edle Qur’an [20: 114]

Vorveröffentlichungen der Dissertation

Teilergebnisse aus dieser Arbeit wurden mit Genehmigung der Fakultät für Lebenswissenschaften, vertreten durch den Mentor der Arbeit, in folgenden Beiträgen vorab veröffentlicht:

Publikationen

Nagia, M., Gaid, M., Biedermann, E., Fiesel, T., El-Awaad, I., Haensch, R., Wittstock, U., and Beerhues, L. Sequential regiospecific gem-diprenylation of tetrahydroxyxanthone by prenyltransferases from *Hypericum* sp. (Submitted).

Nagia, M., Gaid, M., Beuerle, T., and Beerhues, L. Successive xanthone prenylation in *Hypericum sampsonii*. Planta Medica International Open 4, Tu-SL-01 (2017).
doi: 10.1055/s-0037-1608308

Tagungsbeiträge

A. Vorträge

Nagia M., Gaid M., Biedermann E., Beuerle T., Beerhues L., Successive xanthone prenylation in *Hypericum sampsonii*, 65th Annual Meeting of the Society for Medicinal Plant and Natural Product Research, Basel, Switzerland, 3. – 7. September 2017.

Nagia M., Gaid M., Behrends S., Beerhues L., Novel PPAP-related prenyltransferases, 4. SynFoBiA -Kolloquium des Pharmaverfahrenstechnik (PVZ), Braunschweig, Germany, 26. February 2016.

Nagia M., Gaid M., Beurele T., Biedermann E., Beerhues L., Aromatic Prenyltransferases from *Hypericum sampsonii*, Postgraduate workshop of the section „Natural Products“ German Society for Plant Sciences (DBG), Meisdorf, Germany , 11. – 13. September 2016.

Nagia M., Gaid M., Biedermann E., Beuerle T., Beerhues L., Aromatic Prenyltransferases from *Hypericum sampsonii*, 5. SynFoBiA (Neuartige Synthese- und Formulierungsverfahren für schwerlösliche Arzneistoffe und empfindliche Biopharmazeutika) Meeting, Braunschweig, Germany, 10. October 2016

B. Posterbeiträge

Nagia M., Gaid M., Bartels J., Beurele T., Behrends S., Beerhues L., Aromatic prenyltransferases from *Hypericum sampsonii*, Braunschweig International Symposium on Pharmaceutical Engineering Research (SPhERe), Braunschweig, Germany, 19.-20. October 2015.

Nagia M., Gaid M., Fiesel T., Beerhues L., Heterologous expression and functional analysis of novel prenyltransferases from the medicinal plant *Hypericum sampsonii,* 7th International PhD Symposium, organised by the Helmholtz International Graduate School for Infection Research, Braunschweig, Germany, 11. December 2014.

ACKNOWLEDGMENT

All gratitude to the almighty **GOD** for the blessings, wellbeing, and giving me the knowledge and patience to complete this work.

I would like to express my sincere praise to my supervisor Prof. Dr. *Ludger Beerhues* for giving me the opportunity to join his workgroup to work on this interesting research point. I immensely thank him also for his patience, motivation, and immense knowledge. He provided the group members with a suitable environment that supports the growth of *Creative ideas* and *Scientific discussions* on a friendly-cooperative (FC) medium. His smooth and friendly way of guidance and suggesting creative comments that motivate us to work and overcome the scientific challenges arise during the research work are highly appreciated. I have learned from him how to face the scientific problems in a confident way. Finally, I'd like to thank him also for his pleasant character and for keeping a sense of humor when I had lost mine due to the work stress. I find the German word "Doktorvater" suits him better than the English word "supervisor".

Many thanks for Prof. Dr. *Alain Tissier* for his interest in this research work, time, and efforts to referee my dissertation. I also appreciate the acceptance of Prof. Dr. *Stephan Scherneck* to be the chairman of my Ph.D. committee and Prof. Dr. *Ute Wittstock* as an examiner during the Ph.D. defense.

Thanks to Prof. Dr. *Robert Hänsch* for his support of the localization studies done during the Ph.D. and for Prof. Dr. *Sönke Behrends* for the co-operation by insect-cells expression.

My deep thanks go to Dr. *Mariam Gaid* for her sincere guidance, scientific support, and caring throughout the course of the practical work and the revision of the thesis. Her maddening attention to details gleam the importance of such a research item and drove me to finally learn to punctuate prose. Constructive discussion held with her, as well as her scientific experience, facilitate the way to beat the challenges facing me and helped me to find solutions to the tricks of biological systems and molecular biology methods during the accomplishment of my Ph.D.

I am grateful to Dr. *Till Beuerle* for supporting me through the analytical work with Mass spectroscopy and GC-MS, his patience to clarify and discuss all aspects belong to these parts. His sarcastic way of dealing with life helped in relieving the work stress. Many thanks to his kind and friendly guidance during my supervision for the undergraduates' biochemistry courses. I am also thankful to Dr. *Rainer Lindigkeit* for the technical support and valuable discussions.

I'm very thankful to Dr. *Islam Elawaad,* the first person I have met in Braunschweig, who introduced me to the group. His presence accelerated and facilitated my adaptation in the group. His calm attitude in life equalized my dynamic character. His team spirit, sharing of ideas, and tips helped me going through a lot of obstacles. I thank him also for the work-off times we spent together and the shared cheering memories.

Sincere appreciation for my former colleagues Dr. *Eline Biedermann* for her support by the subcellular localization work done in this study and her pleasant character; and Dr. *Tobias Fiesel*, who provided me with the primers of prenyltransferases cloned previously from other *Hypericum* sp. for homology-based cloning of prenyltransferases from my plant *H. sampsonii*.

I'd like to thank my current and former lab mates. Dr. *Benye Liu* for his welcoming approachable personality, kindness, valuable ideas, and co-operation, Dr. *Marco Grull, Ibtisam Ali, Rabeia Ali, Sara Nassar, Philipp Koch, Christian Bunzel* and *Poonam Singh* for the comfortable and friendly atmosphere, valuable and inspiring scientific discussions and continuous encouragement. Special thanks go to Dr. *Mina Noshy* and *Hisham Mohamed* for the work-off times I spent with each of them conducting conversations and laughing to get out of the stringent scientific life for some time. Extended Thanks for all members of the working group of Prof. U. Wittstock, I'm really happy to meet you all.

Bettina Böttner, Doris Glindemann, and Ines Rahaus are acknowledged for their efforts that aid and support every day's work of all IPB members.

For all departed and present colleagues in IPB, I will always remember our happy and joyful conversations and laughter during events and birthday celebrations. I have learned a lot during my stay at our institute at the personal as well as professional levels.

I acknowledge German Academic Exchange Service **(DAAD)** and the Egyptian Ministry of Higher Education **(MOHE)** for granting me this scholarship in the frame of the German-Egyptian Research Long-Term Scholarship **(GERLS)**, which expanded and developed my skills, knowledge and scientific experience and made me acquainted with a new culture.

From the deep of my heart, I'd like to thank *Rania Elmahdy*, my beloved wife, who shares with me every moment of success achieved since more than 10 years ago. Her responsibility, moral support, and love during the ups and downs offered me an excellent and productive atmosphere, alleviated the obstacles from my way, and facilitated my life. Further, I made use of her professional comments and advice that enlighten some ideas concerning the work as she was the first auditor of my seminars and talks. She is the most precious gift from the **GOD**.

Many thanks to my dear sons *Mazen* and *Marawan*. They were doing always their best to draw the smile on my face with their out of the box ideas and kid's logic-solutions for every problem. Their little smiling faces remove all the tiredness and stress after a work-full day.

There are not enough words to thank and express my sincere appreciation and great indebtedness to my **Parents** who expected this day more than 30 years ago. I wished that they were with me now to see one more success added to their stock. They provided me with care, trust, affection, everlasting love, and of course prayers. May **GOD** rest the soul of my father in peace and give my mother a long healthy life. I owe them all the success I achieved in my life. My hearty gratitude to my **brother** and **sister** for their encouragement and help at every moment.

It is absolutely a happy moment to express those feelings to all family members and colleagues. I hope that the words have transferred those feelings in the right way.

To the soul of my father

To my mother

To Rania, Mazen, and Marawan

Table of Contents

Abbreviations

[S]	Substrate concentration
°C	Degree Celsius
µg	Microgram
µl	Microliter
µM	Micromolar
λ_{max}	Maximum absorption wavelength
1356THX	1,3,5,6 -tetrahydroxyxanthone
1367THX	1,3,6,7-tetrahydroxyxanthone
137TrHX	1,3,7-trihydroxyxanthone
246TrHBP	2,4,6-trihydroxybenzophenone
246TrHiBP	2,4,6-trihydroxyisobutyrophenone
246TrHiVP	2,4,6-trihydroxyisovalerophenone
2MBP	2-methyl-2´,4´,6´-trihydroxybutyrophenone
4-CL	4-coumaroyl CoA-ligase
4HB	4-hydroxybenzoic acid
8PX	8-prenyl-1,3,6,7-tetrahydroxyxanthone
*Ac*MNPV	*Autographa californica* multicapsid nucleopolyhedrovirus
ATP	Adenosine triphosphate
aPT	Aromatic renyltransferase
Bam	*Bacillus amyloli*
BCAAs	Branched-chain amino acids
BD	Benzaldehyde dehydrogenase
BLAST	Basic Local Alignment Search Tool
BZL	Benzoate CoA-ligase
bp	Base pair
BPS	Benzophenone synthase
BSA	Bovine Serum Albumin
Bst	*Bacillus stearothermophilus*
BUS	Butyrophenone synthase
C4H	Cinnamate 4-hydroxylase
CCL	Carboxyl CoA-ligase
cDNA	Complementary deoxyribonucleic acid
cGMP	Cyclic guanosine monophosphate
cds	Coding DNA sequence
CHI	Chalcone isomerase
CHS	Chalcone synthase
CNL	Cinnamate CoA-ligase
CoA or CoASH	Coenzyme A
COX-1	Cyclooxygenase I
CTAB	Cetyltrimethylammoniumbromid
CYP	Cytochrome P450
DAD	Diode array detector
dH2O	Deionized water
DMAPP	Dimethylallylpyrophosphate

DMATS	Dimethylallyltryptophan synthase
DNA	Deoxyribonucleic acid
dNTPs	Deoxynucleotide triphosphates
DPPBP	3,3-diprenyl-2,4,6-trihydroxybenzophenone
DTT	1,4-Dithiothreitol
Eco	*Escherichia coli*
EBV-EA	Epstein–Barr virus early antigen
ED_{50}	Effective dose 50
EDTA	Ethylenediaminetetraacetic acid
EPI	Enhanced product ion
ESI	Electrospray ionization
FPP	Farnesyl pyrophosphate
g	Gravitational force
g	Gram
G-246TrHBP	3-geranyl-2,4,6- trihydroxybenzophenone
G-246TrHiBP	3-geranyl-2,4,6- trihydroxyisobutyrophenone
G-246TrHiVP	3-geranyl-2,4,6- trihydroxyisovalerophenone
G-2MBP	2-methyl-3´-geranyl-2´,4´,6´-trihydroxybutyrophenone
GC	Gas chromatography
GPP	Geranylpyrophosphate
GSP	Gene-specific primer
h	Hour
Hin	*Haemophilus influenzae*
HIV	Human immunodeficiency virus
HPLC	High-performance liquid chromatography
IC_{50}	Inhibitory concentration 50
IPP	Isopentenyl pyrophosphate
I^T	Retention index
kDa	Kilodalton
K_m	Michaelis-Menten constant
Kpn	*Klebsiella pneumoniae*
l	Liter
LB	Luria broth
LS	Linsmaier and Skoog
M	Molar
MCS	Multiple cloning site
MDR	Multidrug-resistant
MEP	Methylerythritol phosphate pathway
MIC	Minimum inhibitory concentration
min	Minute
ML	Maximum likelihood
ml	Milliliter
mM	Millimolar
MPAPs	Monocyclic Polyprenylated Acylphloroglucinols
MPPBP	3-prenyl-2,4,6-trihydroxybenzophenone
MPGR	Medicinal plants genomics resource

MRSA	Methicillin-resistant *Staphylococcus aureu*s
mRNA	Messenger RNA
MS	Mass spectroscopy
MSTFA	N-methyl-N-(trimethylsilyl)-trifluoroacetamide
NADPH	Nicotinamide adenine dinucleotide phosphate (reduced form)
NCBI	National Center for Biotechnology Information
NF-κB	Nuclear factor kappa-light-chain-enhancer of activated B cells
Nhe	*Neisseria mucosa* heidelbergensis
nm	Nanometer
NO	Nitric Oxide
OD	Optical density
ORF	Open reading frame
Pac	*Pseudomonas alcaligenes*
PAF	Platelet-activating factor
PAL	Phenylalanine ammonia lyase
PAP	2,4,6-trihydroxyacetophenone
PCR	Polymerase chain reaction
PDE4	Phosphodiesterase-4
PEG 4000	Polyethylene glycol 4000
PDT	Photodynamic therapy
PFTase	Protein farnesyl transferases
PGE2	Prostaglandin E2
PGGTase	Protein geranylgeranyl transferases
pI	Isoelectric point
PKS	Polyketide synthase
PPAPs	Polycyclic Polyprenylated Acylphloroglucinols
PPTS	Protein prenyltransferases
PT	Prenyltransferase
RACE	Rapid Amplification of cDNA Ends
RNA	Ribonucleic acid
rpm	Revolution per minute
R_f	Retention factor
RT	Reverse transcription
R_t	Retention time
s	Second
s.d.	Standard deviation
Sal	*Streptomyces albus*
SDS	Sodium dodecyl sulfate
*Sf*9	*Spodoptera frugiperda* cell line
Sma	*Serratia marcescens*
SMART	Switching Mechanism At 5' end of RNA Transcript
SOC	Super optimal broth with catabolite repression
T_a	Annealing temperature of a primer
TAE	Tris-acetate-EDTA
Taq	*Thermus aquaticus*
TdT	Terminal deoxynucleotidyl transferase

TEMED	N,N,N′,N′-tetramethylethylenediamine
T_m	Tm Melting temperature of a primer
TMH	Transmembrane helices
TP	Transit peptide
TPA	12-*O*-tetradecanoylphorbol-13-acetate
Tris	Tris(hydroxymethyl)aminomethane
TRPC6	Transient receptor potential channel 6
TXS	Trihydroxyxanthone synthase
USER	Uracil-specific excision reagent
UTR	Untranslated region
UV	Ultraviolet
V_{max}	Maximum velocity of an enzyme-catalysed reaction
VPS	Valerophenone synthase
X6H	Xanthone 6-hydroxylase
Xho	*Xanthomonas holcicola*
YFP	Yellow fluorescent protein

Amino acids

Alanine	A	Ala	Leucine	L	Leu
Arginine	R	Arg	Lysine	K	Lys
Asparine	N	Asn	Methionine	M	Met
Aspartic	D	Asp	Phenylalanine	F	Phe
Cysteine	C	Cys	Proline	P	Pro
Glutamic	E	Glu	Serine	S	Ser
Glutamine	Q	Gln	Threonine	T	Thr
Glycine	G	Gly	Tryptophan	W	Trp
Histidine	H	His	Tyrosine	Y	Tyr
Isoleucine	I	Ile	Valine	V	Val

Nucleotides

A	**A**denine		K	**K**eto	G, and T
C	**C**ytosine		R	Pu**r**ine	A, and G
G	**G**uanine		Y	P**y**rimidine	C, and T
T	**T**hymine		B	Not A	C, G, and T
U	**U**racil		D	Not C	A, G, and T
W	**W**eak	A, and T	H	Not G	A, C, and T
S	**S**trong	G, and C	V	Not T	A, C, and G
M	A**m**ino	A, and C	N	A**n**y	A, C, G, and T

1 Introduction

1.1 The genus *Hypericum*

Hypericum is a flowering plant genus, which belongs to the Hypericaceae plant family, previously taxonomically classified as the subfamily Hypericoideae within the family Guttiferae (Clusiaceae). However, recent molecular and phylogenetic analyses showed that it is a distinct family comprising nine genera, namely *Cratoxylum*, *Eliea*, *Harungana*, *Hypericum*, *Lianthus*, *Santomasia*, *Thornea*, *Triadenum*, and *Vismia*. The genus *Hypericum* constitutes the largest genus among those of Hypericaceae (Crockett and Robson, 2011). To date, it contains more than 500 species (Christenhusz and Byng, 2016; Robson, 2016). Commonly, these species appear as herbs, shrubs or, to a lesser extent, trees. The species occupy different habitats worldwide, specifically in temperate regions and high areas in the tropics of North America, North Africa, Europe, and West Asia (Crockett and Robson, 2011; Marrelli et al., 2016). The yellow flowers of members of the genus bloom around the St. John's day on June the 24th, therefore, it is commonly known as St. John's wort (Miller, 1998).

In classical antiquity, *Hypericum* sp. were used as a component of antidote solutions. In the Middle Ages, genus members were thought to ward off evil spirits, which can inhabit a person and cause the symptoms of lack of interest and low mood, defined nowadays as depression. Accordingly, this group of plants was assigned the name *Hypericum* (from the Greek word *hyper* meaning 'above' and *eikon* meaning icon or picture) and they were used to protect the religious symbols and pictures (Crockett and Robson, 2011; Nürk, 2011). In folk medicines, various *Hypericum* species are used for their wide bioactivity range including antidiuretic, antimalarial, hepatoprotective, renal antispasmodic and diuretic effects (Guedes et al., 2012; Stojanovic et al., 2013). These biological activities are attributed to the vast affluence of metabolites belonging to various chemical groups (Tanaka et al., 2010; Crockett and Robson, 2011; Liu et al., 2013b; Zhao et al., 2015; Marrelli et al., 2016; Liu et al., 2017). Representative examples of *Hypericum* secondary metabolites are displayed in Table 1.

Table 1: Examples of secondary metabolites from different chemical classes identified in the genus *Hypericum*

Chemical class	Example	References
Biflavonoids	Amentoflavone	(Baureithel et al., 1997)
Flavonoids	Rutin, hyperoside, isoquercitrin, quercitrin, quercetin	(Noldner and Schotz, 2002; Don et al., 2004)
Naphthodianthrones	Hypericin, pseudohypericin	(Gadzovska et al., 2005; Liu et al., 2007)
Phenylpropanoids	Chlorogenic acid	(Seabra and Correia Alves, 1989)

Polycyclic polyprenylated acylphloroglucinols (PPAPs)	Hyperforin, adhyperforin, sampsoniones, hypericumoxides, hypercohins	(Gurevich et al., 1971; Hu and Sim, 2000; Klingauf et al., 2005; Liu et al., 2013b; Liu et al., 2017)
Tannins and procyanidins	Procyanidin, catechin, epicatechin	(Ploss et al., 2001)
Xanthones	Mangiferin, biyouxanthones, hyperixanthone A	(Chen and Chen, 1985; Tanaka et al., 2004; Xiao et al., 2010)

One of the most important species in the genus is *Hypericum perforatum.* Main chemical constituents of *H. perforatum* are the naphthodianthrones hypericin and pseudohypericin and the polycyclic polyprenylated acylphloroglucinols (PPAPs) hyperforin and adhyperforin (Beerhues, 2011). The former category found application in cancer photodynamic diagnosis and therapy (PDT) (Karioti and Bilia, 2010). Extracts of plants are widely used for the treatment of mild to moderate depression, which is mainly attributed to the content of hyperforins (Kasper et al., 2006). In addition, they are used topically to medicate wounds and abrasions by virtue of the anti-inflammatory, antimicrobial, and tissue growth stimulatory activities, caused by the main constituent and model PPAP hyperforin (Russo et al., 2013; Woelfle et al., 2014). Because of the broad biological activities of hyperforin, PPAPs from other members of the genus *Hypericum* have drawn the attention to be studied. The present research work focuses on PPAPs from *H. sampsonii*.

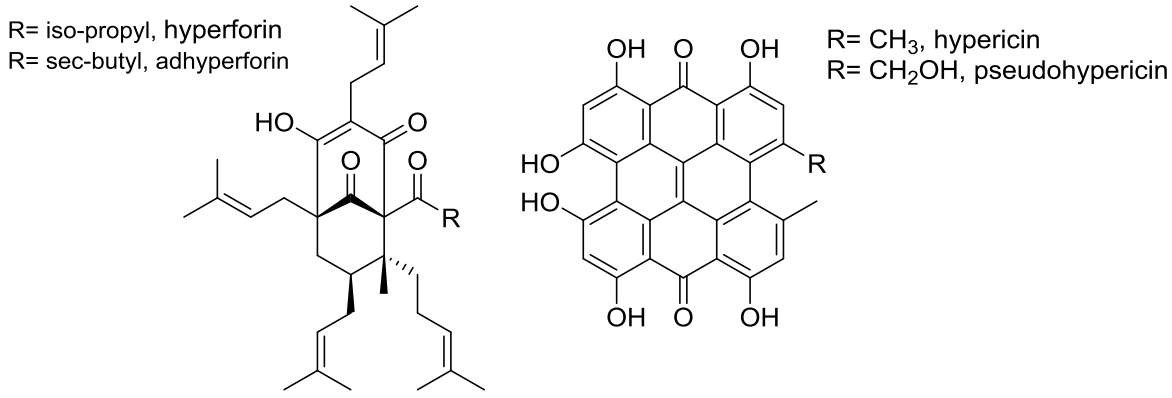

Figure 1: Main active constituents of *H. perforatum*.

1.2 *Hypericum sampsonii*

1.2.1 Botany and occurrence

Hypericum sampsonii Hance is a perennial herbaceous plant. The natural habitats are stream sides, thickets, roadsides, grassy places, and cultivated margins. The plant is native to the Far East countries China, Hong Kong, Northeast India, South Japan, Myanmar, Taiwan, and North Vietnam (Robson, 2016). The erect field herb grows to a length of 20 to 80 cm with single or few stems

originating from decumbent rooting base. Leaves are oblanceolate with an entire margin, rounded to obtuse apex, 1 cm to 3.5 cm, and are arranged in perfoliate pairs having intramarginal dark glands. Venation of the leaves contains 4-5 pairs of main laterals from midrib, branching and uniting near the margin. The corolla has five bright yellow petals with entire or subentire margin and the calyx is composed of five sepals 1-3 mm long. The capsule is 4-5 mm, broadly ovoid exceeding sepals. The seeds are orange-brown, 1 mm long, cylindric, not carinate or appendiculate with finely ribbed-scalariform testa (Robson, 2001). The *in vitro* grown plant, used throughout this study (2.1.1.1 and 3.1.1.1), was shorter, about 10 cm long, and the leaves had nearly the same length as in field grown herb, 1-2.5 cm.

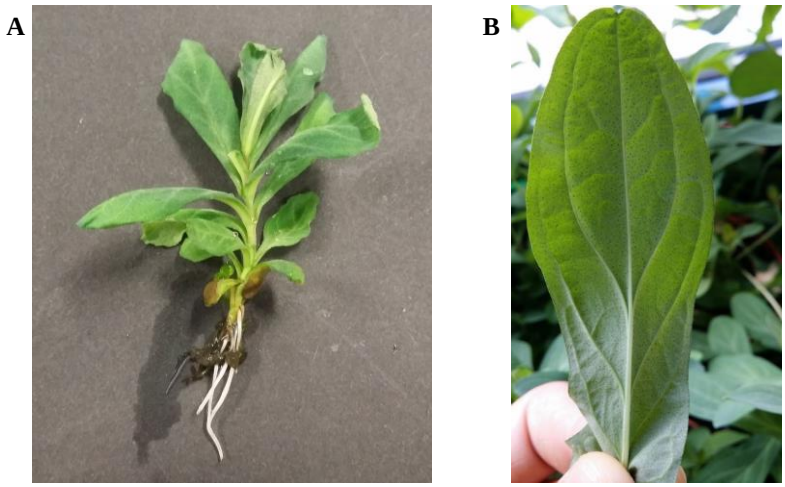

Figure 2: *Hypericum sampsonii*. A) Whole in vitro plantlet. B) Leaf from a pot-grown plant.

1.2.2 Why *Hypericum sampsonii*?

1.2.2.1 Therapeutic Uses

H. sampsonii is a Chinese herb used in folk medicine to treat various disorders. The herbal extracts are used for the treatment of snakebites, diarrhea, backache, burns, and swellings (Xiao et al., 2007). In Taiwan, the plant is used as a detoxifying agent, to relieve swelling, and as anti-hepatitis and anti-hepatoma drug (Lin and Wu, 2003). It contains a wide variety of prenylated acyl- and benzoylphloroglucinol metabolites, including prenylated xanthones. Predominantly, the antibacterial and cytotoxic activities of the plant are largely attributed to the contents of prenylated xanthones and acylphloroglucinols, respectively (Demirkiran, 2007; Xiao et al., 2010; Xin et al., 2011a)

1.2.2.2 Bioactive constituents of *H. sampsonii*

1.2.2.2.1 Xanthones

The first report about *H. sampsonii* secondary metabolites was published by Chen and Chen (1985), who reported five xanthones including the antibacterial xanthone *C*-glucoside mangiferin (Biswas et al., 2015), its isomer isomangeferin, and hyperxanthone. The later was again identified in 2004 from the anti-hepatitis B fraction of the whole herb (Don et al., 2004).

Table 2: Xanthones from *H. sampsonii*.

Name	Plant part	Biological activities	References
Mangiferin and isomangiferin	Whole herb	Antibacterial	(Chen and Chen, 1985; Biswas et al., 2015)
Hypericumxanthone A and B	Aerial parts	Antibacterial	(Xin et al., 2011a)
Hyperixanthone A	Roots	Antibacterial	(Xiao et al., 2008)
Hyperxanthone	Whole herb	Anti-hepatitis B	(Chen and Chen, 1985; Don et al., 2004)
Sulfonated xanthones	Whole herb	Cytotoxic	(Hong et al., 2004)
Patulone	----	Anti-inflammatory and PAF* inhibitor	(Li et al., 2004; Yamakuni et al., 2006)
Sampsone C	Aerial parts	----	(Xin et al., 2011b)
1,3,6,7-Tetrahydroxyxanthone and 2-prenyl-1,3,5,6-tetrahydroxyxanthone	Whole herb	----	(Don et al., 2004)

* PAF= Platelet activating factor

Two sulfonated xanthones, namely 1,3-dihydroxy-5-methoxyxanthone-4-sulfonate and 1,3-dihydroxy-5-O-*β*-D-glycopyranosylxanthone-4-sulfonate, showed moderate activity against the P388 cell line with ED_{50} of 3.46 and 15.69 µmol/l, respectively (Hong et al., 2004). Patulone, 1,2-dihydro-3,6,8-trihydroxy-1,1-bis-(3-methyl-but-2-enyl)-xanthen-2,9-dione, isolated for the first time from *Hypericum patulum* (Ishiguro et al., 1997), was also identified in *H. sampsonii* (Li et al., 2004). It inhibited strongly (more than 60%) the exogenous platelet activating factor (PAF)-induced hypotension in mice. PAF mediates many diseases such as allergy, inflammation, thrombosis, and asthma (Oku et al., 2005). This diprenylated compound also inhibits the release of prostaglandin PGE_2 and COX-1 activity in a dose-dependent manner and inhibits NF-κB, which regulates the transcription of genes involved in the inflammation pathway (Yamakuni et al., 2006). Bioassay-guided fractionation utilizing a multidrug-resistant (MDR) *Staphylococcus aureus* strain resulted in the isolation of a potent antibacterial prenylated agent, hyperixanthone A, which showed minimum inhibitory concentration (MIC) of 2 µg/ml in comparison to the positive standard (norfloxacin) with an MIC of 32 µg/ml (Xiao et al., 2008). Later, Two moderately-active antibacterial prenylated xanthones were isolated from the aerial parts of *H. sampsonii*, namely hypericumxanthone A and B, with an MIC against methicillin-resistant *Staphylococcus aureu*s (MRSA) of 16 and 32 µg/ml, respectively (Xin et al., 2011a).

1.2.2.2.2 Polycyclic polyprenylated acylphloroglucinols (PPAPs)

H. sampsonii is the richest source of PPAPs so far detected. Non-caged derivatives (1.3.1), as well as over 50 PPAPs, belong to adamantane- and homoadamantane-type, have been reported from the plant (Yang et al., 2018). Examples of bioactive *Hs*-PPAPs are represented in Table 3 and Figure 3.

Table 3: PPAPs from *H. sampsonii*.

Name	plant part	biological activity	References
Sampsonione A-R	Whole herb, roots	Cytotoxic	(Hu and Sim, 2000; Xiao et al., 2007; Zhu et al., 2014)
Hypersampsones A-X	Aerial parts	Cytotoxic	(Lin and Wu, 2003; Zeng et al., 2009; Zeng et al., 2012; Tian et al., 2016)
Sampsonols A-F	Aerial parts	Cytotoxic	(Xin et al., 2012)
Hyperisampsines A-O	Aerial parts	Cytotoxic, A, and D are anti-HIV	(Zhu et al., 2014; Zhu et al., 2015; Zhu et al., 2017)
Norsampsones A-E	Aerial parts	Cytotoxic	(Tian et al., 2014; Tian et al., 2017)
Hyperhexanone A	Aerial parts	Cytotoxic	(Zhu et al., 2016)
Dioxasampsone A and B	Aerial parts	Cytotoxic	(Tian et al., 2014)
Sampsone A	Aerial parts	Antibacterial	(Xin et al., 2011b)
Peroxysampsone A and B	Roots	Antibacterial	(Xiao et al., 2010)
Hypersampsonone A-G	Aerial parts	Phosphodiesterase inhibition	(Zhang et al., 2016)
Epoxyplukenetione A	Aerial parts	----	(Zhu et al., 2014)
Plukenetione C	Roots	----	(Xiao et al., 2010)

Sampsoniones A and I showed activity against mouse lymphocytic leukemia (P388) at 13 µg/ml and 6.9 µg/ml, respectively (Hu and Sim, 2000). Hypersampsones A-F had mild cytotoxic activity against MS-G2 hepatoma (Lin and Wu, 2003), whereas the cytotoxicity of hypersampsones S and R was against the HeLa cell line at a concentration of 20 µM (Tian et al., 2016). Sampsonols A and B exhibited significant cytotoxicity against a number of cancer cell lines including human breast (MCF-7), hepatoma (HepG2), colon (HT-29), and lung (A549) tumor cell lines with IC_{50}s ranging from 13 to 28 µM (Xin et al., 2012). All hypersampsin series members had a significant cytotoxicity with IC_{50} values in the range 0.56-3.00 µM against different cell lines. Hypersampsins A and D additionally had an anti-HIV activity with EC_{50} values of 2.97 and 0.97 µM, respectively (Zhu et al., 2014). The decarbonyl PPAP, norsampsone C, caused inhibition of Hela cell proliferation at a concentration of 20 µM (Tian et al., 2014). The underlying mechanism of the cytotoxic activity of *Hs*-PPAPs was attributed to the transcriptional inhibition of the nuclear retinoid x receptor (RXRα), which mediates numerous physiological processes, for example, calcium homeostasis, embryogenesis, and lipid and glucose metabolism, their transcriptional downregulation inducing apoptosis (Wu et al., 2014; Tian et al., 2017).

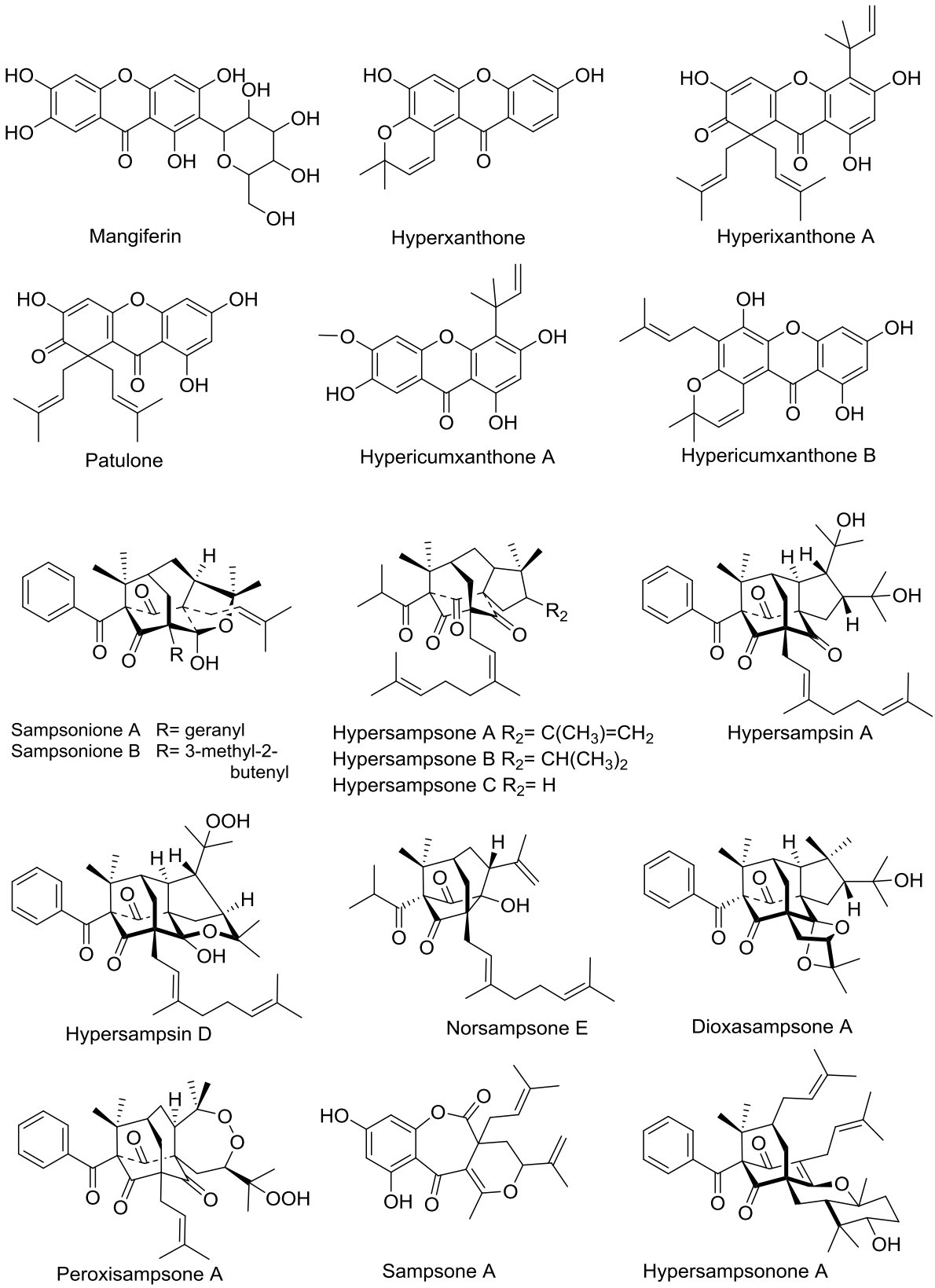

Figure 3: Chemical constituents of *H. sampsonii*.

Peroxisampsone A, a polyprenylated benzophenone peroxide, exhibited norfloxacin-comparable activity against fluoroquinolone-resistant *Staphylococcus aureus* with an MIC value of 110 µM, while the MIC value of the positive control norfloxacin was 100 µM. The activity is assumed to be due to the presence of the peroxide group in its structure (Xiao et al., 2010). Another antibacterial prenylated xanthone, namely sampsone A, showed moderate anti-methicillin-resistant *Staphylococcus aureus* (MRSA) activity with an MIC of 32 µg/ml (Xin et al., 2011b). Hypersamsonone A had a potent phosphodiesterase inhibitory activity with IC_{50} of 8.08 µM (Zhang et al., 2016). Phosphodiesterase-4 (PDE4) plays a crucial rule in cell signaling and is a potential drug target for the treatment of inflammation, asthma, chronic obstructive pulmonary disease and Alzheimer's disease (Zhang et al., 2005).

1.2.2.2.3 Other chemical constituents

Apart from PPAPs, Don et al. (2004) isolated different classes of compounds from the whole herb of *H. sampsonii* including O-prenylated benzophenones assigned the names 2,6-dihydroxy-4-[(*E*)-5-hydroxy-3,7-dimethylocta-2,7-dienyloxy]benzophenone and 2,6-dihydroxy-4-[(*E*)-7-hydroxy-3,7-dimethylocta-2-enyloxy]benzophenone, the anthraquinone emodin, a bisanthraquinone glycoside, two flavonoids kaempferol and quercetin and their 3-O-glucopyranosides. Similar to *H. perforatum*, the plant is characterised by the distribution of dark glands, in which the naphthodianthrones hypericin and pseudohypericin were identified (Liu et al., 2007).

1.3 Polycyclic polyprenylated acylphloroglucinol derivatives (PPAPs)

They are a group of compounds possessing a fascinating highly oxygenated acylphloroglucinol-derived polycyclic nucleus decorated with prenyl groups of different lengths (C_5 or C_{10}), giving them diamond-like structures, high chemical diversity, and intriguing biological activities (Ciochina and Grossman, 2006; Yang et al., 2018). Biosynthetically, PPAPs are a hybrid group of natural products derived from the mevalonate or methylerythritol phosphate and the polyketide pathways (Yang et al., 2015). According to the most recent database of PPAPs published by Grossman (2018), the number of identified natural PPAPs is 618, mainly isolated from members of the Hypericaceae, Clusiaceae and related plant families of the Clusioid clade. A total of 146 structures thereof are caged.

1.3.1 Classification of PPAPs

Based on the complexity of their structures, PPAPs are classified into two main groups: (*i*) the uncaged compounds with either bicyclo[3.3.1]nonane-2,4,9-trione or bicyclo[3.2.1]octane-2,4,8-trione and (*ii*) the caged PPAPs with tri- or tetracyclo structures. According to the relative position of the benzoyl or aliphatic acyl group on the bicyclo scaffold and according to the most recent structural revisions, PPAPs were classified into the two classes A and B (Yang et al., 2018). In contrast, Cuesta-Rubio et al. (2001) and Ciochina and Grossman (2006) classified PPAPs into the three classes A, B, and C **(Figure 4 A)**. Type A PPAPs have the acyl group attached to C-1, which is adjacent to the quaternary carbon C-8. However, the acyl group in type B PPAPs is attached to the C-3 position of the bicyclo skeleton. Interestingly, there are more than 20 PPAPs of type B,

which have a xanthone nucleus and were mainly reported for the genera *Garcinia* and *Symphonia* such as garcimultiflorone I and 3,16-oxyguttiferone A, respectively **(Figure 4 B)** (Cottet et al., 2015; Fu et al., 2015; Grossman, 2018). The rare type C PPAPs have a C-1 acyl group but the quaternary center is distant at C-6 (Ciochina and Grossman, 2006). Type C PPAPs represented only three structures from the 600 naturally occurring PPAPs, namely garcinielliptones K, L and M (Weng et al., 2004).

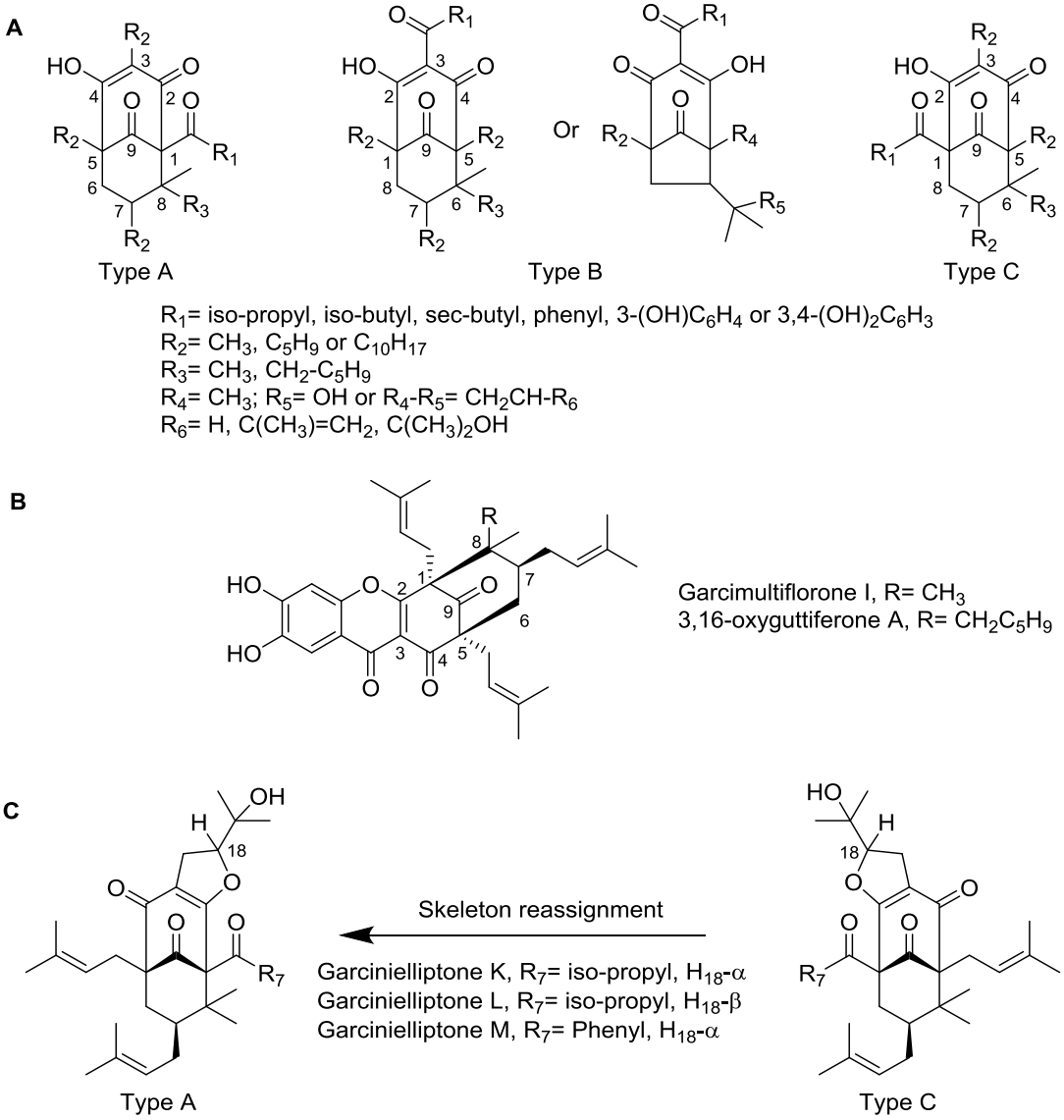

Figure 4: Types of PPAPs. A) Previously described types of PPAPs adapted from Ciochina and Grossman (2006). B) Examples of PPAPs with a xanthone nucleus. Numbering indicates the relative position of the acyl group on the bicycle skeleton. C) Structure reassignment of garcinielliptones K-M to the corresponding type A skeletons, denoting the obsolescence of type C PPAPs. Adapted from Yang et al. (2018).

Yang et al. (2017a) revised and reassigned their structures to the corresponding type A, where the positions of substituents at the bridgehead of the bicyclo skeleton were switched from their original assignment, depending on detailed spectroscopic data and quantum computational chemistry. This led to announce the obsolescence of type C PPAPs **(Figure 4 C)** and to prove that the structure of garcinielliptone K is identical to the previously known compound propolone C (Hernández et al., 2005).

Caged PPAPs are sub-grouped into two classes bearing either adamantane (tricyclo[3.3.1.1]decane) or homoadamantane (tricyclo[4.3.1.1]undecane) cores (Yang et al., 2018). Some examples are represented in Figure 5. Plukenetione A, isolated from *Clusia plukenetii* was the first identified PPAP of the adamantane-type (Henry et al., 1996). Since then, about 33 structure with either type A or type B arrangement or their corresponding *seco*-structures, for example, hypersubone A from *H. subsessile* (Liao et al., 2015), were identified. Homoadamantane-type PPAPs are 49 structures, which follow only type A arrangement, for example, pseudohenone G isolated from *H. pseudohenryi* (Yang et al., 2017b).

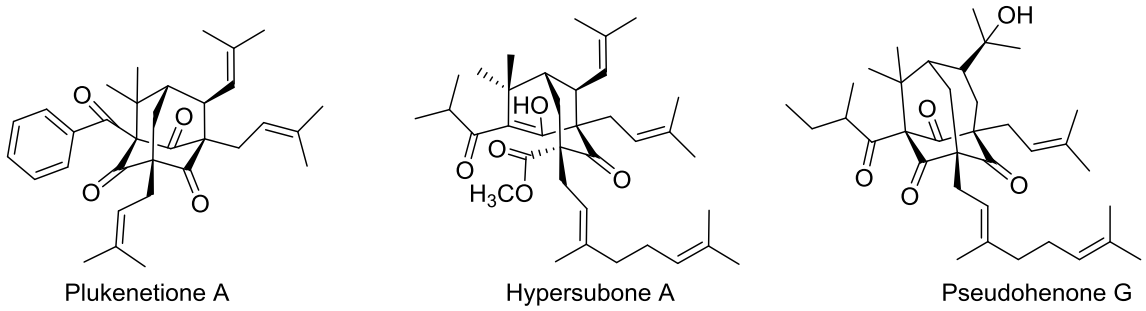

Figure 5: Examples of caged PPAPs of adamantane (plukenetion A), *seco*-adamantane (hypersubone A), and homoadamantane (pseudohenone G) types.

1.3.2 Bioactivities of selected PPAPs

1.3.2.1 Type A PPAPs

Hyperforin **(Figure 1)** is the best-known member of type A PPAPs and responsible for the antidepressant activity of *H. perforatum* (Kasper et al., 2006). The rigorous mechanism of action is not totally defined but the most recent studies suggest neurotransmitters-reuptake inhibition through activating the transient receptor potential channel 6 (TRPC6) (Bouron and Lorrain, 2014; Friedland and Harteneck, 2015) as an action mechanism. Besides, hyperforin has cognitive- and memory-enhancing properties and acts as neuroprotective against Alzheimer's disease neuropathy (Griffith et al., 2010). Through lipoxygenase inhibition (Medina et al., 2006; Sosa et al., 2007) and inhibition of prostaglandin E synthase (Koeberle et al., 2011), hyperforin was proved to have potent anti-inflammatory activities. It can also down-regulate many signaling pathways controlling angiogenesis and proliferation of leukemic cells and induce apoptosis (Quiney et al., 2006; Martinez-Poveda et al., 2010). Furthermore, hyperforin displayed antibacterial (Schiavone et al., 2013; Hernandez-Lopez et al., 2014), antimalarial (Verotta et al., 2007), larvicidal (Mitsopoulou et al., 2014), antioxidant (Meinke et al., 2012), and estrogenic (Kwon et al., 2016) activities.

Garsubellin A **(Figure 6)** is one of the oldest type A PPAPs. It was isolated from the tree *Garcinia subelliptica* (Fukuyama et al., 1998). It boosts the choline acetyltransferase activity in the cultures of P10 rat septal neurons, thus increasing the concentration of the neurotransmitter acetylcholine, and offers a lead opportunity for treating neurodegenerative diseases like Alzheimer's disease (Fukuyama et al., 1997). The compound has a potent anti-inflammatory effect by inhibiting the release of *β*-glucuronidase and the inflammatory mediator histamine (Jing-Ru et al., 2003).

1.3.2.2 Type B PPAPs

Garcinol **(Figure 6)**, isolated from *Garcinia* sp. (Baliga et al., 2011) is a known example for type B PPAPs. Recent reports about the biological activities of the compound showed its high cytotoxic activity, which is mainly mediated by inhibition of several cell signaling pathways (Saadat and Gupta, 2012; Wang et al., 2015b; Behera et al., 2016). Earlier investigations of the compound proved its antioxidant and antifungal activities (Padhye et al., 2009; Jackson et al., 2015). Recently, garcinol showed significant antidiabetic activity against streptozotocin-induced diabetes in rats (Madhuri and Naik, 2017; Mali et al., 2017).

Two C-7 epimeric PPAPs were isolated from *Clusia* sp., namely clusianone and 7-*epi*-clusianone (Piccinelli et al., 2005). Both showed potent HIV inhibitory activity (Garnsey et al., 2011). Moreover, clusianone induced the death of HepG2 cells through the distraction of the membrane potential of rat liver mitochondria (Reis et al., 2014). 7-*epi*-clusianone has an antimicrobial activity against the acid-producing bacteria, *Streptococcus mutans* (Almeida et al., 2008) and is considered a potential agent for fighting worldwide-distributed dental caries (Forssten et al., 2010; Branco-de-Almeida et al., 2011). It also reliefs bronchospasm *via* activation of epithelium-, NO-, and cGMP-dependent pathways (Coelho et al., 2008). Structures of both epimers are shown in Figure 6.

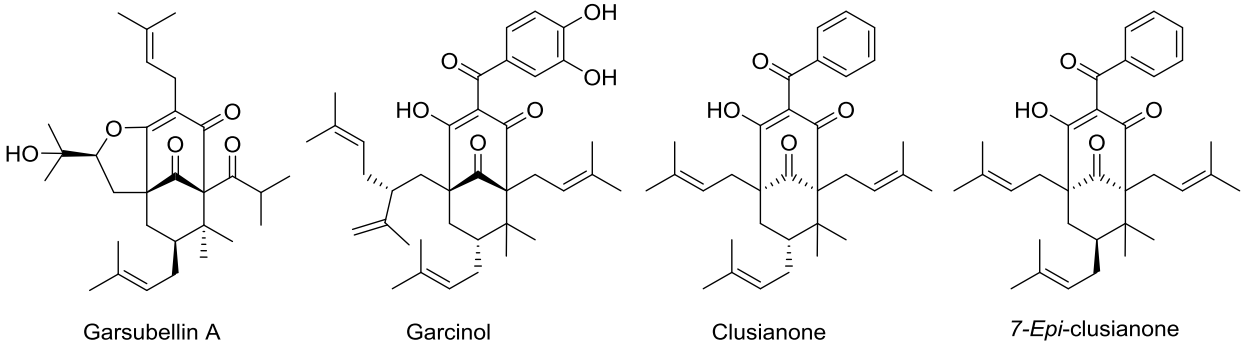

Figure 6: Examples of biologically active PPAPs.

1.3.3 Biosynthesis of PPAPs

Biosynthesis of PPAPs is achieved generally in a two-staged biogenetic scheme. The first step is the construction of the aromatic acylphloroglucinol nucleus, which undergoes the second stage. This decoration involves the attachment of prenyl groups of different lengths at different positions on the skeleton formed (Beerhues, 2011).

1.3.3.1 First stage: formation of aromatic nuclei

Through the catabolism of aliphatic branched chain amino acids (BCAAs), namely leucine, isoleucine, and valine, the branched short-chain acyl-CoAs valeryl-, 2-methylbutyryl- and isobutyryl-CoAs, respectively, are formed. The reaction starts by the transamination of a BCAA, followed by oxidative decarboxylation of the formed ketoacid intermediate (Goese et al., 1999; Karppinen et al., 2007) and a suitable carboxyl CoA ligase (CCL) (Xu et al., 2013). Differently, aromatic-CoA esters are developed *via* the catabolism of the amino acid phenylalanine starting from its deamination by the enzyme phenylalanine ammonia lyase (PAL) to form a *trans*-cinnamic acid (Ritter and Schulz, 2004; Dreßen et al., 2017), which proceeds in either of two ways to form benzoyl-CoA. The first pathway is CoA dependent through cinnamate CoA ligase (CNL) to form cinnamoyl-CoA, followed by *β*-oxidative C_2 shortening. Alternatively, a CoA-independent non-*β*-oxidative pathway is followed through the formation of benzaldehyde and benzoic acid as intermediates (Abd El-Mawla and Beerhues, 2002). Via catalysis of cinnamate 4-hydroxylase (C4H) and *p*-coumarate-CoA ligase, cinnamic acid is converted to *p*-coumaroyl-CoA (Gaid et al., 2011). The CoA thioesters formed, valeryl-, 2-methylbutyryl-, isobutyryl-, benzoyl-, and *p*-coumaroyl-CoA are the starting building blocks for the aromatic nuclei, 2,4,6-trihydroxyisovalerophenone (246TrHiVP), 2-methyl -2´,4´,6´-trihydroxybutyrophenone (2MBP), 2,4,6-trihydroxyisobutyrophenone (246TrHiBP), 2,4,6-trihydroxybenzophenone (246TrHBP), and naringenin chalcone, respectively. The CoA esters are condensed with three molecules of malonyl-CoA by means of suitable type III polyketide synthases, namely isobutyrophenone synthase (BUS), valerophenone synthase (VPS), benzophenone synthase (BPS), or chalcone synthase (CHS) to form a linear tetraketide intermediate, which in turn cyclizes *via* intramolecular Claisen condensation to yield the acylphloroglucinol scaffold (Okada and Ito, 2001; Liu et al., 2003; Klingauf et al., 2005; Karppinen et al., 2007). This polyketide pathway was confirmed for biosynthesis of the phlorisobutyrophenone core by feeding radiolabeled glucose to the sprouts of *H. perforatum* and subsequent analysis of isolated hyperforin (Adam et al., 2002).

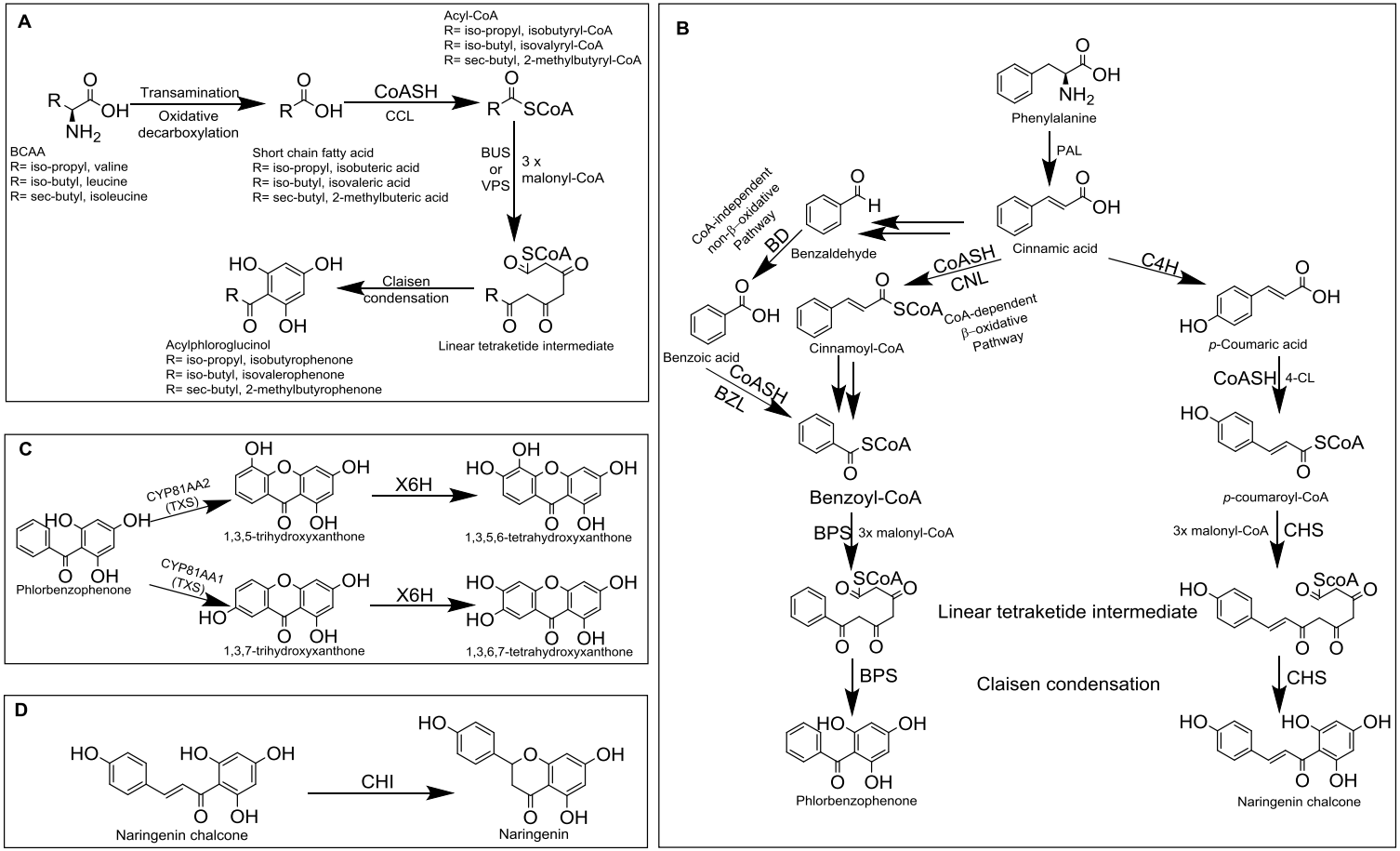

Figure 7: Polyketide biosynthetic cascade for the formation of acyl- and benzoylphloroglucinols. A) Formation of acylphloroglucinols. B) Formation of benzoylphloroglucinols. C) Formation of tetrahydroxyxanthones from phlorobenzophenone. D) Formation of naringenin from naringenin chalcone. 4-CL, 4-coumaroyl CoA-ligase; BD, benzaldehyde dehydrogenase; BPS, benzophenone synthase; BUS, butyrophenone synthase; BZL, benzoate CoA-ligase; C4H, cinnamate 4-hydroxylase; CCL, carboxyl CoA-ligase; CHI, chalcone isomerase; CHS, chalcone synthase; CNL, cinnamate CoA-ligase; CoASH, coenzyme A; CYP, cytochrome P450; PAL, phenylalanine ammonia lyase; TXS, trihydroxyxanthone synthase; VPS, valerophenone synthase; X6H, xanthone 6-hydroxylase.

The phlorbenzophenone (246TrHBP) scaffold can subsequently undergo 3'-hydroxylation and either *ortho* or *para* regiospecific phenol coupling by bifunctional CYP enzymes, namely CYP81AA1 and CYP81AA2, to form 1,3,5- and 1,3,7-trihydroxyxanthone skeletons, respectively (El-Awaad et al., 2016). An additional 6-hydroxylation step is catalyzed by xanthone 6-hydroxylase (X6H) on the trihydroxyxanthone skeletons formed to give rise to either 1,3,5,6- or 1,3,6,7-tetrahydroxyxanthones (1356THX or 1367THX) (Schmidt et al., 2000). The flavanone naringenin is formed in a one-step reaction after naringenin chalcone formation *via* stereospecific cyclization catalyzed by chalcone isomerase (CHI) (Jez et al., 2000). Naringenin is metabolized by further downstream processes to other subgroups of flavonoids (Ferrer et al., 2008).

1.3.3.2 Second stage: attachment of prenyl side chains

This step involves the attachment of isoprenoid units of different hydrocarbon chain lengths (prenyl, C_5; geranyl, C_{10}; farnesyl, C_{15}; etc.) to the formerly formed aromatic prenyl acceptors (1.3.3.1). All isoprenoid units are derived from the five-carbon prenyl diphosphate, dimethylallyl diphosphate (DMAPP), or its structural analog isopentenyl diphosphate (IPP; see 1.4.1). Both C_5 units are biosynthesized through either of two different metabolic pathways **(Figure 8)**. The first one is the cytoplasmic mevalonate pathway, where IPP is built up from the condensation of three molecules of acetyl CoA (Goldstein and Brown, 1990). Finally, an isomerase rearranges it to the more active isomer DMAPP (Cornforth et al., 1966). Alternatively, in higher plants, bacteria, algae, and some protozoa, both C_5 units are formed *via* the methylerythritol phosphate pathway (MEP), which occurs in the plastids. DMAPP and IPP are biosynthesized from a common precursor formed from pyruvate and glyceraldehyde-3-phosphate (Rohmer, 1999; Eisenreich et al., 2004).

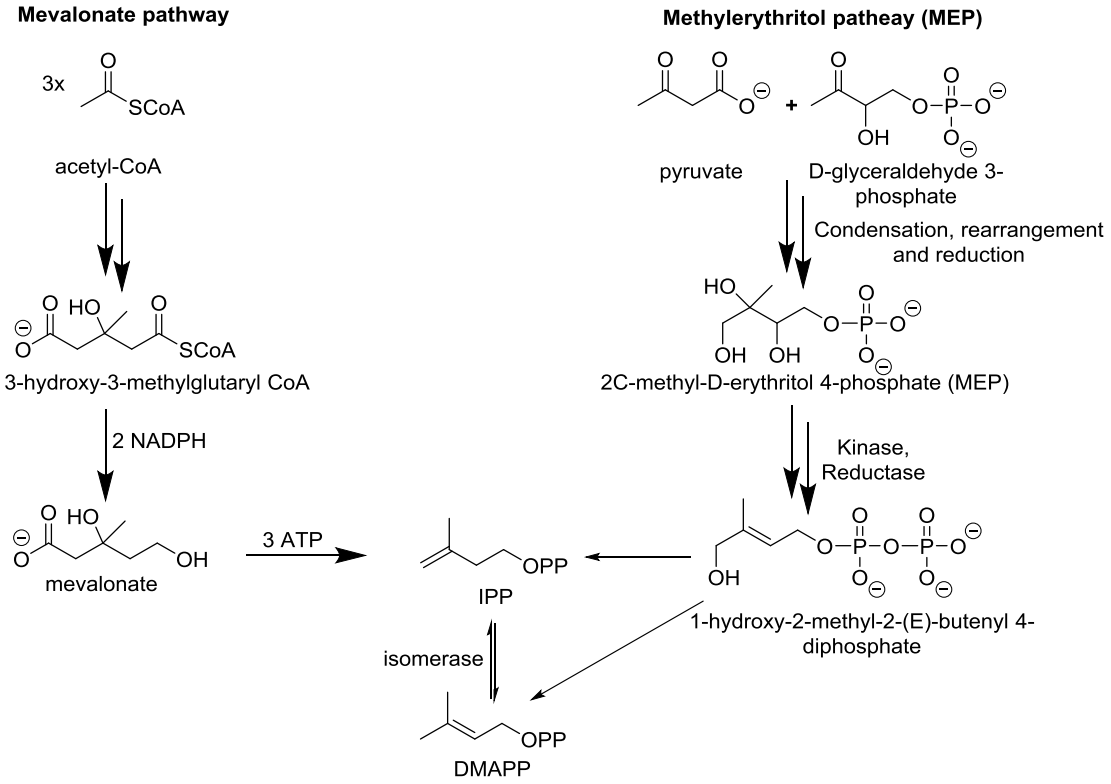

Figure 8: Alternative pathways for the biosynthesis of the five-carbon prenyl diphosphate units. IPP, isopentenyl diphosphate; DMAPP, dimethylallyl diphosphate.

Acylphloroglucinol moieties undergo enzyme-catalyzed addition of prenyl and/or geranyl groups, derived mainly (>98%) from the mevalonate-independent (MEP) pathway (Beerhues, 2011), by the action of a group of enzymes called prenyltransferases (PTs) (Zuurbier et al., 1998). Similar to the biosynthesis of *β*-bitter acids in hop (Li et al., 2015), acylphloroglucinols are prenylated and/or geranylated to afford monocyclic polyprenylated acylphloroglucinol derivatives (MPAP). The MPAP intermediate cyclizes in two different ways to support the formation of all type A and type B PPAPs. An additional DMAPP moiety is added to one of the geminal prenyl groups of the MPAP by a nucleophilic addition mechanism to give rise to a tertiary carbocation. Attack of C-1 of the intermediate on the pendant carbocation (or the analogous pyrophosphate) results in the formation of the bridged system of type A PPAP, whereas C-5-attack gives a type B arrangement of PPAP (Cuesta-Rubio et al., 2001; Liao et al., 2015) **(Figure 9)**. The complexity and structural diversity of PPAPs are created and supported through different types of acyl groups, from which the PPAP is derived, and the downstream processes, which take place on the cyclized and bridged type A or type B skeletons. Examples are the number and position of isoprenoid substituents, their degree of oxidation and respective locations on the formed ether rings, and various secondary cyclization mechanisms, such as aldol, Diels-Alder, etc. (Yang et al., 2018). These mechanisms together with structural diversity due to various down-stream biosynthetic sequences are illustrated by the postulated biosynthesis of the members of the sampsonione series isolated from *H. sampsonii* (Hu and Sim, 2000) **(Figure 10)**.

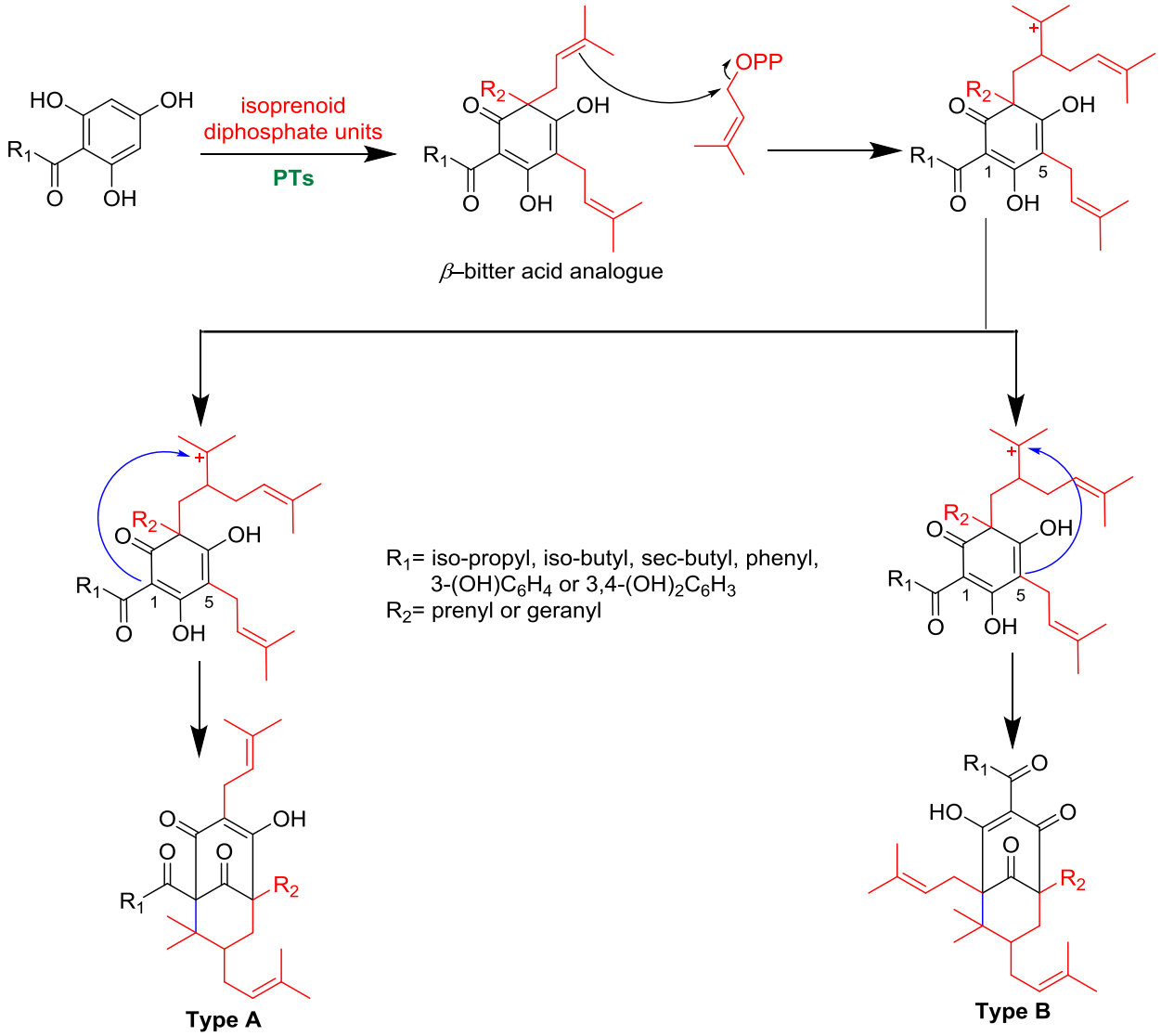

Figure 9: Proposed biosynthetic cascade for type A and type B PPAPs.

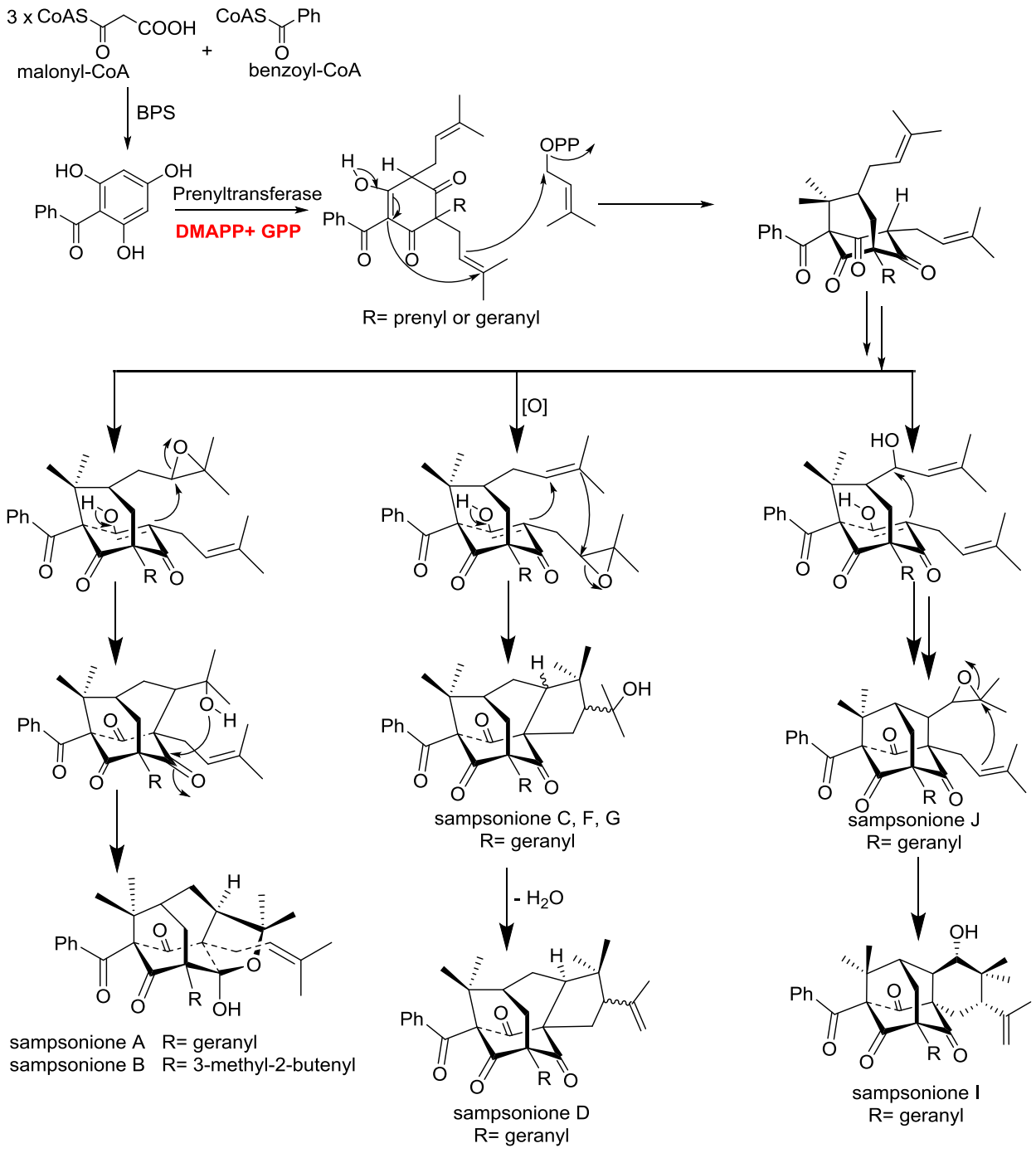

Figure 10: Proposed biosynthesis of sampsoniones A, B, C, D, F, G, J, and I. Adapted from Hu and Sim (2000).

1.4 Prenyltransferases

Prenyltransferases (PTs) are a group of enzymes that catalyze the transfer of prenyl residues from different prenyl donors to an acceptor molecule. PTs constitute an important branch of the larger prenyl converting enzyme family, which is responsible for the biosynthesis of terpenoid and meroterpenoid skeletons (Brandt et al., 2009). According to the most recent estimates, more than

63,000 terpenoid natural products including steroids, carotenoids, ubiquinones, menaquinones, and plastoquinones are identified from microbial, fungal, animal, and mostly plant origins (Winkelblech et al., 2015).

1.4.1 Classification and functions of prenyl converting enzymes

Prenyl converting enzymes are classified mainly into four groups, namely hydrolase/lyases, terpene cyclases (synthases), transferases, and a fourth heterogenous group, which includes members that cannot be assigned to other classes, such as geranylgeranyl hydrogenase or squalene epoxidase **(Figure 11)**. Their catalytic activities begin with the detachment of the diphosphate from a prenyl moiety either by hydrolysis *via* the effect of hydrolases/lyases or as a leaving group forming an intermediate allylic prenyl cation (Brandt et al., 2009). Elimination of the pyrophosphate of GPP through hydrolysis leads to the formation of prototypical acyclic monoterpene geraniol (Banthorpe et al., 1983). Downstream rearrangements, oxidations and/or reduction provide other acyclic monoterpenes such as linalool, citral, citronellol (Banthorpe et al., 1972). Terpene cyclases (synthases) use the allylic cation to execute an intramolecular electrophilic addition to an ethylene double (C=C) bond to result in the formation of a cyclic cation, which mediates the biosynthesis of a broad assortment of mono-, di- or oligo-terpenes such as limonene, α- and β-pinene, and camphene (Bouvier et al., 2005). On the other hand, prenyltransferases require a second aliphatic or aromatic substrate (nucleophilic acceptor) to transfer the allylic carbocation to it. Prenyltransferases (PTs) are subdivided into oligoprenyl diphosphate synthases, protein, tRNA and aromatic prenyltransferases (Heide, 2009; Yazaki et al., 2009; Dumelin et al., 2012; Palsuledesai and Distefano, 2015). Prenyl diphosphate synthases are responsible for the elongation of the carbon backbone of isoprenoids by sequential condensation of C_5 units *via* head-to-tail or head-to-head coupling (head corresponds to the diphosphate group and tail to the prenyl chain). According to the stereochemistry of the formed double bond, they are classified to *trans*- or *cis*-PTs (Poulter, 2006; Liu et al., 2013a; Winkelblech et al., 2015). Protein prenyltransferases (PPTs) like farnesyl transferases (PFTase) or protein geranylgeranyl transferases type I (PGGTaseI) and type II (PGGTaseII) transfer FPP and GGPP, respectively, to the sulfur atom of a cysteine residue of the target protein in a "CaaX box" at the C-terminus. This prenylation enhances the interactions between prenylated proteins and membranes, which is considered as a cellular regulation and post-translational mechanism (Strickland et al., 1998; Gelb et al., 2006; Guo et al., 2008). Other PPTs catalyze C3- or O-prenylation of a tyrosyl residue (McIntosh et al., 2011). Geranylated RNA was discovered in some bacterial species, where the geranyl residue is attached to the sulfur atom in two 5-methylaminomethyl-2-thiouridine nucleotides (Dumelin et al., 2012). Aromatic prenyltransferases (aPTs) catalyse the formation of C-C, C-O, or C-N bonds between a prenyl donor and an aromatic substrate (usually a phenol or indole derivative). Based on differences in structure, sequences, binding motifs, and solubility, they can be classified into two main groups enclosing (*i*) the superfamilies of soluble aPTs, i.e. the ABBA family with the CloQ/NphB group and the dimethylallyl tryptophan synthase (DMATS) family, and (*ii*) the membrane-bound aPTs, e.g. members of the UbiA family (Heide, 2009). Aromatic prenyltransferases are discussed below in detail (1.4.2)

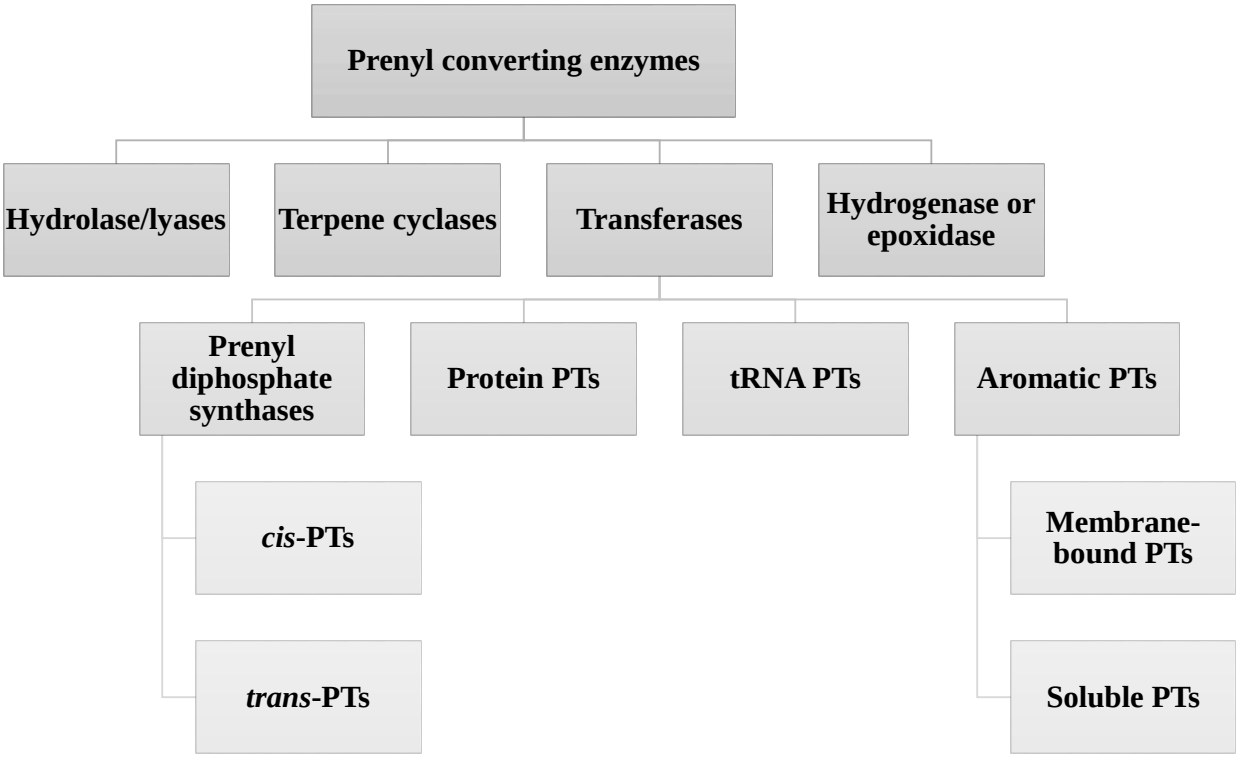

Figure 11: Classification of prenyl converting enzymes.

1.4.2 Aromatic prenyltransferases

Aromatic prenyltransferases illustrate, to a far extent, the chemical and biological diversification of natural products by utilizing a wide range of aromatic substrates (Heide, 2009; Yazaki et al., 2009). Therefore, they were intensively studied during the past decades.

1.4.2.1 Aromatic prenyltransferases of the ABBA family

Members of this family are common among bacteria and fungi. They constitute a soluble aPT group with a distinctive structure of repeating units of *αββα*, after which the family was named and which form a barrel-like cylinder. Based on the nature of the accepted substrates, they are sub-classified into two categories. The first one is the CloQ/NphB group identified from bacteria and fungi, which catalyze the prenylations of quinones, naphthalenes, phenazines, and phenolic compounds (Heide, 2009). The notation of this group is assigned to the first members CloQ and NphB, which were isolated from *Streptomyces roseochromogenes* and several *Streptomyces* sp., respectively (Pojer et al., 2003; Kuzuyama et al., 2005). The former attaches a prenyl residue to 4-hydroxyphenylpyruvic acid as a step in clorobiocin biosynthesis, while the latter catalyzes the geranylation of 1,3,6,8-tetrahydroxynaphthalene. Later, other members belonging to this group were identified (Winkelblech et al., 2015).

The second group is the dimethylallyl tryptophan synthase (DMATS) superfamily, the most investigated sub-class of the aPTs. Members of this family are identified mainly from fungi and to

less extent from bacteria. Structurally, they resemble those of CloQ/NphB (soluble with barrel structure), the characteristic difference lays in the acceptor molecules. They transfer a prenyl moiety to an indole system including tryptophan and tryptophan-containing cyclic dipeptides, from which their name comes. Although their catalytic activities are not dependent on the use of cation, the usage of metal ions enhances their activities (Yu and Li, 2012; Fan et al., 2014; Winkelblech and Li, 2014). The first characterized member of the DMATS superfamily, namely DmaW, was reported from *Claviceps purpurea* (Gebler and Poulter, 1992; Tsai et al., 1995). It catalyzed the prenylation of tryptophan at position C-4 in the biosynthesis of ergot alkaloids.

1.4.2.2 Aromatic prenyltransferases of the UbiA superfamily

The identifier of this family of aPTs is UBiA, a prenyltransferase isolated from *E. coli*, which catalyzes the addition of an all-*trans*-octaprenyl moiety onto 4-hydroxybenzoic acid (4HB; **Figure 12**) within the biosynthetic cascade of ubiquinones, which is important for the mitochondrial respiration inside living cells (Melzer and Heide, 1994). UBiA PTs are distributed in plant and bacteria kingdoms and contribute remarkably to the biosynthesis of primary metabolites (for example vitamin K2, menaquinone; vitamin E, tocopherols) and secondary plant and bacterial natural products (Yazaki et al., 2009; Wang et al., 2014; Zeyhle et al., 2014). UBiA family members greatly differ in their structure, folding and amino acid sequence from the aforementioned ABBA family (1.4.2.1). They are membrane-bound PTs possessing α-membrane spanning peptide helices connected together by amino acid loops containing two highly conserved aspartate-rich motifs with the amino acid sequence DXXXD, where the first motif is thought to be involved in the coordination to the divalent metal ion, which is, apart from the ABBA family, essential for the activity, and the second binds to the aromatic substrates (usually a phenolic system). Through evolution, they acquire a signaling peptide at the N-terminus of the protein targeting it to the membranes of different organelles inside the cell (Heide, 2009; Yazaki et al., 2009; Karamat et al., 2014; Zeyhle et al., 2014).

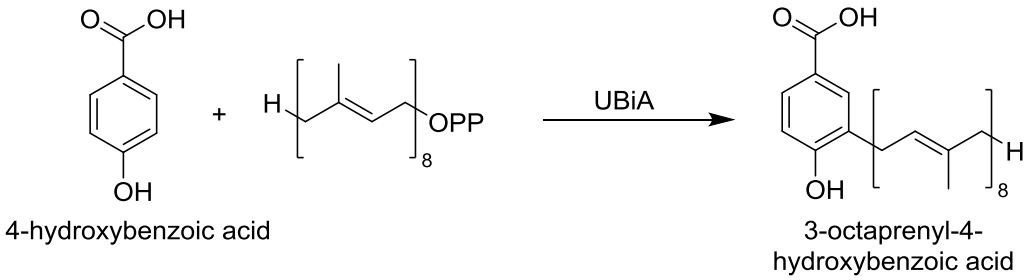

Figure 12: Catalytic activity of UBiA from *E. coli*, the prototype of the UBiA superfamily of aromatic prenyltransferases.

1.4.3 Plant aromatic prenyltransferases

In plants, aromatic prenyltransferases play an important role in both the primary metabolism and the derivatization of natural products. The attachment of isoprene residues to structurally different aromatic skeletons including acylphloroglucins, flavonoids, phenylpropanes, xanthones, and coumarins generates a large number of aromatic or even dearomatized secondary metabolites

(Yazaki et al., 2009). A characteristic feature of plant aPTs is the presence of the extended aspartate-rich motifs N(D/Q)xxDxxxD and KDxxDxxGD. The N-terminal signal peptide targets the proteins mostly to the chloroplast envelop **(Figure 13)**. However, it is still open whether they are localized to the outer or inner membrane (Sasaki et al., 2008; Munakata et al., 2016).

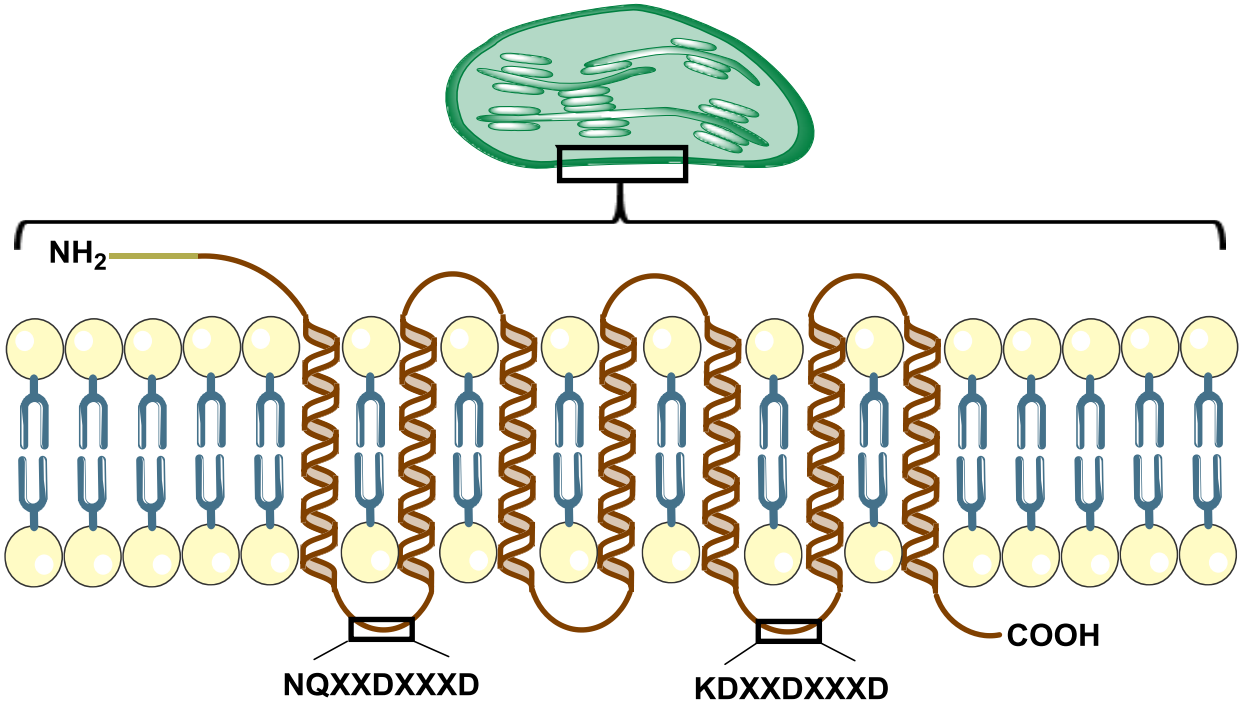

Figure 13: An illustration of the topology of plant aPTs, which possess an N-terminal transit peptide (light green) and a varying number of transmembrane helices connected by amino acid loop regions with two aspartate-rich motifs (boxed), whose orientation within the membrane is still to be defined.

There were only a few reports about plant aPTs in the last 16 years since the discovery of the plant 4HB geranylating enzymes *Le*PGT-1 and *Le*PGT-2 from *Lithospermum erythrorhizon*, which are involved in the biosynthesis of the naphthoquinone shikonin **(Table 4)** (Yazaki et al., 2002).

Table 4: Examples of reactions catalyzed by plant aromatic prenyltransferases (aPT), ordered chronologically.

aPT	Species	Acceptor	Donor	Product	Biosynthetic target	Reference
*Le*PGT-1	*Lithospermum erythrorhizon*	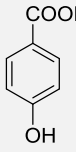 4-hydroxybenzoic acid	GPP	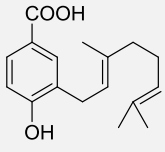 3-geranyl-4-hydroxybenzoic acid	Shikonin	(Yazaki et al., 2002)

*Sf*N8DT	*Sophora flavescens*	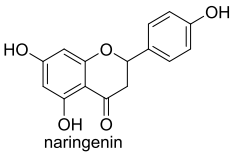	DMAPP	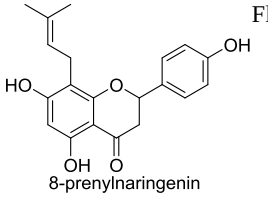	Flavanon G	(Sasaki et al., 2008)
*Gm*G4DT	*Glycine max*	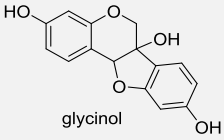	DMAPP	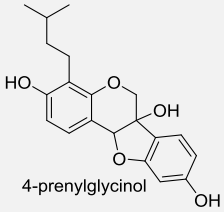	Glyceollin I	(Akashi et al., 2009)
*Hl*PT-1	*Humulus lupulus*	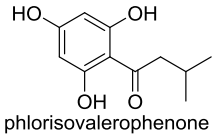	DMAPP	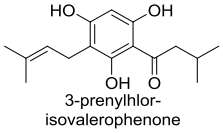	Bitter acids and xanthohumol	(Tsurumaru et al., 2012)
*Cs*PT-1	*Cannabis sativa*	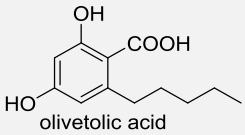	GPP	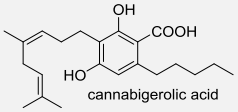	Δ^9-Tetrahydro-cannabinol	(Page and Boubakir, 2014)
*Pc*PT	*Petroselinum crispum*		DMAPP	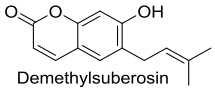	Coumarins	(Karamat et al., 2014)
*Cl*PT1	*Citrus limon*	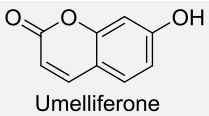	GPP	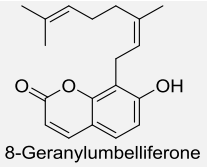	Coumarins	(Munakata et al., 2014)
*Hc*PT	*Hypericum calycinum*	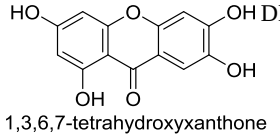	DMAPP	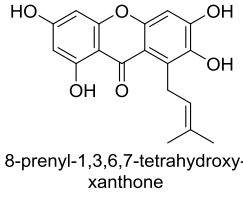	Hyperxanthone E	(Fiesel et al., 2015)
*Ps*PT1/ *Ps*PT2	*Pastinaca sativa*	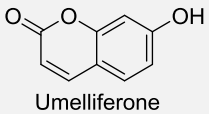	DMAPP	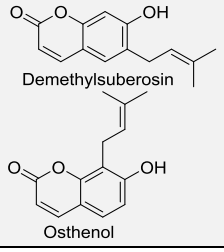	Coumarins	(Munakata et al., 2016)

Despite the great medicinal value of the prenylated natural products, information about aPTs and their role in the biosynthesis of secondary metabolites is still limited. Due to their limited yield and the lack of a full biosynthetic scheme or even a convenient synthetic scheme (see 5.5.1

and 5.5.2), the clinical application of the majority of prenylated natural products is yet restricted. Elucidation of the biosynthetic pathways and characterization of the involved aPTs offer a tool for the biotechnological production of PPAPs either through chemoenzymatic synthesis or genetically engineered microbes.

1.5 The aim of the work

The biosynthesis of polycyclic polyprenylated acylploroglucinol derivatives (PPAPs) involves the prenylation of acyl- and/or benzoylphloroglucinol derivatives, which is achieved by the catalytic action of a group of enzymes named aromatic prenyltransferases (aPTs). Acylphloroglucinol accepting prenyltransferases, involved in the biogenesis of bitter acids, were identified from *Humulus lupulus* (Li et al., 2015). To date, no prenyltransferases using the acylphloroglucinol skeleton were published from the genus *Hypericum*, although it is one of the richest genera in PPAPs. Specifically, no aPTs catalyzing the prenylation of the benzophenone scaffold as an acceptor molecule were identified in planta, neither at the biochemical nor the molecular level.

The goal of the present study is cDNA cloning, functional expression, and characterization of the prenyltransferases involved in the biosynthesis of PPAPs from *H. sampsonii*. Due to the absence of public transcriptomic data for the plant, quite a low expression level, and the membrane integration nature of aPTs, which all hamper the work on plant aPTs, two molecular biological approaches have been appointed in order to identify aPT sequences from *H. sampsonii*. The first one is homology-based cloning, which makes use of the available transcriptomic information about *H. perforatum* and adopts the data of aPTs identified in *H. calycinum*, based on a subtracted library established in our laboratory (Gaid et al., 2012). The second approach is to use degenerate primers designed according to the conserved amino acid sequences of plant aPTs. The work should flow through the following steps:

- Investigation of the metabolic profile of *in vitro*-grown *H. sampsonii* plants for the presence of PPAPs, prenylated intermediates, and aromatic cores.
- Amplification of putative aPT coding sequences or aPT gene core fragments from *H. sampsonii* cDNA and genomic DNA, respectively.
- Obtaining 5'- and/or 3'- ends for the coding sequence fragments by rapid amplification of cDNA ends (RACE).
- Due to the challenging heterologous expression of membrane-integrated enzymes, the full-length aPTs are expressed in insect and yeast expression systems.
- Syntheses of biosynthetic intermediates as enzymatic substrates and reference compounds for production and structural identification of enzymatic products.
- Testing the activity of microsomal fractions using potential substrates.
- Characterization of the active recombinant proteins with respect to molecular and kinetic properties.
- Once the activity of the recombinant enzymes is investigated and their characterization is established, the subcellular localization of the aPTs is determined by transient expression of aPT-yellow fluorescent protein (YFP) fusions in *Nicotiana benthamiana*.

2 Materials

2.1 Biological materials

2.1.1 Plant materials

2.1.1.1 *Hypericum sampsonii*

Hypericum sampsonii Hance is native to East Asia. A sample of the plant was settled in the Herbarium of the Institute of Botany, the Chinese Academy of Sciences, Beijing, China (Specimen number 01262860). The seeds, provided from Zhejiang Normal University, Jinhua, China, were germinated as described elsewhere (Huang et al., 2012) at Key Laboratory of Plant Molecular Physiology, Institute of Botany, The Chinese Academy of Sciences. The seeds and developed seedlings were later used in the current study after propagation by Dr. Benye Liu in our laboratory as described later (3.1.1).

2.1.1.2 *Nicotiana benthamiana*

Pot plant was cultivated at the experimental station of the Institute of Pharmaceutical Biology at the Technical University of Braunschweig, Germany.

2.1.2 Cloning and expression strains

2.1.2.1 Bacterial strain

Strain name	**Genotype**
Escherichia coli DH5α	*F' φ80δlacZΔM15 end A1 rec A1 hsdR17(rk- mk+) supE44 thi-1 λ- gyrA96relA1 Δ(lacZYA-argFV169) deoR*
Agrobacterium tumefaciens	*C58C1(RifR)* *pMP90 (GentR)*

2.1.2.2 Insect cells

Strain name	**Supplier**
Spodoptera frugiperda Gibco® Sf9	Invetrogen™, Life Technologies GmbH

2.1.2.3 Yeast strain

Strain name	Genotype
***Saccharomyces cerevisiae* INV*Sc*1 (Invetrogen)**	*MATa his3D1 leu2 trp1-289 ura3-52 MAT his3D1 leu2 trp1-289 ura3-52*

2.2 Chemicals

Chemical	**Manufacturer**
2,3′,4,4′,6-Pentahydroxynenzophenone (maclurin)	Aldrich
2,3′,4,6-Tetrahydroxybenzophenone	Lab collection
2,4,6-Trihydroxybenzophenone	ICN Biomedicals
2-Hydroxybenzophenone	Merck
2-Mercaptoethanol (β-ME)	Roth
4-Hydroxybenzophenone	Fluka
Acetic acid	Roth

Acrylamide/Bisacrylamide 30%	Bio-Rad
Acetosyringone	Sigma-Aldrich
Agar Kobe	Applichem
Ammonium bicarbonate	Fischer scientific
Ammonium hydroxide	Riedel-de Haën
Ammonium persulfate (APS)	Roth
Ampicillin	Roth
Bacto casamino acids	Difco
Betaine	Sigma-Aldrich
Bovine serum albumin (BSA)	Sigma-Aldrich
Bromophenol blue	Aldrich
$CaCl_2.2H_2O$	Roth
Cellulose MN 2100	Merck
Chloroform	Sigma-Aldrich
Chloroform (GC grade)	Sigma-Aldrich
$CoCl_2.6H_2O$	Riedel-de Haën
Coomassie blue (G250 and R250)	Merck
$CuCl_2$	Fluka
$CuSO_4.5H_2O$	Riedel-de Haën
DOWEX® AG 50W-X8, 100–200 mesh	Sigma-Aldrich
Ethanol	VWR
Ethyl acetate	VWR
$Na_2EDTA.2H_2O$	Roth
Ferric chloride	Roth
$FeSO_4.7H_2O$	Riedel-de Haën
Formic acid	Roth
Galactose	Roth
Geranyl chloride	Sigma-Alderich
Glass beads	Sigma-Aldrich
Glucose	Roth
Glycerol	Roth
Glycine	Roth
HCl	VWR
Isobutyric acid	Sigma-Alderich
Isopropanol	VWR
KCl	Roth
KH_2PO_4	Roth
KI	Riedel-de Haën
KNO_3	Roth
Mangiferin	Avachem
Methanesulfonic acid	Sigma-Aldrich
Methanol	VWR Chemicals
Methanol HPLC	Fischer Chemicals
$MgCl_2.6H_2O$	Fluka
$MgSO_4.7H_2O$	Roth
Midori Green	Nippon Genetics GmbH

$MnCl_2$	Merck
$MnSO_4.H_2O$	Riedel-de Haën
Myo-inositol	Roth
$Na_2MoO_4.2H_2O$	Merck
NaCl	Roth
NaOH	Roth
NH_4NO_3	Roth
N-methyl-N-(trimethylsilyl)-trifluoroacetamide (MSTFA)	ABCR
o-Phosphoric acid	Fischer-Scientific
PEG 4000	Fluka
Peptone from casein	Roth
peqGold Universal Agarose	Peqlab
Phenol	Roth
Phloroglucinol	Acros
Phosphorus pentoxide	Acros
Polyvinylpyrrolidone	Sigma-Aldrich
Potassium acetate	Roth
Prenyl bromide	Sigma-Alderich
Prenyl chloride	Sigma-Aldrich
silica gel 60 (0.040–0.063 mm)	Merck
Silica C_{18} (reversed phase)	Merck
Sodium dodecyl sulfate (SDS)	Roth
Sorbitol	Roth
Sucrose	Diadem
Sulfosalicylic acid	Merck
Tetramethylethylenediamine (TEMED)	Roth
Tetrabutylammonium hydrogen pyrophosphate	Sigma-Alderich
Thiamine hydrochloride	Sigma-Aldrich
tris(hydroxymethyl) aminomethane (Tris)	Roth
Xylene cyanol FF	Roth
Yeast extract	Applichem
Yeast nitrogen base without amino acids	Sigma
$ZnSO4.7H_2O$	Riedel-de Haën

2.3 Vectors

Plasmid Name	**Use**	**Origin**
pJET1.2	Blunt cloning of PCR products	CloneJET PCR Cloning Kit (Thermo Fisher)
pESC-URA	Functional expression in yeast cells	Agilent
pFastBac™ 1	Transfer vector for expression in insect cells	Invetrogen™, Life Technologies GmbH
pCAMBIA2300-35S-N-term-YFP u	USER cloning for localization	university of Copenhagen (Nour-Eldin et al., 2006)

pCAMBIA2300-35S-C-term-YFP u	USER cloning for localization	university of Copenhagen (Nour-Eldin et al., 2006)
Helper plasmid K19	To prevent the rejection of the transfected heterologous PTs in *N. benthamiana* during localization study	AG Prof. Dr. Hänsch, Institute of plant biology, TU Braunschweig
EqFP611-DsRED	Cytoplasmic control during localization study	AG Prof. Dr. Hänsch, Institute of plant biology, TU Braunschweig

2.4 Primers

2.4.1 Primers derived from *Hypericum* sp.

Primer no.	Primer Name	Sequence 5′ → 3′
1F	*Hc*PT-2_*NheI*_for	AATGCTAGCATGGAGCTCTCCCGGATGCTTAAATTTCC
1R	*Hc*PT-2_*HindIII*_re	AATAAGCTTCTAAACGAAAGGAAGCAGAATATACTGCACAACG
2F	290_pFastBac_For	ATTGAATTCATGGAGCTCTCCCGGATGC
2R	290_pFastBac_Re	ATTCTCGAGCTAAACGAAAGGAAGCAGAATATACTGC
3F	hpa_8393_for	AATGGATCCATGGAGCTCTCCATTTTCCCGTCCTCTC
3R	hpa_8393_rev	AATCTCGAGTTAGATGAAAGGGAAGAGGGCGTACTCGG
4F	PT4472_R_EX	AATGGTACCCTAAATAAACGGGAACAATAAAGTTTG
4R	PT4472_F_EX	AATGGATCCATGGAAATCTCCCGATTGC
5F	339F	ATTGAATTCATGGAGGTTTCTCGATTGCCATCG
5R	339R	ATTAAGCTTCTAGATGAAGGGGAGCAAGATAAATTGC
6F	Tex-for	ATTGGATCCATGGACGTTTCCAGTTCTGCTTTCACAC
6R	Tex-rev	ATTGGTACCCTAGAGGAATGGAAGCGTGATAAACTGC
7F	*Hp*PT015370*BamHI*- F	ATTGGATCCATGGAGTCTCTACGTTTGGTCTC
7R	*Hp*PT015370*KpnI*-R	ATTGGTACCTCATCTAATGAATGGGATCAGTAAG
8F	*Hc*PT1_*XhoI*_F	AATCTCGAGATGGATAATCTATCCCTCTCCCTTCC
8R	*Hc*PT1_*KpnI*_R	AATGGTACCCTAAATAAAAGGAAATATGGCCCACTCTGC
9F	470F	ATTGAATTCATGGAGATCTCTCTTGCTTTCCTTCATCTGC
9R	470R	ATTCTCGAGCTAGATGAAGGGAAGTAGGATTAAGTGGGC
10F	9252-for_*BamHI*	ATTGGATCCATGGCCTTCTCTCCATTACTTTCATC
10R	9252-rev_*KpnI*	ATTGGTACCCTAGATAAAAAGAAATAGGATGTACTCGG
11F	15764_*BamHI*_f	AATGGATCCATGGAGACCTTTCGCTTTCCCTC
11R	15764_ *XhoI*_r	AATCTCGAGTTAAATGAATGGAAACAGCAAAATTTGGACAAG
12F	*Hp*PT19471*BamHI*-F	ATTGGATCCATGGATATCTCACGCACAATATC
12R	*Hp*PT19471*KpnI*-R	ATTGGTACCCTAAATAAAAGGATGAAGTATAAACTCG

2.4.2 Primers used for core fragments amplification, 3′ and 5′ RACE

Primer Name	Sequence 5′ → 3′
PT_Deg_for	GAAMYWGAYARGATWAAYAARCC
PT_Deg_rev	ATCTCCNTYNRYRTCWGRWANATC
*Hs*_deg2_5R_rev_1	ATGGAGTACGATGATGCAACCAAC
*Hs*_deg2_3R_for_1	GAATGGATTCGGTCAATTCTTCGTC
*Hs*_deg6_5R_rev_1	GTCGGTGTCTGGAAGATCTTTTAATATG
*Hs*_deg6_5R_rev_2	ACACCGCTCCGACTATTAGTAAGCAG
*Hs*_deg6_5R_rev_3	TAGAGCTCCGGCTATGACCAAGCCG
*Hs*_deg6_3R_for_1	GCCTTACTTACCTTTAGCTTCC
*Hs*_degL_5R_rev_1	TGCTGACGCCACCAACAATAACAAGAC

*Hs*_degL_5R_rev_2	AGAATTTAGTGTTCCCGCTGTTAGC
*Hs*_degS_5R_rev_1	AACGGAATATAATGAATGCACCACC
*Hs*PT5_Fragment_f	TTCTGACATGGACGGAGATAG
3'UTR_*Hs*_290	TCGACACATACGCATATGTTCG

2.4.3 Primers used for cloning in pFastBacI

Primer Name	Sequence 5′ → 3′
*Hs*PT1_*EcoR*I_fo	AAAGAATTCATGGAGCTCTCCCGGATGCCTTCATC
*Hs*PT1_*Xho*I_rev	ATTCTCGAGCTAAATGAAAGGGAACAATAAC
*Hs*PT2_*BamH*I_for	ATTGGATCCATGGAGGTTTCTCGGTTGC
*Hs*PT2_*Kpn*I_rev	AAAGGTACCCTAGATGAATGGAAGCATG
*Hs*PT3_*EcoR*I_for	ATTGAATTCATGGAGACCTTCCGCTTTCC
*Hs*PT3_*Xho*I_rev	AAACTCGAGTCAGATGAATGGAAACAAC
*Hs*PT4_*BamH*I_for	AATGGATCCATGGAAATCTCCCGATTGCCTTCATC
*Hs*PT4_*Kpn*I_rev	AATGGTACCCTAGATGAACGGAAACAGGAAAAG
*Hs*PT5_*EcoR*I_for	ATTGAATTCATGGAGCTCTCCCGGATGC
*Hs*PT5_*Xho*I_rev	ATTCTCGAGCTAGATGAAAGGAAGCAGAACATACTG

2.4.4 Primers used for cloning in pESCUra

Primer Name	Sequence 5′ → 3′ *
*Hs*PT1_y_*Sal*I_fo	AATGTCGACATGGAGCTCTCCCGGATGCCTTCATC
*Hs*PT1_y_*Pac*I_rev	AAATTAATTAACTAAATGAAAGGGAACAATAAC
*Hs*PT3_y_*BamH*I_fo	AATGGATCCATGGAGACCTTCCGCTTTCC
*Hs*PT5_Y_*EcoR*I_for	ATTGAATTCATGGAGCTCTCCCGGATGC
*Hs*PT5_Y_*Pac*I_rev	ATATTAATTAACTAGATGAAAGGAAGCAGAACATACTGC
*Hs*PT6_Y_*Eco*RI_for	ATTGAATTCATGGAGTCTCTACGTTTGGTCTCC
*Hs*PT6_Y_*Pac*I_rev	ATATTAATTAATCATCTAATGAATGGGATCAG
*Hs*PT7_*EcoR*I_for	ATTGAATTCATGGCCTTCTCTCCATTAC
*Hs*PT7_*Pac*I_rev	AAATTAATTAACTAGATAAAAAGAAATAGG

* Restriction sites added to the primers were underlined

2.4.5 Primers used for cloning in *N. benthamiana*

Primer Name	Sequence 5′ → 3′
PT2_SP_For	GGCTTAAUATGATGGAGGTTTCTCG
PT2_YatC_Rev	GGTTTAAUccGCAGATGAATGGAAGC *
PT2_YatN_Rev	GGTTTAAUCTAGATGAATGGAAGC
PT2_NoSP_For	GGCTTAAUATGTTTGCCTCCCGTAGTAAGC **
PT5_SP_For	GGCTTAAUATGGAGCTCTCC
PT5_YatC_Rev	GGTTTAAUccGCAGATGAAAGGAAGC *
PT5_YatN_Rev	GGTTTAAUCTAGATGAAAGGAAGC
PT5_NoSP_For	GGCTTAAUATGCGCCGGATGGTTGC **

* cc is added to compensate frameshift with YFP and GCA false stop codon, ** ATG artificial start codon

2.4.6 SMART II RACE primers

Primer Name	Sequence 5′ → 3′
SMART II™ oligo	AAGCAGTGGTATCAACGCAGAGTACGCGGG
3′-RACE CDS primer	AAGCAGTGGTATCAACGCAGAGTAC(T)30VN
5′-RACE CDS primer	(T)25VN
RACE long	CTAATACGACTCACTATAGGGCAAGCAGTGGTATCAACGCAGAGT
RACE short	CTAATACGACTCACTATAGGGC
RACE nested	AAGCAGTGGTATCAACGCAGAGT

2.5 Enzymes

2.5.1 Enzymes used for reverse transcription (RT)

Enzyme name	Manufacturer
BD PowerScript™ Reverse Transcriptase	BD Biosciences
RevertAid™ HMinus Reverse Transcriptase	Thermo Scientific
SMARTScribe™ Reverse Transcriptase	Takara

2.5.2 Enzymes used for polymerase chain reaction (PCR)

Enzyme name	Manufacturer
peqGOLD *Taq* DNA polymerase	Peqlab
Phusion® Hot Start II High-Fidelity DNA Polymerase	Thermo Scientific

2.5.3 Restriction endonucleases

Enzyme name	Restriction site sequence 5′→ 3′	Manufacturer
*BamH*I	G▼GATCC	Thermo Scientific
*Bst*BI	TT▼CGAA	Thermo Scientific
EcoRI	G▼AATTC	Thermo Scientific
HindIII	A▼AGCTT	Thermo Scientific
KpnI	GGTAC▼C	Thermo Scientific
NheI	G▼CTAGC	Thermo Scientific
Nt.BbvCl	CC▼TCAGC	New England Biolabs
PacI	TTAAT▼TAA	Thermo Scientific
SalI	G▼TCGAC	Thermo Scientific
SmaI	CCC▼GGG	Thermo Scientific
XhoI	C▼TCGAG	Thermo Scientific

2.5.4 Miscellaneous enzymes

Enzyme name	Manufacturer
DNA Blunting Enzyme (CloneJET PCR Cloning Kit)	Thermo Scientific
FastAP Thermosensitive Alkaline Phosphatase	Thermo Scientific
RiboLock™ RNase Inhibitor	Thermo Scientific

RNase A	Thermo Scientific
RNase-free DNase I	Qiagen
T4 DNA ligase	Thermo Scientific
USER-Enzyme mix	New England Biolabs GmbH

2.6 Kits

Name	Purpose	Manufacturer
Bac-to-Bac® Baculovirus Expression System *	Insect expression system	Invitrogen™, Life Technologies GmbH
BD SMART™ RACE cDNA Amplification Kit	5'- and 3'-rapid amplification of cDNA ends (RACE)	BD Biosciences
Cellfectin® II reagent *	Insect expression system	Invitrogen™, Life Technologies GmbH
CloneJET PCR Cloning Kit	Blunt cloning of PCR products	Thermo Fisher
COMBINA 11 S	Testing presence/absence of glucose in yeast media	HUMAN Gesellschaft für Biotechnica und Diagnostica GmbH
innuPREP DOUBLEpure Kit	DNA purification from PCR, digestion mixture and agarose gel	Analytik Jena
RNeasy® Plant Mini Kit	RNA isolation from *H. calycinum* cell cultures	Qiagen
S.c. EasyComp™ Transformation Kit	Preparation and transformation of yeast competent cells	Invitrogen

* Materials used for insect expression were kindly provided by Prof. Sönke. Behrends (Institute of Pharmacology, Toxicology and Clinical Pharmacy, Technical University of Braunschweig)

2.7 Culture media

2.7.1 Plant cultivating media

MS medium		Final concentration	
Macro-nutrients	**10X stock solution**		
$CaCl_2.2H_2O$	4.4 g/l	440.0	mg/l
$FeSO_4.7H_2O$	278.0 mg/l	27.8	mg/l
KH_2PO_4	1.7 g/l	170.0	mg/l
KNO_3	19.0 g/l	1900.0	mg/l
$MgSO_4.7H_2O$	3.7 g/l	370.0	mg/l
$Na_2EDTA.2H_2O$	413.0 mg/l	41.3	mg/l
NH_4NO_3	16.5 g/l	1650.0	mg/l
Micro-nutrients	**1000X stock solution**		
H_3BO_3	6.54 g/l	6.54	mg/l

$CoCl_2.6H_2O$	25.0	mg/l	25.0	µg/l
KI	830.0	mg/l	830.0	µg/l
$MnSO_4.H_2O$	16.9	g/l	16.9	mg/l
$Na_2MoO_4.2H_2O$	250.0	mg/l	250.0	µg/l
$ZnSO_4.7H_2O$	8.6	g/l	10.6	mg/l
Vitamins and amino acids	**100X stock solution**			
Glycine			2	mg/l
Myo-inositol	1.0	g/100ml	100.0	mg/l
Nicotinic acid			0.5	mg/l
Pyridoxine hydrochloride			0.5	mg/l
Thiamine hydrochloride	1.0	mg/100ml	0.1	mg/l

- The pH is adjusted to 6.0 and the medium is autoclaved at 120° C for 20 minutes.

2.7.2 Bacterial culture media

SOC medium			**Final concentration**	
Yeast extract	5.0	g/l	0.5	% (w/v)
Peptone from casein	20.0	g/l	2.0	% (w/v)
NaCl	467.6	mg/l	10.0	mM
KCl	186.4	mg/l	2.5	mM
$MgSO_4$. $7H_2O$ (1M)	5.0	ml/l	5.0	mM
$MgCl_2$ (1M)	5.0	ml/l	5.0	mM
Dextrose (1M)	20.0	ml/l	20.0	mM

- The pH is adjusted to 7.5.

- The first four components are dissolved in 970 ml distilled water and autoclaved. Afterward, the sterile-filtered solutions of the last three components are added.

YEP medium			**Final concentration**	
Bacto peptone	10	g/l	1	% (w/v)
NaCl	4.69	g/l	0.085	M
Yeast extract	10	g/l	1	% (w/v)
Agar (for solid medium)	20	g/l	2	% (w/v)

***A. tumefaciens* activation medium**	**Final concentration**	
Acetosyringone	150	µM
MES buffer	0.01	M
$MgCl_2$	0.01	M

2.7.3 Yeast culture media

YPD medium			**Final concentration**	
Yeast extract	10.0	g/l	1.0	% (w/v)
Peptone from casein	20.0	g/l	2.0	% (w/v)
Dextrose	20.0	g/l	2.0	% (w/v)

- The first two components are dissolved in 900 ml distilled water and autoclaved. Afterward, 100 ml of sterile filtered 20% (w/v) dextrose solution are added.
- For solid medium, 2% (w/v) agar is added before autoclaving.

Synthetic dextrose minimal medium (SD dropout or SGI medium)			**Final concentration**	
Bacto casamino acids	1.0	g/l	0.10	% (w/v)
Dextrose	20.0	g/l	2.0	% (w/v)
Yeast nitrogen base (with or without amino acids)	6.7	g/l	0.67	% (w/v)

- The first two components are dissolved in 900 ml distilled water and autoclaved. Afterward, 100 ml of sterile filtered 20% (w/v) dextrose solution are added.
- For solid medium, 2% (w/v) agar is added before autoclaving.

YPGE medium			**Final concentration**	
Yeast extract	10.0	g/l	1.0	% (w/v)
Peptone from casein	10.0	g/l	1.0	% (w/v)
Dextrose	5.0	g/l	0.5	% (w/v)
Ethanol	30.0	ml/l	3.0	% (v/v)

- The first two components are dissolved in 945 ml distilled water and autoclaved. Afterward, 25 ml of sterile-filtered 20% (w/v) dextrose solution and 30 ml absolute ethanol are added.

2.7.4 Insect culture media

Basic medium		**Final concentration**	
Sf-900^{TM} SFM	Invitro ^{TM}, Life Technologies GmbH		
Sf9-medium			
Sf-900^{TM} SFM			
Fetal bovine serum		100	g/l
Penicillin/ Streptomycin		10	g/l

2.8 Buffers and solutions

2.8.1 Buffers used for RNA extraction

RNA extraction buffer	**Final concentration**	
CTAB	20	mg/ml
EDTA	25	mM
NaCl	2	M
PVP	20	mg/ml
Spermidin	0,5	mg/ml
TRIS-HCl	100	mM
β-Mercaptoethanol	20	ml/l

- pH was adjusted at 8
- β-Mercaptoethanol was added directly before use

SSTE buffer	Final concentration
EDTA	1 mM
NaCl	1 M
SDS	5 mg/ml
Tris-HCl	10 mM

- pH was adjusted to 8

2.8.2 Buffers used for plasmid isolation from *E. coli*

Buffer I	Final concentration
$Na_2EDTA.2H_2O$	10 mM
RNase A	10 Mg/ml
Tris	50 mM

- The pH is adjusted to 8 with 1N HCl
- RNase is added immediately before use

Buffer II	Final concentration
NaOH	0.2 M
SDS	1 % (w/v)

Buffer III	Final concentration
Potassium acetate	3 M

- The pH of buffer III is adjusted to 5.5 with glacial acetic acid

2.8.3 Buffer used for plasmid isolation from yeast

Yeast cracking solution	Final concentration
Tris	10 mM
$Na_2EDTA.2H_2O$	1 mM
NaCl	100 mM
SDS	1 % (w/v)
Triton X-100	2 % (v/v)

- The pH is adjusted to 8.5 with 1N HCl

2.8.4 Buffers used for microsomal protein isolation from Insect cells

Sonication Buffer	Final concentration
Glycerol	0.1 ml/ml
$Na_2EDTA.2H_2O$	1 mM
Tris-HCl	50 mM

Buffer A	Final concentration
Glycerol	0.1 ml/ml
NaCl	300 mM
Tris-HCl	50 mM

- The pH of both buffers was adjusted to 7.5

2.8.5 Buffers used for microsomal protein isolation from yeast

TEK buffer	Final concentration	
$Na_2EDTA.2H_2O$	1	mM
KCl	0.1	M
Tris-HCl pH 7.4 *	50	mM

TES buffer	Final concentration	
$Na_2EDTA.2H_2O$	1	mM
Sorbitol	0.6	M
Tris-HCl pH 7.4 *	50	mM

- The pH of both buffers was adjusted to 7.4

* From 1M stock buffer

2.8.6 Buffers and solutions used for agarose gel electrophoresis

50X TAE buffer			Final concentration	
$Na_2EDTA.2H_2O$	18.612	g/l	50	mM
Tris	242.28	g/l	2	M

- The pH is adjusted to 8.0 with glacial acetic acid

6X DNA loading dye			Final concentration	
Bromophenol blue	15	mg/50 ml	0.03	% (w/v)
Glycerol	30	ml/50 ml	60	% (v/v)
$Na_2EDTA.2H_2O$	1.117	g/50 ml	60	mM
Tris	60.6	mg/50 ml	10	mM
Xylene cyanol FF	15	mg/50 ml	0.03	% (w/v)

- The pH is adjusted to 7.6 with 1N HCl
- Stored in -20 °C without autoclaving

2.8.7 Solution for the determination of protein concentration

Bradford dye solution			Final concentration	
Coomassie blue G250	100	mg/l	0.01	% (w/v)
Ethanol absolute	50	ml/l	5	% (v/v)
o-phosphoric acid (85%)	100	ml/l	10	% (v/v)

- Coomassie blue is dissolved first in ethanol and then *o*-phosphoric acid is added.
- The solution is filtered before use and kept at 4 °C away from light.

2.8.8 Buffers used for the synthesis of geranyl pyrophosphate

Ion exchange buffer			Final concentration	
NH_4HCO_3	2	g	0.25	mM
Isopropyl alcohol	20	ml	2%	v/v
Deionized water	980	ml		
Chromatography buffer buffer			**Final concentration**	
NH_4HCO_3 (dissolved in 250 ml dH_2O)	4	g	0.5	mM

Isopropyl alcohol	500	ml	50%	v/v
Acetonitrile	250	ml	25%	v/v

Spray reagents	**Volume**	
1st reagent		
Sulfosalicylic acid	1	g
Ethanol	60	ml
water	40	ml
2nd reagent		
$FeCl_3$	2	g
Ethanol	80	ml
Water	20	ml

2.9 Equipment

2.9.1 General equipment

Equipment	**Model**	**Manufacturer**
Autoclave	Systec VX-120	Systec
Balance	2254	Sartorius
Balance	Kern 572	Kern & Sohn Gmbh
Balance	LA230S	Sartorius
Centrifuge	1-15K	Sigma
Centrifuge	Avanti J-30I	Beckmann Coulter
Centrifuge	Avanti J-E	Beckmann Coulter
Centrifuge	Biofuge 13	Heraeus
Centrifuge	GS6R	Beckmann Coulter
Centrifuge	Universal 32 R	Hettich
Deep freezer (-80 °C)	MDF-U53V	Sanyo
Dry block heater	Dri-Block DB-3D	Techne
Electrophoresis chamber for agarose gels	Wide Mini-Sub Cell GT	Bio-Rad
Fraction collector	Ultrorac® 7000	LKB-Produkter
Glass column	dimensions 40 X 11 cm	-
Glass column	dimensions 25 X 6.5 cm	-
Heating circulator water bath	TopTech MW-4	Julabo
Laminar air flow	LaminAir HLB2472 BS	Heraeus
Lyophilizer	Gamma -20	Christ Lyophilizing apparatuses GmbH
Magnetic stirrer	MR Hei-standard	Heidolph Instruments GmbH & CO. KG
Magnetic stirrer	Ret basic	IKA®-Werke GmbH & CO. KG
MicroPulser		BioRad laboratories GmbH
Microscope	Laborlux 11	Leitz
Microscope (confocal laser scanning)	cLSM-510META connected to Axiovert 200M	Carl Zeiss

pH meter	pH 325	WTW GmbH
Rotary evaporator	W60	Heidolph
Rotational Vacuum Concentrator	RVC 2-18	Christ
Shaker incubator	Multitron	Infors HT
Shaker incubator	KF4	Infors HT
Sonifier	250	Barson Ultrasonics corporation
Spectrophotometer	SimpliNano™	GE Lifesciences
Spectrophotometer	Ultrospec 1000	Pharmacia Biotech
Spectrophotometer	UVmini-1240	Schimadzu
Thermocycler	T-Professional basic gradient	Biometra
Ultrasound water path	SonorexTK30	BANDELIN electronic GmbH & CO. KG
Diaphragm vacuum pumps with programmable digital vacuum controller	VCZ 224	Ilmvac
Vortex shaker	VF2	IKA
Vortex shaker	Vortex Genie 2 Digital	Scientific industries (Si)
Water purification system	Arium 611	Sartorius

2.9.2 Equipment for chromatographic and spectroscopic analysis

Equipment	Model	Manufacturer
HPLC	**Agilent 1260 Infinity System**	Agilent
Pump	G1311C Quaternary Pump VL	Agilent
Auto sampler	G1329B ALS	Agilent
Column oven	G1316A TCC	Agilent
Column	HyperClone ODS 120A (C18, 4.6 × 150 mm, 5 μ)	Phenomenex
Diode Array Detector	G1315D DAD VL	Agilent
Software	Agilent ChemStation for LC 3D System Rev. B.04.03(16)	Agilent
HPLC	**LaChrom Elite System**	VWR-Hitachi
Pump	L-2130	VWR-Hitachi
Degasser	Model 2005 Degasser	VWR-Hitachi
Auto sampler	L-2200	VWR-Hitachi
Column	ZORBAX Eclipse Plus (C_{18}, 4.6 × 100 mm, 3.5 μ)	Agilent
Diode Array Detector	L-2455	VWR-Hitachi
Software	EZChrom Elite vers. 3.3.2 SP1	Agilent

GC-MS	6890 gas chromatograph	Agilent
Column	ZB5-MS column (30 m, 0.25 mm i.d., 0.25 mm ft)	Phenomenex
Derivatization's oven	GC 5890 A	Hewlett-Packard Company
Mass spectrometer	Joel	Agilent
Software	chemstation	Agilent
Mass spectrometer	**3200 QTRAP LC/MS/MS System**	AB Sciex
Software	Analyst vers. 1.4.2	AB Sciex
NMR spectrometer	**Avance II 600, 5 mm TCI CryoProbe**	**Bruker Co.**
Thin layer chromatography	**0.1 cellulose (20 x 20 cm)**	**Merk Millipore Co.**
Thin layer chromatography	**0.2 silica gel 60 F_{254} (20 x 20 cm)**	**Merk Millipore Co.**
Thin layer chromatography	**0.2 Nano-Sil C_{18}-100 UV_{254} (10 x 10 cm)**	**MACHEREY-NAGEL GmbH & Co. KG**

2.10 Databases and software

2.10.1 Software

Name, web address*	Use
Bioedit 7.2.5	Multiple sequence alignment
Chromas Lite 2.1.1 http://technelysium.com.au/	Visualization of the sequencing chromatograms from *.ab1 files.
Lasergene - DNAStar 7.0	A package composed of various individual programs for DNA and protein sequence analysis. Those programs include: MegAlign: generates pairwise and multiple sequence alignments of protein or DNA showing consensus strength and percent identity matrices. EditSeq: helpful in editing protein and nucleotide sequences. SeqMan: assembles Contigs from individual overlapping sequences. SeqBuilder: generates plasmid maps, shows existing restriction sites within a given nucleotide sequence and predicts restriction digestion results.
Primer premier 5.0	Design of primers for RACE experiments.
MEGA 7.0 http://www.megasoftware.net/	Construction of phylogenetic trees (Kumar et al., 2016)
Wsearch Pro http://www.wsearch.com.au	Mass spectral date reduction
ZEN 2.3 (Carl Zeiss)	Visualization of images generated by LASER scanning microscope.

2.10.2 Online databases and tools

Databases name and web address	Use, description
NCBI protein and nucleotide databases http://www.ncbi.nlm.nih.gov/protein http://www.ncbi.nlm.nih.gov/nuccore	Retrieving amino acid and nucleotide sequences of deposited prenyltransferases.
MPGR database http://medicinalplantgenomics.msu.edu/	A repository of the transcriptomic and metabolomic data of 14 medicinal plants, including *H. perforatum*.
OneKP database http://www.onekp.com	Transcriptomic data of over 1000 plants including *H. perforatum*.
PhytoMetaSyn database http://www.phytometasyn.ca/index.php	Transcriptomic data of 75 plant species including *H. perforatum*.

Online tools:	Website
BLAST	http://blast.ncbi.nlm.nih.gov/Blast.cgi
ChloroP 1.1 Server	http://cbs.dtu.dk/services/ChloroP/
DoubleDigest Calculator	https://www.thermofisher.com/de/de/home/brands/thermo-scientific/molecular-biology/thermo-scientific-restriction-modifying-enzymes/restriction-enzymes-thermo-scientific/double-digest-calculator-thermo-scientific.html
ExPASy translate tool	http://web.expasy.org/translate/
iPSORT	http://ipsort.hgc.jp/index.html
MWG Primer-check	http://ecom2.mwgdna.com/services/oligo/apploligos.tcl?ot=OLIGO_PCR
Oligo Analysis Tool	https://www.eurofinsgenomics.eu/en/ecom/tools/oligo-analysis/
Oligo Calc	http://basic.northwestern.edu/biotools/OligoCalc.html
PROTEIN CALCULATOR v. 3.4	http://protcalc.sourceforge.net/
SOSUI Prediction of Membrane Proteins	http://harrier.nagahama-i-bio.ac.jp/sosui/
TargetP 1.1 Server	http://cbs.dtu.dk/services/TargetP/
TMHMM Server v. 2.0	http://cbs.dtu.dk/services/TMHMM/

* All listed websites have been successfully accessed on Juni 01, 2018

3 Methods

3.1 Eukaryotes Cultivation Methods

3.1.1 Cultivation of plants used in the current study

3.1.1.1 *Hypericum sampsonii*

In vitro plantlets were grown on Murashige and Skoog medium (MS; section 2.7.1) (Murashige and Skoog, 1962) enriched with 3% (w/v) sucrose and 0.6% (w/v) agar. Prior to autoclaving the pH value of the medium was adjusted to 5.7. A 16/8 hours light/dark photoperiod at 25 ± 2 °C was employed as the growth conditions for the seedlings. Four and six-week-old seedlings were used for RNA extraction and metabolite identification, respectively (Gaid et al., 2016).

3.1.1.2 *Nicotiana benthamiana*

Nicotiana benthamiana was cultivated in steamed potting soil at acclimatized room at 24 °C, 65% humidity and with lighting for 12 hours per day (30 μmol/m^2s). Plants were re-cultivated under the same conditions after 2 to 3 weeks after seeding time.

3.1.2 Cultivation of *Spodoptera frugiperda* (*Sf*9 cell line)

The immortalized insect cell line *Sf*9 (2.1.2.2) derived from ovarian cells of the Moth *Spodoptera frugiperda* served as a host. *Sf9* cells were easily transfected with the baculovirus *Autographa californica* multicapsid nucleopolyhedrovirus (*Ac*MNPV), which was very well suited for the expression of proteins based on recombinant bacmids/baculoviruses. The *Sf9* cells were analyzed as 50-500 ml samples in *Sf9* medium (2.7.4) at 27 °C and 140 rpm in shaker incubator under sterile conditions and after every 3-4 days, by diluting the cell suspension with fresh *Sf*9 medium, the optical density (OD) of the cells was maintained between 1 x10^6- 10 x10^6 cells/ml (Schneider and Seifert, 2010). The procedure was maintained at the lab. of Prof. Sönke Behrends (Institute of Pharmacology, Toxicology and Clinical Pharmacy, Technical University of Braunschweig).

3.2 Chemical Methods

Some of the potential substrates were not commercially available, which necessitates their synthesis *via* chemical or enzymatic approaches.

3.2.1 Synthesis of 3-mono- and 3,5-di-prenylated-2,4,6-trihydroxybenzophenone

A modified method according to Pepper et al. (2014) was used. KOH (1 g) was added to a suspension of 1 g of 2,4,6-trihydroxybenzophenone in 8 ml water. Prenyl bromide (1 ml; Sigma-Aldrich, Steinheim, Germany) was added dropwise over 30 min to the mixture and stirred in ice for 90 min then the reaction was stopped by the addition of 4 ml 1 N HCl. The reaction mixture was extracted with ethyl acetate (3 X 10 ml) and the organic extract was dried over anhydrous Na_2SO_4 followed by concentration under vacuum. The extract was fractioned over a silica gel column (silica gel 60, 0.040–0.063 mm from Merck, Darmstadt, Germany; column dimensions 40 X 11 cm) with a gradient of dichloromethane/ methanol the fractions collected and screened by TLC (silica gel 60 F254; Merck, Darmstadt, Germany) and developed using a system of

dichloromethane: methanol 95:5 to result in 3 fractions. 3-Monoprenylated 2,4,6-trihydroxybenzophenone (MPPBP) was purified from fraction no. 2 employing a reversed phase silica C18 (column dimensions 25 X 6.5 cm) using a methanol/ water gradient to yield 60 mg of a yellow solid, which was identified by ^{1}H NMR and ^{13}C NMR. Data for MPPBP: R_f = 0.58 (DCM/MeOH, 95:5); 1H NMR (600 MHz, MeOD) δ 7.54 (m, 2H), 7.42 (m, 1H), 7.32 (m, 2H), 5.87 (s, 1H), 5.22 (t, *J*= 1.4 Hz, 1H), 3.23 (d, *J*= 7.1, 2H), 1.75 (s, 3H), 1.66 (s, 3H) ; ^{13}C NMR (150 MHz, $CDCl_3$) δ 201.1 (Cq, C=O), 164.3 (Cq, C-O), 163.4 (Cq, C-O), 160.5 (Cq, C-O), 143.6 (Cq, C-C), 131.7 (CH), 131.2 (Cq, C-C), 129.2 (CH), 128.5 (CH), 124.5 (CH), 108.3 (Cq, C-C), 105.3 (Cq, C-C), 95.3 (CH), 26.0 (CH_3), 22.3 (CH_2), 17.9 (CH_3).

3,5-Diprenylated 2,4,6-trihydroxybenzophenone (DPPBP) was purified from fraction 1 over a reversed phase column using a reversed phase silica C_{18} using a methanol/ water gradient. It was identified by ^{1}H NMR and ^{13}C NMR. Data for DPPBP: R_f = 6.9 (DCM/MeOH, 95:5); ^{1}H NMR (600 MHz, $CDCl_3$) δ 7.64 (dd, *J*= 8, 1.5, 2H), 7.57 (t, *J*= 1.2, 1H), 7.5 (m, 2H), 5.22 (t, *J*= 1.3, 2H), 3.35 (d, *J*= 7.4, 4H), 1.78 (s, 6H), 1.74 (s, 6H); ^{13}C NMR (150 MHz, $CDCl_3$) δ 198.0 (Cq, C=O), 161.0 (Cq, C-O), 157.6 (Cq, C-O), 140.3 (Cq, C-C), 135.1 (Cq, C-C), 132.1 (CH), 129.0 (CH), 128.0 (CH), 121.8 (CH), 106.3 (Cq, C-C), 104.5 (Cq, C-C), 25.8 (CH_3), 21.8 (CH_2), 17.9 (CH_3).

A third reaction product (bi-product) was purified from fraction 1, which was mis-conducted before identification as DPPBP due to the same molecular mass indicated by ESI-MS/MS analysis. It was then identified as a benzopyran derivative, which can be formed due to the intramolecular cyclization of the adjacent *o*-prenyl group with the hydroxyl group on the adjacent carbon atom or formed as an artifact after synthesis during extraction or purification.

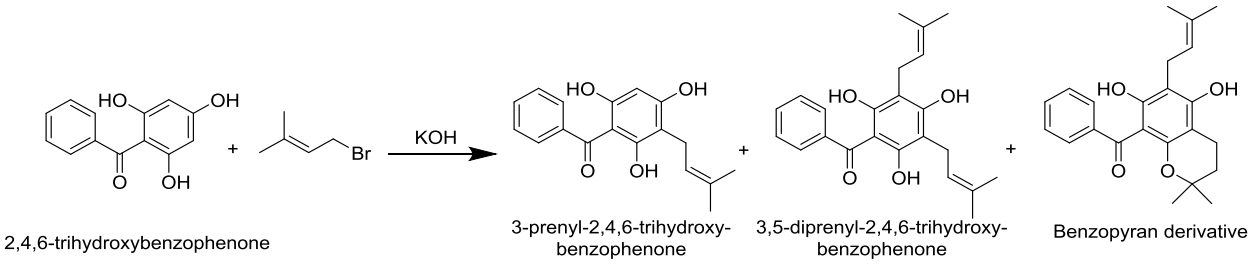

3.2.2 Synthesis of 2,4,6-trihydroxyphlorisobutyrophenone

2,4,6-Trihydroxyisobutyrophenone (246TrHiBP) was obtained employing Friedel-Crafts acylation (van Klink et al., 1999) through the reaction of 3.15 g phloroglucinol (Merck, Darmstadt, Germany) with 1.159 ml isobutyric (Sigma-Aldrich, Steinheim, Germany) acid in the presence of 6.67 g $AlCl_3$ (Merck, Darmstadt, Germany) and 25 ml $POCl_3$ (Sigma-Aldrich, Steinheim, Germany) under argon gas. The reaction mixture was poured over ice to break the reaction which was later extracted with dichloromethane. The product was purified on preparative silica gel plates (silica gel 60 F254, 20 X 20 cm plates, thickness 1mm; Merck, Darmstadt, Germany) using a

mobile system of Petroleum ether: Ethylacetate 7: 3 (R_f = 0.28). The structure was confirmed by comparing its MS/MS fragmentation pattern with an authentic reference.

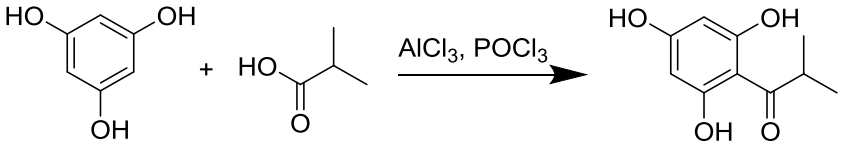

Ploroglucinol 2-methyl-propionic acid 2,4,6-trihydroxyiso-butyrophenone

3.2.3 Synthesis of 1,3,6,7-tetrahydroxyxanthone

1,3,6,7-Tetrahydroxyxanthone (1367THX) was prepared by Dr. Gaid. The product was obtained *via* acid hydrolysis of mangiferin (Avachem, San Antonio, TX, USA) (Guo et al., 2015). Mangiferin (30 mg) was dissolved in 5 ml HI and 111 mg phenol (Mainland, Pharmazeutische Fabrik, Frankfurt am Main, Germany). The mixture was refluxed for 6 hours at 150 °C. Saturated $NaHCO_3$ (3 ml) was then added and the mixture was fractioned with ethyl acetate and water. The aqueous phase was heated under reflux to evaporate the left iodide, acidified with HCl and extracted twice with equal volume ethyl acetate. The combined organic extract was dried with a rotary evaporator to yield 1367THX whose structure was confirmed based on a comparison of its mass fragmentation with a reference.

3.2.4 Synthesis of geranyl pyrophosphate (GPP)

The protocol applied for the synthesis of GPP was modified after the original one described by Woodside et al. (1988). Here, the synthesis was started from the second stage because of the commercial availability of the starting material 1-chloro-3,7-dimethylocta-2,6-diene (geranyl chloride). The reaction was performed in absolutely dry conditions under nitrogen gas in 3 neck flask. One neck was equipped with a septum to allow the drawing of air (with a syringe) while flushing the flask with nitrogen from the other neck. 5 gm tetrabutylammonium hydrogen pyrophosphate trihydrate ($(Bu_4N)_3P_2O_7H$) dissolved in dry acetonitrile were stirred under nitrogen with 4.8 ml 1-chloro-3,7-dimethylocta-2,6-diene (geranyl chloride) which is added after the evacuation of the air through the septum with a syringe. The entire reaction mixture was then dried using a rotary evaporator to result in a viscous yellowish-brown mass.

The residue was dissolved in ion exchange buffer (2.8.8), applied to the DOWEX® AG 50W-X8 cation exchange column (ammonium form). One day before the reaction, The NH_4^+ form of the resin was generated by washing Dowex AG 50W-X8 (H^+ form) in a fritted-glass funnel with four portions (each 200 ml) of concentrated ammonium hydroxide. Afterward, the resin was washed with deionized water until the pH of the filtrate drops to pH 7, then twice with 200 ml portions of the ion-exchange buffer. The washed resin is suspended in 200 mL of ion exchange buffer and slurry was packed into the column (4 × 15 cm column). The column was loaded and eluted with 360 ml ion exchange buffer and the resulting bale yellow eluate was frozen then lyophilized.

The resulting white powder was dissolved in 5 mL of 0.05 M ammonium bicarbonate (2.8.8), and the solution was mixed with 20 ml of 1:1 (v/v) acetonitrile: isopropyl alcohol and the contents are mixed vigorously by vortexing and a white precipitate was brought about. The suspension was centrifuged for 5 min at 2000 rpm. The supernatant was transferred with a pipette in a new tube, and the precipitate was suspended again in 5 mL of 0.05 M NH_4HCO_3, and the extraction was repeated. This was followed by three additional extractions using a solution composed of (2 ml 0.05 M ammonium bicarbonate + 4 ml acetonitrile + 4 ml isopropyl alcohol). The supernatant was pooled (nearly 80 ml) was concentrated to a volume of 5 ml then dissolved in 5 ml chromatography buffer (2.8.8).

The desired compound was then purified on a cellulose column washed with deionized water, 0.1 N HCl, 0.1 NaOH and 1:1 2-propanol: water and packed exactly as mentioned in the original protocol (Woodside et al., 1988) eluted with chromatography buffer. About 150 fractions each 15 ml were collected employing a fraction collector. Each third fraction was run over a cellulose TLC plate (2.9.2) with the chromatography buffer as a mobile phase. The plate was sprayed with a freshly prepared sulfosalicylic acid solution, dried in the air then with fresh ferric chloride solution (2.8.8). Pyrophosphate group- containing compounds appear as white spots on a pink background. GPP-containing fractions were combined together and freeze-dried. The resulting solid (with strong lemon odor) was dissolved in MeOH: NH_4OH 7: 3 solution to a final concentration of 50 mM.

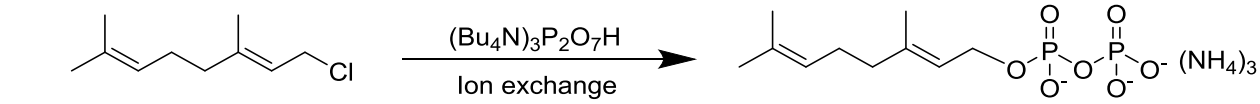

1-chloro-3,7-dimethylocta2,6-diene
(geranyl chloride)

Trisammonium-GPP

3.2.5 Synthesis of dimethylallyl pyrophosphate (DMAPP)

Based on the same protocol, the synthetic step described previously (3.2.4) were applied with the alteration of the starting material as 1-chloro-3-methylbut-2-ene (prenyl chloride) instead of prenyl chloride to obtain the corresponding pyrophosphate derivative.

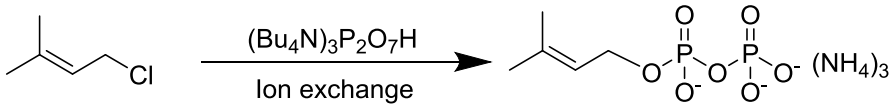

1-chloro-3-methylbut2-ene
(prennyl chloride)

Trisammonium-DMAPP

3.2.6 Upscaled enzymatic production of 8-prenyl-1,3,6,7-tetrahydroxyxanthone

The potential substrate 8-prenyl-1,3,6,7-tetrahydroxyxanthone is not available commercially. Based on the current study the regioselective enzymatic formation is the optimum way for its production. One thousand time standard incubations (3.5.5.1) were done utilizing the optimum

conditions for maximum yield where 2.5 mg THX was incubated with 0.4 mM DMAPP and ≈ 100 mg of membrane protein prepared from yeast-expressing *Hs*PT8PX (*Hs*PT2). Products were extracted 3 times with ethyl acetate and evaporated under vacuum (106 bar, 45 °C) till dryness. Pure 8PX was isolated from the extract using semi-preparative HPLC (3.6.1). The resultant pure 8PX (1.5 mg) was dissolved in 457 µl methanol to give a 10 mM stock solution.

3.2.7 Profiling of PPAPs core from *Hypericum sampsonii*

Three grams whole *in vitro* 6 weeks-old seedlings were collected and homogenized with sea-sand. The homogenate was ground again with the addition of ≈ 10 ml methanol for 5 min at room temperature. The entire mixture was filtered under vacuum. Extraction and filtration were repeated twice. The combined methanol extract was then dried on a rotary evaporator at 50 ℃ till complete dryness. The residue was dissolved in 1 ml methanol HPLC, a 25 time diluted 25 µl aliquots were analyzed by HPLC (3.6.1). After initial analysis, the extract was fractioned by semi-preparative HPLC via injecting successive aliquots of 50 µl to result in 5 fractions. Fractions were then evaporated under nitrogen gas, each dissolved in 1 ml methanol afterward the molecular masses were confirmed via ESI-MS/MS. Lastly, GC-MS analyses were performed using the silylated fractions (3.6.3).

3.3 Molecular Biology Methods

3.3.1 Isolation of nucleic acids

3.3.1.1 Isolation of total RNA

Various methods were performed to confirm a high RNA quality and yield. Extraction of RNA was carried out with special caution due to the single-stranded nature of RNA and the ubiquitous occurrence of RNases that can degrade it.

3.3.1.1.1 Extraction with commercial kits

Entire 4-week-old *H. sampsonii* seedlings were collected and washed. One sample of 100 mg was used for RNA extraction using (Qiagen) following the manufacturer's protocol.

3.3.1.1.2 Extraction according to Jaakola protocol

Based on RNA extraction developed by Jaakola et al. (2001) an RNA extraction protocol suitable for phenol-rich plant tissues was developed similar to that modified by Fiesel (2016). Plant tissue was disrupted and homogenized in liquid nitrogen. Two samples of plant material, each approximately 100 mg, were added each with 750 µl preheated RNA extraction buffer (section 2.8.1) and incubated at 65 °C for 10 min and was vortexed briefly every 2 min. CTAB was added as a detergent for the separation of polysaccharides, EDTA as a complexing agent, *β*-mercaptoethanol as antioxidant and PVP as stabilizer and adsorbent of polyphenols. The mixture was centrifuged at 4 °C and 10,000 x *g* for 10 min. The supernatant was separated and extracted twice with chloroform: isoamyl alcohol (24:1) phases were then separated by centrifugation at 13000 rpm at room temperature for 10 min. RNA was precipitated overnight at 4 °C by adding a ¼ volume of 10 M LiCl to the hydrophilic supernatant. The RNA was trapped at 4 °C and 18,000 x *g* for 20 min, the supernatant was decanted and the pellets were washed two times successively

with 500 µl cold ethanol 70% (v / v) and dissolved each in 100 µl SSTE buffer (section 2.8.1). Dissolved samples were combined and extracted once with phenol: chloroform: isoamyl alcohol (125: 24: 1) and once with chloroform: isoamyl alcohol (24: 1) to remove any residual DNA contamination. RNA was re-precipitated by the addition of ice-cold ethanol at -20 °C for 2 h, centrifuged at 4 °C washed twice with cold ethanol and, after removal of the supernatant dried at 37 °C for 30 min in a vacuum concentrator finally suspended in 30- 50 µl RNase-free dH_2O.

3.3.1.2 Isolation of plasmid DNA from *E. coli*

Alkaline lysis method was used which based on selective lysis of large linear DNA in alkaline medium but leaving the small circular DNA intact (Birnboim and Doly, 1979). The denatured DNA together with proteins are neutralized and precipitated while plasmid DNA remains dissolved. A single colony of transformed *E. coli* was inoculated in a 5 ml LB tube supplemented with 10 µl of 100 mg/ml ampicillin solution for positive selection of bacterial cells accommodating plasmids contain an ampicillin resistance gene. After overnight (16- 18 h) incubation at 37 °C and 200 rpm, cells in 2 ml of the overnight culture were pelleted in by centrifugation for 5 min at 5000 rpm. Pellets were resuspended in 300 µl of ice-cooled buffer I containing freshly-added RNase A (2.8.2). 300 µl of the alkaline buffer (buffer II, 2.8.2) were added, then the tubes were mixed by moving upside down 6 times and incubated at room temperature for 5 min. An equal amount of neutralizing buffer III (2.8.2) was gently mixed, then the whole mixture was incubated on ice for 20 min which resulted in the precipitation of chromosomal DNA and proteins. The precipitate was discarded through centrifugation for 10 min at 14000 rpm, while 800 µl of the supernatant were vigorously vortexed with an equal volume of chloroform; separation of the two phases achieved after centrifugation for 10 min at 14000 rpm. Precipitation of plasmid DNA was done by the addition of 490 µl isopropanol to 700 µl of the aqueous phase after transferring to a new 1.5 ml Eppendorf (70 % of the aqueous phase volume), followed by vortexing and centrifugation for 30 min at 14000 rpm. After discarding the supernatant the pellet was washed with 500 µl of 70 % ethanol, centrifuged for 10 min at 14000 rpm. The supernatant was again removed and the precipitated plasmid was dried in a rotational vacuum concentrator and finally dissolved in 30- 50 µl of deionized water.

The isolated plasmids were tested either by restriction digestion or by PCR for the presence of the insert before sequencing the results were analyzed as would be described later by agarose gel electrophoresis (3.3.6).

3.3.1.3 Isolation of plasmid DNA from *Saccharomyces cerevisiae*

To control whether the tested transformed yeast colony contains the expected plasmid, plasmids were isolated according to the protocol developed by Hoffman and Winston (1987). Colonies harboring the right plasmid were selected for subsequent expression procedure.

Two ml overnight yeast culture were centrifuged for 5 min at 5000 rpm to pellet the cells, the cells were again suspended in the residual medium left after discarding the supernatant. To the suspension 200 µl of the yeast cracking solution (2.8.3), 200 µl of phenol: chloroform (1:1) and

300 mg of acid-washed glass beads were added. The whole suspension was vigorously vortexed for 2 min, then centrifuged for 10 min at 13000 rpm. The aqueous phase was separated and further used to precipitate the DNA by adding 70% of its volume isopropanol. After precipitation of DNA, washing, drying, dissolution was continued as described under section 3.3.1.2. A disadvantage of this method is the low quality of the isolated plasmids (protein and RNA contaminations), nevertheless, it was enough to be used as a template to confirm the correct inserts by PCR amplification.

3.3.1.4 Isolation of DNA from agarose gels

DNA fragments with the right expected size were purified using the innuPREP DOUBLEpure Kit (Analytik Jena). First, the gel matrix was solubilized in 650 µl solubilizing buffer for 10 min at 50 °C. The solubilized gel was transferred to nucleospin column where DNA is adsorbed to the silica membrane, and other components of the mixture were removed after centrifugation (1 min at 8000 rpm) and washing twice by the washing buffer. Then the column was dried by centrifugation at maximum speed for 2 minutes. Finally, DNA was eluted by the addition of ≈ 15 µl of the dH_2O.

3.3.1.5 Direct isolation of target DNA from reaction mixtures

The same principle and kit as mentioned in 3.3.1.4 but the digestion or dephosphorylated reaction mixture was mixed with 500 µl of the binding buffer then transferred to the separation column, centrifuged at 12000 rpm for 1 min, washed once and then the process is continued as before.

3.3.2 Quantification of nucleic acids

The concentration of nucleic acids was determined spectrophotometrically by measuring the absorbance of a 1:100 diluted sample at wavelength 260 nm. Beer-Lambert equation was applied.

$$C = \frac{A_{260}}{L}\ x\ \varepsilon\ x\ D$$

Where,

- C is the concentration of the nucleic acid sample in ng/µl
- A_{260} is the absorbance of the nucleic acid sample at 260 nm
- L is the path length in cm
- ε is the extinction coefficient (50 µg/ml for double-stranded DNA, 33 µg/ml for single-stranded DNA and 40 µg/ml for RNA)
- D is the dilution factor

The ratio A_{260}/A_{280} was obtained for the determination of the purity of the isolated nucleic acid. Due to the interference of genomic DNA, proteins or some reagents commonly used in nucleic acids isolation a value of ≥ 1.8 and ≤ 2 was sought. Unlogical higher values indicate contamination with genomic DNA and lower values imply the high amount of contaminants that have absorption at λ_{280} like proteins and/ or phenols.

3.3.3 Reverse transcription

3.3.3.1 General reverse transcription

Total RNA was revers-transcribed to get complementary DNA (cDNA) for subsequent cloning of prenyltransferases. A special RNA-dependant DNA polymerase (RevertAid™ H Minus Reverse Transcriptase (RT; 2.5.1) was used. In reverse transcription, the use of an oligo (dT) primer directed to the polyadenylated sequence at the 3' end of each mRNA molecule, specifically transcribing the mRNA from the total RNA. The synthesized cDNA was used to search for new prenyltransferase (PT) fragments using degenerate primers as well as cloning of complete PT genes. This process was done as reported by the manufacturer. Initially, the reaction components with RNA were pipetted together **(Table 5)**. For initial denaturation of secondary structures, RNA was heated briefly and after a short incubation on ice added to Master Mix (MM). Finally, the reaction was stopped completely by heat inactivation of the RT. The obtained cDNA utilized as a template for PCR (3.3.5) or stored at -20 °C until use.

Table 5: Standard reverse transcription protocol.

Step	Components	Volume	
	Template RNA	3-7	µl *
	Oligo(dT)-Primer (10 µM)	1	µl
	dH_2O	ad 12.5	µl
Denaturation	65 °C for 5 min		
	Put on ice for 5 min		
	5x Reaction buffer	4	µl
	RiboLock™ RNase Inhibitor	0.5	µl
	dNTP-Mix (each 10 mM)	2	µl
	RevertAid™ H Minus Reverse Transcriptase	1	µl
	Total volume	20	µl
Reverse transcription	42 °C for 90 min		
Heat deactivation	70 °C 10 min		

* correspond to 1- 2 µg

3.3.3.2 Reverse transcription for SMART RACE suitable cDNA

For the identification of unknown 3' and 5' ends of genes and for the two-sided extension of incomplete cDNA fragments to the untranslated region (3'-UTR / 5'-UTR) finds Clontech's SMART™ RACE cDNA Amplification Kit a good use (Chenchik et al., 1998). In the reverse transcription of this RACE application (rapid amplification of cDNA ends), the cDNA strand was simultaneously supplemented by a known anchor sequence at the 3' or 5' end during the synthesis, which allowed, in a subsequent RACE-PCR, the amplification of unknown cDNA sequences between known middle fragment and the respective anchor sequence.

The 3'-RACE was accomplished as described under 3.3.3.1. An oligo (dT) primer with an additional known sequence at its 5 'end (3'-RACE CDS primer A; 2.4.6) was used, After attaching the primer to the complementary poly (A) tail of the mRNA, the 3' end of the newly synthesized cDNA strand can be amplified.

Specific reverse transcription for the 5' extension (5'-RACE) is required, in addition to a gene-specific or an oligo (dT) -Primers (5'-RACE primer A; 2.4.6), a special reverse transcriptase with built-in terminal transferase activity (SMARTScribe ™ RT). After reading and reaching the 5' end of the mRNA template, it adds 3- 5 cytosine moieties to the 3' end of the newly synthesized cDNA strand. Thus, allowing the SMART II™ A oligo to complement the introduced cytosine, which known as template switching, thus allow the oligo to serve as a template for the SMARTScribe™ RT. The RT recognized this single-stranded overhang, changed the template of mRNA on the SMART II™ A oligo, hence introducing the anchor into the RACE-ready cDNA. The SMART™ RACE cDNA Amplification Kit was used according to the manufacturer's instructions. Pipetting scheme and thermocycler program steps are listed in Table 6.

Table 6: 5`- RACE reverse transcription's protocol.

Step	Components	Volume	
	Template RNA	2.75	µl
	5'-CDS Primer A (10 µM)	1	µl
Denaturation	72 °C for 3 min		
	42 °C for 2 min		
	5x Reaction buffer	2	µl
	DTT (20 mM)	1	µl
	dNTP-Mix (each 10 mM)	1	µl
	SMARTer II™ A Oligo (12 µM)	1	µl
	RiboLock™ RNase Inhibitor (40 U/ µl)	0.25	µl
	SMART Scribe™ RT (100 U/µl)	1	µl
	Total volume	10	µl
Reverse transcription	42 °C for 90 min		
Heat deactivation	70 °C 10 min		

3.3.4 Primer design

Several points should be taken into consideration while designing primers to bind specifically to the desired gene or fragment and yield a good amount of it.

1. Primer length: should be between 18-24 nucleotides
2. GC content: a GC content between 40- 60% is ideal. Long stretches of guanine or cytosine bases should be avoided to prevent mispriming and it is better to end the primer with G or C. This clamp allows to anchor the primer on its template for efficient priming.
3. Melting temperature of the primer: T_m ranges between 55 °C and 65 °C would be sufficient for most of the templates. Ideally, the difference between forward and reverse primers should not be more than 2 °C. A primer with rather higher T_m is needed when the template is a mix of DNA or cDNA.
4. It is advisable to prevent complementarity within a primer to avoid hairpin formation or between forward and reverse primers to hamper the development of primer dimers which affect the yield of the desired band. This could be checked using the oligo cal. online tool http://biotools.nubic.northwestern.edu/OligoCalc.html

5. Sequence homology to other parts of the template should be as minimal as possible to avoid amplification of undesired regions of the template.
6. A restriction site at 5′-end of the primer is added when the next step was restriction digestion for subsequent cloning. In this case, 3 more nucleotides are added before the restriction site to help the enzyme cut the linear amplified DNA. The introduced nucleotides (anchor sequence and the restriction site) should not be considered while calculating the melting temperature of the primer.
7. By designing a reverse primer the reverse complementary sequence of the template is taken into consideration.

Uracil-containing primers that are compatible with USER cloning technique (2.4.5) were generated by the introduction of a tail of 8 nucleotides, present in the PacI cassette inserted into pCAMBIA2300-35S, to their specific PT sequence. The sequence GGCTTAAU was added to the forward primer to have the arrangement 5′-GGCTTAAU+ target PT-specific sequence-3′, the reverse primer is 5′-GGTTTAAU+ target PT-specific reverse complementary sequence-3′. Reverse primers for amplifying PTs were inserted into C-terminal fusion vectors, where the YFP is in frame with PT, were designed by replacing the stop codon with non-stop codon triplet (false stop codon). Two cytidine residues were also introduced to compensate frame shift to result in a primer with the structure 5′-GGTTTAAU+cc+ false stop codon+ reverse complementary upstream sequence of stop codon-3′. Truncated PTs, lacking the transit peptide, were amplified using a forward primer that inserts an artificial start codon before the TP-downstream sequence to result in a primer that has the arrangement 5′-GGCTTAAU+ artificial ATG+ downstream sequence of TP-3′. The primer design for amplifying the reverse primer depends whether the YFP was fused before the N-terminal or after the C-terminal of the introduced truncated PT.

3.3.5 Polymerase Chain Reaction (PCR)

Kary Mullis was awarded the Nobel Prize for Chemistry in 1993 for inventing the polymerase chain reaction (PCR). This technique is applied to obtain a high copy number of the template DNA through an exponential amplification of a desired target of the template by means of an enzyme called DNA polymerase, where the newly formed DNA is used as a template for the next amplification cycle, from which comes the name chain reaction (Mullis, 1994). The enzyme adds nucleotides to the 3′ end of a primer that anneals specifically to the DNA template. Thus the components of a PCR are DNA template, a pair of primers that are hybridized in opposite directions, a mixture of deoxynucleotide triphosphates (dNTPs) and a DNA polymerase.

The reaction is completed in 3 stages:

1. Denaturation: the separation of the DNA double strands to produce single-stranded DNA by heating the DNA for 30 s at 95–98 °C to disrupt the hydrogen bonds between the complementary bases.
2. Annealing: allowing the primers anneal to their target at the template via dropping off the temperature to 45–70 °C. Usually, the annealing temperature (T_a) used is 3–5 °C below

the T_m of the primers, to prevent non-specific annealing to other template DNA molecules present in the reaction mixture.

3. Extension: this step is carried out at 72 °C, the best temperature for DNA polymerase activity. The duration of this step depends on the length of the amplified fragment and the speed by which the enzyme adds nucleotides to the newly synthesized strand. Roughly it should be 1 min for each 1 kDa.

This three-stage amplification can be repeated within a single PCR. Providing sufficient supply of all required synthesis components, 25- 35 cycles could be done, thus generating large amounts of DNA in a short time. Various PCR applications differ by the temperature programs used, additives and by the DNA polymerases used. The PCR product is analyzed by agarose gel electrophoresis (3.3.6) and could be separated as previously described (3.3.1.4)

3.3.5.1 Standard PCR

This PCR approach was used during the course of this work for amplification of PT fragments, to check the presence of expected inserts in the ligation constructs and RACE amplicons. For this PCR Taq-polymerase served as DNA polymerase. The reaction runs as described in **Table 7**.

Table 7: Standard PCR components and thermocycler steps.

Step no.	Function	Components	Volume
		Template DNA (250- 500 ng)	1 µl
		For. Primer (10 µmol)	1 µl
		Rev. Primer (10 µmol)	1 µl
		dH_2O	12 µl
1	Pre-heating	95 °C then pause	
2	Initial denaturation	95 °C for 180 sec	
3	Adding the second reaction mix	72 °C then pause	
		10x Reaction buffer	2.5 µl
		dNTP-Mix (each 10 mM)	1 µl
		dH_2O	6.25 µl
		Taq-polymarase (1.25 U/µl)	0.25 µl
		Total volume	25 µl
4	Denaturation	95°C for 30 sec	
5	Annealing	T_a °C for 30 sec	
6	Extension Go to step 4, 34 x	72 °C for 150 sec	
7	Final extension	72 °C for 600 sec	
8	Storage	12 °C then pause	

3.3.5.2 High-fidelity DNA polymerases PCR

In this type of PCR, a polymerase with exonuclease activity is used, which is able to excise an inserted mismatched nucleotide. Consequently, the fidelity of replication is assured and the resulting products have always blunt ends. Phusion Hot Start II DNA Polymerase was used for this PCR. Proofreading PCRs were applied when absolutely correct DNA sequences are required

such as cloning of genes into expression vectors. Reaction components and thermocycler program steps are demonstrated in **Table 8** and **Table 9** respectively.

Table 8: proofreading PCR components.

Components	Volume	
Template DNA (1- 10 ng)	1	µl
For. Primer (10 µmol/µl)	1.25	µl
Rev. Primer (10 µmol/µl)	1.25	µl
5x Reaction buffer	5	µl
dNTP-Mix (each 10 mM)	0.5	µl
Phusion Hot Start II DNA Polymerase (2/µl)	0.5	µl
dH_2O	ad 25	µl

Table 9: cycling program of proofreading PCR.

Step	Function	Temperature	Time (sec)	Cycles	Go to step
1	Lid and pre-heating	98 °C	Pause		
2	Initial denaturation	98 °C	30		
3	Denaturation	98 °C	10		
4	Annealing	T_m* + 3 °C	30		
5	Extension	72 °C	150	34	3
6	Final extension	72 °C	600		
7	Storage	12 °C	Pause		

* Lower T_m of the primer pair

3.3.5.3 Touchdown PCR

The reaction ingredients of this PCR type are the same as standard PCR. However, the main difference is in the cycling program **(Table 10)**. Touchdown PCR was applied to enhance the efficacy and specificity of amplification through stepwise coverage of a wider range of annealing temperatures. Here, during the first phase of cycling the chosen T_a is equal or 2 °C below the lower Tm of the primers followed by 10 cycles each with 0.5 °C decrease in the T_a to enrich the target DNA.

Table 10: Thermocycler program for touchdown PCR.

Step	Function	Temperature	Time (sec)	Δ T	Cycles	Go to step
1	Lid and pre-heating	95 °C	Pause			
2	Initial denaturation	95 °C	180			
3	Denaturation	95°C	30			
4	Annealing	T_m -2 °C	30	− 0.5 °C		
5	Extension	72 °C	150		9	3
6	Denaturation	95 °C	10 s			
7	Annealing	T_m -7 °C	30 s			
8	Extension	72 °C	150		34	6
9	Final extension	72 °C	600			

10	Storage	12 °C	Pause

3.3.6 Agarose gel electrophoresis

It was used for the analysis and separation of PCR or digestion products. Electrophoresis is mainly a sieving process where DNA fragments are separated according to their sizes in a cross-linked agarose matrix by applying an electric field across the gel matrix. DNA molecules migrate along the gel matrix to the positive pole as a result of having negatively charged phosphate groups in the DNA backbone. A linear relation exists between the logarithm of the fragment size and its relative migration distance through the gel. A typical agarose gel is 1% which is suitable for DNA fragment sizes range 0.2- 20 Kb but the concentration can be modified for some purposes. A lower or higher concentration of 0.5 % or 2% were used to increase the resolution efficiency for better detection of large and small fragments (≈ 500 bp) respectively.

For the preparation of standard 1% agarose gel, 800 mg of agarose was boiled with 80 ml of 1X TAE buffer (2.8.6) till complete dissolution of agarose powder. The gel is cooled out to about 60 °C then 3 µl Midori Green were added and comprehensively mixed with gel solution, the mixture is added to suitable gel tray and a comb is applied to it. After solidification of the gel, the comb is removed and the tray is transferred to the gel chamber. A mixture of the samples to be analyzed with the loading dye (2.8.6) is loaded in the gel wells. The gel was run in TAE buffer for 30–35 min at 120 V and 400 mA. To identify the size of analyzed DNA fragments 5 µl of DNA ladder were loaded into one of the wells. When the run is completed the gel was visualized with a UV-equipped transilluminator. When needed a gel band was cut and the DNA entrapped inside it was purified as described under 3.3.1.4).

In addition, agarose gel electrophoresis was utilized to control the purity and integrity of RNA. In this respect, the gel was prepared as described above and the RNA sample is mixed carefully with RNase inhibitor in addition to the loading buffer.

3.3.7 RACE

DNA sequences that lack the information at 5′- or 3′- ends can be elongated by applying RACE techniques to get the full-length sequence (Frohman et al., 1988). For the preparation of RACE suitable cDNA during reverse transcription, a known anchor sequence synthesized and fused behind the unknown end of the cDNA strand (3.3.3.2). Special RACE primers are added to the reaction, which can anneal specifically to the anchor sequences introduced to cDNA ends. In addition, a gene-specific primer (GSP) was added to the reaction that was derived from the known middle fragment to obtain the unknown sequence lying between the GSP and the anchor sequence. In case of 5′-RACE the GSP is designed as a reverse primer and 5′-RACE ready cDNA is employed as a template, while in 3′-RACE it would be a forward primer and 3′-RACE ready cDNA served as a template.

Practically, the cDNA template was used to extend the target CDS either in the direction of the 3′ or the 5′ end (3′-RACE PCR / 5′- RACE PCR) in separate PCRs. The RACE long primer used in the first PCR (2.4.2) lengthened the anchor sequence in the DNA synthesis towards a GSP. This PCR product served as a template for a second RACE PCR in which a primer, whose sequence is complementary to the extended anchor sequence of RACE long, called RACE short primer (2.4.2) is applied. RACE short was combined with a more downstream GSP within the known CDS sequence from the first PCR at the respective desired end. In this way, both the yield and the specificity of RACE-PCR products was greatly enhanced. However, the RACE technique was combined with standard, proofreading or touchdown PCR applications to identify the missing CDS ends.

3.3.8 Sequencing

The DNA sequences of purified plasmids and/or DNA constructs were controlled on behalf of the companies Eurofins MWG Operon or Source Bioscience Sequencing. The concentration of the samples was adjusted with dH_2O to nearly 100 ng/µl according to the requirements of the service providers and, if required, premixed with the sequencing primers matching the respective plasmid. Sequencing results were bio-informatically analyzed using Lasergene - DNAStar 7.0 (2.10.1).

3.3.9 Construction of sequencing and expression plasmids

3.3.9.1 pJET 1.2 cloning

All identified prenyltransferases, their middle fragments, and RACE products were ligated into the vector pJET1.2/blunt (CloneJET PCR Cloning Kit; 2.6) for the purpose of sequencing. This linear cloning vector benefits from an interesting selection mechanism based on the existence of a lethal gene which is disrupted by insertion of DNA molecule into the vector's cloning site. Therefore, only cells containing the recombinant plasmids can survive and proliferate which cancels the need for blue/white screening.

After manufacturing instruction, the kit can be used for ligating blunt-end proofread PCR products directly using blunt-end ligation protocol **(Table 11)** or 3′-dA overhang-bearing *Taq*-polymerase PCR products through doing an initial blunting step employing the supplied blunting enzyme that possesses an exonuclease activity **(Table 12)**. Ligation mixture can be used immediately for transformation or stored at -20°C.

Table 11: pJET 1.2 blunt-end ligation protocol.

Function	Component	Volume	
	2X Reaction Buffer	5	µl
	purified blunt-end DNA fragment	1	µl *
	pJET1.2/blunt Cloning Vector (50 ng/µl)	0.5	µl
	T4 DNA Ligase	0.5	µl
	dH_2O	ad 10	µl
	Total volume	10	µl
Ligation	Incubate at 22°C for 10 min		

Table 12: pJET 1.2 Sticky-end ligation protocol.

Function	Component	Volume
	2X Reaction Buffer	5 µl
	purified PCR product with sticky-ends	1 µl *
	DNA blunting Enzyme	0.5 µl
	dH_2O	2.5 µl
	Total volume	9 µl
Blunting	Incubate 70 °C for 5 min, then Chill on ice	
	pJET1.2/blunt Cloning Vector (50 ng/µL)	0.5 µl
	T4 DNA Ligase	0.5 µl
	Total volume	10 µl
Ligation	Incubate at 22 °C for 10 min	

* Containing 50- 150 ng

3.3.9.2 Cloning of expression vectors

3.3.9.2.1 Restriction digestion

Restriction endonucleases of type II that recognize a palindromic nucleotide sequence (usually 4-8 bases, known as restriction site) were used. Type II restriction Enzymes cut within or near their restriction sites generating sticky or blunt ends suitable for subsequent ligation with the vector when it is cut by means of the same enzymes. During the course of this work, only sticky end ligation was used to insert a gene into an expression vector (2.3). The restriction sites introduced to the primers during the designing process were chosen so that they are absent from the insert DNA but present in multiple cloning sites of the utilized vector.

For each ligation procedure, two restriction digestion reactions were needed. These reactions could be done separately according to the instruction provided with each enzyme, where the products of the first digestion process were purified and re-digested with the second enzyme or, when possible, a double-digestion process using both enzymes simultaneously according to the instructions of Thermos Fischer DoubleDigest Calculator (2.10.2). Digestion was also used to check the presence of some inserts after ligation and transformation and the digestion reactions were visualized with agarose gel electrophoresis. The vector and insert digestions were incubated for 3 h at 37 °C, while plasmid digestion was incubated for 1 h at 37 °C.

Table 13: Single digestion reaction components.

Component	Insert	Vector	Plasmid
10x Reaction buffer	1 µl	2 µl	1
DNA	ad 10 µl	ad 20 µl	2 µl
Restriction enzym (10 U/µl)	0.5 µl	1 µl	0.5 µl
dH_2O	-	-	ad 10 µl

Table 14: Double digestion reaction components.

Component	Inserts	Vectors	Plasmids
DNA solution	ad 10.0 µl	ad 20.0 µl	2.0 µl
10X buffer	1.0 µl	2.0 µl	2.0 µl
1st restriction enzyme	0.5–1.0 µl	0.5–1.0 µl	0.5–1.0 µl
2nd restriction enzyme	0.5–2.0 µl	0.5–2.0 µl	0.5–2.0 µl
dH_2O	-	-	ad 20.0 µl

3.3.9.2.2 Dephosphorylation of the digested vectors

To minimize the possibility of re-circularization of the linearized vector after digestion during the ligation process through removing 5′ terminal phosphates. The vector sticky ends can ligate together again (self-ligation) instead of ligating to the sticky ends of the insert and result in an empty vector which could be transformed to the host competent cells like any positive plasmid and this will be detected only after plasmid isolation. FastAP Alkaline Phosphatase (2.5.4) was used for the dephosphorylation of the digested vectors. The reaction was incubated for 12 min at 37 °C followed by heat-inactivation of the enzyme for 5 min at 75 °C. The dephosphorylated product was purified as described under 3.3.1.5 to get rid of salts and proteins in the reaction mixture.

Table 15: Dephosphorylation reaction components.

Component	Volume
Digested vector	5-17 µl
10X reaction buffer for AP	2 µl
FastAP Alkaline Phosphatase	1 µl
dH_2O	ad 20 µl

3.3.9.2.3 Ligation

By means of this molecular biology tool, the free ends of DNA fragments can be connected together via the formation of a phosphodiester bond between a 5′ phosphate group in one fragment and a 3′ hydroxyl group in the other. Ligation was used during the course of this work to insert PT fragments, full-length genes via blunt-end ligation into sequencing vector (pJet 1.2, 2.3) or by sticky-end ligation to incorporate full genes into expression vectors (pESC-URA and pFastBac-1). T4 DNA ligase, which is dependent on the presence of ATP and Mg^{2+} as cofactors are used to catalyze the reaction. This enzyme is suitable for blunt or sticky end ligations. Optionally 50 % PEG 4000 as an enhancer can be added. Ideally, the insert: vector ratio should be 3: 1. During the course of the work, work ratios between 2: 1 and 5: 1 were used. Ligation reaction mixture **(Table 16)** was incubated at 4 °C overnight.

Table 16: Ligation reaction components.

Component	Volume

Insert DNA	6.5	µl
Linearized vector DNA	2	µl
10X T4 DNA ligase buffer	1	µl
T4 DNA ligase	0.5	µl
50 % PEG 4000 (optional)	1	µl

3.3.9.3 USER cloning

USER™ stands for uracil-specific excision reagent. This special type of ligation-free cloning was used to build constructs for subsequent transformation of *Agrobacterium tumefaciens* as a step of the subcellular localization sequence procedure for xanthone-related prenyltransferases (4.6.1.2). The linearized pCAMBIA2300-35S vector that harbors a yellow fluorescent protein (YFP) either at C- or N- terminus of the predicted gene to be inserted was kindly provided by our former colleague Dr. Elina Biedermann (AG Prof. Dr. Ute Wittstock; IPB-TU Braunschweig). Briefly, the vector was linearized by a two-step prolonged digestion first with PacI then with the nicking enzyme Nt.*BbvCl* (2.5.3; **Table 17**). PTs to be inserted, were amplified from yeast expression vectors by means of specific uracil-containing primers (2.4.5) in a proof-reading PCR.

Purified linearized vector and uracil-containing PTs were mixed with USER enzyme mix (Nour-Eldin et al., 2006). USER cloning reaction components and protocol are described in Table 18. The whole reaction was finally transformed to competent *E.coli* as a preliminary step for transformation in *Agrobacterium tumefaciens.*

Table 17: Digestion protocol of pCAMBIA2300-35S vector.

Function	Component	Volume	
	pCAMBIA2300-35S	1.3	µg
	PacI	1	µl
	10x cut Smart buffer	5	µl
	H_2O	ad 50	µl
	Total volume	50	µl
1st digestion	37°C for at least 18 h		
	10x cut Smart buffer	0.5	µl
	PacI	0.5	µl
	Nt.*BbvCl*	0.5	µl
	H_2O	3	µl
2nd digestion	37°C for 2 h		

Table 18: USER reaction protocol.

Component	Volume	
pCAMBIA2300-35S	2	µl
Uracil-containing PT	8- 10	µl
USER enzyme mix	1	µl
Total volume	11- 13	µl

37 °C for 20 min
25 °C for 20 min

3.3.10 Construction of prenyltransferases phylogenetic tree

An evolutionary tree was constructed using protein sequences of plant aromatic prenyltransferases and a soluble fungal aromatic prenyltransferase that lacks the aspartate conserved motifs *At*aPT (Zhou et al., 2017) was used as an out-grouping to root the tree. Accession numbers are listed in the appendix (8.1), and sequences were aligned using the Clawstal W method in BioEdit software. The alignment output file positioned in MEGA 7 (Kumar et al., 2016) and an initial tree was constructed by a neighbor-joining method which was used then as a base for a final tree built up by Maximum-likelihood algorithm (ML). Poisson correction mode (Zuckerkandl and Pauling, 1965) was used to calculate amino acid differences with partial deletion arrangement for the adjustment of gaps. Replicates of 1000 bootstrap are estimated for the reliability of the constructed tree.

3.4 Microbiological Methods

3.4.1 Determination of microbial count

One ml of bacterial or yeast culture was used for photometric determination of *E.coli* or *S. cerevisiae* microbial count by virtue of measuring the optical density at 600 nm using a spectrophotometer against 1 ml of fresh media as blank. 0.1 OD_{600} corresponds to 1×10^8 cells/ml of bacteria or 3×10^6 cells/ml of yeast (Lech and Brent, 2001; Treco and Winston, 2001)

3.4.2 Preparation of competent cells

3.4.2.1 Preparation of competent *E. coli* cells

Chemically competent DH5α *E. coli* (2.1.2.1) cells were prepared by calcium chloride method described by Mandel and Higa (1970). A single colony of the bacteria was incubated overnight with shaking at 220 rpm in 5 ml LB medium. One ml from the pre-culture was used as an inoculum for 50 ml LB medium until an OD_{600} of 0.2- 0.3 was reached. Th

e culture was grown again to obtain an OD_{600} of 0.7. Bacterial cells were then harvested from the medium by centrifugation at 8.000 rpm at 4 °C for 10 min. After discarding the supernatant, bacterial pellet was resuspended in 50 ml 50 mM ice-cold $CaCl_2$ solution and centrifuged again under the same conditions. Again, the pellet was suspended in 20 ml 50 mM $CaCl_2$ solution and directly incubated in ice for 20 min. The incubate was centrifuged again and the pellet was separated, suspended in 860 µl 50 mM $CaCl_2$ solution, and kept on ice for another 15 min. Finally, 140 µl sterile glycerin was mixed with the suspension and the mixture was divided into 50 µl aliquots. The aliquots were stored at -80 °C until used for transformation.

3.4.2.2 Preparation of competent *Saccharomyces cerevisiae* cells

S.c. EasyComp Transformation Kit (Invitrogen) which make use of lithium acetate method illustrated in (Dohmen et al., 1991; Becker and Lundblad, 2001). One yeast colony grown on selective medium was picked, used to inoculate 10 ml YPD medium (2.7.3), and incubated at 30

°C and 250 rpm for about ≈ 26 h. when the OD_{600} reached 2.6–5.0 about 600 µl of the starter culture were added to 10 ml fresh YPD medium until an OD_{600} of 0.2–0.4 was reached. The YPD culture was allowed to grow for about 6 h. by reaching an OD_{600} of 0.6–1.0 the culture was centrifuged for 5 min at 1500 rpm and the cells were collected. Cells were resuspended in 10 ml of Solution I (provided with the kit), centrifuged and the supernatant was discarded. The pellet was resuspended in 1 ml of Solution II (provided with the kit) then divided into 50 µl aliquots, stored at -80 °C.

3.4.2.3 Preparation of competent *Agrobacterium tumefaciens* cells

A. tumefaciens cells were made competent according to a modified protocol after McCormac et al. (1998). Ten ml YEP pre-culture (2.7.2) of *A. tumefaciens* (2.1.2.1) were incubated overnight at 28 °C under shaking at 220 rpm. The medium was supplemented with the antibiotics rifampicin and gentamycin at a concentration of 100 µg/ml each. The complete overnight culture was diluted with 300 ml of YEP medium (2.7.2) augmented by antibiotics as previous and allowed to grow until reaching an OD_{600} of 0.5- 0.7 under the same conditions. The media was then divided into 6 sterile falcon tubes, centrifuged (10 min at 4000 x *g*) and the pellet was harvested, washed three times with 25 ml ice-cooled 10% sterile-filtered glycerin and combined in 2 sterile falcon tubes. After centrifugation for 10 min at 5000 x *g*, pellets were collected and resuspended in 2 ml ice-cooled 10% sterile-filtered glycerin, again centrifuged and cells were combined together and incubated with 10% glycerin at 4 °C for 24 h. in the next day, the suspension was aliquoted and stored at -80 °C.

3.4.3 Transformation of competent cells

3.4.3.1 Transformation of competent *E. coli* cells

The ligation mixture (3.3.9.2.3) was gently mixed with 50 µl aliquot of competent on ice-thawed DH5α *E. coli* cells (3.4.2.1). The mixture was kept on ice for 20 min. Heat shock transformation method was carried out by heating the mixture for 45 sec on 42 °C followed by rapid cooling on ice for 5 min. The transformation mixture was later incubated in 250 µl of SOC medium for 75 min at 37 °C and 220 rpm. After incubation, 250 µl were spread on LB plate supplemented with ampicillin and incubated at 37 °C overnight. Plasmid isolation for control for the positive insert is done as described under (3.3.1.2).

3.4.3.2 Transformation of competent *Saccharomyces cerevisiae* cells

Transformation of competent INV*Sc*1 strain (3.4.2.2) is performed using *S.c.* EasyComp Transformation Kit (Invitrogen). First plasmids were isolated from *E.coli* and tested for the presence of desired inserts (3.3.1.2). A maximum of 5 µl containing 1-5 µg of positive plasmids was mixed with a thawed competent cells aliquot. Afterward, 500 µl of solution III was added to the mixture and vortexed vigorously. The transformation mixture was incubated in a water bath for 90 min at 30 °C with vigorous vortexing at time intervals of 15 minutes. Employing the auxotrophic selection, about 200 µl were spread over SD dropout plates that lack the presence of the marker.

1.1.1.1 Transformation of competent *Agrobacterium tumefaciens* cells

Transformation of competent *A. tumefaciens* (3.4.2.3) was conducted by electroporation in a pre-cooled electroporation cuvette. The transformation mixture was treated with an electric impulse with the conditions (2.5 kV, 400 Ω, and 25 µF) using MicroPulser (BioRad laboratories GmbH). The mixture was mixed afterward with 1 ml antibiotic-free YEP medium then transferred to 10 ml of YEP and incubated for 3h at 28 °C and 220 rpm. 50-100 µl were then spread on YEP agar plates supplemented with the antibiotics rifampicin, gentamycin and kanamycin at concentrations 100 µg/ml, 100 µg/ml and 50 µg/ml respectively. Plates were incubated then at 28 °C for 2- 4 days.

3.4.4 Transfection of *Spodoptera frugiperda* (*Sf*9) cells

3.4.4.1 Production of recombinant Bacmid

Bac-to-Bac® Baculovirus Expression System (2.6) was used for the cultivation of the recombinant bacmid. The first step is the construction of respective PT genes into pFastBac™ 1 (2.3). The expression cassette of the donor vector pfastBac is flanked by left and right regions of Tn7 and composed of gentamycin resistance gene, *Ac*MNPV polyhedrin promoter, the MCS (including the DNA sequence to be expressed) and an SV40 polyadenylation signal to form a miniTn7 **(Figure 14)**. Purified constructs of each PT into pFastBac were transformed into a special *E. coli* strain called (DH10Bac ™). This bacterial strain harbors baculovirus shuttle vector bacmid carrying a mini-attTn7 target site (bacmid bMON14272; 136 kb) and kanamycin resistance gene and the so-called helper plasmid (pMON7124; 13.2 kb) which encodes for tetracycline resistance enzyme and transposition proteins which allow the transposition of gene of interest from pfastBac to bacmid (Luckow et al., 1993). After transformation and with the help of helper plasmid, the transposition takes place between lacZ-mini-attTn7 and mini-Tn7 transposon to generate a recombinant bacmid. Successful transposition disturbs the *β*-galactosidase gene within the lacZ-mini-attTn7 and the colonies appear white using the blue/white selection.

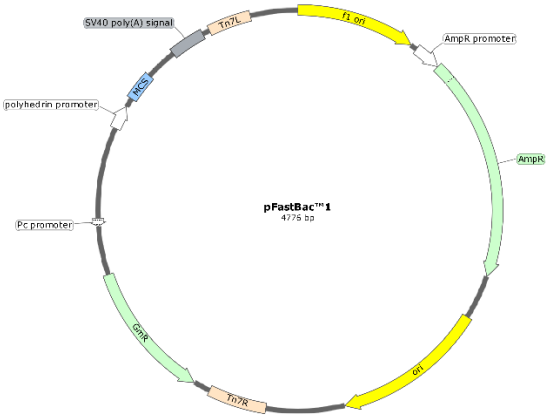

Figure 14: The map of pFastBac™ 1 donor vector.

Agar plates were incubated at 37 °C for 48 h. A single white bacterial colony is used to inoculate 5 ml LB medium containing gentamycin, kanamycin, and tetracycline with a concentration of 7 µg/ml, 50 µg/ml, and 10 µg/ml respectively. Tubes were incubated at 37 °C and 220 rpm for 16-

24 h overnight. Bacmid can be isolated as described under (3.3.1.2) and used for further work in the Bac-Bac system or stored at -20 °C.

3.4.4.2 Production and amplification of recombinant baculovirus

One µg of the purified, recombinant bacmid DNA and 8 µl Cellfectin® II reagent (2.6) were separately and gently mixed with 100 µl basic medium. Both solutions were combined with caution, mixed gently, and allowed to stand at room temperature for 15-30 minutes. A complex was being formed between of the anionic bacmid DNA and the cationic lipophilic Cellfectin® II, which led to an inclusion in or an adsorption on the existing liposomes. Meanwhile, cultivated *Sf9* cells (2.1.2.2) should be first diluted with the basic medium Sf-900 ™ II SFM (2.7.4) to reach a cell density of 4 x 10^5 cells/ml. Two ml of the diluted culture was transferred to a 6-well culture plate and incubated at room temperature for 15 min.

For the first baculovirus production, the bacmid-liposome mixture was added successively drop by drop on the *Sf9* cells and afterward incubated at 27 °C for 3-5 hours, so that the liposomes fused with the cell membrane of the *Sf9* cells by endocytosis and the bacmid DNA was transfected into the insect cells. Thereafter, the supernatant bacmid-liposome mixture was removed and replaced by 2 ml of Sf9 medium and the whole blend was then incubated at 27 °C for 3-5 days.

After the onset of the death of the infected *Sf9* cells, they were harvested by centrifugation at 4 °C and 4000 rpm for 2 min. The baculovirus-containing supernatant served the infection of fresh 100 ml *Sf9* cells having a cell density of 1 × 10^6 cells/ml, which were cultured in a shaker incubator, for the multiplication of baculoviruses, at 27 °C and 140 rpm for 5-7 days. After incubation, If the viability of *Sf9* cells decreased below 40%, insect cells should be separated from virus by 10 min centrifugation at 4 °C and 4000 rpm. The virus-containing supernatant was sterile-filtered through a syringe filter with a pore size of 0.22 µm, amplified and used for a new infection-turn employing 500 ml of fresh *Sf9* cells (cell density 1×10^6 cells/ml) to be infected with 5 ml baculovirus solution, incubated as described above, centrifuged off and filter sterilized. Finally, the supernatant was used for protein expression in *SF9* cells (3.5.1).

3.4.5 Preparation of stock cultures

3.4.5.1 *E. coli* stock cultures

A single colony of transformed *E. coli* was inoculated in a 5 ml LB tube supplemented with 10 µl of 100 mg/ml ampicillin solution for positive selection of bacterial cells accommodating plasmids contain an ampicillin resistance gene. After overnight (16- 18 h) incubation at 37 °C and 200 rpm, 1.35 ml of the grown culture was mixed with 450 µl of sterile LB- glycerol (40: 60 v/v) in a screw-capped 2 ml tubes. The prepared tubes were stored at -80 °C.

3.4.5.2 *S. cerevisiae* stock cultures

One colony of transformed *S. cerevisiae* grown on the selective medium was picked and used to inoculate 5 ml of the same selective liquid medium to allow auxotrophic selection of cells accommodating desired plasmids. After incubation for 24 h at 30 °C and 220 rpm, 500 µl of the

grown culture was mixed with 500 µl of YPD medium and 750 µl of sterile glycerol in a screw-capped 2 ml tubes. The prepared tubes were stored at -80 °C.

3.4.5.3 *A. tumefaciens* stock cultures

A single colony of transformed *A. tumefaciens* grown on YEB-agar medium supplemented with rifampicin and gentamycin at a concentration of 100 µg/ml each was picked and cultivated in a 5 ml YEB tube supplemented with the same antibiotics to allow selection. After a 16-18 h overnight incubation at 28 °C under shaking of 220 rpm, 1.35 ml of the grown culture was mixed with 450 µl of YEB- glycerol (40: 60 v/v) in a screw-capped 2 ml tubes. The prepared tubes were stored at -80 °C.

3.5 Biochemical methods

3.5.1 Protein expression in Insect cells-Baculovirus System

3.5.1.1 Infection of *Sf9* cells and expression of PTs

A suspension culture of *Sf*9 cells bearing a cell density of 2×10^6 cells/ml was pipetted with 10% v/v baculovirus supernatant, arising from the amplification turns (3.4.4.2), expression batches were incubated in 27 °C and 140 rpm for 72-96 h in a shaking incubator. Based on the viral *Ac*MNPV polyhedrin promoter, the introduced recombinant gene was highly expressed in virus replication. The heterologously expressed prenyltransferases were eventually extracted including the membrane proteins from the *Sf*9 cells and used for further in-vitro enzyme studies.

3.5.1.2 Protein extraction from insect cells

Protein extraction protocol was developed after Ohara et al. (2013). The complete volume of the culture was transferred to sterile falcon tubes and insect cells were harvested via centrifugation 4 °C and 6000 rpm for 6 min. after discarding the culture, the pellet was gently resuspended by pipetting in 5 ml sonication buffer (2.8.4). The tube containing the suspension was placed in an ice-filled beaker and the cells were disrupted three times each 1 min (with 30-sec pause in-between) by means of an ultrasound Sonifier (2.9.1) with the settings (Duty Cycle = 20 and Output Control = 1.5). Aliquots of intact and broken cells were stained with Trypan blue solution controlled microscopically to ensure the disruption of the cells for efficient extraction. Cells residue were removed by centrifugation at 4 °C and 5.000 rpm for 5 min. The crude protein extract (supernatant) was then ultra-centrifuged in pre-cooled ultracentrifuge using ultracentrifugation-suitable tubes (the volume of the supernatant was adjusted by adding sonication buffer) at 4 °C and 100000 x g for 80 min. After pouring off the supernatant, 2 ml of ice-cold buffer A (2.8.4) were added to the residue, and the pellet was carefully resuspended on ice by slow successive drawing up and draining using a syringe. The obtained microsomal protein fraction was quantified (3.5.4) and either used directly for activity testing (3.5.5) or stored at -80 °C.

3.5.2 Protein expression in Yeast cells

3.5.2.1 Induction of protein expression in yeast cells

The induction of heterologous protein expression in INV*Sc*1 yeast cells was carried out according to Pompon et al. (1996). A single colony of the transformed *S. cerevisiae* (3.4.3.2) grown on SGI-

agar medium was picked and cultivated in liquid SGI at 30 °C and 220 rpm for 24 h. 1.5 ml of it was used to inoculate 150 ml of YPGE medium (2.7.3) and incubated at 30 °C and 220 rpm for ≈ 26 h. When an OD_{600} of ≈ 1.6 is reached, which means the consumption of entire glucose in the media, induction of protein expression was initiated by adding 16.7 ml of 20% sterile-filtered galactose solution to the culture to obtain a final concentration of 2% galactose. Additionally, the absence of glucose was ensured also tested by COMPINA 11 S strips (2.6). The cells were further cultivated at 30 °C and 220 rpm for 14- 16 h.

3.5.2.2 Protein extraction from Yeast

The culture was transferred to 50 ml falcon tube and the cells were harvested by centrifugation at 5000 rpm for 5 min then resuspended in 10 ml TEK buffer (2.8.5), transferred to 15 ml falcon tube and centrifuged again under the same conditions. Pellet was again resuspended in 5 ml TEK buffer by vortexing and kept at room temperature subsequently centrifuged and the supernatant was discarded. The obtained pellet was resuspended by vortexing in 3 ml of TES buffer, mixed with 3 g of 0.45-mm acid-washed glass beads, and shaken using vortex shaker (Vortex Genie 2 Digital equipped with the Si-H512 Horizontal 15 ml tube holder) at 4 °C for 20 min to mechanically break the yeast cells. The suspension including the glass beads was centrifuged (5000 rpm for 5 min at 4 °C). The resulted supernatant was transferred to a new falcon tube and kept on ice. Pellets (broken cells + glass beads) were resuspended again in 3 ml of TES buffer and the entire process of mechanical breaking was repeated twice. Supernatants were combined together to obtain the crude protein extract. Crude protein extract was ultra-centrifuged as described before (3.5.1.2) and the precipitated microsomal fraction was suspended in buffer A (2.8.4) instead of TEG buffer mentioned in the original protocol (Pompon et al., 1996) as TEG buffer contains EDTA which may negatively affect the subsequent activity testing (3.5.5) through chelating the divalent cation added to the assay.

3.5.3 Transient expression in *Nicotiana benthamiana*

This transient expression technique was used to study the subcellular localization of the xanthone-related HsPTs. Transformed Agrobacteria (1.1.1.1) were grown on YEP-agar medium (2.7.2) at 28 °C. One colony was selected and incubated overnight with 10 ml YEP medium provided with 100 µg/l Rifampicin, 50 µg/L kanamycin and 100 µg/L gentamycin at 28 °C and 220 rpm for ≈ 30 h. In the next day, cultures were centrifuged at room temperature and 4000x g for 15 min and the cells were suspended in activation medium (2.7.2) (Gehl et al., 2009) till OD_{600} reaches 1. Likely, helper *A. tumefaciens* bearing K19 gene were grown and mixed with activation medium till the OD_{600}= 0.6. Cultures carrying fusion constructs of *Hs*PTs were mixed 1:1 with K19-containing cultures to enhance the transformation efficiency (Pan et al., 2018). After incubation for 2 h at 28 °C and 100 rpm, this mix was then co-infiltrated to the lower surface of 6-8 weeks old *N. benthamiana* leaves grown in soil in a climate chamber (24 °C, 65% humidity, 12 h light intensity) using 2 ml needleless syringe. For a maximum of 3 leaves per plant were infiltrated with suspension mix. *A. tumefaciens* harboring the localization cytoplasmic control (modified DSred

gene) treated equally and infiltrated as well. Three days after infiltration leaf discs were cut and visualized under LASER-scanning microscope (3.7).

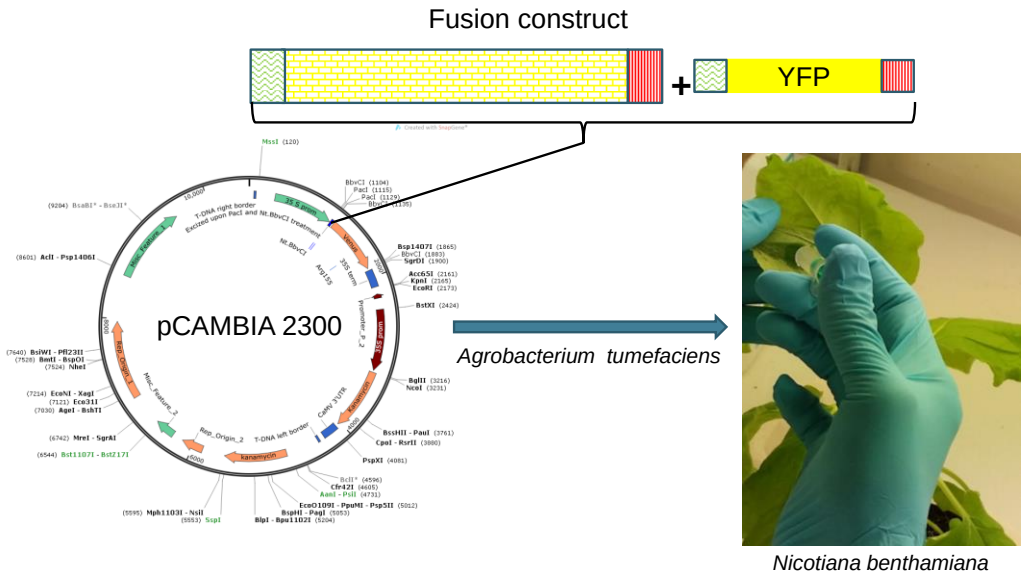

Figure 15: Schematic diagram for the transient expression of fusion constructs in *Nicotiana benthamiana* leaves.

3.5.4 Determination of protein concentration

The quantification of proteins was done as described by Bradford (1976), when the dye Coomassie Brilliant Blue G-250 binds to the protein, shifted its absorption maximum from 465 to 595 nm. The absorption of the protein test solution was measured at 595 nm against blank to cancel the effect of salts and pH on the test quality. Both test and blank solutions are blended separately and incubated for 5 min at room temperature. Test and blank solutions' components are demonstrated in Table 19.

Table 19: Bradford's reaction components for determination of protein concentration.

Test solution			Blank		
Component	Volume		Component	Volume	
Protein suspension (dissolved in buffer A)	2- 5	µl	-		
Buffer A	ad 100	µl	Buffer A	100	µl
Bradford solution	900	µl	Bradford solution	900	µl
Total volume	1000	µl	Total volume	1000	µl

An important factor for the determination of protein concentration by this method is the factor of Bradford' solution which is the slope of the calibration curve by plotting absorbance (Y-axis) of the different known concentration of BSA (1- 10 µg/ml) against the amount of BSA in µg (X-axis). The following formula was used to calculate microsomal protein concentration:

$$C = \frac{A_{595}}{F_B \; x \; V}$$

Where,

C is the calculated concentration of protein in µg/µl
A_{595} is the absorbance of the test solution at λ=595 nm normalized by blank solution
V is the volume of the protein solution used for measuring in µl
F_B is the factor of Bradford solution

3.5.5 Enzymatic assays

3.5.5.1 Standard PT *in vitro* enzymatic assay

For the determination of prenyltransferase activity of all recombinant proteins, a standard 250 µl enzymatic incubation was applied. The aromatic substrate (prenyl acceptor) was mixed with an equimolar concentration of the prenyl donor (DMAPP or GPP) in the presence of $MgCl_2$ as a co-factor. The final reaction volume was adjusted by the calculated volume of water and the reaction was initiated by the addition of 100 µg microsomal fraction. Reaction components and their exact concentrations are illustrated in Table 20. The reaction was performed in a shaker incubator for 90 min at 35 °C with gentle mixing at 60 rpm, modified after Ohara et al. (2013). After incubation, the reaction was stopped via the addition of 35 µl 2N HCl, extracted twice with 350 µl ethyl acetate. The combined organic extracts were air-dried, dissolved in 80 µl methanol (HPLC grade) and analyzed by HPLC (3.6.1).

Table 20: Standard PT *in vitro* enzymatic assay components.

Component	Volume		Final concentration	
Aromatic substrate (10 mM)	5	µl	0.2	mM
Prenyl donor (50 mM)	1	µl	0.2	mM
$MgCl_2$ (100 mM)	15	µl	6	mM
Tris-HCL pH 7 (1 M)	25	µl	0.1	M
100 µg protein	x	µl	0.4	mg/ml
H_2O	ad 250	µl	-	
Total volume	250	µl		

3.5.5.2 Characterization of prenyltransferase activity

The optimum assay conditions for enzymatic reactions catalyzed by active recombinant PTs were investigated. In this respect, each reaction parameter was individually changed and the influence of the modification on the activity of the enzyme was investigated as follows:

1. pH optima of the reaction: the pH was analyzed over a pH range of 6-10 in 0.5 pH unit increments with mainly 2 buffer systems to cover a wide pH span, namely K_3PO_4 (pH range 5- 8) and TRIS-HCl (pH range 7- 11)

2. Reaction time: the reaction was inspected at different time points ranging from 2 to 180 minutes and tested against zero time control.
3. Protein amount: A range of 5- 500 µg membrane protein/assay was investigated to select the optimum amount to be used while determining kinetic parameters of each active PT.
4. Incubation temperature: temperature spans from 20 °C to 50 °C with 5 °C intervals were tested.
5. Co-factor: different divalent cations were used (Ca^{2+}, Co^{2+}, Cu^{2+}, Fe^{2+}, Mg^{2+}, Mn^{2+}, Zn^{2+}).

After the determination of the optimum reaction parameters of each enzymatic reaction, the kinetic parameters for each enzyme with the respective accepted aromatic substrate or preyl donor were explored. To achieve this aim, different concentrations of each accepted substrate (2.5- 1000 µM) were tested considering the optimum reaction conditions.

3.6 Analytical methods

3.6.1 High-performance liquid chromatography (HPLC)

The analysis of all enzymatic assays was done by HPLC (Agilent 1260 Infinity Quaternary LC System; Agilent Technologies, Santa Clara, CA, USA) supplied with a diode array detector (DAD; G4212A) and a column (XBridge BEH C_{18} Column, 3.5 µm, 4.6 mm X 100 mm). The liquid system consisted of double distilled acidified water (A; 1 mM formic acid) and methanol (B). For optimum separation of enzymatic reaction components, different gradients of water/ methanol were used based on the nature of prenyl acceptor used. By analyzing enzymatic products using xanthone substrates, Gr. 1 was utilized. On the other hand, using patulone (diprenylated 1367THX) as a substrate, the expected products would have been less polar so Gr. 2 was used. When acyl- or benzoylphloroglucinol derivatives were used as prenyl acceptors, a different gradient was used, namely, Gr. 3. All used mobile phase gradients are listed in Table 21. Detection wavelengths for main substrates and enzymatic products are mentioned in Table 22. For the detection of other substrates or trace products, the detection wavelength was the respective absorption maximum for each compound.

Table 21: Mobile phase gradients used for HPLC analyses of enzymatic assays using different aromatic prenyl acceptors. Gr. 1 for xanthone substrates except for patulone; Gr. 2 for patulone; Gr. 3 for acylphloroglucinols; Gr. 4 for semi-preparative purification of 8PX. 8PX, 8-prenyl-1,3,6,7-tetrahydroxyxanthone.

Gr. 1	
Time (min)	% B
0	40
5	60
10	80
19	95
20	40
25	40

Gr. 2	
Time (min)	% B
0	60
6	80
12	95
32	95
34	60
40	60

Gr. 3	
Time (min)	% B
0	40
4	60
10	80
12	95
19	95
20	20
25	20

Gr. 4	
Time (min)	% B
0	20
2	40
5	55
12	75
30	100
32	20
35	20

For semi-preparative purification of 8PX (3.2.6), the enzymatic extract was dissolved in 1.5 ml methanol HPLC grade and purified in aliquots of 75 µl using Gr.1 and the same column described above for the analysis of enzymatic incubations.

Fractions of *H. sampsonii* extract were obtained utilizing Gr. 4 on reversed phase column (5 µm C_{18}, 250 x 4.6 mm; phenomenex jupitar). The extract was dissolved in 1 ml methanol HPLC grade, then successive aliquots of 50 µl were injected and fractioned by semi-preparative HPLC procedure.

Table 22: Detection wavelengths for main substrates and enzymatic products.

Compound	Detection wavelength (nm)
1367THX	254
246TrHBP	306
246TrHiBP	286
246TrHiVP	286
2MBP	286
8PX	254
G-246TrHBP	312
G-246TrHiBP	292
G-246TrHiVP	292
G-2MBP	292
Patulone	292

3.6.2 Liquid chromatography-Mass spectrometry (LC-MS)

For analysis of individual reaction products, about 10-25 times enzymatic reactions were combined together and the corresponding peak was purified and collected by HPLC. Aliquotes of the purified components (~10 µg/ml) were analysed *via* mass spectrometry (3200 QTrap mass spectrometer; Applied Biosystems/MDS SCIEX, Darmstadt, Germany), supplied with an electrospray ionization interface (Turbo V), employing the integrated 3200 QTrap syringe pump of the instrument (Syringe; 1,000 ml, i.d. 2.3 mm; Hamilton, Nevada, USA) at a flow rate of 10 ml/min. The MS/MS mode was carried out using a voltage source and declustering potential of 5.5kV and 76V, respectively. Nitrogen was used as a nebulization gas, with the curtain gas, gas 1, and gas 2 settings at 10, 14 and 0, respectively. Products' molecular ion peaks were additionally investigated by MS/MS in the instrument's enhanced product ion (EPI) mode by means of nitrogen gas for collision-induced dissociation. 30–50V was used as collision energy. Processing of data was performed using the Analyst software (version 1.4.2; Applied Biosystems/MDS SCIEX) was used.

3.6.3 Gas chromatography-Mass spectrometry (GC-MS)

Fractions obtained from *H. sampsonii* extract were evaporated under nitrogen gas and each dissolved in 1 ml methanol. Aliquots of 100-300 µl were transferred to inlets of HPLC vials and left to evaporate under nitrogen gas. The residue was derivatized with 50 µl N-methyl-N-

(trimethylsilyl)-trifluoroacetamide (MSTFA; ABCR, Karlsruhe, Germany) at 60 °C for 30 min. One microliter from each silylated fraction was injected directly into GC-MS (2.9.2). The apparatus is equipped with a ZB5MS column (30 m long, 0.25 mm i.d., 0.25 µm ft). The temperature program used was 70 °C for 3 min, followed by a linear temperature increase from 70 °C to 310 °C over 24 min at a rate of 10 °C/min and finally 310 °C for 5 min. The split ratio was varied according to the concentration of the sample from 1:10 to zero. Helium was used as a carrier gas. The retention index (I^T) for the compounds was calculated in comparison to a mixture of even-numbered hydrocarbons (C_{12} to C_{24}) according to the following equation:

$$I^T = 100[\left(\frac{t^T_{\mathrm{Ri}} - t^T_{\mathrm{Rz}}}{t^T_{\mathrm{R(z+1)}} - t^T_{\mathrm{Rz}}}\right) + z]$$

Where,

I^T	is the retention index for temperature programmed GC analysis, constant heating rate
t^T_{Ri}	is the retention time of sample peak
t^T_{Rz}	is the retention time of n-alkane peak eluted immediately before sample peak
$t^T_{\mathrm{R(z+1)}}$	is the retention time of n-alkane peak eluted immediately after sample peak
z	Is the carbon number of n-alkane peak eluted immediately before sample peak

3.6.4 Nuclear Magnetic Resonance (NMR)

For structure elucidations of synthetic mono- and diprenylated phlorbenzophenones, NMR spectroscopy was carried out at the lab of Prof. Dr. Ludger Ernst (Institute of Inorganic and Analytical Chemistry, TU Braunschweig) on Bruker Avance II 600 NMR spectrometer (600 MHz ^{1}H and 150 MHz ^{13}C). Samples were dissolved in a suitable deuterated solvent (CD_3OD for monoprenylated derivative and $CDCl_3$ for diprenylated) and analyzed at room temperature.

3.7 Laser scanning microscopy

Leaf discs of the lower epidermis of the transgenic leaves of *N. benthamiana*, four days after *A. tumefaciens* infiltration, were visualized by confocal laser scanning microscopy with the CLSM-510META scan head connected to an Axiovert 200M (Carl Zeiss, http://www.zeiss.de) as described previously (Gehl et al., 2009). The excitation was carried out by Argon LASER (488 nm for YFP and chlorophyll auto-fluorescence). Primary beam-splitting mirrors (458/514 or 488 nm) and a secondary beam splitter at 545 nm were used for the separation of emitted light. For the detailed examination of samples, C-Apochromat 403/1.2 water immersion objective was us

4 Results

4.1 Metabolic screening of PPAP aromatic cores from *H. sampsonii*

Hypericum sampsonii seedlings (six-week-old) were investigated for the presence of prenylated intermediates and their aromatic cores. Seedlings were extracted with MeOH and the resulting extract was analyzed by HPLC using gradient 4 (3.6.1). When comparing the UV spectra and the retention times (R_t) of the eluted compounds with authentic reference compounds, this preliminary investigation sketched an overview of the metabolite pattern of the *in vitro* plantlets. Peaks at R_t = 7.22, 8.77, 12.12 and 18.22 min showed 1367THX-like UV spectra. In addition, peaks at 18.54 and 24.85 min exhibited patulone-like spectra with a bathochromic shift in the absorption maximum from 292 to 318 nm. The peak at R_t = 22.47 min had a UV spectrum mimicking that of prenylated 246TrHBP with an absorption maximum at 314 nm. The most lipophilic peaks had the characteristic absorption maxima of reported benzoyl- and acylphloroglucinol derivatives from *H. sampsonii* (Hu and Sim, 2000), with the peaks at R_t = 22.01, 26.34, 29.65 and 32.41 min exhibiting similar UV spectra. The methanolic extract was fractioned *via* semi-preparative HPLC according to the retention times to result in five fractions **(Figure 16; Figure 17)**. The properties of each fraction are summarized in **Table 23**.

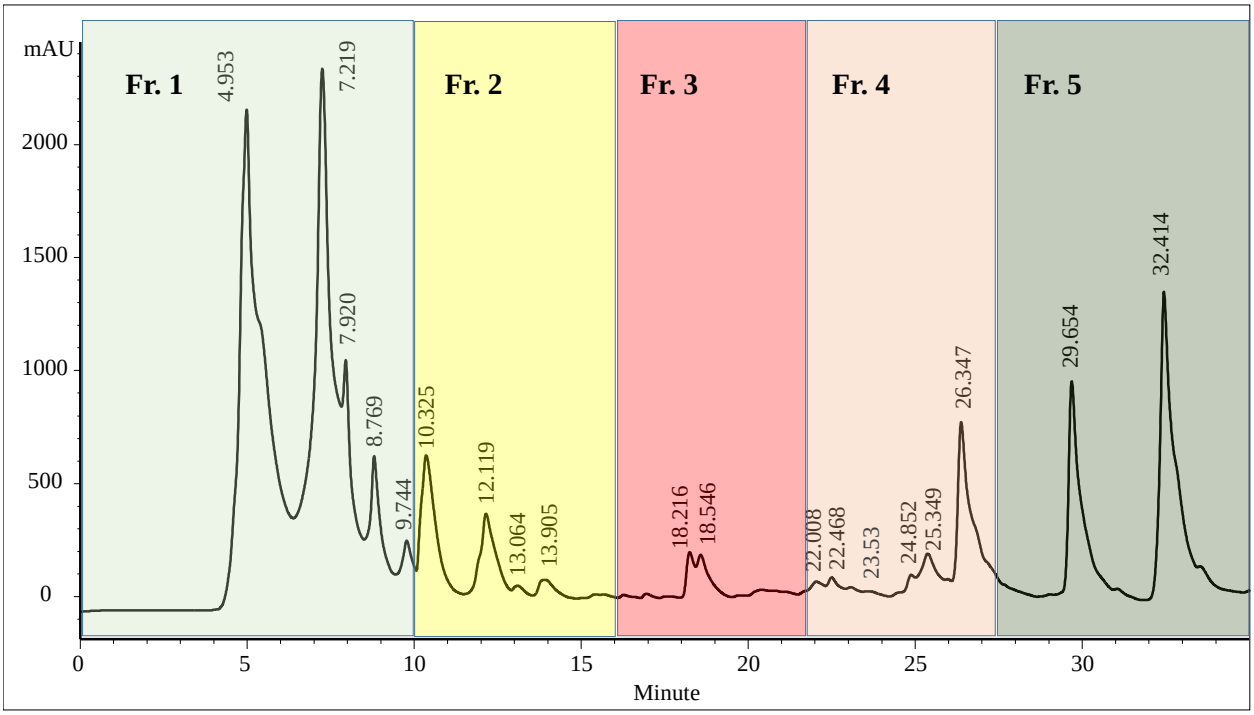

Figure 16: HPLC-DAD chromatogram of *H. sampsonii* MeOH extract. The color code correlates to the fractions shown in Figure 17.

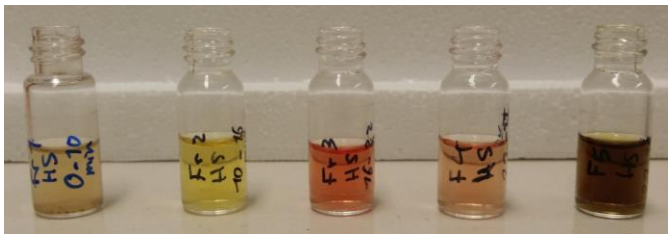

Figure 17: Photo of *H. sampsonii* extract fractions.

Table 23: Fractionation of the methanolic extract prepared from *H. sampsonii in vitro* seedlings.

Fr. no.	Collection time (min)	Color	Weight (mg)	Expected compounds
1	0- 10	Pale yellow	12.3	Polar compounds *
2	10- 16	Yellow	0.6	Aromatic cores
3	16- 22	Red	0.5	Prenylated intermediates
4	22- 27	Pale red	0.6	Prenylated intermediates
5	27- 35	Dark green	2.9	Highly prenylated compounds **

* For example amines, flavonoids, and phenolic acids
** Compounds having more than C_{10} prenyl moieties

The fractions obtained were deeply investigated by ESI-MS. The first fraction did not show significant results. On the other hand, the EMS-MS spectrum of Fr. 2 enclosed molecular ion peaks of some known compounds at m/z 195, 209, 229 and 259, which may correspond to $[M-H]^-$ of 246TrHiBP, 2MBP or 246TrHVP, 246TrHBP and 1367THX, respectively **(Figure 18 A)**. By studying the fragmentation spectra of those peaks, the presence of 246TrHiBP, 2MBP or 246TrHVP, 246TrHBP and 1367THX in this fraction was confirmed because their fragmentation patterns agreed with those of the reference compounds **(Figure 18 B, C, D, and E)**. The presence of acylphloroglucinols (246TrHiBP, 2MBP, and 246TrHBP) as potential prenylation acceptors was further confirmed through a GC-MS check of the fraction **(Figure 19)**. First, Fr. 2 was derivatized by silylation (3.6.3). A mixture of the three references, silylated Fr. 2 and an alkane mixture were injected in the same GC-MS run. According to the EI-MS fragmentation of the references **(Figure 19 A, B, and C),** an extracted ion chromatogram at m/z 431, 411, 397 and 369 was generated for both the reference mixture and Fr. 2. Peaks appeared at 17.9, 18.6 and 21.25, confirmed to be 246TrHiBP, 2MBP, and 246TrHBP, respectively. They shared the same R_t and EI-MS spectra as well as the retention indices calculated for the reference peaks, which were 1819.70, 1858.08 and 2050.86 for 246TrHiBP, 2MBP, and 246TrHBP, respectively. In addition, hits generated by the GC-MS database confirmed the aforementioned results.

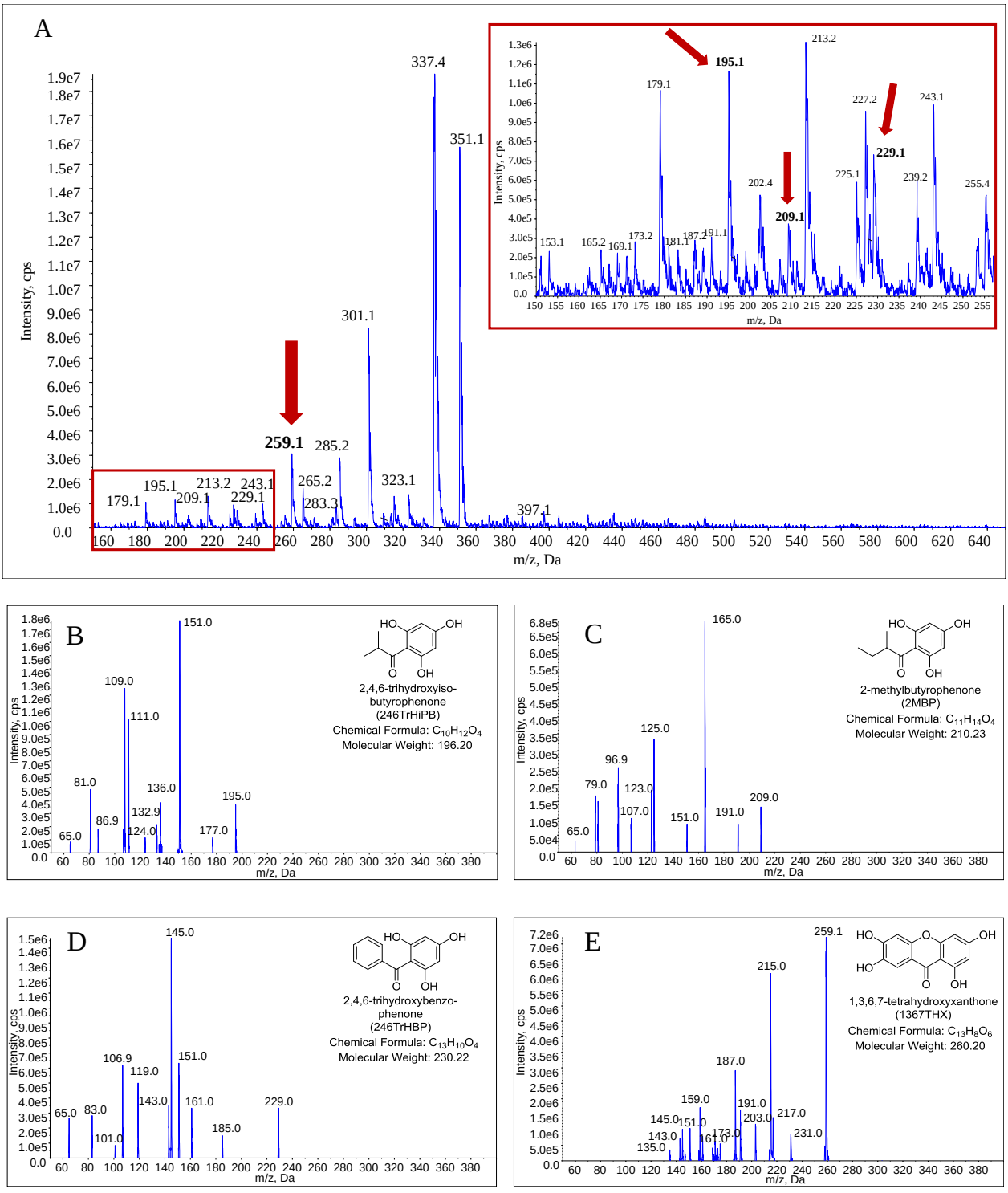

Figure 18: MS analyses of fraction 2 prepared from the methanolic extract of *H. sampsonii*. A) EMS spectrum showing molecular ion peaks corresponding to some known aromatic prenyl acceptors. B-E) ESI-MS/MS spectra of m/z 195 (B), 209 (C), 229 (D), and of 259 (E). Analyses were done in negative ion mode.

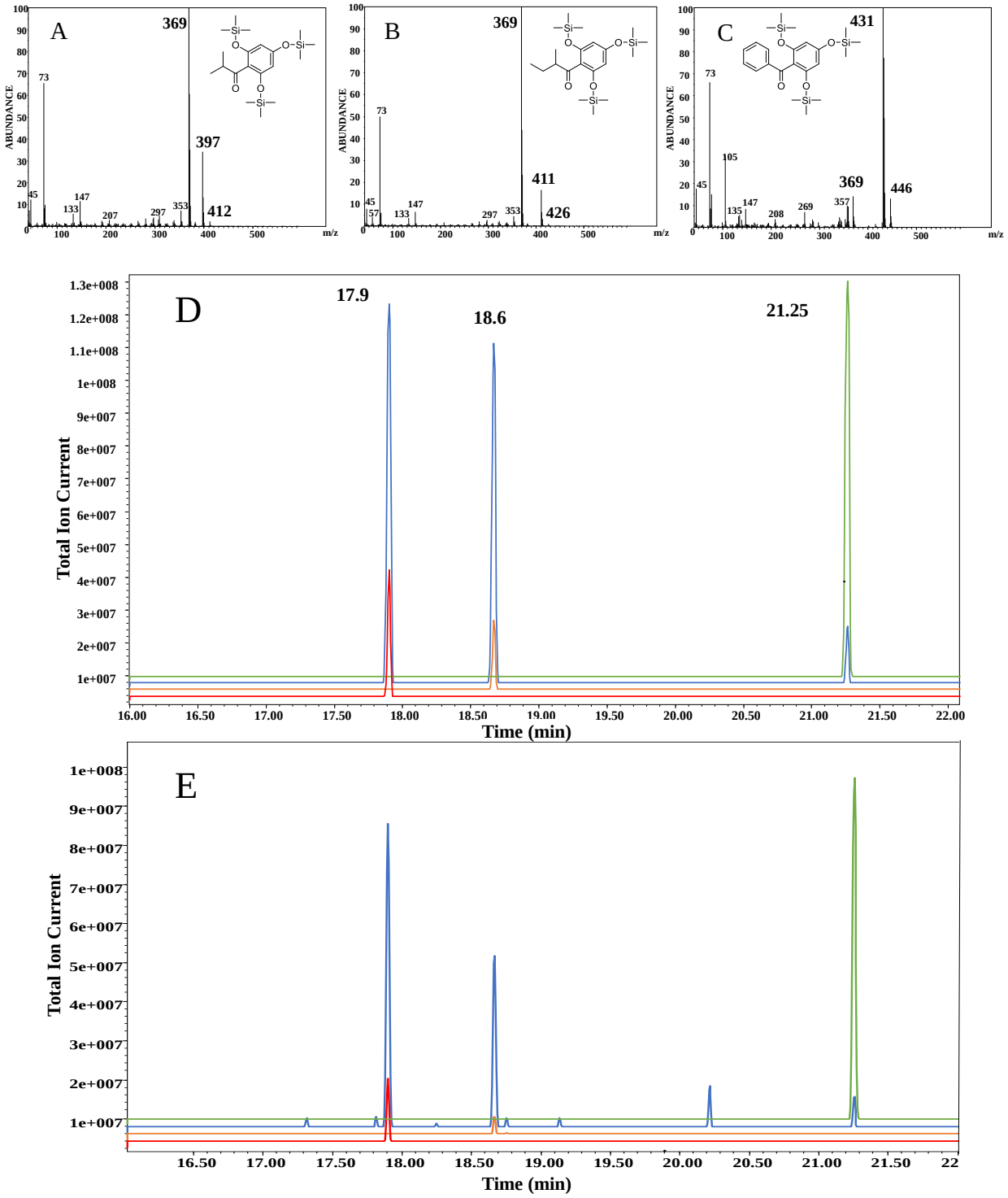

Figure 19: GC-MS analysis of fraction 2 prepared from the methanolic extract of *H. sampsonii*. A-C) EI spectra of 246TrHiBP (A), 2MBP (B), and246TrHBP (C). D, E) Extracted ion chromatograms at m/z 431 (green), 411 (orange), 397 (red) and 369 (blue) for reference mix (D) and fraction 2 (E).

Data acquisition from MS/MS analysis of fraction 3 confirmed the presence of a couple of prenylated xanthone intermediates. By comparing the mass fragmentation pattern of molecular ion peaks at $[M-H]^-$ m/z 327.1 and 395.2 with reference compounds, these ion peaks were elucidated as 8-prenyl-1,3,6,7-tetrahydroxyxanthone (8PX) and the diprenylated xanthone derivative patulone, respectively **(Figure 20 B and C)**. Another ion peak at $[M-H]^-$ m/z 365 was confirmed to be either 3,5-diprenylated-2,4,6-trihydroxybenzophenone or 3-geranyl-2,4,6-trihydroxybenzophenone due to its ESI spectrum (see 4.5.1 and 4.6.1.2). Mass fragmentation spectra of ion peaks at m/z 517, 519, 533 and 549 possibly correspond to the known compounds sampsonion B, a caged benzoylphloroglucinol derivative isolated previously from *H. sampsonii* extract (Hu and Sim, 2000), pseudohypericin, hypersampsone A and adhyperforin, respectively. The ion peak at m/z 519 proved to be pseudohypericin according to its ESI mass spectrum (Gadzovska et al., 2005), which justifies the red color of the fraction **(Figure 17; Figure 20 D)**. The MS/MS spectrum of the ion peak at m/z 549 did not agree with that of an authentic adhyperforin reference (Gaid et al., 2016) and it is still unknown. Analysis of fractions 4 and 5 gave more insight into the metabolite profiling of *in vitro*-grown *H. sampsonii* plants. Ion peaks found in those two fractions may coincide to molecular weights of known acyl- and benzoylphloroglucinol derivatives, but the reported spectral data for those metabolites is scarce. In addition, their structural elucidation is out of the scope of the current study.

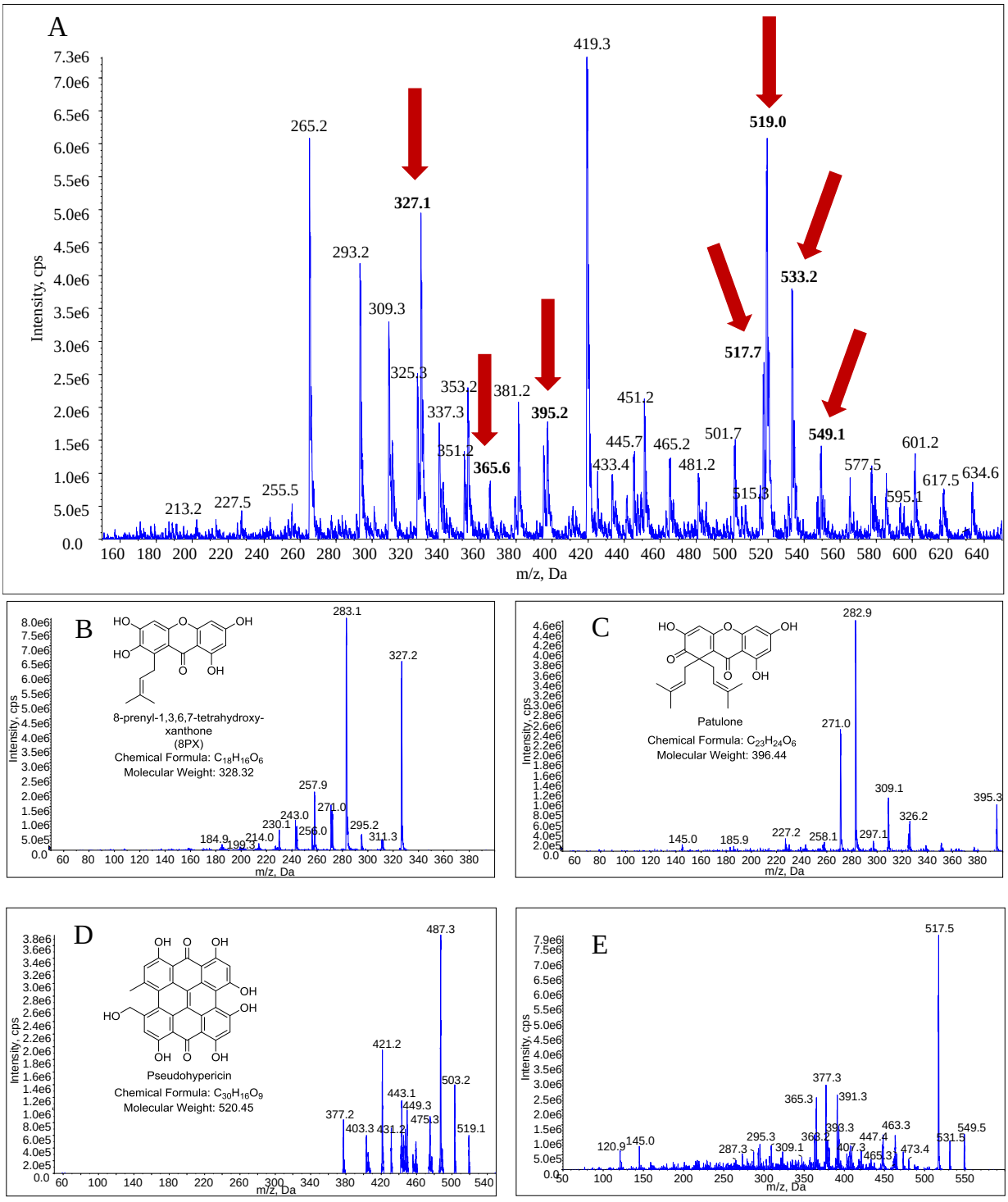

Figure 20: MS analyses of fraction 3 prepared from the methanolic extract of *H. sampsonii*. A) EMS spectrum of Fr. 3 showing molecular ion peaks corresponding to some known aromatic prenyl acceptors. B-E) ESI-MS/MS spectra of m/z 327 (B), 395 (C), 519 (D), and 549 (E). Analyses were done in negative ion mode.

4.2 RNA extraction from *H. sampsonii*

H. sampsonii RNA was extracted from the entire *in vitro* seedlings using the RNeasy® Plant Mini Kit and the LiCl precipitation method (3.3.1.1). The concentration of the isolated RNA, calculated as described under 3.3.2, was determined as 14, 260 and 280 ng/µl for RNA samples isolated by the RNeasy kit and the samples 1 and 2 from LiCl precipitation, respectively. The integrity of RNA samples was checked and verified by running them on agarose gels. The characteristic bands proving the presence of 28S and 18S ribosomal RNA subunits appeared clearly for the samples isolated according to Jaakola et al. (2001), which indicated the higher suitability of this method to isolate RNA from *H. sampsonii*. Furthermore, the integrity of RNA samples was confirmed by the band intensity ratio 28S/18S of ≈ 2 **(Figure 21)**. All samples showed good purity as indicated by the ratio $A_{260}/A_{280,}$ which was around 1.9 for all samples.

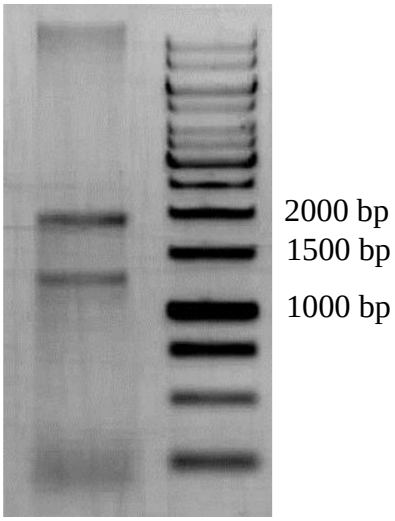

Figure 21: Agarose gel electrophoresis of one RNA sample after LiCl precipitation (750 ng) demonstrating 18S (below) and 28S (above) subunits. Right lane: ladder.

4.3 Cloning of prenyltransferases

4.3.1 Homology-based cloning of PT transcripts from *H. sampsonii*

Overexpression primers (forward and reverse primers) derived from prenyltransferases identified in other *Hypericum* species (Müller, 2013; Fiesel, 2016) were applied to the reverse-transcribed RNA derived from *H. sampsonii*. Nine primer pairs were designed according to an American transcriptome database for *H. perforatum* (http://medicinalplantgenomics.msu.edu/) and another three were derived from the results of a subtracted cDNA library of the xanthone-producing yeast-extract-treated *H. calycinum* cell culture (Gaid et al., 2012). cDNA from *H. sampsonii* was used as a template with each pair of primers. Some of the employed primers failed to give amplification products with *H. sampsonii* cDNA. In some cases, however, amplicons were formed. Each amplification product was purified from the gel, ligated to the vector pJet 1.2, and sequenced. Sequence information was blasted against the NCBI database using the "tblastn" online tool to examine homology with common PTs. Amplification results are listed in **Table 24**.

Table 24: Investigation of the amplification results obtained by applying *Hypericum* sp. derived primers to *H. sampsonii* cDNA.

Primer pair no.	Amplification	NCBI accession (nearest hit) *	Name of later *Hs*PT sequence
1	No		
2	Yes	PT, homogentisate solanesyltransferase, chloroplastic [*Ricinus communis*], XP_002531591.2, 39%	Core fragment of *Hs*PT5
3	Yes	Nonspecific amplification	
4	Yes	Nonspecific amplification	
5	yes	Nonspecific amplification	
6	yes	Nonspecific amplification	
7	yes	PT, hypothetical protein MANES_06G022400 [*Manihot esculenta*], OAY46726.1, 72%	*Hs*PT6. *H*sPT6a
8	Yes	Nonspecific amplification	
9	No		
10	Yes	PT, homogentisate solanesyltransferase, chloroplastic isoform X1 [*Jatropha curcas*], XP_012090862.1, 49%	*Hs*PT7
11	Yes	PT, probable homogentisate phytyltransferase 2, chloroplastic isoform X2 [*Musa acuminata* subsp. malaccensis], XP_018679846.1, 38%	*Hs*PT8
12	No		

* NCBI nearest hit, if available. The description follows the order: name of a hit, accession number and % identity.

4.3.2 Applying degenerated primers

All known plant membrane-bound aromatic prenyltransferases have two aspartate-rich motifs with the characteristic amino acid sequences N(D/Q)xxDxxxD and KDxxDxxGD (Akashi et al., 2009; Tsurumaru et al., 2010). In our group, degenerate primer pairs corresponding to the amino acid

sequences of these two conserved regions were previously derived (Müller, 2013), a forward primer from the 1st region and a reverse one from the 2nd motif. The forward degenerate primer was employed with either reverse degenerate, RACE long or RACE nested in so-called different amplification sets to amplify core fragments from 3′-ready *H. sampsonii* cDNA. The obtained amplification products were cut and purified from the gel, cloned into pJet. Many colonies belonging to each of the amplification sets were tested for the presence of the desired inserts (3.3.1.2). A number of plasmids showed positive inserts (5, 2 and 2), corresponding to the amplification set number 1, 2 and 3, respectively, and were sent to sequencing. After analysis of the sequence results, four different middle fragments were identified **(Table 25)**. The results from those amplifications are shown in **Figure 22**.

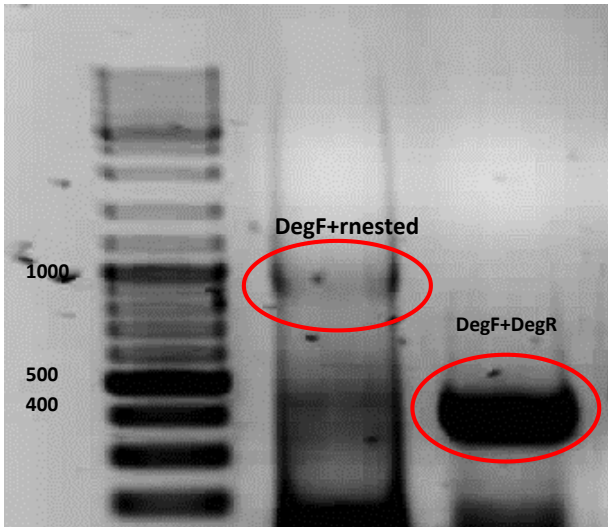

Figure 22: Agarose gel electrophoresis shows the amplification products obtained upon using the degenerate forward primer with either RACE_nested or degenerate reverse primer.

Table 25: Investigation of the amplification results from using degenerate primers with *H. sampsonii* cDNA.

Set no.	For. Primer	Rev. Primer	Plasmid no.	Product	Length	Temp. name	Core for
1	PT_Deg_for	PT_Deg_rev	1 2 4	Identical	396	Deg_2	*Hs*PT1, 1a, 1b
			5 6	Identical	402	Deg_6	*Hs*PT2
2	PT_Deg_for	RACE_long	1	1 fragment	690	Deg_L	*Hs*PT3
			2	Identical	648	Deg_S	*Hs*PT4
3	PT_Deg_for	RACE_nested	1				
			2	1 fragment			Nonspecific

4.3.3 Amplification of full-length PTs

4.3.3.1 *Hs*PT1

One forward and one reverse primer were derived from fragment Deg_2 **(Table 25)**, namely Hs_deg2_3R_for_1 and Hs_deg2_5R_rev_1 (2.4.6), to obtain 3′- and 5′- ends of the targeted *Hs*PT. Firstly, the 3′-RACE was done using 3′-ready cDNA as a template to yield a fragment with 453 bp including the stop codon, followed by a 3′-UTR of 151 bp and 29 adenine nucleotides. To extend this fragment toward its 5′-terminus, three forward primers from close *H. perforatum* PT sequences (having similarities towards the Deg_2 fragment from 71.4 to 71.9 %, namely 2F, 5F, and 6F; 2.4.1) were used as a forward primer mix together with the reverse primer *Hs*_deg2_5R_rev_1 in a single PCR round. An amplicon of 680 bp was gleaned. Overexpression primers were designed using assembled sequence information from 5′-end, core and 3′-end fragments. The ORF sequence of *Hs*PT1 was confirmed *via* proofreading, followed by sequencing of the blunt-ligated pJET 1.2/*Hs*PT1 construct (3.3.9.1).

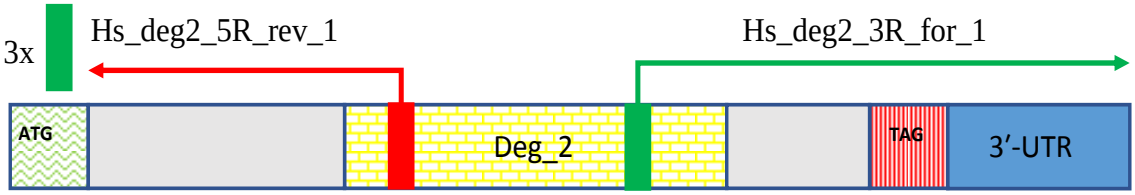

Figure 23: Schematic representation of RACE reactions done to obtain full-length *Hs*PT1, displaying the primers employed to get the sequence. The core fragment is displayed in yellow, missing sequence parts are shown in grey, forward primers and start codon are shown in green, the reverse primer is in red and the 3′-UTR is in blue.

The amplified sequence of *Hs*PT1 was composed of 1191 bp ORF followed by 151 bp 3′-UTR and a poly-A tail of 29 bases. It coded for 396 amino acids with a predicted molecular mass of 43.8 kDa and an isoelectric point of 9.55. The protein contained the two conserved regions NQIFDIETD and KDLPDVEGD. Based on the prediction by the online tool “TMHMM”, the number of transmembrane helices (TMH) for *Hs*PT1 was eight. *Hs*PT1 has a transit peptide length of 21 amino acids, which targets it to the chloroplasts according to the prediction results of the TargetP v1.1 online tool.

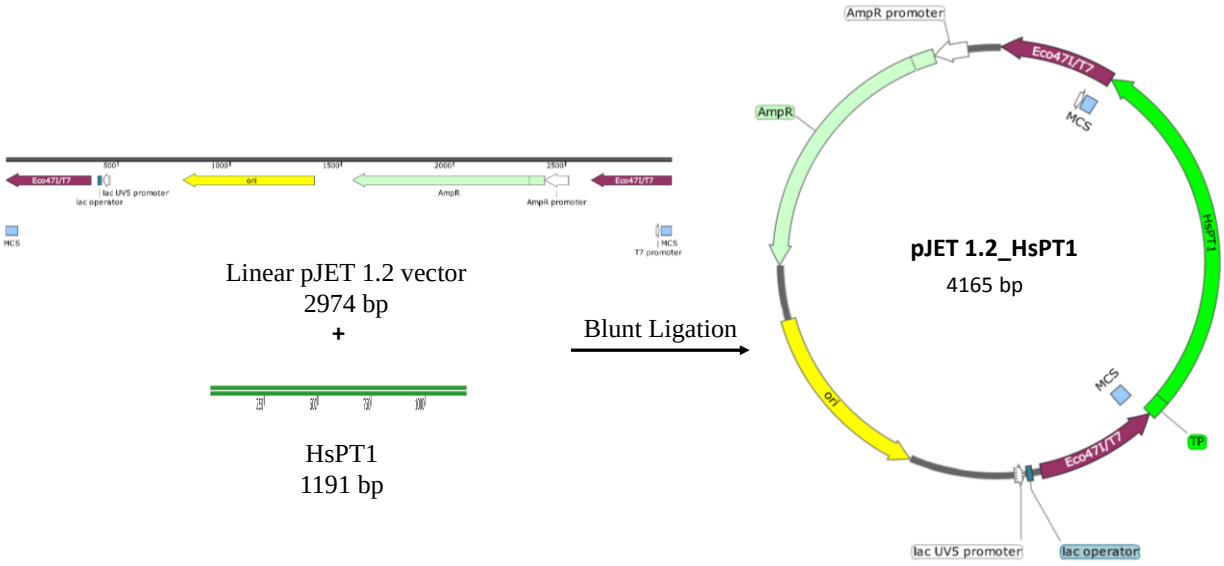

Figure 24: Representative example of an *Hs*PT1-pJET1.2 construct.

4.3.3.2 *Hs*PT1a

While screening positive clones for *Hs*PT1, two new sequences were observed. Both sequences shared high identity with *Hs*PT1 at nucleotide and protein levels. They were named *Hs*PT1a and *Hs*PT1b (4.3.3.3). *Hs*PT1a has an open reading frame of 1176 bp encoding 391 amino acids, which indicates a 15 bp (5 amino acids) shorter sequence due to a gap between positions 120 and 126 in *Hs*PT1 upon aligning the two sequences. It shared 99.6% and 99% similarity at the nucleotide and peptide levels, respectively. It was predicted that it has two TMH less, the same signal peptide length and the same target organ inside the cell as *Hs*PT1.

4.3.3.3 *Hs*PT1b

This sequence has a smaller gap of only six bp to give an ORF of 1185 bp and encodes for two amino acids less than does *Hs*PT1, which are between positions 71 and 74 upon comparing with the peptide sequence of the longer allele. At the nucleotide level, it showed similarity to *Hs*PT1 and *Hs*PT1a of 99.2% and 99.7%, respectively. Its anticipated properties using the online tools are the same as those of *Hs*PT1. Differences between those three polymorphs are demonstrated in **Figure 25**.

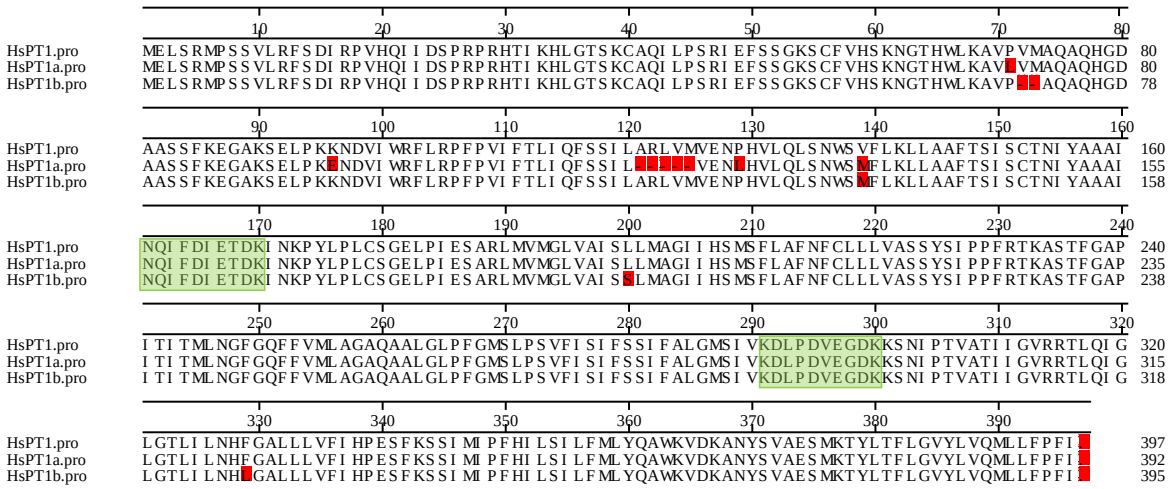

Figure 25: Multiple sequence alignment of the protein sequences of *Hs*PT1, *Hs*PT1a, and *Hs*PT1b, showing sequence differences and gaps among the three polypeptides. Differences are marked in red. Numbering line is according to the sequence of the longest allele, *Hs*PT1. Conserved aspartate motifs are marked in green.

4.3.3.4 *Hs*PT2

The fragment Deg_6 of 402 nucleotides was stretched to its 5′- and 3′-ends by applying RACE techniques. The forward gene-specific primer (2.4.2; Hs_deg6_3R_for_1) was used for 3′-racing to extend the middle fragment by 693 bp until the stop codon. To get the 5′-end of the gene, the first amplification was done using RACE_long and Hs_deg6_5R_rev_2 (2.4.2) as forward and reverse primers, respectively. The PCR product was purified and used as a template for a second amplification using the complementary sequence to RACE-Long primer, RACE_short in addition to Hs_deg6_5R_rev_3. Sequence results of the later amplicon confirmed the extension toward the start codon.

The resulting full-length sequence comprised 1452 nucleotides enclosing an ORF of 1179 bp surrounded by 71 bp 5′-UTR and 182 bp 3′ UTR with a tail of 20 adenine nucleotides. The recombinant polypeptide comprised 392 amino acid with a theoretical molecular weight of 42.9 kDa and pI of 9.88. The conserved motifs NQIFDIETD and KDISDVEGD were present, denoting an aromatic prenyltransferase, which was designated *Hs*PT2. The predicted number of TMH was eight. N-terminal 24 amino acids were expected to be the signal peptide targeting the gene product to the chloroplasts inside the plant cell.

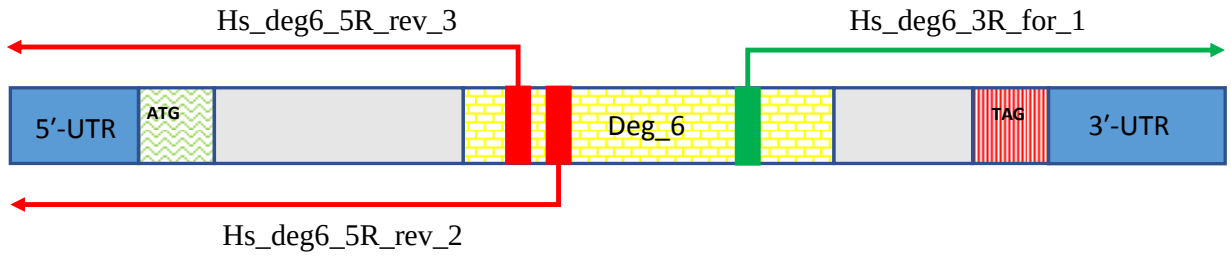

Figure 26: Schematic representation of RACE reactions performed to obtain full-length *Hs*PT2, displaying the primers employed to get the sequence. The core fragment is displayed in yellow, missing sequences are shown in grey, forward primers and start codon are shown in green, reverse primers and stop codon in red and UTRs are shown in blue.

4.3.3.5 *Hs*PT3

The fragment generated from the PCR employing the degenerate forward primer (PT_Deg_for) and RACE_long **(**Deg_L; **Table 25)** was extended to its 5′-end in a 2-stage-amplification where the product of the first amplification served as a template for a second amplification using the upstream primer (Hs_degL_5R_rev_2; 2.4.2) to get a full-length cDNA of 1179 bp flanked by 5′-UTR and 3′-UTR of 90 and 232 bp, respectively. The 3′-untranslated region was followed by 21 adenine bases. A protein sequence of 392 amino acids involved the conserved motives NQIFDLETD and KDIPDIEGD. The expected molecular weight of the protein was 43.1 kDa with a pI of 9.88. This protein has eight integrated membrane domains as anticipated by the TMHMM online tool. The results of SignalP prediction indicated a signal peptide length of 18 amino acids. Plastidial subcellular localization was shown by the results of TargetP v1.1 and chloroP online tools.

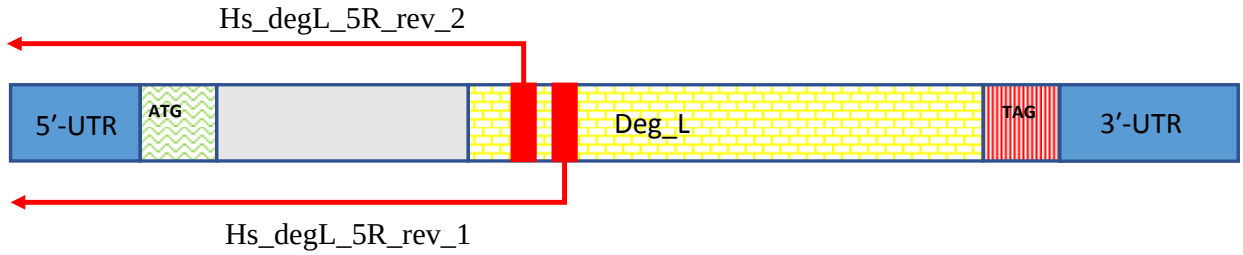

Figure 27: Schematic representation of RACE reactions performed to obtain full-length *Hs*PT3, displaying the primers employed to get the sequence. The core fragment is displayed in yellow, missing sequence part is shown in grey, forward primers and start codon are in green, reverse primer and stop codon are in red and UTRs are in blue

4.3.3.6 *Hs*PT4

Based on the core fragment, Deg_S, amplified from cDNA using the forward degenerate primer with reverse RACE_short primer **(Table 25)**, one reverse primer designated Hs_degS_5R_rev_1 was designed for extending this sequence to its 5′-end. This primer was used in an amplification program together with a mixture of nine primers belonging to previously cloned *H. perforatum*

prenyltransferases. The resulted amplicon had a length of 663 bp. By compiling it with the previously identified core fragment Deg_s, a full-length cDNA of 1354 nucleotides was obtained. 1173 bp, 152 bp, and 29 bp were identified as ORF, 3′-UTR, and poly A-tail, respectively. High fidelity PCR was done to proofread the sequence, which was named *Hs*PT4. The predicted protein product of 390 amino acids with a molecular mass of 43.4 kDa and pI 9.51 contained the two conserved regions NQIFDIEID and KDIPDIEGD. As predicted by online tools, it showed seven integrated membrane domains and a signal peptide of 18 amino acids targeting it to the plastidial membrane.

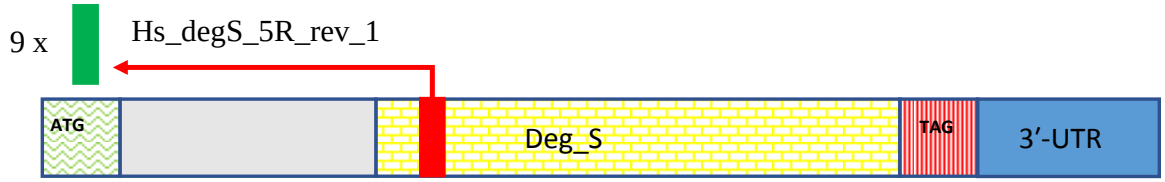

Figure 28: Schematic representation of RACE reaction performed to obtain full-length *Hs*PT4, displaying the primer employed to get the sequence. The core fragment is displayed in yellow, missing sequence part is shown in grey, forward primers and start codon are shown in green, stop codon is in red and the UTR is in blue.

4.3.3.7 *Hs*PT5

Although the PCR product primed by primer pair no. 2 (2.4.1) showed the size of a full ORF, sequence analysis of the PCR product lacked the correct stop codons. However, it shared 88% sequence identity to the ortholog sequence isolated from *H. calycinum* when the same primer pair was used. A forward primer (HsPT5_Fragment_f; 2.4.2) was designed from the regions near the 3′- ends of the CDS to serve in RACE reactions.

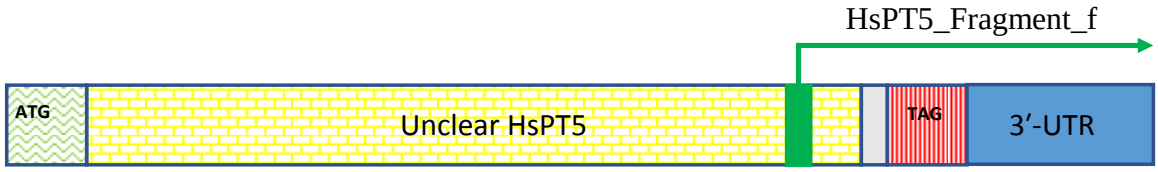

Figure 29: Schematic representation of RACE reactions performed to obtain full-length *Hs*PT5 displaying the primers employed to get the sequence. The core fragment is displayed in yellow, missing sequence parts are shown in grey, forward primers and start codon are shown in green, reverse primers and stop codon are in red and UTR is shown in blue.

The stop codon was identified to reveal an ORF of 1143 nucleotides, followed by 173 bp 3′-UTR and a poly-A-tail of 28 bp. The predicted protein structure consisted of 380 amino acids and housed the NQISDIETD and KDISDMDGD aspartate-rich motives. The protein had an expected size of 42.1 kDa and an isoelectric point of 9.43. SignalP assigned a transit peptide of 20 amino acids. The confirmed sequence was then submitted to TMHMM to show predictable nine membrane helices. Unexpectedly, the prediction results for localization of this protein were contradictory, as TargetP predicted it as mitochondrial and chloroP as plastidial.

4.3.3.8 *Hs*PT6

*Hs*PT6 was obtained as full-length coding sequence using the forward and reverse primers 7F and 7R, respectively (2.4.1). The proofread-confirmed sequence was 1188 bp long and encoded 395 amino acids with the conserved motives NQLTDIEID and KDIPDIDGD. It showed 97.4% and 96% sequence similarity to its homolog identified from *H. perforatum* by aligning their nucleotide and translated polypeptide sequences, respectively. The size of the translation-resulted protein was 44.6 kDa with a pI of 9.73. The number of membrane-spanning polypeptide chains of this PT was assigned to be seven with a targeting signal of 21 amino acids, which directs the enzyme to the membrane of the plastids.

4.3.3.9 *Hs*PT6a

Sequence analysis of *Hs*PT6 constructs revealed the existence of another shorter sequence. The new sequence named *Hs*PT6a had an open reading frame of 1176 bp. The protein product of this polymorph was 391 amino acids long and shared 86.7 and 85.2% sequence similarity to *Hs*PT6 and the *H. perforatum* homolog, respectively. Similar to its homologue in *H. perforatum*, *Hs*PT6a was predicted to have nine TMH. The length of the transit peptide (TP) was predicted to be three amino acids shorter than that of *Hs*PT6 but the online software failed to forecast the target of the protein inside the plant cell.

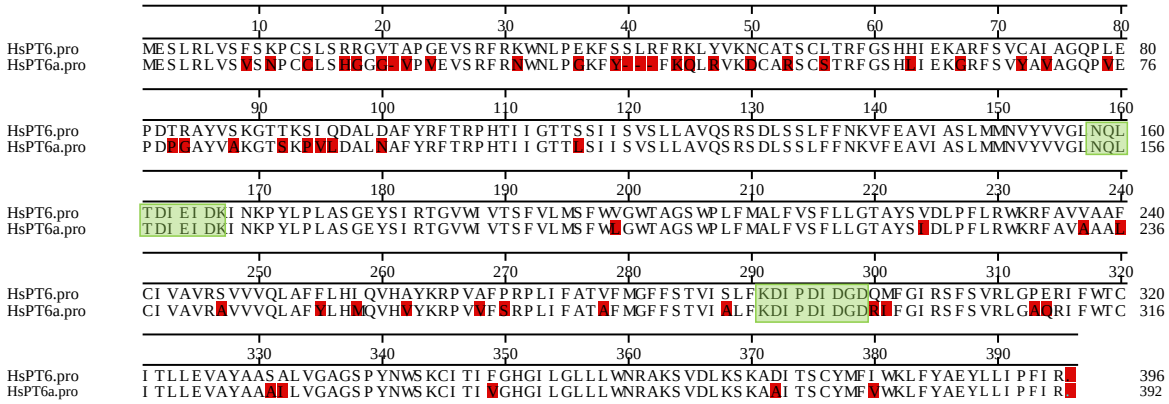

Figure 30: Alignment of the protein sequences of *Hs*PT6 and *Hs*PT6a showing sequence differences and gaps between the polypeptides. Differences are marked in red. Numbering is according to the sequence of the longer allele *Hs*PT6. Conserved aspartate motifs are marked in green.

4.3.3.10 *Hs*PT7

It was amplified from *H. sampsonii* cDNA adopting the primer pairs numbered 10 (2.4.1) in a touchdown PCR. The sequence of the amplified product was affirmed after a proofreading with a high fidelity DNA polymerase. The attained sequence was a PT ORF of 1176 bp encoding a protein chain of 391 amino acids with 43.7 kDa and a pI of 9.22. Similar to other aromatic PTs, the D-rich regions NQIFDVEID and KDLSDIDGD were identified. *Hs*PT7 had only eight bp difference from the corresponding coding sequence amplified with the same primers from *H. perforatum*. This enzyme has seven TMH. A short targeting signal was anticipated by SignalP, which is only 10

amino acids long and targets the protein to the membrane of chloroplasts, as predicted by the two online software with a high probability.

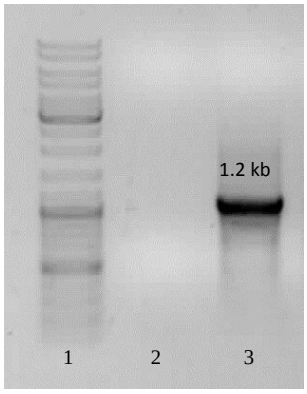

Figure 31: Representative example of agarose gel electrophoresis, displaying in lane 1 DNA marker, in lane 2 negative control PCR with no template and in lane 3 the PCR product that was called later *Hs*PT7.

4.3.3.11 *Hs*PT8

A primer pair (11F and 11R; 2.4.1) was employed to get an ORF, which had the tentative name of *Hs*PT8. Its length was likewise 1176 bp and encoded for a protein of 391 amino acids. The conserved regions NQIFDLETD and KDIPDIEGD were observed. The protein sequence possesses eight TMH, a molecular weight of 43.1 kDa and a pI of 9.88. The sequence shared identities of 88.1% and 83.7% with its *H. perforatum* homolog (*Hp*PT6) (Fiesel, 2016) at the nucleotide and amino acid levels, respectively, with sixty four-amino acids difference **(Figure 32)**. A plastidial targeting signal of 18 amino acids was anticipated. Upon alignment of all *Hs*PTs, it shared 99.6 % and 100 % similarities with nucleotide and peptide sequences of *Hs*PT3, amplified by degenerate primers and RACE (4.3.3.5). Thus, it was not considered for further investigation.

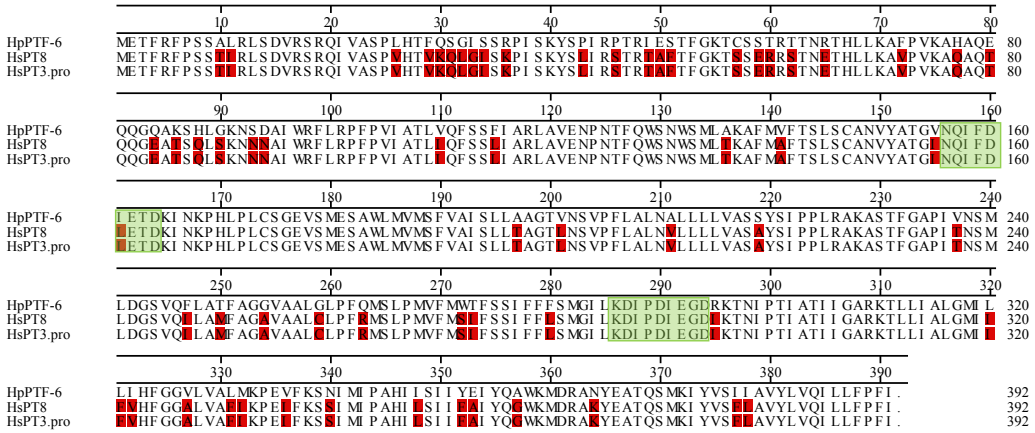

Figure 32: Alignment of the protein sequences of *Hp*PT6, *Hs*PT8, and *Hs*PT3 highlighting the differences between these polypeptides. The differences are marked in red. Numbering is according to the sequence of the *H. perforatum* homolog *Hp*PT6. Conserved aspartate motifs are marked in green.

Table 26: Summary of the properties of the PTs isolated from *H. sampsonii*.

Name	ORF (bp)	Peptide (Amino acid)	TMH	D-Motives*		Size (KDa)	pI	TargetP	ChloroP
*Hs*PT1	1191	396	8	NQIFDIETD	KDLPDVEGD	43.8	9.55	C	-
*Hs*PT1a	1176	391	6	NQIFDIETD	KDLPDVEGD	43.3	9.33	C	-
*Hs*PT1b	1185	394	8	NQIFDIETD	KDLPDVEGD	43.6	9.55	C	-
*Hs*PT2	1179	392	8	NQIFDIETD	KDISDVEGD	42.9	9.88	C	C
*Hs*PT3	1176	391	8	NQIFDLETD	KDIPDIEGD	43.1	9.88	C	C
*Hs*PT4	1173	390	7	NQIFDIEID	KDIPDIEGD	43.4	9.51	C	C
*Hs*PT5	1143	380	9	NQISDIETD	KDISDMDGD	42.1	9.73	M	C
*Hs*PT6	1188	395	7	NQLTDIEID	KDIPDIDGD	44.6	9.73	C	C
*Hs*PT6a	1176	391	9	NQLTDIEID	KDIPDIDGD	43.7	9.68	-	-
*Hs*PT7	1176	391	7	NQIFDVEID	KDLSDIDGD	43.7	9.22	C	C

* D is aspartate

4.4 Heterologous expression of prenyltransferases

According to the properties of the aforementioned PTs, which were confirmed by software prediction, all prenyltransferases are membrane-bound enzymes. Thus, the eukaryotic production platforms are expected to be superior to prokaryotes for the expression of the membrane integral proteins (Buchanan, 1999; Yazaki et al., 2002; Sasaki et al., 2008; Farrokhi et al., 2013; Ohara et al., 2013). This is discussed in detail in the discussion part under section 5.4. For the development of this study, two host systems for expression of identified aromatic *Hs*PTs were chosen, namely, the insect cell-baculovirus system and yeast cells.

Overexpression primers were designed for each prenyltransferase coding sequence from *H. sampsonii*. Specific restriction sites were added to every primer according to its sequence map and the multiple cloning site of the vector used later for expression (3.3.4). The coding sequence was then proofread from cDNA and subsequently cloned into the expression vector (3.3.9.2).

4.4.1 Building up expression constructs for the insect cell-baculovirus system

Each of the identified sequences and the vector pFastBacI were separately digested or, when possible, double-digested with corresponding restriction endonucleases **(Table 27)** and ligated into the expression cassette of the donor vector pfastBac under the control of the polyhedron promoter. After expression in *Sf9* cells (3.5.1), the microsomal protein fraction was collected and used in activity testing, as described under sections 3.5.1.2 and 3.5.5, respectively.

Table 27: The restriction enzymes used for digestion and subsequent cloning of the *Hs*PTs into pFastBacI carrier vector.

Gene Name	Restriction enzymes used	
	Forward	Reverse
HsPT1	*Eco*RI	*Xho*I
HsPT1a	*Eco*RI	*Xho*I
HsPT1b	*Eco*RI	*Xho*I

HsPT2	*BamH*I	*Kpn*I
HsPT3	*Eco*RI	*Xho*I
HsPT4	*BamH*I	*Kpn*I
HsPT5	*Eco*RI	*Xho*I
HsPT6	*BamH*I	*Kpn*I
HsPT6a	*BamH*I	*Kpn*I

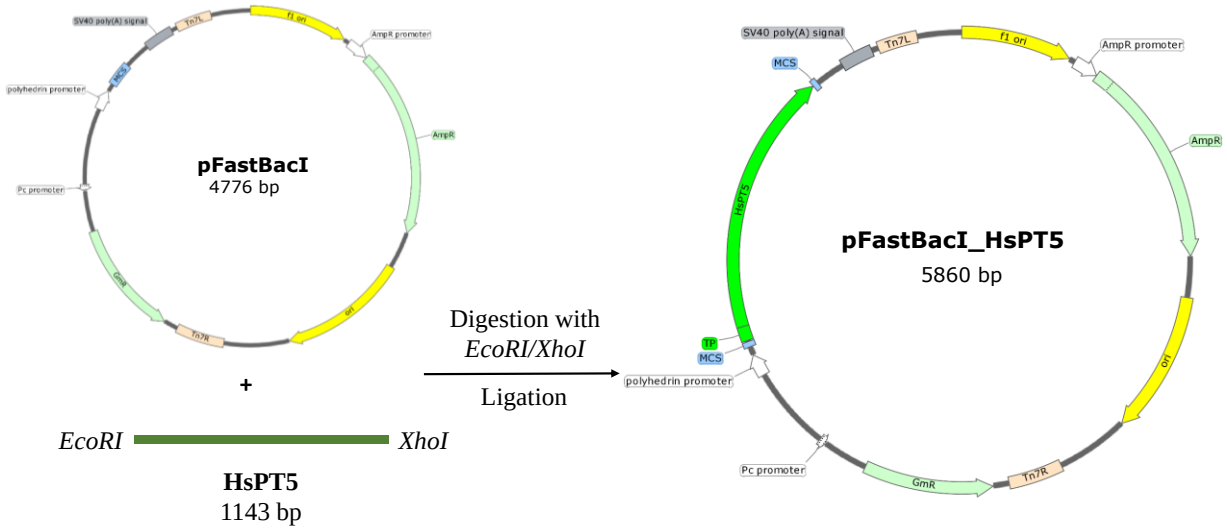

Figure 33: Construction of the pFastBacI_*Hs*PT5 plasmid by cloning the *EcoR*I/*Xho*I-digested *Hs*PT5 ORF into the donor vector *EcoR*I/*Xho*I-linearized pFastBacI for *Sf9* expression.

4.4.2 Building up expression constructs for yeast cells

Prenyltransferases cloned from *H. sampsonii* cDNA were integrated into pESC-URA. Firstly, genes and vector were independently digested or, when possible, double-digested with corresponding restriction enzymes and then ligated into either multiple cloning site 1 or 2 of the vector under the control of GAL 10 and GAL 1 promotors, respectively. The constructed plasmids were transformed into INVSc1 yeast cells for expression (3.5.1; 3.5.2), the membrane protein fraction was isolated and subjected to prenyltransferase assays, as described under sections 3.5.1.2, 3.5.2.2 and 3.5.5, respectively.

Table 28: The restriction enzymes and MCSs targeted for digestion and subsequent cloning of *Hs*PTs into pESC-URA vector.

Gene Name	Restriction enzymes used		MCS	Promoter
	Forward	Reverse		
HsPT1	*Eco*RI	*Pac*I	1	GAL 10
HsPT1a	*Eco*RI	*Pac*I	1	GAL 10
HsPT1b	*Eco*RI	*Pac*I	1	GAL 10
HsPT2	*BamH*I	*Kpn*I	2	GAL 1
HsPT3	*BamH*I	*Xho*I	2	GAL 1

HsPT4	*BamH*I	*Kpn*I	2	GAL 1
HsPT5	*Eco*RI	*Pac*I	1	GAL 10
HsPT6	*Eco*RI	*Pac*I	1	GAL 10
HsPT6a	*Eco*RI	*Pac*I	1	GAL 10
HsPT7	*Eco*RI	*Pac*I	1	GAL 10

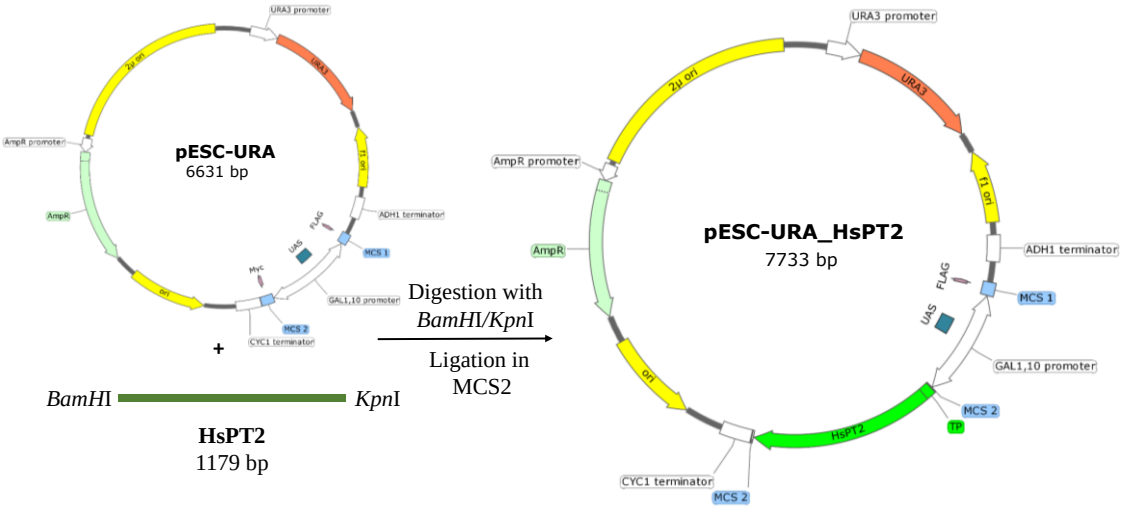

Figure 34: Construction of the pESC-URA_*Hs*PT2 plasmid by cloning the *BamH*I/*Kpn*I-digested *Hs*PT2 into MCS2 of the *BamH*I/*Kpn*I-linearized pESC-URA for expression in yeast.

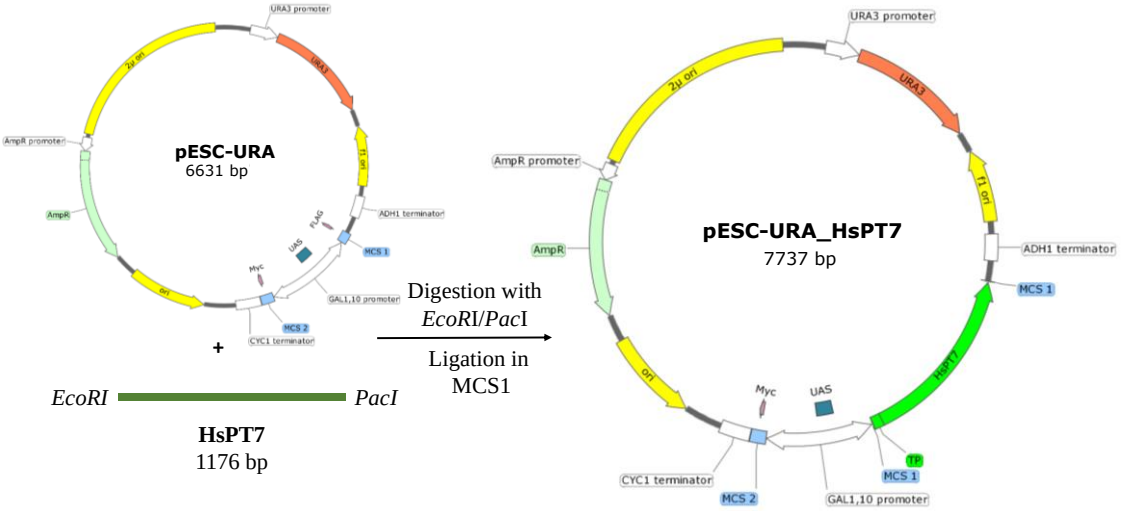

Figure 35: Construction of the pESC-URA_*Hs*PT7 plasmid by cloning the *Eco*RI/*Pac*I-digested *Hs*PT7 into MCS1 of the *Eco*RI/*Pac*I-linearized pESC-URA for expression in yeast.

4.5 Chemical synthesis of substrates

4.5.1 Synthesis of 3-mono- and 3,5-diprenylated-2,4,6-trihydroxybenzophenone

The prenylation reaction of 246TrHBP was performed as described under 3.2.1. After terminating the reaction, the mixture was subjected to fractionation by silica gel column chromatography. Three fractions were identified by TLC using a system of dichloromethane: methanol 95:5. Each fraction was then purified on a reversed phase silica gel column. Of fraction no. 2, 60 mg of yellow solid was purified, analyzed by HPLC-MS and NMR for detailed structure elucidation of the compound. Its MS/MS pattern showed the molecular ion peak at m/z 299 equivalent to $[M+H]^+$. According to the ^1H NMR and ^{13}C NMR data described under 3.2.1, the compound was identified as 3-prenylated-2,4,6-trihydroxybenzophenone (MPPBP; **Figure 36 A**).

Two compounds were purified from Fr. 1, both of which had a molecular weight of 366 as concluded from MS/MS spectral data. They were sent to NMR for structure elucidation. The NMR spectral data of the first one did not match the expected data of 3,5-diprenylated-2,4,6-trihydroxybenzophenone. The ^1H NMR spectrum contained two triplet peaks at a chemical shift of 1.6 ppm and 2.55 ppm, each integrating to two protons which could be interpreted as two adjacent methylene groups. The ^{13}C-DEPT spectrum showed two methylene carbons at 16 ppm and 32 ppm. One more quaternary carbon at 75 ppm was observed in ^{13}C NMR. The pure compound was identified as the benzopyran derivative of the diprenylated 246TrHBP, namely (5,7-dihydroxy-2,2-dimethyl-6-(3-methylbut-2-en-1-yl)chroman-8-yl)(phenyl)methanone. The second purified compound from Fr. 1 was identified after interpreting its spectral data to be the desired product, i.e. 3,5-diprenylated-2,4,6-trihydroxybenzophenone (DPPBP; NMR data of the compound are described under 3.2.1).

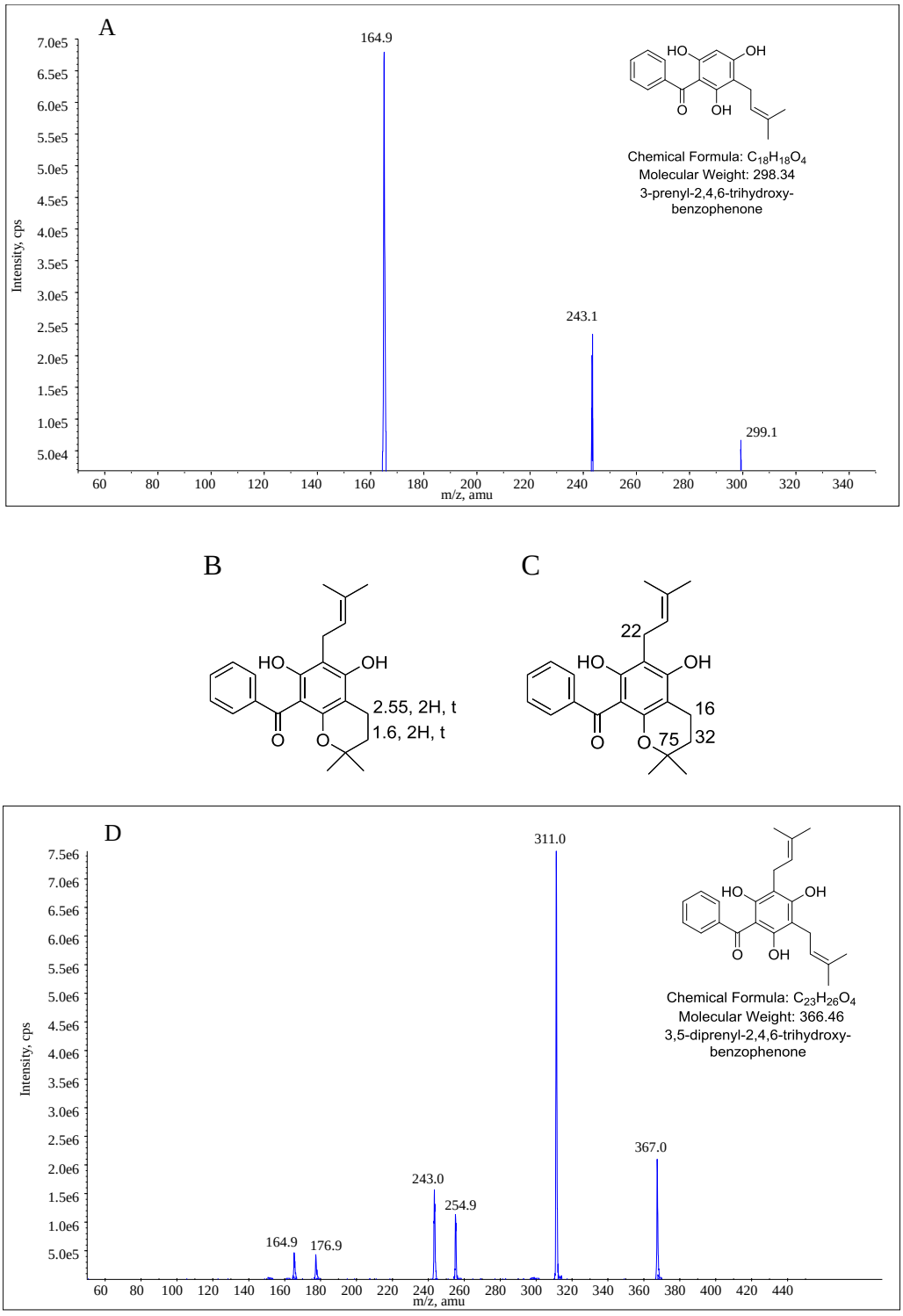

Figure 36: Spectral data of the products of the prenylation reaction of 246TrHBP. A) Positive ionization mode for EPI mass spectrum of MPPBP. B-C) Differential NMR data between benzopyran derivative and DPPBP for ^{1}H NMR (B) and ^{13}C NMR (C). D) The positive ionization mode EPI mass spectrum of DPPBP.

4.5.2 Synthesis of 2,4,6-trihydroxyisobutyrophenone

After analyzing the reaction mixture with TLC, a UV-active spot was observed at R_f= 0.37 corresponding to the reference 2,4,6-trihydroxyisobutyrophenone (246TrHiBP; 3.2.2). The UV-absorbing band was purified on preparative silica gel TLC plates (2.9.1) using a mobile system of petroleum ether: ethyl acetate 7: 3. The silica band bearing the desired spot was scratched and extracted with MeOH. The extract was dried under vacuum to result in 700 mg pure 2,4,6-trihydroxyisobutyrophenone residue, which was dissolved in MeOH to a concentration of 0.01 M.

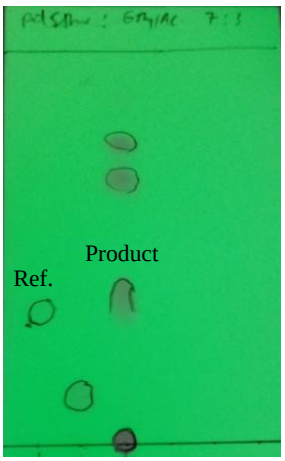

Figure 37: TLC analysis of the synthesis of 246TrHiBP under UV light (366 nm). Lane 1 is reference 246TrHiBP. Lane 2 is the starting material (phloroglucinol). Lane 3 is the reaction mixture after consumption of reactants.

4.5.3 Synthesis of geranyl (GPP) and prenyl (DMAPP) donors

GPP was synthesized as described under 3.2.4. Fractions collected from a cellulose column (each 15 ml) were subjected to cellulose TLC plates. After spraying with a freshly prepared sulfosalicylic acid solution, they were dried in the air and then sprayed with fresh ferric chloride solution (2.8.8). Fractions 79-112 exhibited white spots on a pink background with an R_f = 0.34. Pyrophosphate group-containing fractions were combined together and freeze-dried. A 380 mg amount of white powder with strong lemon odor was produced. The resulting solid was dissolved in 24.5 ml of MeOH: NH_4OH 7: 3 solution and divided into 1 ml aliquots, each having a final concentration of 50 mM. The product (tris-ammonium salt) was analyzed by MS/MS and it showed a molecular ion peak of 313 corresponding to the anion $[M-H]^-$ **(Figure 38)**. The fragmentation pattern of the product displayed peaks at m/z 295 corresponding to $[M-H_2O]^-$ and peaks at m/z 158.9 and m/z 78.8, which correspond to pyrophosphate and phosphate moieties, respectively (Jauhiainen et al., 2009).

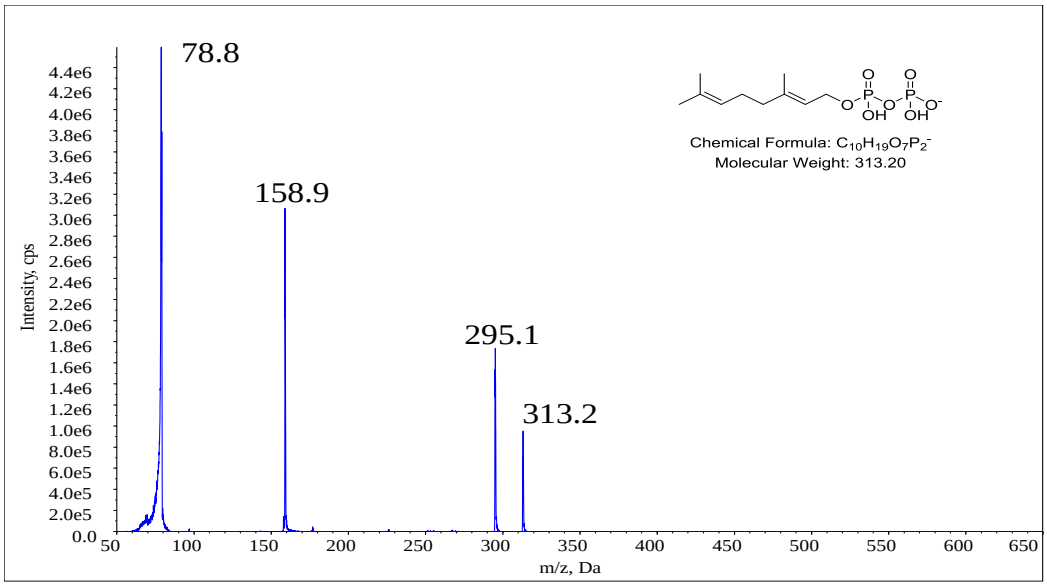

Figure 38: EPI mass spectrum of GPP in negative ionization mode.

DMAPP was synthesized and identified employing the same methods as for GPP. Its MS/MS analysis exhibited a molecular ion peak at m/z 245 of $[M-H]^-$. The corresponding peaks at *m/z* 226, *m/z* 159 and *m/z* 79 according to Jauhiainen et al. (2009) were also present. After lyophilization, 640 mg of DMAPP were produced, dissolved in MeOH: NH_4OH 7: 3 solution and divided into 1 ml aliquots, each having a final concentration of 50 mM.

4.5.4 Chemo-enzymatic production of 8-prenyl-1,3,6,7-tetrahydroxyxanthone

Since 8PX was accepted by both xanthone-related *H. sampsonii* PTs, it had to be produced in sufficient amounts to be used as a substrate for further characterization of *Hs*PT8PX and *Hs*PTpat (see later sections 4.6.2.1 and 4.6.2.2). The lack of a commercial source or a convenient synthetic scheme for 8PX necessitated its enzymatic production through the reaction of 1367THX with DMAPP catalyzed by *Hs*PT8PX. Thus, a 1000-fold scale-up was done applying the conditions that produce the maximum yield of the product (see later section 4.6.2.1). Both the prenyl donor and the aromatic substrate were incubated at 37 °C using Tris-HCl buffer pH 7 with $MgCl_2$ as a cofactor for 90 min. A portion of 1.5 mg pure 8PX (yield ≈ 60%) was produced, purified and further employed as a substrate.

4.6 Functional characterization of membrane proteins from *H. sampsonii*

4.6.1 *In vitro* activity screening

Microsomes isolated either from *Sf9*- or INV*Sc*1- cells were subjected to activity screening with a number of potential aromatic substrates including acyl- and benzoylphloroglucinol, xanthone and flavonoid chemical groups (**Figure 39**) in the presence of DMAPP or GPP as prenyl donors according to the method mentioned under section 3.5.5.1. The formed products were analyzed by HPLC-DAD and ESI-MS (3.6.1; 3.6.2). The detected activities not only indicated the presence of prenyltransferase activity but also proved the successful expression process.

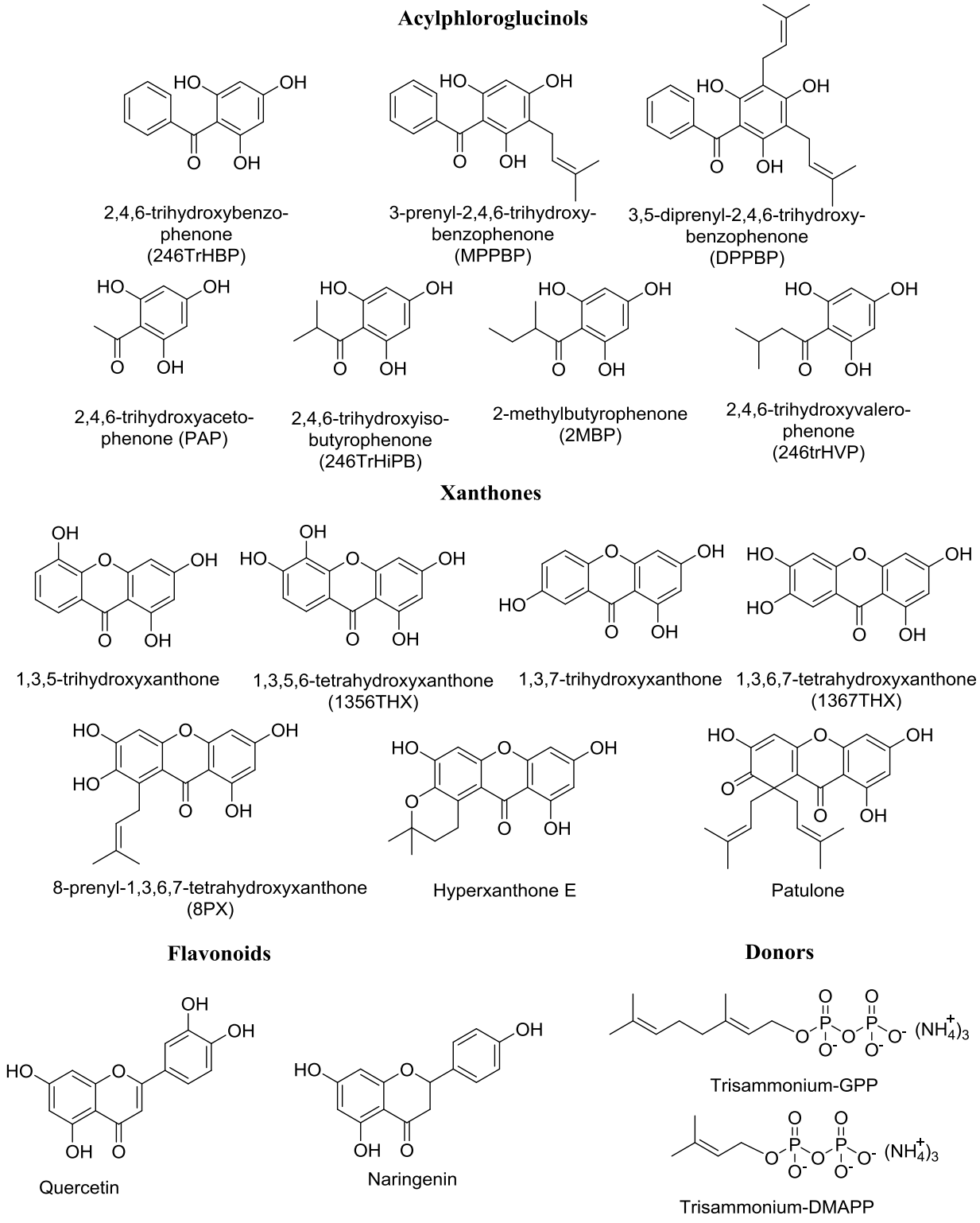

Figure 39: Aromatic prenyl acceptors and prenyl donors used for activity screening of *Hs*PTs.

4.6.1.1 Insect cell-expressed recombinant proteins

Activity assays of membrane preparations after individual expression of *Hs*PTs in insect cells with potential substrates are displayed in **Table 29**. Out of nine PTs, only *Hs*PT5 showed an activity under the applied test conditions. Enzymatic incubations of insect microsomes bearing *Hs*PT5 with 1,3,6,7-tetrahydroxyxanthone (1367THX) and DMAPP resulted in a single product. As indicated by HPLC-DAD analysis, the enzyme catalyzed the geminal addition of two prenyl groups to 1,3,6,7-tetrahydroxyxanthone at C-8, which interrupts the skeleton conjugation with simultaneous oxidation of the adjacent hydroxyl group **(Figure 40)**. The product has the same retention time (14.4 min) and the same characteristic absorption maxima at 236 and 292 nm like the authentic reference patulone (purified from cell suspension cultures of *H. calycinum* by Dr. Mariam Gaid). Furthermore, the fragmentation pattern in the mass spectral analysis was in agreement with the authentic reference compound exhibiting the molecular ion peak at m/z 395 equivalent to $[M-H]^-$. After confirmation of the activity, this recombinant enzyme was named after its product as *Hs*PTpat.

The three alleles, namely *Hs*PT1, *Hs*PT1a, and *Hs*PT1b showed prenyl- and geranyltransferase activity for substrates with an acylphloroglucinol skeleton. However, the observed activities were not reproducible, thus the approval of these *Hs*PTs as active prenyltransferases is still open.

Table 29: Summarized results of activity assays with insect cell-expressed *Hs*PTs

Recombinant PT	Accepted Substrates		Product
	Acceptor	Donor	
*Hs*PT1	?	?	
*Hs*PT1a	?	?	
*Hs*PT1b	?	?	
*Hs*PT2	-	-	
*Hs*PT3	-	-	
*Hs*PT4	-	-	
*Hs*PTpat	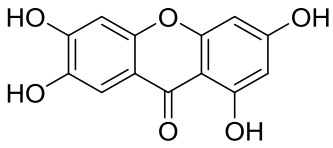 1,3,6,7-tetrahydroxyxanthone	DMAPP	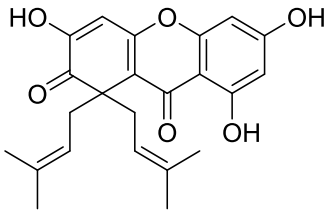 Patulone
*Hs*PT6	-	-	

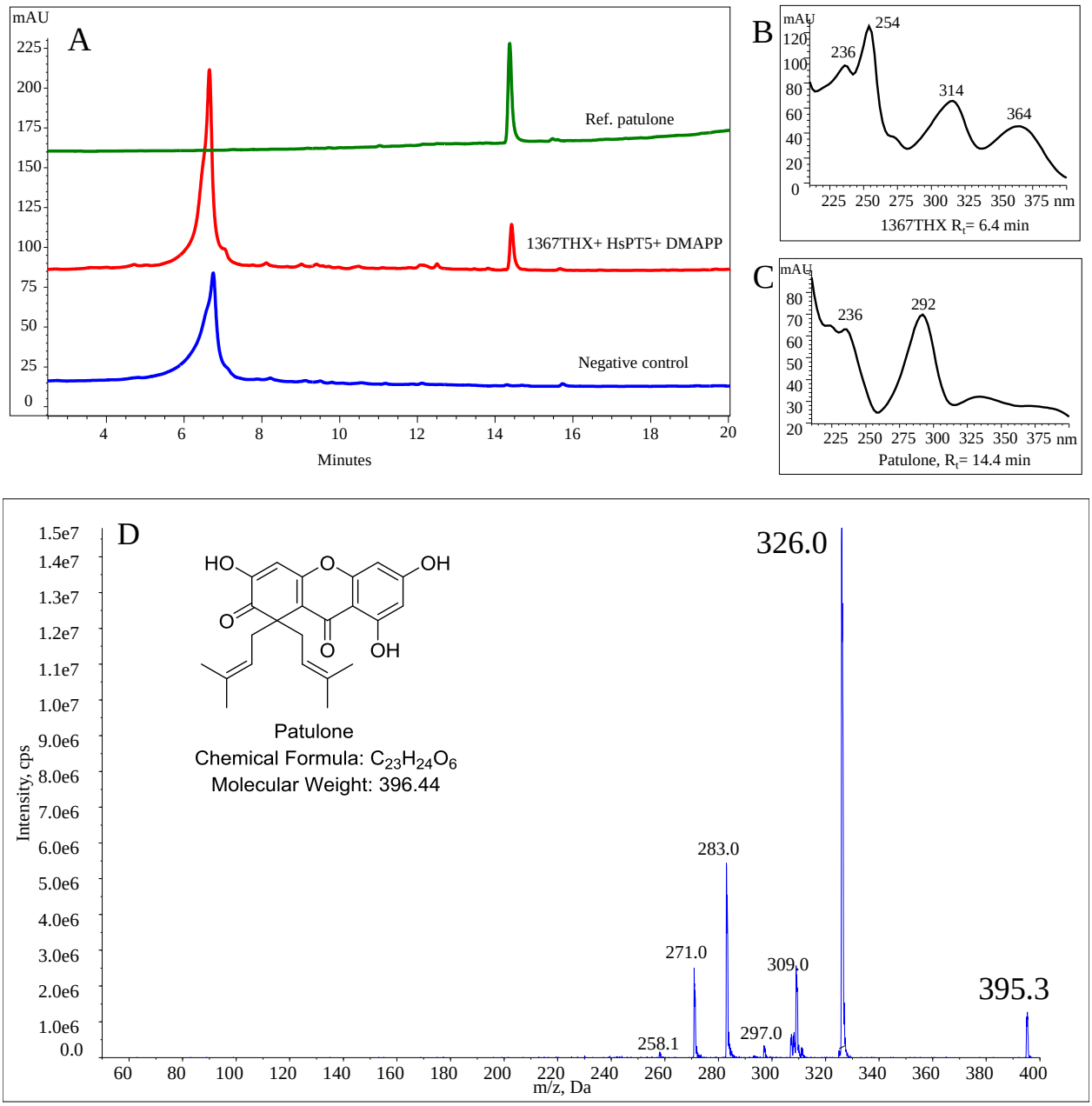

Figure 40: Incubation of insect microsomes containing *Hs*PTpat with 1367THX. A) Stacked HPLC-DAD chromatograms for enzymatic reaction (red), standard (green) and negative control (blue). B and C) UV spectra of the aromatic substrate (B) and enzymatic product (C). D) Negative ion EPI mass spectrum of the enzymatic product.

4.6.1.2 Yeast cell-expressed recombinant proteins

Expression of *Hs*PTs in yeast exhibited activity profiles different from those expressed in insect cells (**Table 30, page 99**). The enzymatic activity of the microsomal preparations from yeast cells harboring the pESC-URA-*Hs*PT2 ORF was tested *via* incubation with potential substrates belonging to different chemical classes (**Figure 39**). Products were analyzed as discussed in the

methods section (3.6). *Hs*PT2 was able to convert 1,3,6,7-tetrahydroxyxanthone (1367THX) to its 8-monoprenyl derivative as the major product **(Figure 41 A).** Thus, the name *Hs*PT8PX was used to refer to this enzyme. The product peak shared the retention time (R_t = 12.2 min) and UV spectrum with authentic 1,3,6,7-tetrahydroxy-8-prenylxanthone (8PX; **Figure 41 C**). The mass spectra (molecular ion peak at m/z 327 equivalent to $[M-H]^-$) of the enzymatic product and the reference compound were in agreement (Fiesel et al., 2015). 8PX was further metabolized by the microsomal fraction *via* the addition of another prenyl group to the same carbon atom (C-8) to produce patulone (8,8-diprenyl-1,3,6,7-tetrahydroxyxanthone) as a minor product. Direct use of 8PX as a substrate in a separate incubation led to the formation of patulone as the sole product **(Figure 42)**. The retention time and UV spectrum, as well as the molecular ion peak and MS/MS fragmentation pattern of the enzymatically formed patulone, matched those of an authentic reference compound.

When the yeast-expressed *Hs*PTpat (previous name *Hs*PT5) was incubated with 1367THX, it gave the same results as the insect-expressed protein. The diprenylated xanthone derivative patulone was formed **(Figure 40)**. *Hs*PTpat was able to catalyse the enzymatic conversion of 8PX to patulone **(Figure 43)**. Thus, the recombinant protein *Hs*PTpat produced only patulone as a sole product, independent of using 1367THX or its 8-prenyl derivative as a prenyl acceptor.

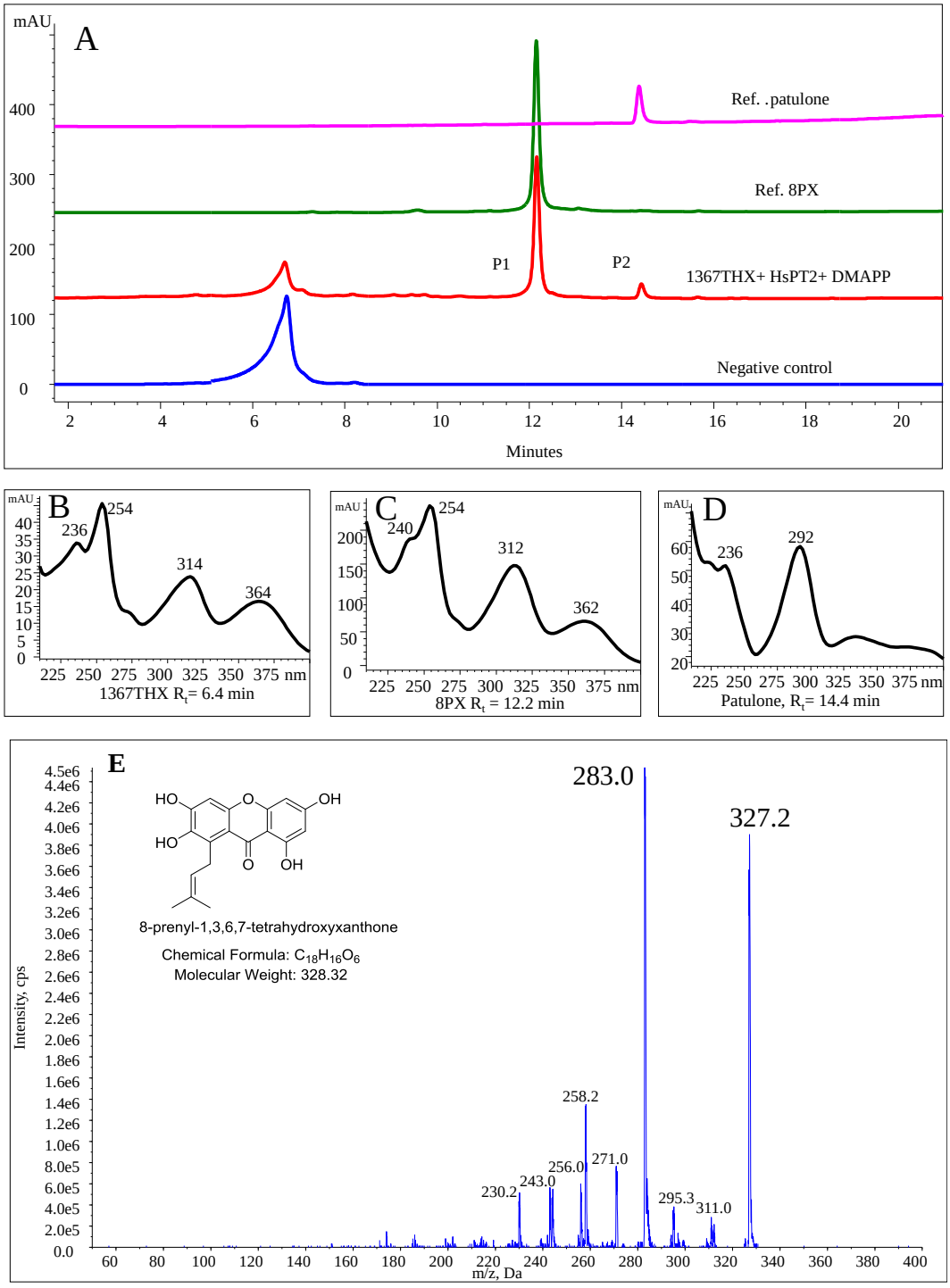

Figure 41: Incubation of yeast microsomes containing *Hs*PT8PX with 1367THX. A) Stacked HPLC-DAD chromatograms for the enzymatic reaction, standards, and negative control. B) UV spectrum of the aromatic substrate, 1367THX. C) UV spectrum of the enzymatic product P1. D) UV spectrum of the enzymatic product P2. E) EPI mass spectrum of the main enzymatic product.

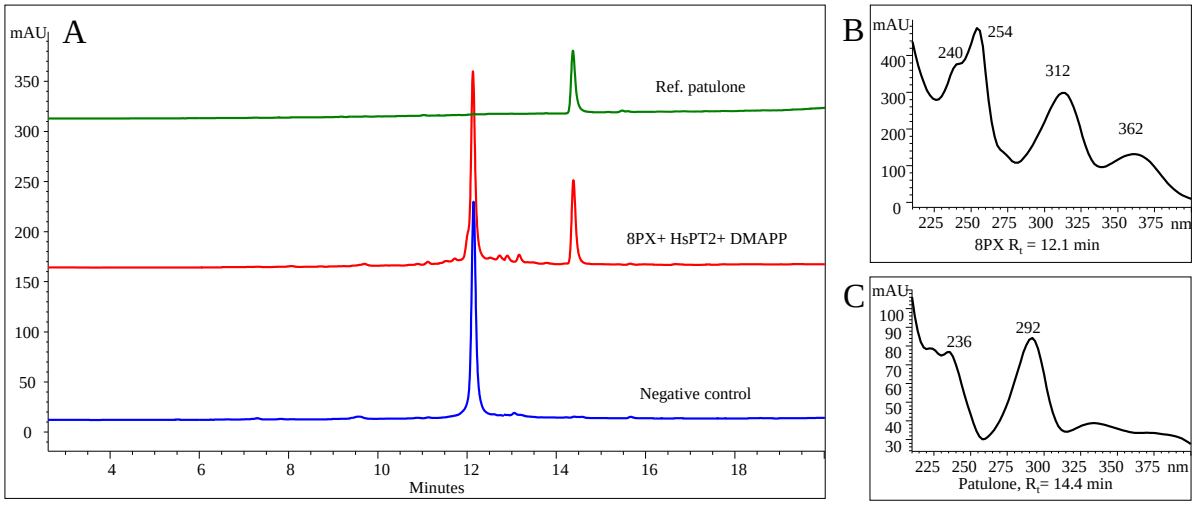

Figure 42: Incubation of yeast microsomes containing *Hs*PT8PX with 8PX. A) Stacked HPLC-DAD chromatograms for enzymatic reaction, references and negative control. B and C) UV spectra of the aromatic substrate (B) and enzymatic product (C).

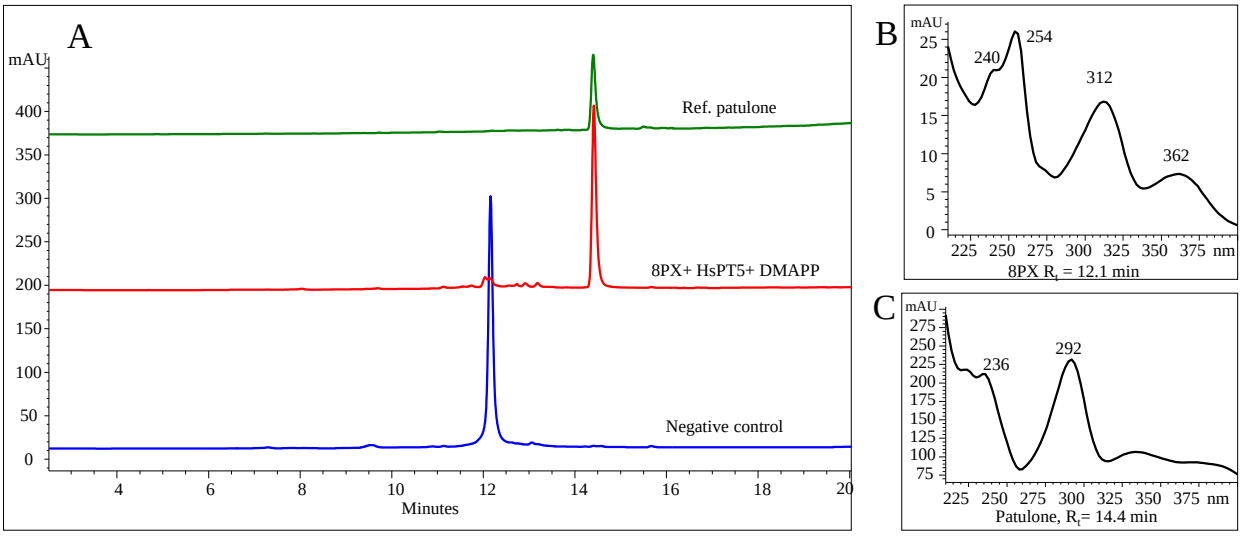

Figure 43: Incubation of microsomes containing *Hs*PTpat with 8PX. A) Stacked HPLC-DAD chromatograms for the enzymatic reaction, reference, and negative control. B and C) UV spectra of the aromatic substrate (B) and the enzymatic product (C).

A third recombinant yeast-expressed prenyltransferase from *H. sampsonii*, namely *Hs*PT7, exhibited a geranyl transferase activity, this time, with unsubstituted acyl- and benzoylphloroglucinol aromatic substrates. Thus, it produces mono-geranyl derivatives from each of the accepted substrates belonging to this group. *Hs*PT7, after confirmation of its geranyl transferase activity, was given the name *Hs*PTAPG.

An enzymatic assay of *Hs*PTAPG with 2,4,6-trihydroxyisobutyrophenone (246trHiBP) resulted in the formation of a single product (R_t = 15.0 min; **Figure 44 A**). This product was identified as 3′-geranyl-2,4,6-trihydroxyisobutyrophenone (G-246TrHiBP). Its UV spectrum showed a

characteristic absorption maximum at 292 nm, which resembled that of the substrate with ≈ 4 nm bathochromic shift **(Figure 44 B and C)**. In addition, its MS spectra showed molecular ion peaks at m/z 331 and 333 equivalent to $[M+H]^-$ and $[M-H]^+$, respectively **(Figure 44 D and E)**, which matched previously published data (Li et al., 2015).

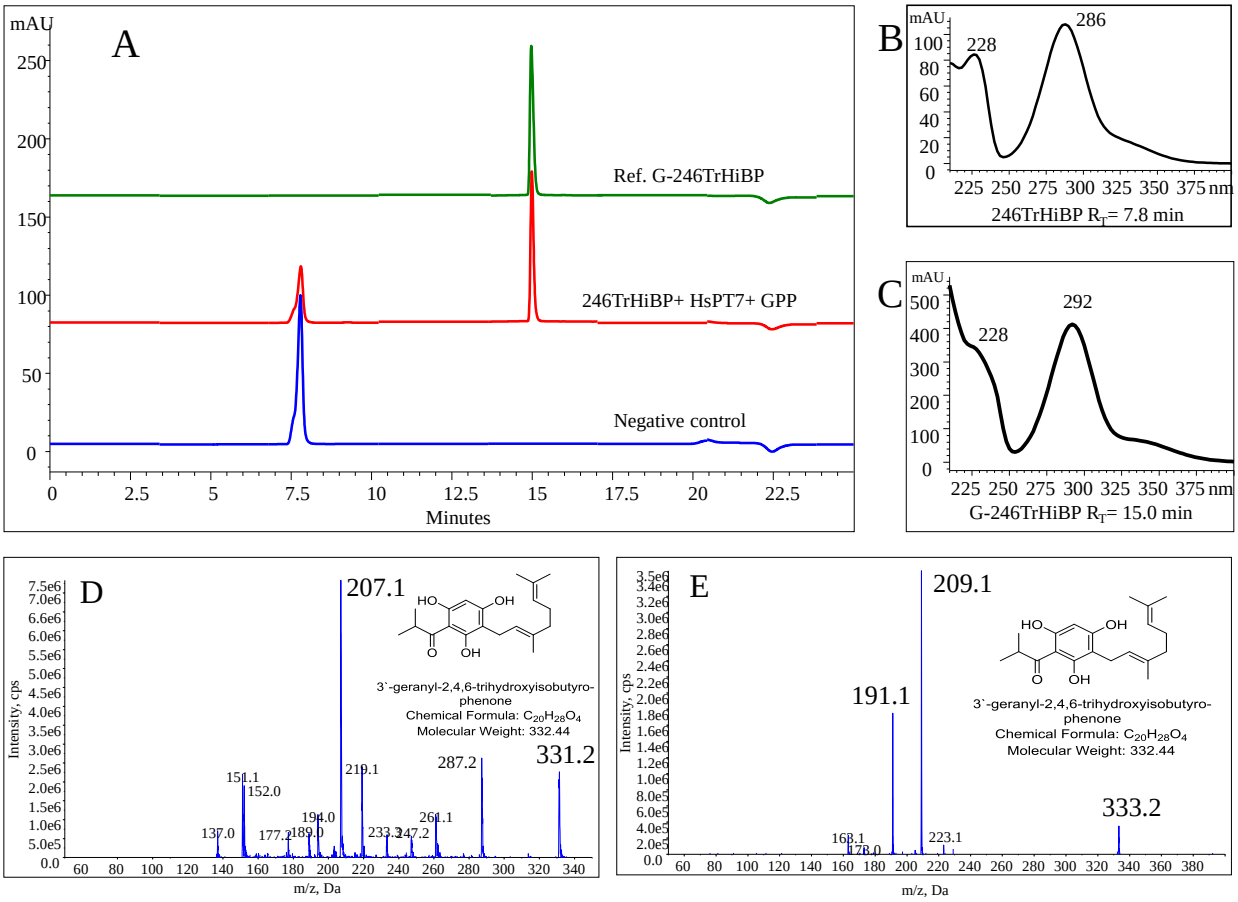

Figure 44: Incubation of yeast microsomes containing *Hs*PTAPG with 246TrHiBP. A) Stacked HPLC-DAD chromatograms for enzymatic reaction (red), reference (green) and negative control (blue). B and C) UV spectra of the aromatic substrate (B) and enzymatic product (C). D and E) EPI mass spectra in negative ion mode (D) and positive ion mode (E).

Another acylphloroglucinol derivative was accepted when incubated with recombinant *Hs*PTAPG, namely, 2,4,6-trihydroxy-2-methylbutyrophenone (2MBP; synthesized in our laboratory by a former colleague, Marco Grull). A peak at R_t = 15.2 min was detected with a similar UV spectrum to that of the substrate, again with a bathochromic shift, to have an absorption maximum at 292 nm. MS/MS fragmentation of the product demonstrated a molecular ion peak at m/z 347 equivalent to $[M+H]^+$ **(Figure 45 D)**. Accordingly, the product was identified as 2-methyl-3´-geranyl-2´,4´,6´-trihydroxybutyrophenone (G-2MBP).

Similarly, membrane preparations from yeast were incubated with the benzoylphloroglucinol derivative 2,4,6-trihydroxybenzophenone to bring out one product with R_t = 14.8 min (**Figure 46**),

whose UV spectrum had an absorption maximum at 314 nm with ≈ 8 nm red-shift from its starter substrate (absorption maximum at 306 nm; **Figure 46 B and C**). The product was identified as the mono-geranylated derivative of the substrate according to its MS/MS pattern with the molecular ion peak at m/z 367 equivalent to $[M+H]^+$ (**Figure 46 D**). Other acyl- and benzoylphloroglucinols were poorly accepted substrates and the resulting products were, according to their R_t and UV patterns, identified as mono-geranylated derivatives of the corresponding substrates.

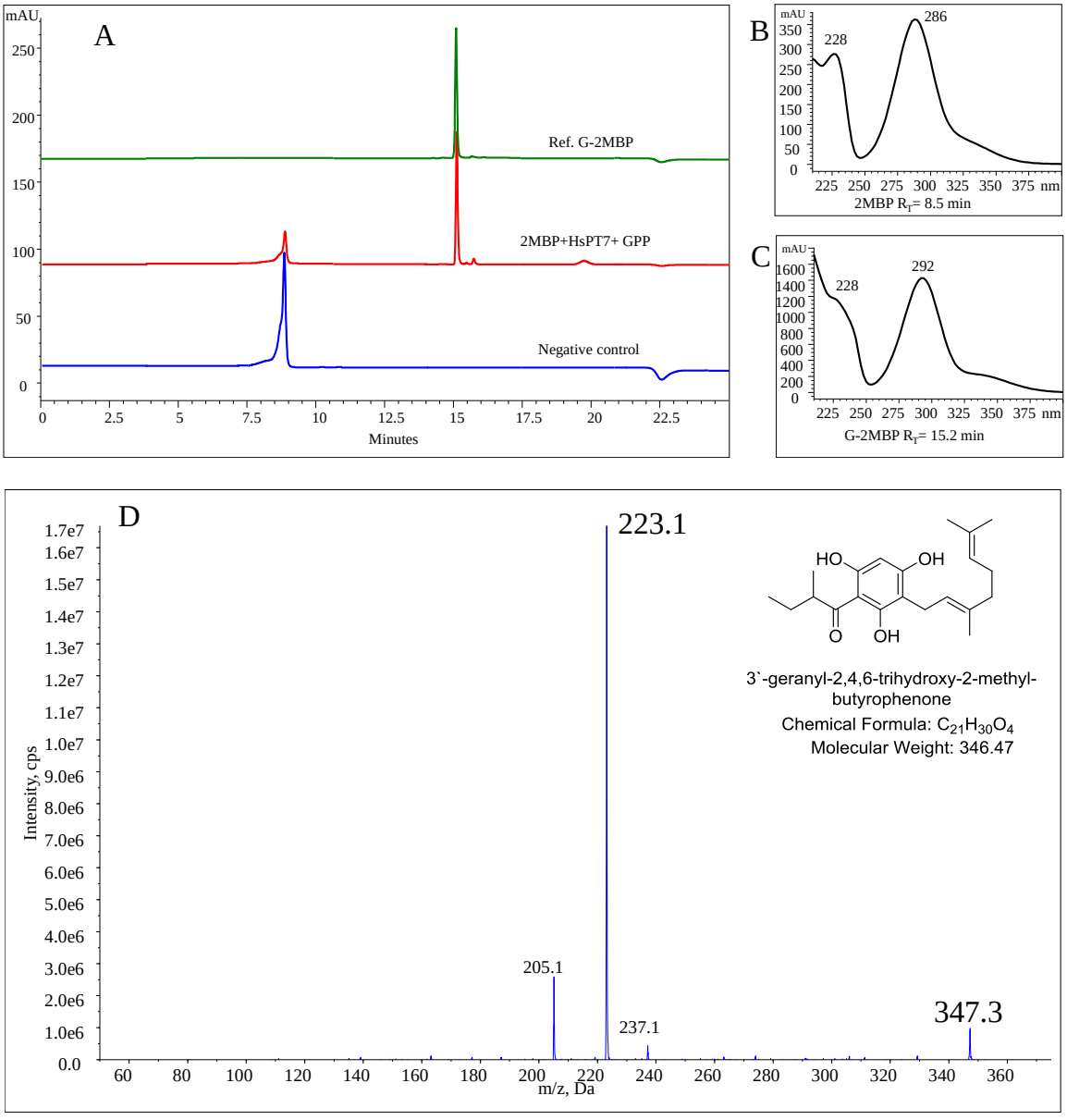

Figure 45: Incubation of yeast microsomes containing *Hs*PTAPG with 2MBP. A) Stacked HPLC-DAD chromatograms for enzymatic reaction (red), reference (green) and negative control (blue). B and C) UV spectra of the aromatic substrate (B) and enzymatic product. D) The positive ion mode EPI mass spectrum of the enzymatic product.

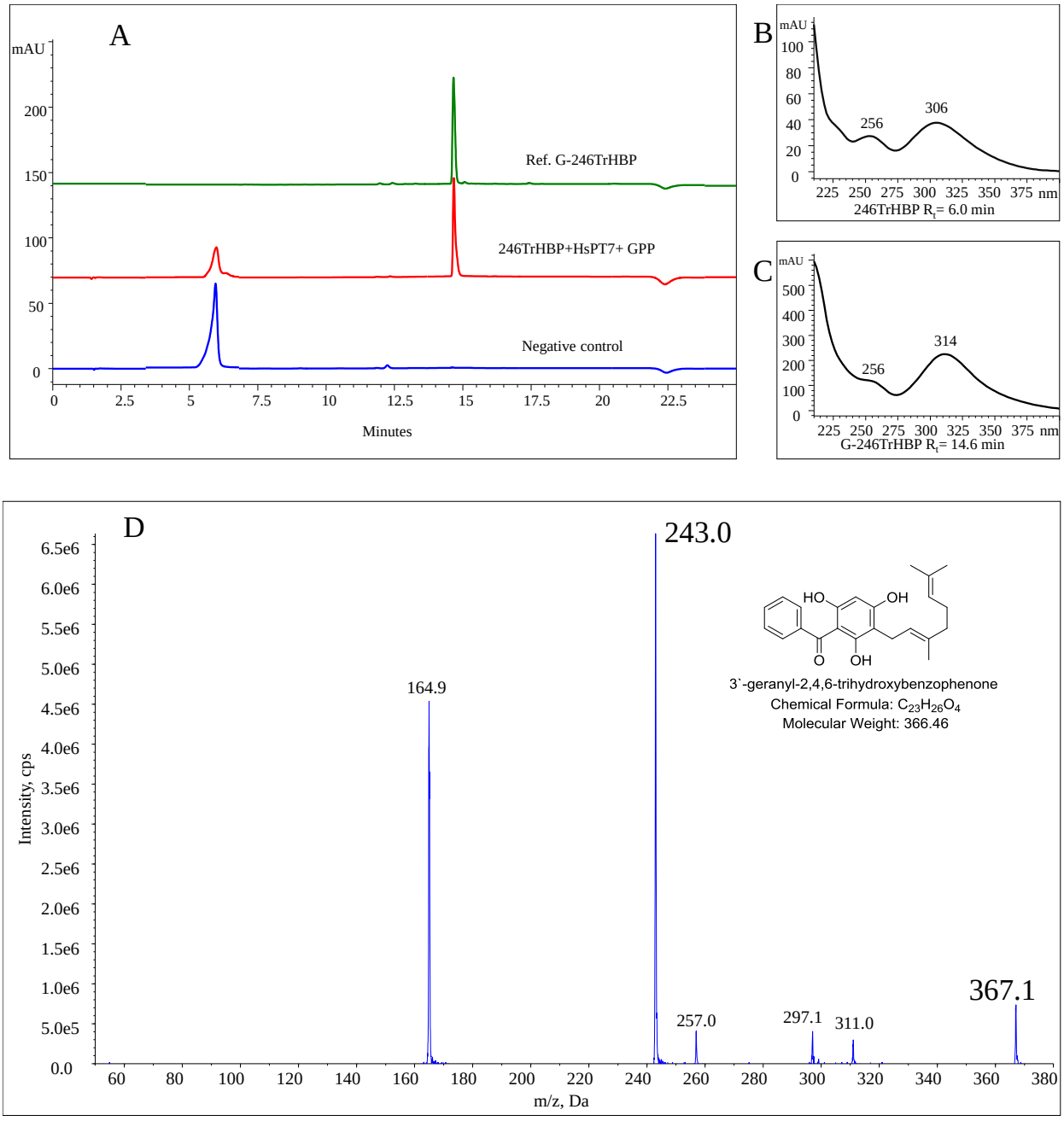

Figure 46: Incubation of yeast microsomes containing *Hs*PTAPG with 246TrHBP. A) Stacked HPLC-DAD chromatograms for enzymatic reaction (red), reference (green) and negative control (blue). B and C) UV spectra of the aromatic substrate (B) and enzymatic product (C). D) The positive ion mode EPI mass spectrum of the enzymatic product.

Different sets of combinations of yeast microsomes harbouring recombinant proteins without detected catalytic activities were co-incubated, under the above-used assay conditions, with *Hs*PTs that had confirmed activities. This co-incubation principle was applied to test the possibility that any of these inactive proteins may catalyse further prenylation on any of the products of the active *Hs*PTs. Unfortunately, no further prenylated products were detected, even for the *Hs*-homologue

of *H. perforatum* sequence (*Hp*PT6), which was able to add a prenyl group to the geranylated acylphloroglucinols, produced by the *H. perforatum Hs*PT7-homologue (Fiesel, 2016).

Table 30: Summarized results of activity assays with yeast cell-expressed *Hs*PTs

Recombinant PT	Accepted Substrates		Products
	Acceptor	Donor	
*Hs*PT1	-	-	
*Hs*PT1a	-	-	
*Hs*PT1b	-	-	
*Hs*PT2 (*Hs*PT8PX)	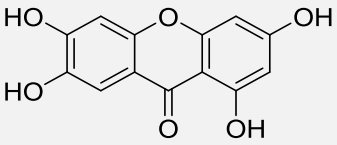 1,3,6,7-tetrahydroxyxanthone	DMAPP	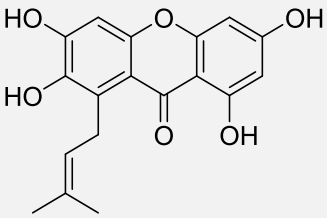 8-prenyl-1,3,6,7-tetrahydroxyxanthone and 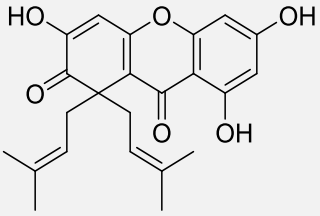 patulone
	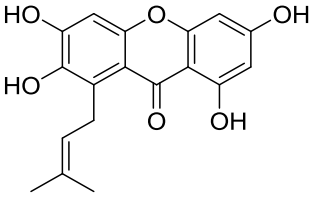 8-prenyl-1,3,6,7-tetrahydroxy-xanthone	DMAPP	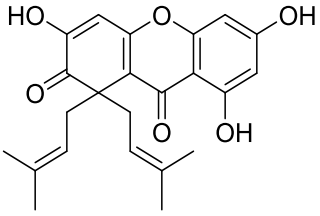 patulone
*Hs*PT3	-	-	
*Hs*PT4	-	-	

*Hs*PT5 (*Hs*PTpat)	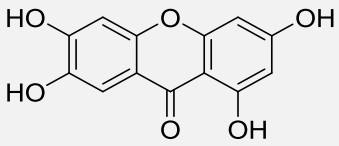 1,3,6,7-tetrahydroxyxanthone	DMAPP	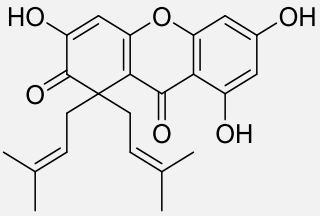 patulone
	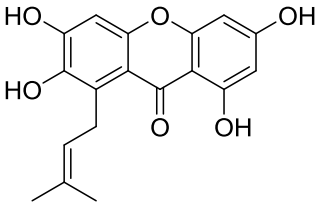 8-prenyl-1,3,6,7-tetrahydroxy-xanthone	DMAPP	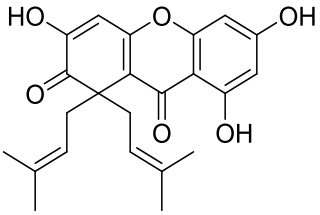 patulone
*Hs*PT6	-	-	
*Hs*PT7 (*Hs*PTAPG)	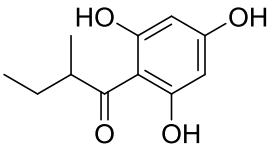 2-methyl-2´,4´,6´-trihydroxybutyrophenone	GPP	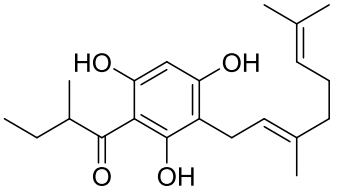 2-methyl-3´-geranyl-2´,4´,6´-trihydroxybutyrophenone
	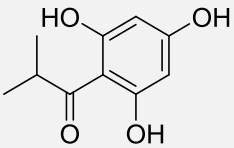 2,4,6-trihydroxyisobutyro-phenone	GPP	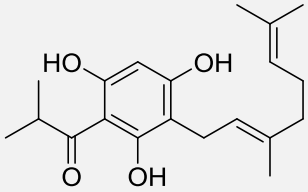 3-geranyl-2,4,6-trihydroxyiso-butyrophenone
	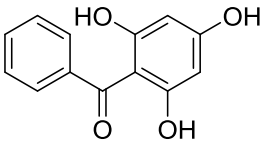 2,4,6-trihydroxybenzo-phenone	GPP	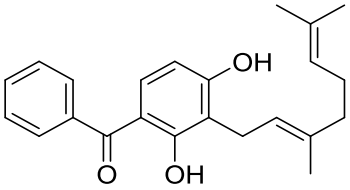 3-geranyl-2,4,6-trihydroxy-benzophenone

4.6.2 Characterization of active recombinant proteins

For a better understanding of the enzymatic reactions observed, the optimum conditions for each of the *Hs*PT-catalyzed conversions were investigated. Optimum pH was necessary to be determined as the pH value can directly affect the ionization state of the protein and consequently its folding. Thus, the activity of proteins is commonly decreased outside of a certain range of pH values. Likewise, the increase in temperature, to a certain limit, can affect the activity positively, before the hydrogen bonds within the polypeptide start to labilize, leading to partial denaturation of the protein and gradual loss of the activity. The accumulation of the products is time-dependent. The best co-factor (divalent cation) for each reaction was investigated, testing the effect of different divalent cations on the amount of the resulting product.

4.6.2.1 *Hs*PT8PX

This enzyme can accept two xanthones, namely, 1367THX and its prenylated derivative 8PX (4.6.1.2; **Table 30**). The reaction with the unprenylated substrate showed the highest yield at a pH value of 7 using a Tris-HCl buffer. Increasing or decreasing the pH value of the reaction by 0.5 unite demonstrated a decline in the activity by ≈ 10 and 30%, respectively.

The preferred divalent cation for the catalytic activity of *Hs*PT8PX for the formation of either 8PX (the substrate is 1367THX) or patulone (the substrate is 8PX) was Mg^{2+}. The rate of accumulation of enzymatically formed 8PX was linear over the first 15 minutes. However, a slow increase in the product formation was observed until three hours. Incubation temperatures between 35 °C - 40 °C showed the highest amount of product. A 5 °C increase in the temperature caused a loss of 18% of the activity. The product increased in a linear manner until a protein amount of 10 µg (**Figure 47**). Incubation with the prenylated derivative, 8PX, showed similar results, except that the time-dependent product accumulation rate was linear till 20 min.

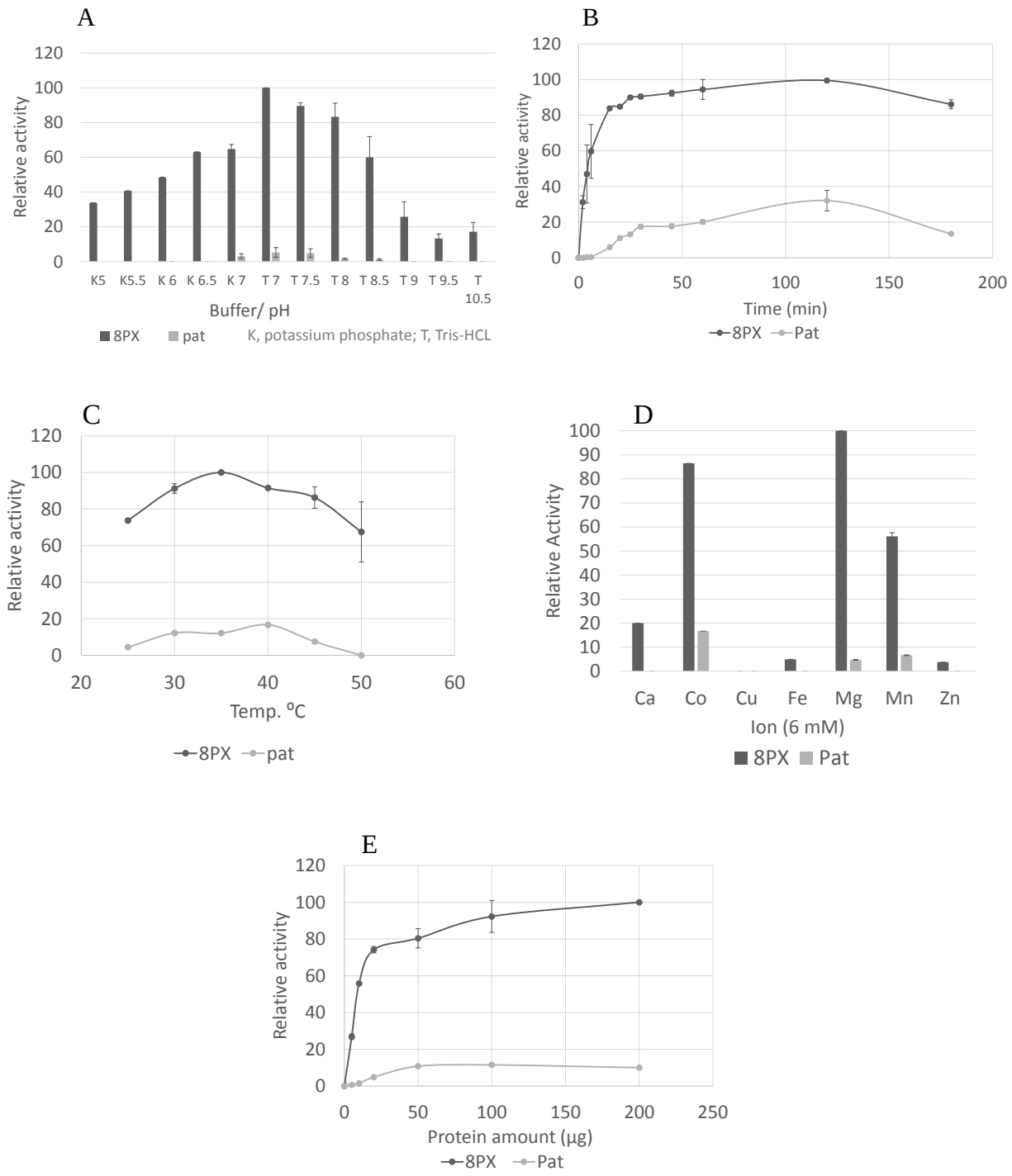

Figure 47: Effect of variation of enzymatic reaction conditions on the activity of *Hs*PT8PX using 1367THX as a substrate. A) pH. B) Incubation time. C) Temperature. D) Divalent cations. E) Protein amount. Data represent means ± s.d. (n = 3).

4.6.2.2 *Hs*PTpat

*Hs*PTpat is a second xanthone-related prenyltransferase, which catalyzes the geminal addition of either two prenyl groups or only one at C-8 of the xanthone skeletons 1367THX and its 8-prenyl

derivative, respectively. Best conditions for the utilization of both substrates by this aPT were determined and are summarized in **Table 31**. The optimum pH for the reaction with 1367THX was at the weakly basic pH of 7.5 and the preferred co-factor was assigned Mn^{2+}. With 8PX, the neutral pH was preferred and, like in the reactions catalyzed by *Hs*PT8PX, the best divalent cation was Mg^{2+}.

Table 31: Optimum incubation conditions for the xanthone-related PT *Hs*PTpat with 1367THX and 8PX as substrates. Conditions used for the determination of Michaelis-Menten kinetics are also stated.

Factor	1367THX		8PX	
	Highest yield	Kinetics	Highest yield	Kinetics
pH value*	7.5	7.5	7	7
Time	60 min	20 min	30 min	12 min
Temperature	35- 40 °C	37 °C	35- 40 °C	37 °C
Divalent cation	Mn^{2+}	Mg^{2+}	Mg^{2+}	Mg^{2+}
Protein amount	Linear product accumulation up to 200 µg	100 µg	Linear product accumulation up to 50 µg	15 µg

* The preferred buffer was Tris-HCl

4.6.2.3 *Hs*PTAPG

The enzyme was able to catalyze the geranylation of almost all tested acyl- and benzoylphloroglucinols in the study. The first three substrates (246TrHiBP, 2MBP, and 246TrHBP) were considerably utilized under the standard incubation conditions (3.5.5.1) and were thus considered for further characterization. The first investigated substrate was 246TriBP, where the best pH value for the reaction was 7.5 using a Tris-HCl buffer. The activity was changed slightly by increasing or decreasing the pH by 0.5 units. The product formed, G-246TrHiBP, accumulated linearly until an incubation time of 10 min, whereafter the reaction velocity decreased. An incubation temperature between 40 °C and 45 °C was assigned to be the optimum for this reaction. Around 13-17% loss of activity was observed for incubations done at 35 °C and 50 °C, respectively. Opposite to Co^{2+} and Ca^{2+}, which caused 90 and 85% loss of activity, respectively, Mg^{2+} was the most effective co-factor for catalysis. Linear accumulation of the geranylated product was observed till 16 µg protein in the reaction mixture, however, higher protein amounts were accompanied by decreases in the reaction rate.

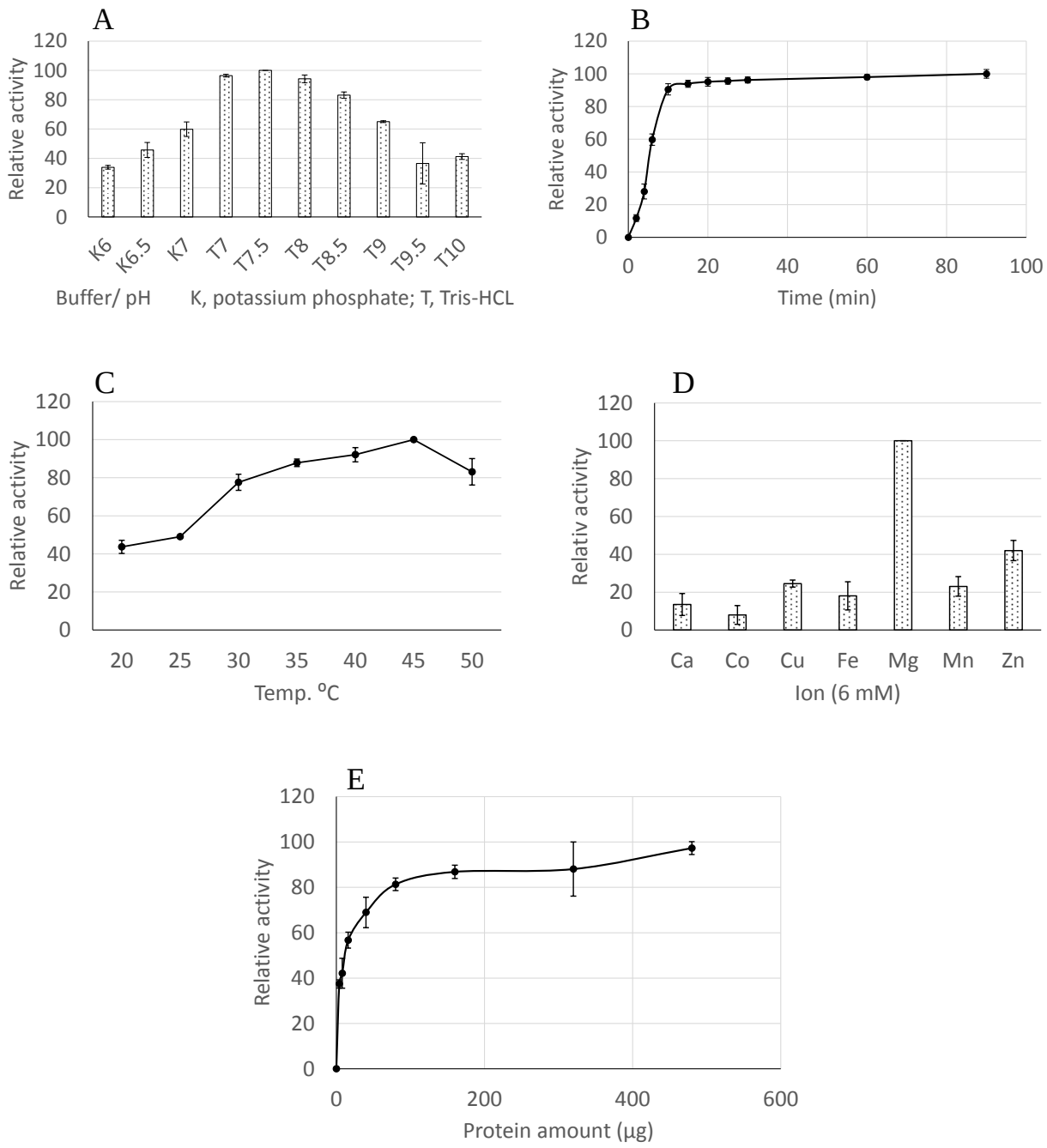

Figure 48: Effect of varied reaction conditions on the activity of *Hs*PTAPG using 246TrHiBP as a substrate. A) pH. B) Incubation time. C) Temperature. D) Divalent cations. E) Protein amount. Data represent means ± s.d. (n = 3).

Similar characterization results were observed when another acylphloroglucinol was employed as an aromatic geranylation acceptor, namely, 2MBP, except for a slightly higher pH optimum. The same conditions were used for the investigation of Michaelis-Menten kinetics for both substrates. On the other hand, the enzymatic reaction with the benzoylphloroglucinol needed a slightly basic pH (Tris-HCl pH 8), more protein amount and longer incubation time to reach the maximum yield

of the produced G-246TrHBP. The characterization results of *Hs*PTAPG are summarized in **Table 32**.

Table 32: Optimum incubation conditions for the acylphloroglucinol-related PT *Hs*PTAPG with 2MBP and 246TrHBP. Conditions used for the determination of Michaelis-Menten kinetics are also stated.

Factor	2MBP		246TrHBP	
	Highest yield	Kinetics	Highest yield	Kinetics
pH value*	8	8	8	8
Time	90 min	6 min	120 min	20 min
Temperature	40- 45 °C	42 °C	40- 45 °C	42 °C
Divalent cation	Mg^{2+}	Mg^{2+}	Mg^{2+}	Mg^{2+}
Protein amount	Linear product accumulation up to 16 µg	8 µg	Linear product accumulation up to 80 µg	40 µg

* The preferred puffer was Tris-HCl

The series of potential substrates were used to test the substrate preference of *Hs*PTAPG at pH 8 and 42 °C for 6 min in the presence of GPP and Mg^{2+} as a co-factor (conditions for linear velocity of the enzyme with acylphloroglucinol substrates). The most preferred substrate for the enzyme was 2MBP. The activity towards this aromatic substrate was assigned to 100% and the relative activity for other geranyl acceptors was calculated as a percentage in terms of nmol product for each substrate **(Figure 49)**. The second best substrate was 246TrHiBP (55%), followed by the benzoyl derivative 246TrHBP (13%). Other substrates such as tetrahydroxybenzophenone (THBP), phloracetophenone (PAP), and phlorisovalerophenone (246THiVP) were poorly accepted (3- 9.5%; **Figure 49**). By applying the preferred for 246TrHBP (increasing the incubation time and amount of protein used), the utilization of this substrate increased from 13% to ≈ 30%. However, trials to change the incubation conditions of *Hs*PTAPG failed to enhance the enzymatic acceptance of prenylated substrates and maclurin.

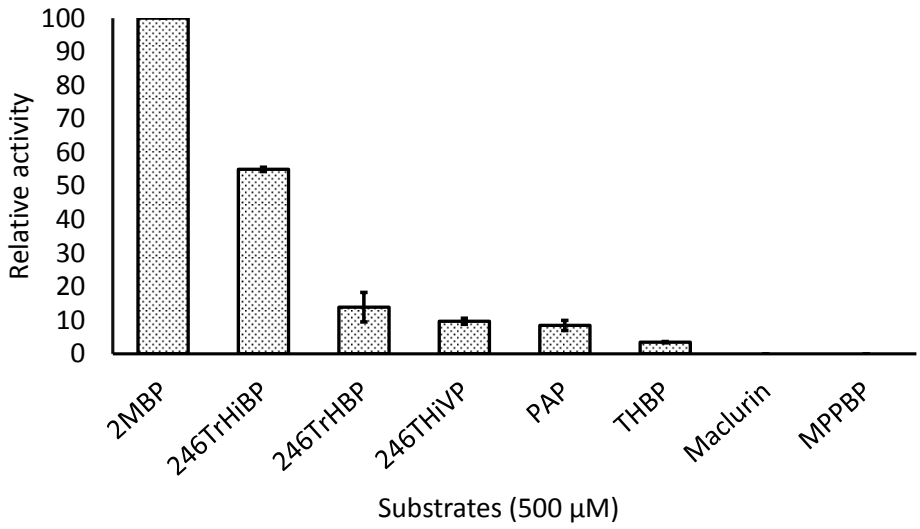

Figure 49: Substrate specificity of yeast-expressed *Hs*PTAPG using various acyl- and benzoylphloroglucinol derivatives as geranyl acceptors. The relative enzyme activity is calculated as a percentage of the most accepted substrate in terms of nmol product for each substrate. Data represent means ± s.d. (n = 3).

4.6.3 Kinetic parameter determination

4.6.3.1 Xanthone prenyltransferases

Both xanthone-related PTs accept 1367THX and 8PX as prenyl acceptors to produce xanthone derivatives with different degrees of prenylation. *Hs*PT8PX catalyzes the formation of 8PX from 1367THX and, at the same time, it can add a second prenyl group to 8PX to form patulone. In contrast, *Hs*PTpat produces always patulone from either 1367THX or 8PX. Thus, the affinities of this pair of enzymes, in terms of Michaelis-Menten constants (K_m), for both substrates had to be determined to assure the preferred substrate for each recombinant aPT **(Table 33)**.

The K_m values for 1367THX and 8PX upon reaction with *Hs*PT8PX were 53.17 ± 1.5 µM and 83.8 ± 8.3 µM, respectively. On the other hand, the V_{max} values for these reactions were greatly different (9.46 ± 0.083 nkat/µg and 0.26 ± 0.007 nkat/µg, respectively). In the reactions with the second enzyme *Hs*PTpat, the values for the two substrates were almost reversed. The K_m values for 1367THX and 8PX were 200.27 ± 16.38 µM and 73.56 ± 6 µM, respectively, and the V_{max} values were 0.24 ± 0.012 and 5.2 ± 0.2 nkat/µg for the reactions with 1367THX and 8PX, respectively. These results indicate that the main substrate for the enzyme *Hs*PT8PX is the tetrahydroxyxanthone and the main substrate for *Hs*PTpat is the prenylated xanthone.

The K_m values of each enzyme for DMAPP in the presence of its main substrate were also determined. Calculated K_m and V_{max} values for *Hs*PT8PX with DMAPP in the presence of 1367THX were 15.82 ± 5.7 µM and 8.24 ± 0.5793 nkat/µg, respectively. Similarly, the kinetic parameters for DMAPP in the reaction *Hs*PTpat + 8PX + DMAPP were 23.7 ± 3.26 µM and 4.1 ± 0.27 nkat/µg, respectively.

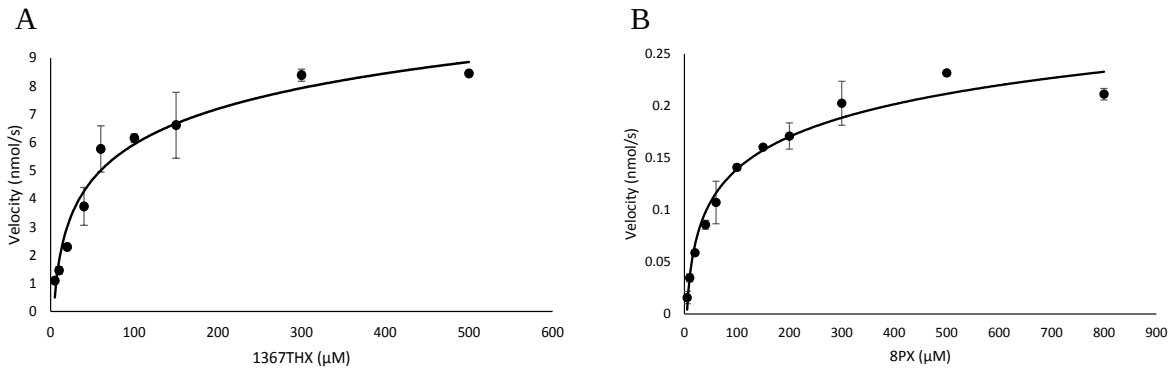

Figure 50: Hyperbolic regression curves for the determination of the Michaelis-Menten constants (K_m values) of *Hs*PT8PX with the substrates 1367THX (A) and 8PX (B).

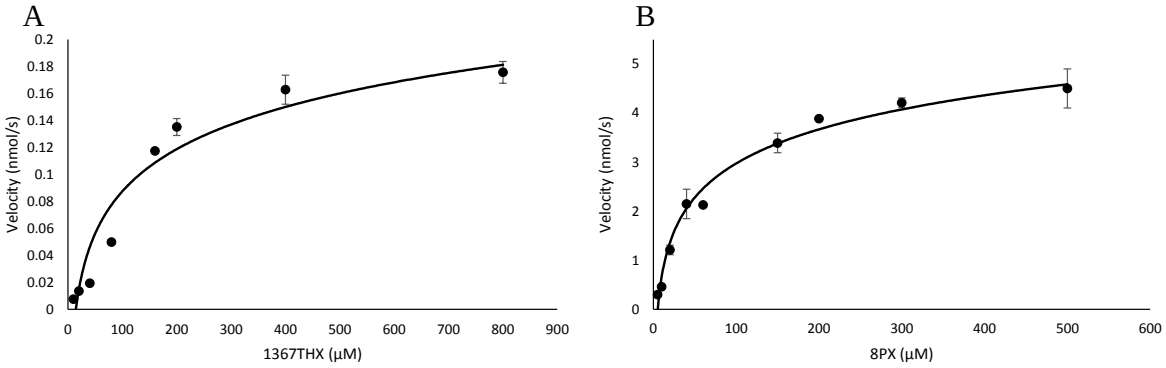

Figure 51: Hyperbolic regression curves for the determination of the Michaelis-Menten constants (K_m values) of *Hs*PTpat with the substrates 1367THX (A) and 8PX (B).

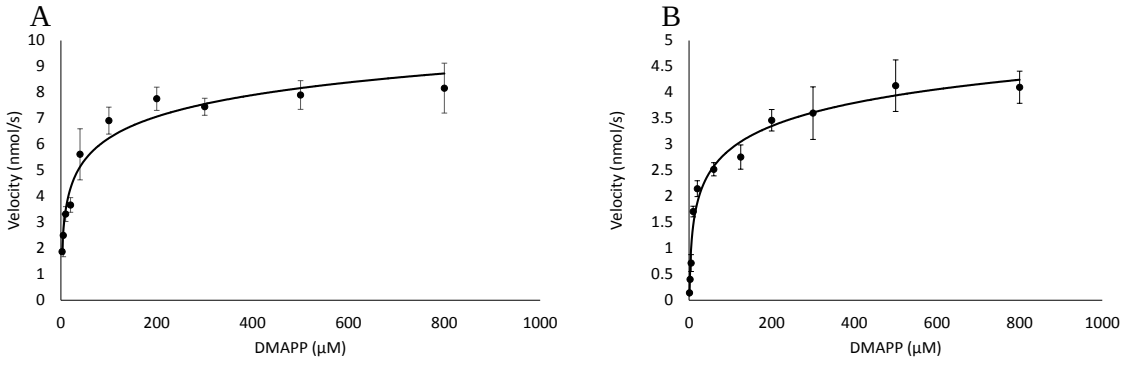

Figure 52: Hyperbolic regression curves for the determination of the Michaelis-Menten constants (K_m values) of *Hs*PT8PX for DMAPP in the presence of 1367THX (A) and of *Hs*PTpat for DMAPP in the presence of 8PX (B).

Table 33: Kinetic parameters of *Hs*PT8PX and *Hs*PTpat

	1367THX		8PX	
	K_m (μM)	V_{max} (nkat/μg)	K_m (μM)	V_{max} (nkat/μg)
*Hs*PT8PX	53.17 ± 1.5	9.46 ± 0.083	83.8 ± 8.3	0.26 ± 0.007
*Hs*PTpat	200.27 ±16.38	0.24 ± 0.012	73.56 ± 6	5.2 ± 0.2

4.6.3.2 Acyl/benzoyl prenyltransferase

The affinity of the enzyme *Hs*PTAPG towards the first three accepted substrates, as indicated by its substrate specificity (4.6.2.3), was also measured. The lowest K_m and highest V_{max} values were confirmed for the substrate 2MBP, calculated as 62.68 ± 1.6 μM and 20.82 ± 1.065 nkat/mg, respectively **(Figure 53)**. The measured kinetic parameters for *Hs*PTAPG supported the results obtained for the substrate specificity **(Table 34)**. In addition, the kinetic parameters for *Hs*PTAPG with GPP were determined as 33.7 ± 3.37 μM and 15.48 ± 1.85 nkat/μg for K_m and V_{max}, respectively. Michaelis-Menten constants and maximum velocities of the enzyme with other substrates are listed in **Table 34**.

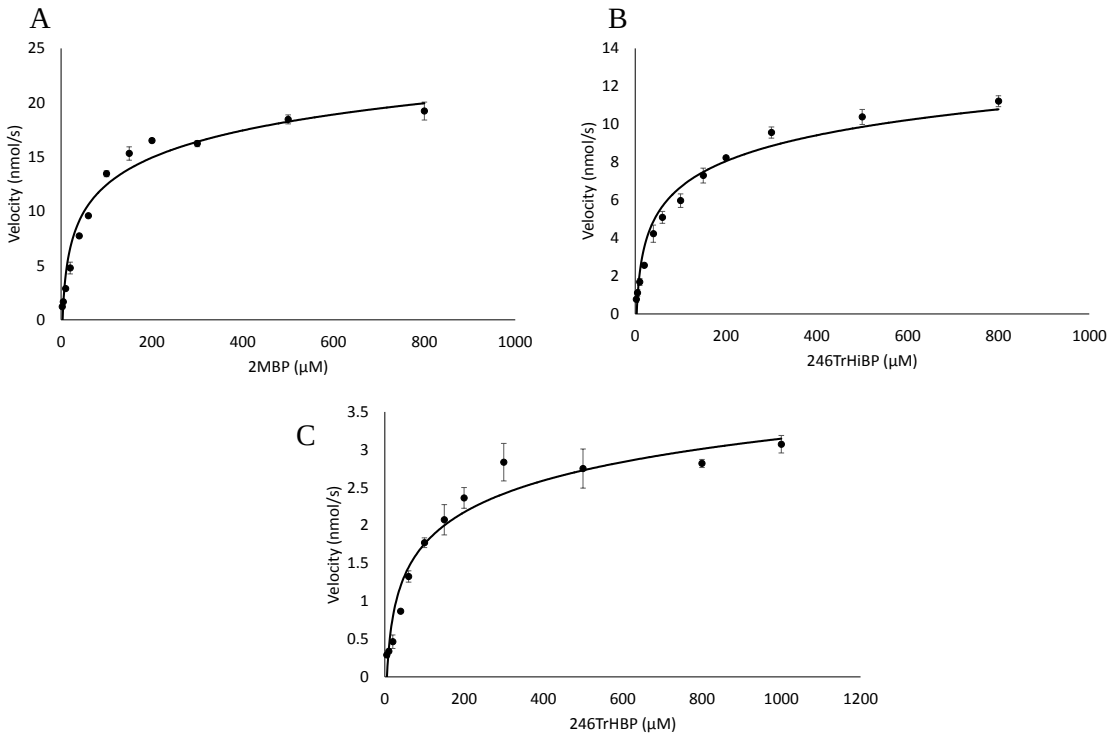

Figure 53: Hyperbolic regression curves for the determination of the Michaelis-Menten constants (*K*m values) of *Hs*PTAPG with the substrates 2MBP (A), 246TrHiBP (B), and 246TrHBP (C).

Table 34: Kinetic parameters of *Hs*PTAPG with 2MBP, 246TrHiBP, and 246TrHBP

Substrate	*Hs*PTAPG	
	K_m (μM)	V_{max} (nkat/μg)
2MBP	62.68 ± 1.6	20.82 ± 1.065
246TrHiBP	87.65 ± 3.1	12.17 ± 0.1
246TrHBP	91.54 ± 6.2	3.34 ± 0.04

4.7 Phylogenetic analysis of *H. sampsonii* prenyltransferases

Another important characterization tool was employed to infer the evolutionary history of the identified *H. sampsonii* PTs and to correlate them to their previously published ancestors, which supports the right positioning of these functionally novel aPTs among other aPTs. Amino acid sequences of membrane-bound aPTs from various bacterial and plant (monocots, dicots) origins, which shared low to moderate homology (12.7- 61.3%) with the *Hs*PTs, were used to construct a phylogenetic tree. A soluble fungal aPT, which lacked the conserved aspartate motifs (Zhou et al., 2017) was used as an outgroup to root the tree.

The resulting tree was functionally clustered by the nature of the accepted aromatic substrates into aPT groups specific for xanthones, flavonoids, homogentisate, coumarins, plastoquinones, phloroglucinols, and 4-hydroxybenzoate **(Figure 54)**. All *H. sampsonii* PTs identified in the present study, except for *Hs*PT6 and its isoform *Hs*PT6a, originated from the same clade with almost 100% strapping. The xanthone-specific PTs *Hs*PT8PX and *Hs*PTpat grouped together with *Hc*PTpat and the recently published xanthone-specific *Hc*PT (Fiesel et al., 2015) into the same subclade. *Hc*PT8PX and *Hs*PTAPG represented individual subbranches within the clade of *Hypericum* PTs. Thus, *Hs*PTAPG did not group together with the acylphloroglucinol-related prenyltransferases isolated from hop and cannabis (Tsurumaru et al., 2012; Page and Boubakir, 2014). The two isoenzymes *Hs*PT6 and *Hs*PT6a were incorporated with low bootstrapping value (10) into the clade consisting of homogentisate PTs, which might suggest their involvement in the primary metabolism of *Hypericum*.

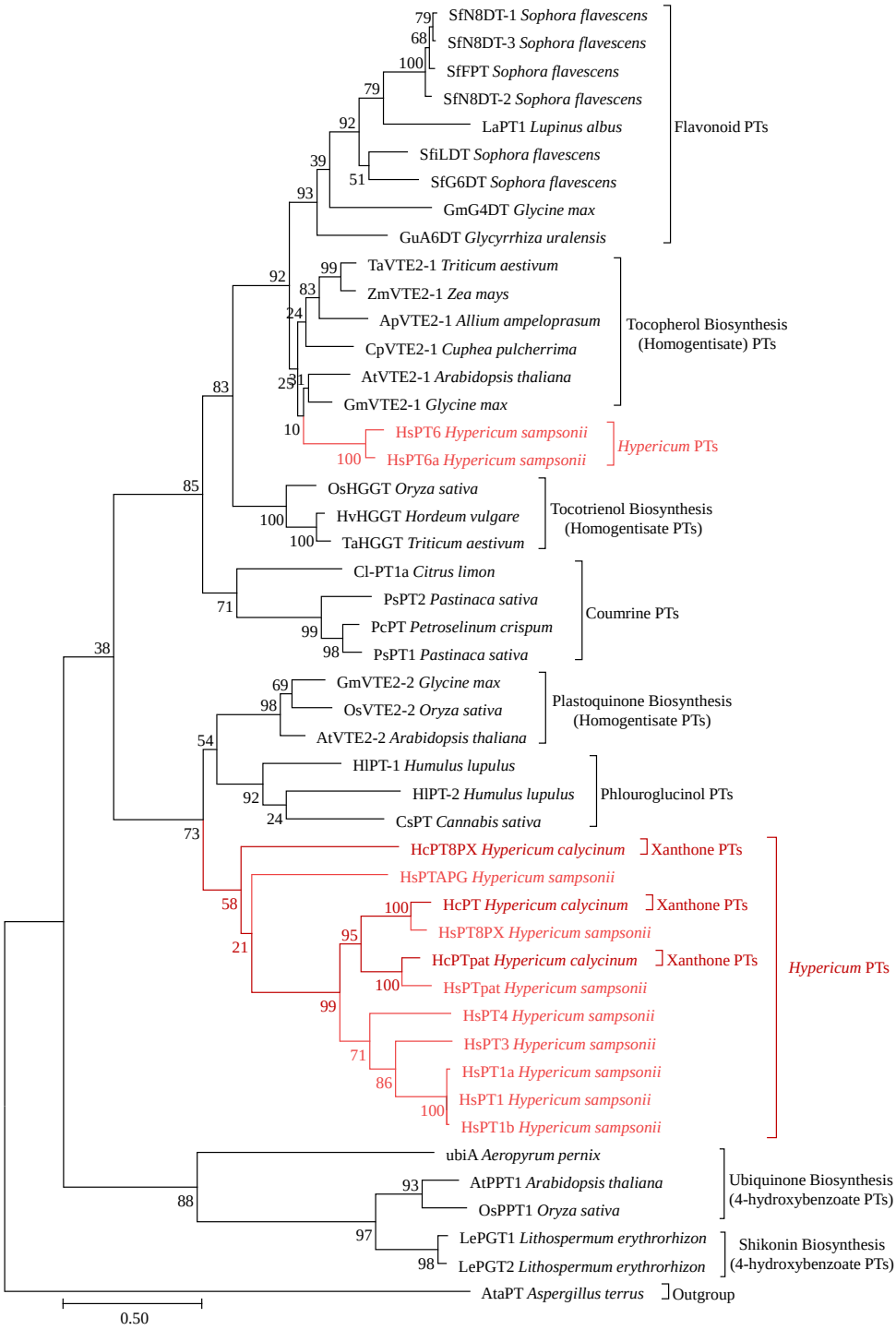

Figure 54: Phylogenetic tree illustrating the evolutionary relationships between aPTs from *Hypericum* sp. and previously identified aPTs from other plants. The maximum likelihood tree was constructed using amino acid sequences through MEGA 7 with 1000 bootstrapped value support and a Poisson model. The bootstrap values are indicated at the branch points. The scale bar represents 0.5 of amino acid substitution per site.

4.8 Localization of xanthone specific *H. sampsonii* prenyltransferases

The subcellular localization of the PTs was determined through the generation of fusion constructs with yellow fluorescent protein (YFP), which were transiently expressed in *Nicotiana benthamiana* leaves (3.5.3). *Hs*PT8PX and *Hs*PTpat were fused with YFP at both the N- and the C-termini. N-terminal and C-terminal fusion proteins were also generated for the truncated proteins, which lacked the targeting signal. For C-terminal fusions, the stop codons of the PT sequences were deleted. A construct of truncated DsRed was co-expressed to act as a cytoplasmic control.

4.8.1 Subcellular localization of *Hs*PT8PX in fusion with YFP

Four fusion constructs with yellow fluorescent protein were established as described under 3.3.9.3. The full-length and transit peptide-lacking sequence (truncated *Hs*PT8PX, formerly assigned as *Hs*PT2) were assembled with the YFP sequence at either the N- or the C-terminus of the PT **(Figure 55)**. The *Hs*PT2 fusion constructs were transferred into the DH5α *E. coli* strain. Afterward, the plasmids were extracted and transferred into *A. tumefaciens*, which was cultivated for infiltration into the lower surface of *N. benthamiana* leaves. At the same time, *A. tumefaciens* harboring truncated DsRed as a cytoplasmic control were co-infiltrated. The leaves were allowed for three days to transiently express the different fusion proteins (3.5.3). *N. benthamiana* leaf discs were cut and visualized *via* laser scanning microscope (3.7). Strong yellow fluorescence was observed around the red autofluorescence of chlorophyll, indicating an integration of this aPT into the membranes of the chloroplasts and thus its plastidial subcellular localization. The truncated version of the aPT exhibited a cytoplasmic localization, as the yellow fluorescence of the fusion construct coincided with that of the cytoplasmic control, truncated DsRed **(Figure 56)**. Similar results as with the truncated versions were obtained with the N-terminal fusions due to the masking of the aPT transit peptide.

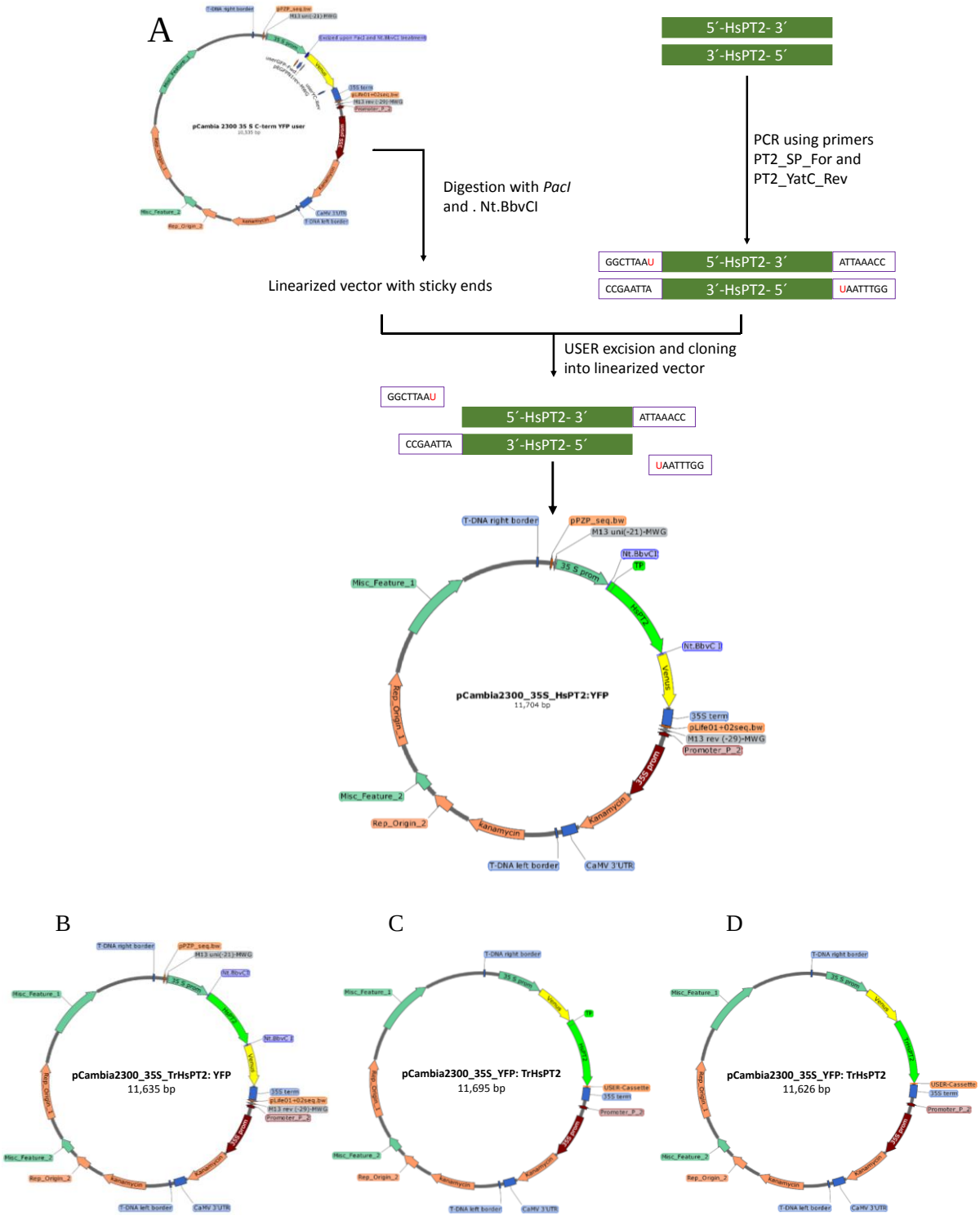

Figure 55: Fusion constructs of *Hs*PT2 (*Hs*PT8PX) with YFP. A) Schematic representation of the stepwise assembly of the fusion construct for full-length *Hs*PT2 with YFP. B, D) Fusion construct of truncated *Hs*PT2 with YFP. (A, B) YFP at the C-terminus of the protein. (C, D,) YFP at the N-terminus of the protein.

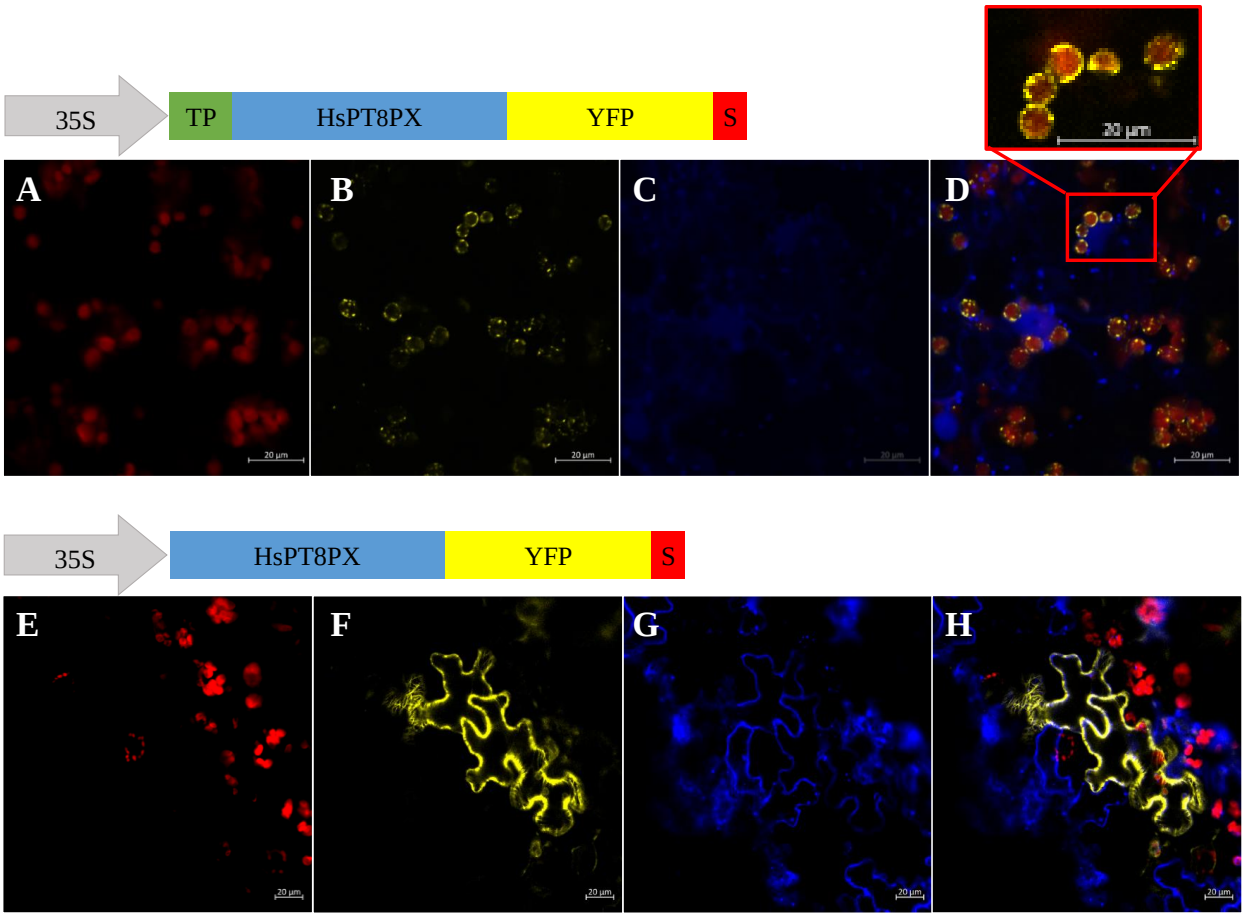

Figure 56: Subcellular localization of *Hs*PT8PX and its truncated version lacking the signal peptide in *N. benthamiana* leaves. (A, E) Red autofluorescence of chlorophyll. (B, F) Yellow fluorescence of the PT-YFP fusion. (C, G) Blue fluorescence of the truncated version of DsRed. (D, H) Superimposed photos. TP, transit peptide; S, stop codon.

4.8.2 Subcellular localization of *Hs*PTpat in fusion with YFP

Fusion plasmids of the *Hs*PTpat (*Hs*PT5) with YFP were generated employing the corresponding primers in the manner described under scetion 3.3.9.3. They were co-expressed together with the DsRed control in *N. benthamiana* leaves (3.5.3; **Figure 57**). Results detected *via* laser-scanning microscopy were similar to those observed for *Hs*PT8PX. The full-length fusion construct showed its yellow fluorescence at the membranes of the plastids. When the signal peptide was removed, the fluorescence remained in the cytoplasm of the plant cell, as it exhibited the same fluorescence pattern like the cytoplasmic control, truncated DsRed **(Figure 58)**.

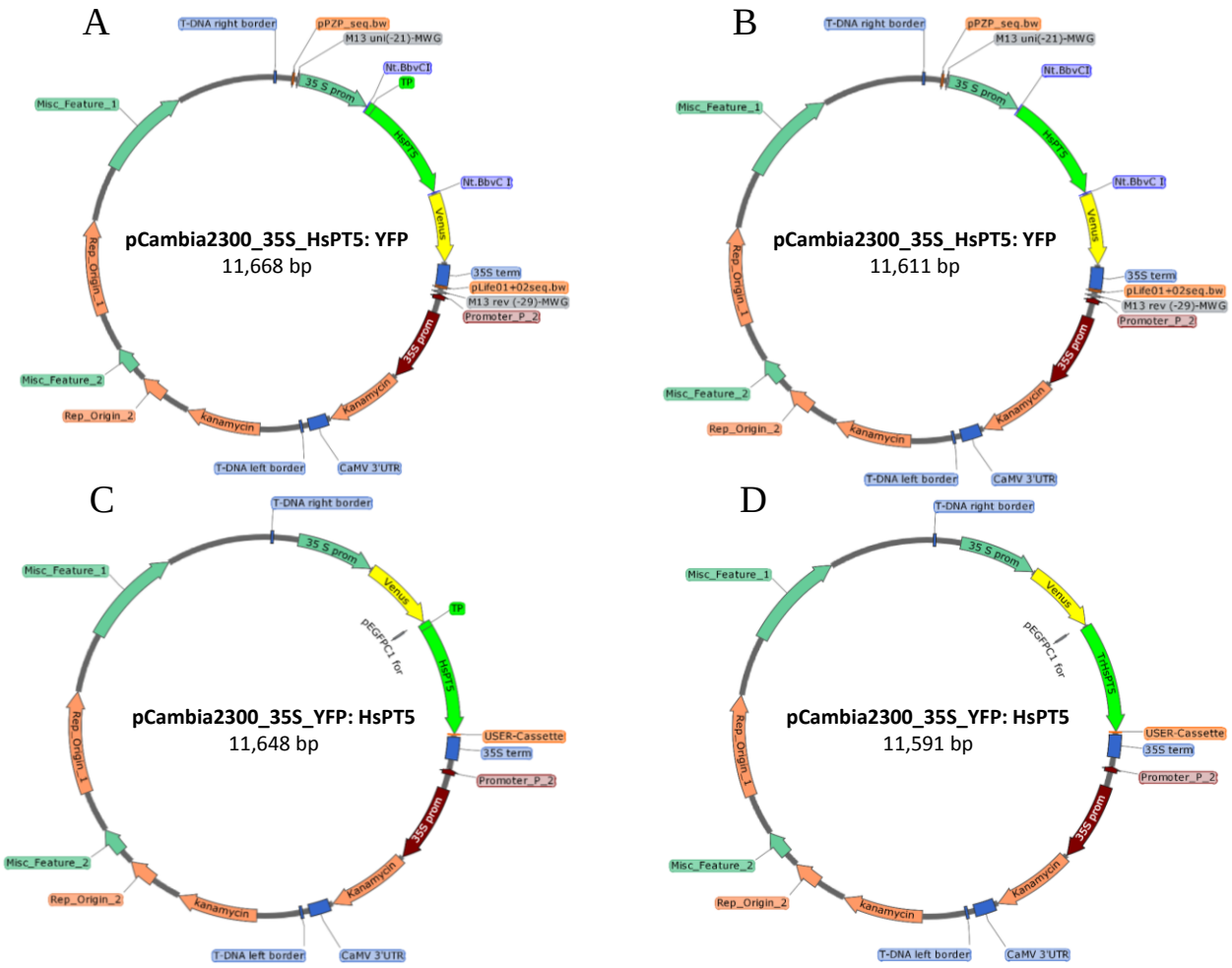

Figure 57: Fusion constructs of *Hs*PT5 (*Hs*PTpat) with YFP. (A, C) Fusion construct of full-length *Hs*PT5. (B, D) Fusion constructs of truncated *Hs*PT5 lacking the coding sequence for the signal peptide. (A, B) Fusion constructs with YFP at the C-terminus. (C, D) YFP at the N-terminus.

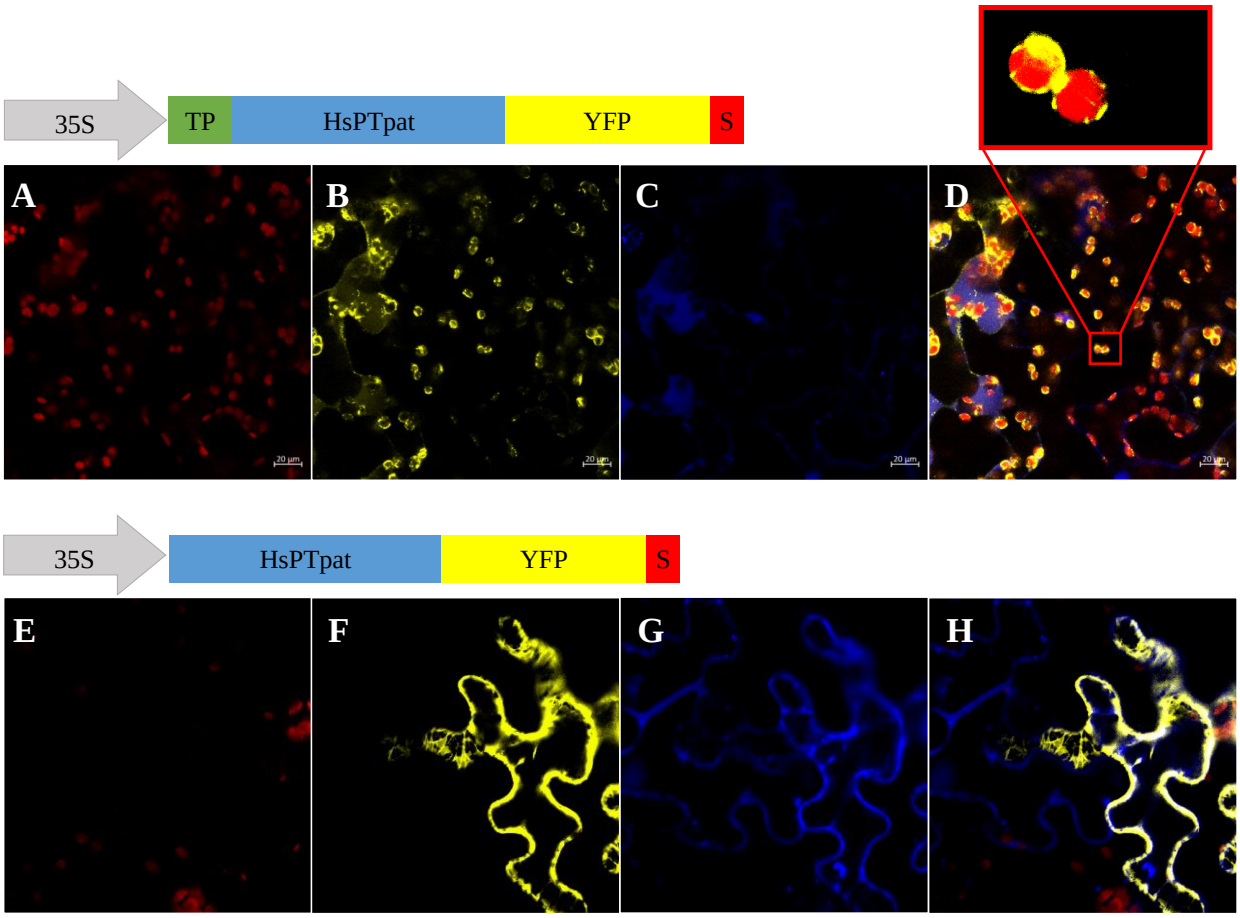

Figure 58: Subcellular localization of *Hs*PTpat and its truncated version lacking the signal peptide in *N. benthamiana* leaves. (A, E) Red autofluorescence of chlorophyll. (B, F) Yellow fluorescence of the aPT-YFP fusion. (C, G) Blue fluorescence of the truncated version of DsRed. (D, H) Superimposed photos. TP, transit peptide; S, stop codon.

5 Discussion

5.1 *In vitro* cultivated *Hypericum sampsonii* as a source of PPAPs

Metabolite profiling provoked by HPLC-MS/MS and/or GC-MS is an important biochemical readout, which can be used for numerous applications. For example, chemotaxonomical classification of organisms, analysis of environmental stimuli, chemical characterization of a plant to estimate the risk of using it medicinally, assessment of plant breeding effects (Robinson et al., 2005; Hill and Roessner, 2013), and better understanding of plant biosynthetic mechanisms (Vickery et al., 2016). In the current study, the metabolic screening of six-week-old *H. sampsonii in vitro* seedlings by HPLC, MS-MS, and GC-MS provided an overview of the metabolic profile and assured the existence of biosynthetic aromatic precursors, which could accept prenyl groups after comparing the results with previous metabolic reports of field-grown *H. sampsonii* (Li et al., 2004; Zhu et al., 2017) In this respect, eight compounds bearing different chemical structures were identified in the extract. Xanthones, namely 1,3,6,7-tetrahydroxyxanthone (1367THX), its 8-prenylated derivative (8PX) and its 8,8-diprenylated derivative (patulone) were identified in the extract. The 1,3,6,7-tetrahhydroxyxanthone precursor was previously reported for the plant (Don et al., 2004). Furthermore, the identified prenylated derivatives were isolated from the wild plant growing in the Yunnan province of China (Li et al., 2004). Acyl- and benzoylphloroglucinols with caged and complex structures bearing the basic scaffolds of 2,4,6-trihydroxyisobutyrophenone and 2,4,6-trihydroxybenzophenone were repeatedly described for the plant (Hu and Sim, 2000; Li et al., 2004; Xiao et al., 2007; Xin et al., 2012; Zhu et al., 2016). This reasonably justifies the finding of these scaffolds and the geranylated-PBP in the extract investigated in the current work. In addition, the geranylated benzoyl derivative was identified along with complex acyl- and benzoyl-metabolites in the plant (Lin and Wu, 2003). The current study reports the presence of 2-methyl-2´,4´,6´-trihydroxybutyrophenone (2MBP) for the first time because neither 2MBP itself nor a polyprenylated compound derived from this precursor have been reported before for *H. sampsonii*. Hyperjapones C and E, isolated recently from *Hypericum japonicum* (Lam et al., 2016), and adhyperforin occurring in the *H. perforatum* (Klingauf et al., 2005), are examples of polycyclic polyprenylated compounds bearing this core structure. Similar to previous reports, a naphthodianthrone, pseudohypericin, was identified in the *H. sampsonii* extract (Liu et al., 2007). Furthermore, MS/MS analysis of most non-polar *H. sampsonii* fractions revealed a number of peaks that corresponded to molecular weights of known PPAPs from *H. sampsonii*. Due to the limited Ms/Ms spectral data available for these metabolites, the compounds corresponding to the detected peaks could not be fully identified and, anyway, full structural elucidation of the constituents was beyond the scope of this study. However, the confirmed existence of PPAP core structures and prenylated intermediates validated the *in vitro*-cultivated plant material as a source of aromatic PTs. Together with reported metabolic data, it also supported a proper experimental design and gave a good idea of the chemical classes of aromatic prenyl acceptors to be used later in functional characterization of the identified *Hs*PTs.

5.2 Prenylation as a key for the structural and biological diversity of plant metabolites

5.2.1 Structural diversity

Prenylation is a key step in the diversification of natural aromatic compounds from different chemical groups due to the number and length of prenyl chains, such as prenyl (C_5), geranyl (C_{10}), farnesyl (C_{15}) or longer side chains, as well as the positions of prenylations on the aromatic nucleus. Furthermore, subsequent biosynthetic modifications can occur to the added prenyl groups, for example, cyclization or hydroxylation (Adam et al., 2002; Yazaki et al., 2009). As a result, various secondary metabolites with diverse chemical and biological characters can arise from one common precursor. Demethylsuberosin, osthenol, and 8-geranylumbelliferone are three compounds that are derived from the same core structure, umbelliferone, using different aromatic prenyltransferases. A prenyltransferase from *Petroselinum crispum* (parsley), namely *Pc*PT, was able to add a prenyl group (C_5) to either position C-6 or C-8 on the coumarin structure to form demethylsuberosin and osthenol, respectively (Karamat et al., 2014). These C6- and C8-prenylated coumarin derivatives are intermediates in the biosynthetic pathways of the furanocoumarins psoralen and angelicin, respectively. Umbelliferone can undergo a C8-geranylation reaction catalyzed by another aPT identified from lemon (*Citrus limon*), namely *Cl*PT1. The enzymatic product, 8-geranylumbelliferone, was identified in the peel of some species belonging to the citrus family, Rutaceae (Munakata et al., 2014). *Pastinaca sativa* prenyltransferases (*Ps*PT1 and *Ps*PT2) also catalyzed the attachment of a prenyl moiety to either C-6 or C-8 of the coumarin structure, respectively (Munakata et al., 2016). Examples of modification by prenylation on a xanthone structure are clearly given by the polyprenylated 1367THX metabolites identified in roots of *Hypericum chinense* (Tanaka et al., 2010) and later in root cultures of *H. perforatum* (Tocci et al., 2013; Tocci et al., 2017). Biyouxanthones A and B differed only in the number of prenyl groups attached to the basic xanthone structure. Prenyltransferases responsible for the formation of those compounds are not yet fully explored. Different α- and β-bitter acids are derived from acylphloroglucinols by the action of two aPTs identified in hop. They differ in the number of the prenyl moieties attached to the starter units. Furthermore, hydroxylation occurs on the α-acids. Examples of structural diversity due to prenylations are shown in **Figure 59**.

Prenyltransferases account for the amazing diversity among *H. sampsonii* metabolites. The first example from *H. sampsonii*, which highlights this chemical variation, is the isolation of mono- and diprenylated 1,3,6,7-tetrahydroxyxanthone (8PX and patulone, respectively), which arise from the same 1367THX chemical scaffold (Li et al., 2004). Two series of complex and caged metabolites, assigned the names sampsoniones A-R (Hu and Sim, 2000; Xiao et al., 2007) and hyperisampsins A-O (Zhu et al., 2014; Zhu et al., 2015; Zhu et al., 2017) were described from *H. sampsonii*. They shared the precursor phlorbenzophenone but differed not only in the arrangement of the prenyl and geranyl groups but also in the downstream biosynthetic steps done by cyclases and hydroxylases on the prenyl side chains. In the same context, hypersampsone A, B, C and S are examples of *H. sampsonii* metabolites that have the acylphloroglucinol scaffold

phlorisobutyrophenone and are differentiated through the substitutions on the cyclized prenyls (Lin and Wu, 2003; Chen et al., 2014). The structural diversity of metabolites in *H. sampsonii* sharing a common precursor is displayed graphically in the introduction and results parts of this study **(Figure 3)**.

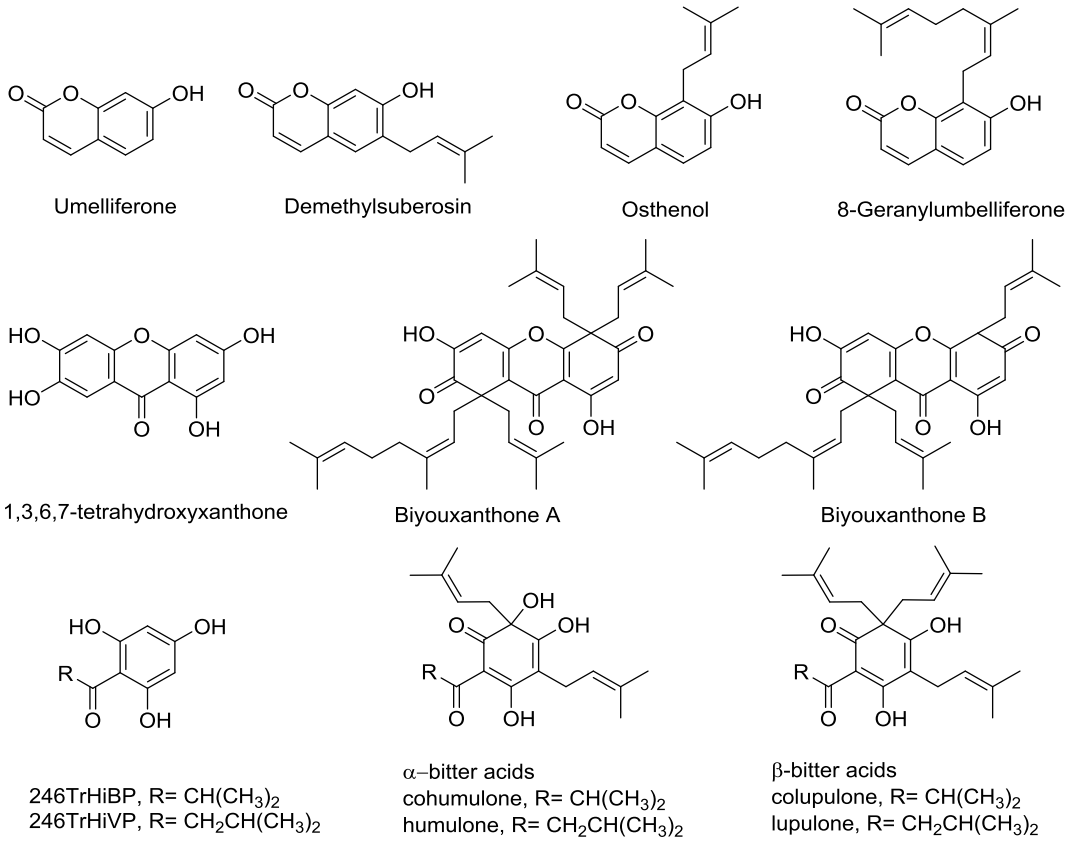

Figure 59: Examples of the structural diversity of plant secondary metabolites due to changes in the prenylation pattern on a core scaffold.

5.2.1 Biological diversity

Introduction of one or more prenyl groups to an aromatic system results in the formation of more lipophilic compounds with enhanced affinity for the interaction with biological membranes. This augmented lipophilicity accounts for better pharmacological activities of prenylated plant secondary metabolites, derived from different chemical nuclei, over their unprenylated ancestors (Alhassan et al., 2014; Gaid et al., 2018).

Prenylated acridone alkaloids, isolated from members of the family Rutaceae, glycocitrine-II and *O*-methylglycocitrine II, showed more inhibitory effect on 12-*O*-tetradecanoylphorbol-13-acetate (TPA)-induced Epstein–Barr virus early antigen (EBV-EA) activation (short-term *in vitro* assay), when compared to 1,3-dihydroxy-10-methylacridone without prenyl side chains, as concluded from the IC_{50} values of the prenylated alkaloids (8.96 and 8.99 nmol against 32 pmol TPA-induced activation) (Itoigawa et al., 2003). Furthermore, the naturally occurring oxyfarnesyl coumarin

derivative umbelliprenin, isolated from *Ferula persica* (Iranshahi et al., 2004) exhibited antioxidant, anti-inflammatory and lipoxygenase inhibitory activities (Khaghanzadeh et al., 2017).

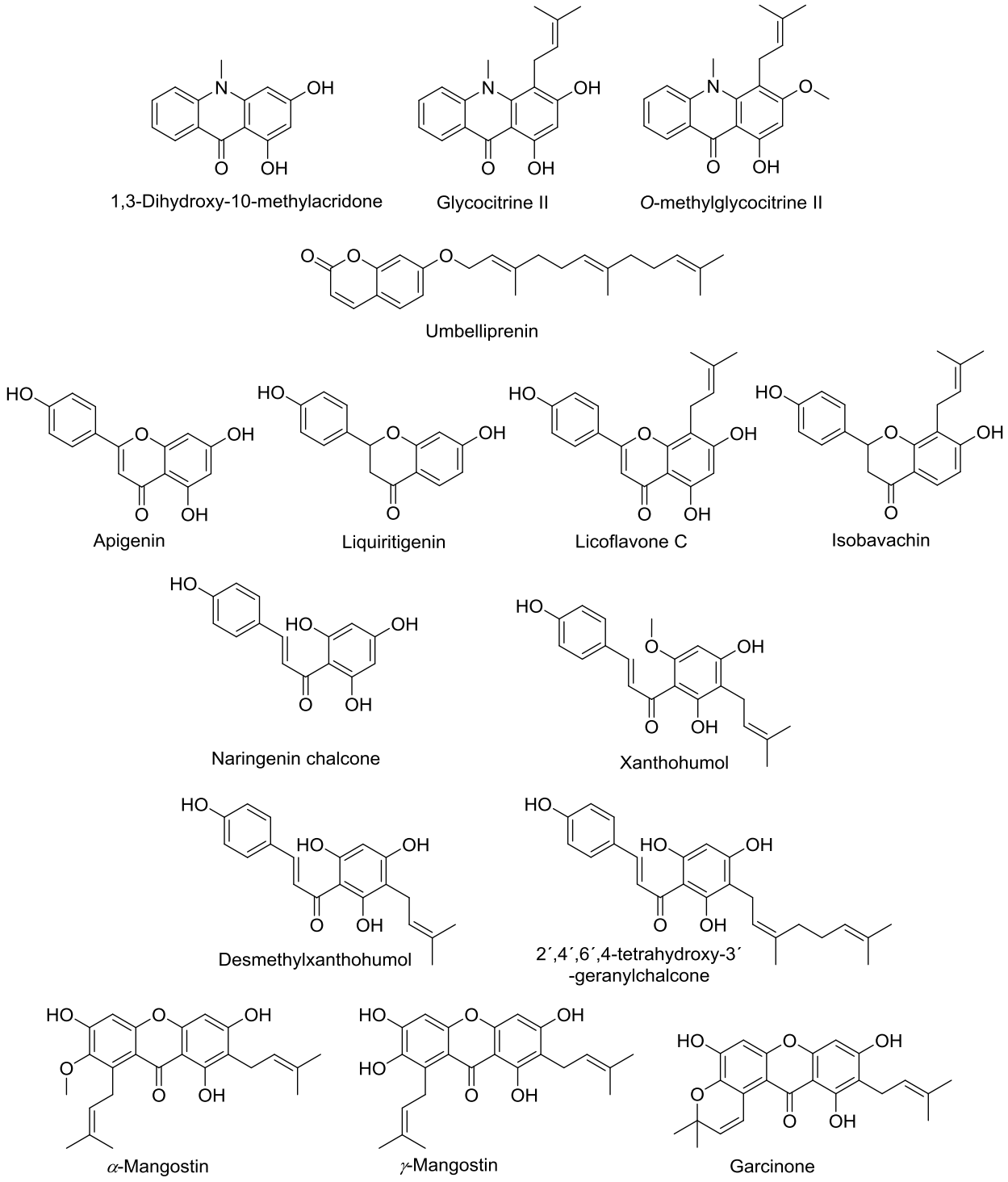

Figure 60: Prenylated plant secondary metabolites of different chemical classes exhibiting a wider biological activity range than their non-prenylated core structures.

These activities were further supported by a series of research works, in which a number of oxyprenyl-, oxygeranyl- and oxyfarnesylcoumarine derivatives were synthesized and their lipoxygenase inhibitory effect was tested against soybean 15-lipoxygenase (SLO) and human 15-lipoxygenase-1 (HLO-1). Interestingly, the most active inhibitors were the oxyfarnesyl coumarins, namely 5-farnesyloxycoumarin, 2-oxyfarnesylcoumarin and umbelliprenin (7-oxyfarnesylcoumarin), with IC_{50} values of 0.8 ± 0.1, 1.7 ± 0.1 and 3.1 ± 0.1 μM, respectively (Iranshahi et al., 2012). In contrast, 5-hydroxycoumarin did not have any significant antioxidant activity (Steffan et al., 2010). Attaching a prenyl group at the C-8 position of the flavone or flavanone skeleton of apigenin and liquiritigenin, respectively, boosted the cytotoxic activity of their derivatives. Applying increasing concentrations of the unprenylated flavonoids or even of apigenin-*C*8-glucoside (vitexin) up to 250 μmol/L displayed no cytotoxic effect on H4IIE and C6 cell lines. In comparison, licoflavone C (8-prenylapigenin) and isobavachin (8-prenylliquiritigenin) had IC_{50} values of 42 ± 5 and 96 ± 19 μmol/L and IC_{50} values of 37 ± 6 and 69 ± 3 μmol/L against the two cell lines, respectively Upon assessing the inhibitory effect of naringenin chalcone and its prenylated and geranylated derivatives, especially xanthohumol, desmethylxanthohumol and 2´,4´,6´,4-tetrahydroxy-3´-C-geranylchalcone, on the copper-mediated oxidation of LDL, only prenylated compounds exhibited around 70% inhibition after 5 hours of incubation at a concentrations of 5 and 25 μmol/L, whereas non-prenylated naringenin chalcone had a pro-oxidation effect (Miranda et al., 2000). The formation of desmethylxanthohumol from naringenin chalcone was catalyzed by *Hl*PT-1, an acylphloroglucinol-specific PT identified in hop (*Humulus lupulus*) female flowers (Tsurumaru et al., 2010; Tsurumaru et al., 2012). The identified aPT together with another aPT, namely *Hl*PT-2, forms a metabolon, which is responsible for the biosynthesis of *α*- and *β*-bitter acids (Tsurumaru et al., 2012; Li et al., 2015). Humulone induced apoptosis in promyeloid leukemia HL-60 cells in concentrations of 1 to 100 μg/mL. In addition, the overall content of bitter acids proved to be responsible for the sedative effects of hop cones (Schiller et al., 2006; Van Cleemput et al., 2009).

Biological activities of prenylated 1367THX derivatives, which are common among members of the family Hypericaceae, were also reported. Biyouxanthones A and B **(Figure 59)** showed antiviral activity against the hepatitis C virus (Tanaka et al., 2010). Biyouxanthone D also isolated from the roots of *H. chinense* (Tanaka et al., 2010) and later from the root cultures of *H. perforatum* had a significant antifungal activity against *Cryptococcus neoformans* and dermatophytes with MICs of 20.16 and 22.63 μg/ml, respectively (Tocci et al., 2013). Other species of the family like *Garcinia mangostana* contain a number of pharmacologically active poly-prenylated xanthones. α-Mangosgtin induced apoptosis in PC12 rat pheochromocytoma cells with an EC_{50} of 4 μM (Sato et al., 2004) It also constricted the aggregation of *β*-amyloid in primary rat cerebral cortical neurons, which may be a method for controlling the progression of Alzheimer's disease (Wang et al., 2012). γ-Mangostin and garcinone B, another two poly-prenylated 1,3,6,7-tetrahydroxyxanthones from *Garcinia* sp., inhibited COX-1 and COX-2 with potent anti-inflammatory effects (Yamakuni et al., 2006). This broad activity range is not reported for the lead compound tetrahydroxyxanthone, from which all above mentioned prenylated xanthones

originate. A cytotoxic prenylated xanthone, elliptoxanthone A, was isolated from the aerial parts of *Hypericum ellipticum* and it showed moderate cytotoxic activity (IC_{50} = 104 µg/mL) against a number of human colon cancer cell lines (Manning et al., 2011). *Hc*PT and *Mal*DT are two plant aPTs, which were identified recently in cell cultures of *Hypericum calycinum* (Fiesel et al., 2015) and *Morus alba* (Wang et al., 2016) and were able to catalyze the regiospecific attachment of a prenyl group to positions C-8 and C-2 on the xanthone skeleton of 1367THX and 137TrHX, respectively.

H. sampsonii metabolites are not excluded from the prenylation-enhanced pharmacological activities. Biological activities of PPAPs, which were reported for this plant and descend from prenylated xanthones and acyl/benzoylphloroglucinols, are discussed in detail in the introduction part of this work (1.2.2.2). Aromatic prenyltransferases responsible for the biosynthesis of some xanthone-PPAP metabolites along with aPTs involved in the biosynthesis of complex *Hs*-PPAPs are extensively discussed in the sections 5.5.1 and 5.5.2, respectively.

5.3 Aromatic prenyltransferases from *H. sampsonii*

Based on the transcriptomic data available for a plant of the same genus, *Hypericum perforatum*, and previous cloning done in the workgroup using degenerate primers targeting the conserved motifs of aPTs, ten full-length aromatic prenyltransferase sequences were isolated and identified from *Hypericum sampsonii*. To date, the plant is not explored at the genetic and proteomic levels. Thus, the identified genes and the described enzymatic activities of their expressed recombinant proteins are functionally novel. Sequence analysis of these enzymes proved that they possess not only the structural but also the common functional features characterizing plant aromatic prenyltransferases and differentiate them from members of the ABBA PT-superfamily. Explicitly mentioned are the presence of a signal peptide at the N-terminus of the protein, the presence of transmembrane α-helices (Sasaki et al., 2008; Yazaki et al., 2009; Tsurumaru et al., 2010) as well as the occurrence of two aspartate-rich motifs having the amino acid sequences NQxxDxxxD and KDxxDxxGD (Akashi et al., 2009; Tsurumaru et al., 2010). Functionally, active *Hs*PTs showed a narrow range of accepted aromatic prenyl substrates and absolute dependence on a divalent cation as a cofactor for the catalysis

Previously, X-ray crystallography showed that soluble aromatic prenyltransferases from bacteria and fungi have in their secondary structure a 10-stranded, antiparallel β-sheet of five repeating $\alpha\beta\beta\alpha$ structural motifs, after which they were named as ABBA family. This β-sheet structure forms a barrel-like reaction cylinder, in which the prenylation takes place (Heide, 2009; Saleh et al., 2009; Winkelblech et al., 2015). This large reaction pocket rationalizes the wide substrate specificity of bacterial and fungal aPTs and distinguishes them from plant aPTs, which have a quite limited spectrum of accepted substrates (Schuller et al., 2012; Winkelblech et al., 2015; Chen et al., 2017). All known plant membrane-bound aromatic prenyltransferases have two aspartate-rich motifs, which are essential for the enzymatic activity (Akashi et al., 2009; Tsurumaru et al., 2010). The first one with the amino acid sequence N(D/Q)xxDxxxD is proposed to be involved in

prenyl diphosphate binding via metal ions (Guo et al., 2005; Brandt et al., 2009). The second motif KDxxDxxGD assigned to membrane-bound prenyltransferases is responsible for the binding of their aromatic substrates (Kuzuyama et al., 2005; Stec and Li, 2012). On the other hand, aPTs of the ABBA family have no aspartate-rich conserved motifs and, as a result, their catalytic mechanism does not involve the coordination of Mg^{+2}. Instead, the active center of soluble aPTs bears positively charged amino acids to take over the function of Mg^{2+} (Tello et al., 2008). There is only one exception among the bacterial aPTs, namely NphB, whose activity is dependant on the presence of Mg^{2+} in the enzymatic reaction (Heide, 2009). This enzyme, together with CloQ, forms a subfamily of soluble a PTs (Winkelblech et al., 2015).

Multiple sequence alignment of *Hs*PTs with reported plant aPTs **(Figure 61)** revealed that all known plant aPTs, including the currently identified aPTs, have not only the conserved aspartate-rich motifs essential for the catalytic activity but also another highly conserved three-amino-acid motif directly behind the first motif, assigned as asparagine-lysine-proline. However, no report about the role of these amino acids is available. The extended first motif has the amino acid sequence N(Q/E)xxDxxxD(K/R)(I/V)NKPx(L/S)P. The next motif has the amino acid arrangement KDx(P/S)DxxGD.

All sequences identified in this study express the availability of membrane-spanning helices, as predicted by the results of TMHMM and SOUIS online tools. The number of predicted TMH ranged from six to nine. In addition, the usage of the TargetP and ChloroP online platforms for the prediction of the targeting signal revealed that all *Hs*PTs have a targeting signal directing them to chloroplasts, except for *Hs*PT5 (*Hs*PTpat) whose prediction results for the signaling peptide were contradictory. TargetP predicted it as mitochondrial whereas chloroP resulted in expected chloroplast targeting **(Table 26)**. The incidence of these typical plant aromatic prenyltransferase traits was confirmed practically for two representative examples of *Hs*PTs, namely *Hs*PT2 (*Hs*PT8PX) and *Hs*PT5 (*Hs*PTpat). As indicated by the subcellular localization of C-YFP-marked fusion constructs of the two proteins (4.8), they were localized to the membranes of chloroplasts in comparison to the cytoplasmic subcellular localization of their corresponding truncated versions **(Figure 56 and Figure 58)**. With the exception of the geranyltransferase *Le*PGT-1, which was found to be integrated into the membranes of the endoplasmic reticulum (Ohara et al., 2009), all other reported members of the plant aPT family showed subcellular localization in the plastids (Sasaki et al., 2008; Akashi et al., 2009; Karamat et al., 2014; Munakata et al., 2014; Munakata et al., 2016).

The phylogenetic positioning of *H. sampsonii*-identified prenyltransferases fulfilled the expectation that most of them were grouped in the same clade, which included the *Hs*PT xanthone-DMAPP transferases (*Hs*PT8PX and *Hs*PTpat) and the closely related xanthone PTs characterized from *H. calycinum* (Nagia et al., submitted). *Hs*PTAPG did not cluster together with the functionally related aPTs that utilize phloroglucinol derivatives as prenyl acceptors. *Hl*PT1 and *Hl*PT2 catalyze the formation of bitter acids in hop (Li et al., 2015) and *Cannabis sativa* PT1(*Cs*PT1) catalyses the geranylation of olivetolic acid to form cannabigerolic acid in *Cannabis*

sativa (Page and Boubakir, 2014). This evolutionary positioning of the *Hs*PTs emphasizes and bioinformatically justifies the enzymatic activities settled in the current study. Two polymorphs also identified in *H. sampsonii* and assigned the names *Hs*PT6 and *Hs*PT6a were located on the clade together with homogentisate phytyltransferases involved in the biosynthesis of tocopherol (Venkatesh et al., 2006; Wang et al., 2015a), which rationalizes the lack of activity towards any of the substrates used in this study.

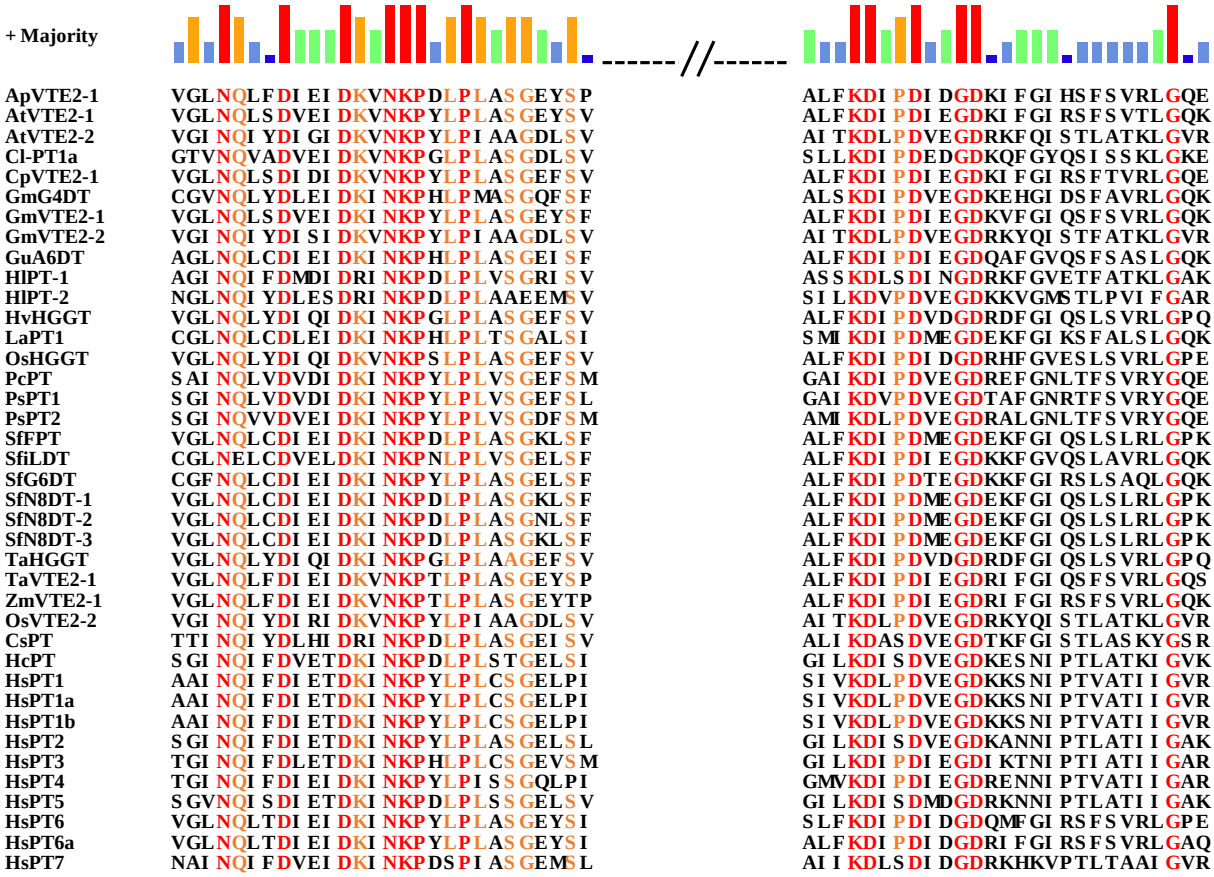

Figure 61: Multiple sequence alignment of *Hs*PTs with known aPTs denoting the highly conserved aspartate regions. Highly conserved amino acids are colored red and less conserved amino acids are colored orange.

An observable phenomenon among the analyzed aPT genes is the polymorphism, where the same primer pair can fish different alleles whose sequences are closely related to each other (Biedermann, 2017). *Hs*PT1, *Hs*PT1a, and *Hs*PT1b are three alleles with high sequence similarity. The longer isoform, *Hs*PT1, has a high homology of 99.6% and 99.7% at the nucleotide level and 99.0% and 99.2% at the polypeptide level to *Hs*PT1a and *Hs*PT1b, respectively **(Figure 62 A and B)**. Shorter alleles have a sequence identity of 99.5% and 99.7% at the nucleotide and amino acid levels, respectively. Comparing the amino acid sequences revealed, besides a 4-amino acid-gap, four amino acid differences between *Hs*PT1 and *Hs*PT1a, of which the only significant one was the exchange of positively charged lysine (K_{96}) with negatively charged glutamic acid (E_{96}) at the corresponding position. In addition, one of the two amino acid differences between *Hs*PT1 and the

third allele, *Hs*PT1b, may be considered compelling and affect the structure or function of the protein because the hydrophilic serine moiety S_{198} is replaced with the small hydrophobic leucine L_{200} in the *Hs*PT1 structure. Mostly, these amino acid changes are considered as silent polymorphism, when they are far from the active site and do not affect the conformation. After sequencing the amplicon of *Hs*PT6, another allele emerged which was more divergent than described in the previous situation with *Hs*PT1. *Hs*PT6 and *Hs*PT6a have a similarity of 91.2% and 86.7% at nucleotide and protein levels, respectively **(Figure 62 C and D)**. *Hs*PT6a encodes four amino acid less than its longer polymorph *Hs*PT6 and they differ by 52 amino acids. This high level of polymorphism expresses the fast evolutionary rate within the species (Wang et al., 2015a).

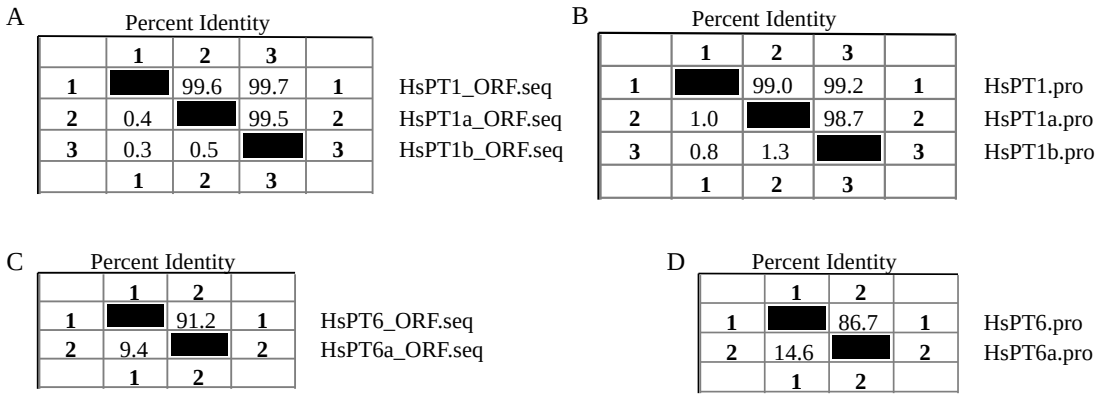

Figure 62: Sequence similarity percentages between polymorphs. A, B) Alleles *Hs*PT1, *Hs*PT1a, and *Hs*PT1b at nucleotide and amino acid levels, respectively. C, D) Alleles *Hs*PT6 and *Hs*PT6a at nucleotide and amino acid levels, respectively.

5.4 Challenging heterologous expression system

The natural abundance of proteins is too low to provide sufficient amounts for their isolation, identification, and structural or functional characterization, thus heterologous overexpression is a crucial molecular biology tool to get a considerable supply of naturally occurring proteins (Wagner et al., 2006; Wagner et al., 2008). A second advantage of the heterologous expression is ensuring the study of only one isoform of the desired protein, thus bypassing overlapping substrate specificities and providing proteins for further purposes, such as purification of enzymes for kinetic and structural studies (Anna et al., 2005).

Despite the fact that protein overexpression in *E. coli* affords a robust system for heterologous protein expression, it is not applicable for the production of eukaryotic membrane proteins (Farrokhi et al., 2013). Expression of such proteins interferes with the membrane viability and is toxic for the prokaryotic cell system (Wagner et al., 2006). Most of the overexpressed membrane proteins are located in the cell membrane of the bacteria and the toxicity is primarily caused by the narrow capacity of the Sec translocon, resulting in aggregation of the overexpressed protein and formation of inclusion bodies with a severe negative effect on not only the plasma membrane

but also the cytoplasmic proteome (Buchanan, 1999; Wagner et al., 2007). In addition, heterologous membrane protein overexpression disturbs the cytoplasmic protein homeostasis and reduces the level of energy-producing enzymes in the cell. Wagner and co-workers (2007) reported that the degree of bacterial cell toxicity was dependent neither on the number of TMH nor on the length of the proteins but only on the amount of the expressed material (Wagner et al., 2007). Out of the toxicity on the bacterial cells, the eukaryotic post-translational machinery is not always functional in prokaryotic cells (Bencúrová et al., 2003), which necessitates the production of stable, active and accurately folded proteins (Drew et al., 2003; Pagny et al., 2003). One *E. coli* strain, namely Lemo21 (DE3, New England Biolabs) was developed for the overexpression of membrane proteins, where the activity of T7 RNA polymerase can be tuned by its natural inhibitor T7 lysozyme (T7 lys), which in turn is under the control of the well-titrable L-rhamnose promotor (*rha* BAD) to regulate the extent of overexpression. The fusion construct of YidC-GFP was used to test the suitability and the yield of expression in the Lemo21 strain (Wagner et al., 2008). YidC is prokaryotic membrane integrated insertase and constitutes a part from the Sec translocon in *E. coli* (Samuelson et al., 2000), which can facilitate the insertion of membrane proteins either autonomously or in cooperation with SecYEG14–16 (Sachelaru et al., 2017). However, overexpression of *Hs*PT5 in the Lemo21 strain failed to yield active protein (data not shown). A reasonable explanation of this unexpected result lays in the difference in structural features between eukaryotic and prokaryotic membrane proteins as the partial folding of the β-barrel of the later occurs before insertion into the prokaryote membrane (Eppens et al., 1997). In addition, β-barrel enzymes contain a relatively high number of charged residues that make their insertion quite easier than that of heterologous plant membrane integral proteins with highly hydrophobic α-helices (Booth and Curran, 1999).

A model of comparison between the eukaryotic against bacterial platforms was introduced by Farrokhi et al. (2013), who compared the overexpression of plant membrane proteins involved in the biosynthesis of plant cell wall in bacteria (*E.coli*), yeast (*Pichia pastoris*), *N. benthamiana*, insect, and mammalian cells was compared. The prokaryotic expression system failed to produce any functionally active protein, whereas, all eukaryotic systems yielded biochemically active, accurately folded proteins because they are expected to have the eukaryotic post-translational modification machinery, which simulates processes found in higher plants.

The aforementioned discussion reflects, to a far extent, the superiority of eukaryotic expression systems over the prokaryotic platform for the overexpression of plant membrane proteins including prenyltransferases. Furthermore, to date, no published recombinant plant aPT was functionally expressed in any of the bacterial systems. Most of the identified recombinant plant prenyltransferases were overexpressed in yeast (*Saccharomyces cerevisiae*) (Yazaki et al., 2002; Sasaki et al., 2008; Akashi et al., 2009; Shen et al., 2012; Munakata et al., 2014). Some others were heterologously expressed either in insect, namely *Hl*PT-1 (Tsurumaru et al., 2012) and *Le*PGT1 (Ohara et al., 2013) or plant systems like *Petroselinum crispum*, namely *Pc*PT (Karamat et al., 2014) and *Ps*PT1 and *Ps*PT2 (Munakata et al., 2016). According to the published literature,

there is no homogeneous or generalized best eukaryotic expression system for the production of recombinant plant aromatic PTs. Therefore, three overexpression systems were used throughout the course of the current study. Yeast and insect systems were used for overexpression of proteins for activity testing and the plant system was used to express fusion constructs with yellow fluorescent marker gene to test the subcellular localization of xanthone *Hs*PTs. The difference in the number of active *Hs*PTs between yeast- and insect-expressed proteins confirmed the fact that there is no united system for overexpression for the aPTs.

5.5 Functional characterization of recombinant *Hs*PTs

5.5.1 Xanthone-related *Hs*PTs

5.5.1.1 Enzymatic activity screening

Activity testing of *Hs*-identified PTs revealed two xanthone-prenylating enzymes, namely *Hs*PT8PX and *Hs*PTpat. The former converts 1367THX to its monoprenylated derivative, and patulone is formed as a minor product within the same reaction. *Hs*PT8PX can also catalyze further prenylation on its own product (8PX) to produce patulone (4.6.1.2; **Figure 63 A**). *Hs*PTpat can form patulone as a single product either from 1367THX by attaching two geminal prenyl moieties at C-8 on the xanthone skeleton or by adding only one prenyl group to the prenylated xanthone derivative (8PX) when this is utilized as a substrate (4.6.1.2; **Figure 63 B**). Two paths were suggested for the biosynthesis of the diprenylated patulone. The first route is the stepwise attachment of two prenyl-groups, where *Hs*PT8PX catalyzes the formation of the monoprenylated intermediate (8PX), which then undergoes prenylation to the diprenylated derivative (patulone) catalyzed by *Hs*PTpat (path A; **Figure 63 C**). The second path postulates a direct formation of patulone by successive addition of two prenyl groups to 1367THX employing only *Hs*PTpat (path B).

Upon analyzing the kinetic parameters of both enzymes, it was apparent that the K_m value for 1367THX with *Hs*PT8PX is about 4-fold less than that upon the use of the same substrate by *Hs*PTpat. Furthermore, the V_{max} of the reaction catalyzed by *Hs*PT8PX is 40-fold higher than that for the reaction catalyzed by *Hs*PTpat. Both enzymes showed comparable K_m values for 8PX. However, the rate of the reaction with *Hs*PTpat was ≈ 20 times higher than that with *Hs*PT8PX, which explains the significant consumption of 8PX by *Hs*PTpat. Thus, it was experimentally supported that the main substrate for *Hs*PT8PX is 1367THX and the major substrate for *Hs*PTpat is 8PX. As a result, path A is confirmed where these enzymes catalyze two successive prenylation steps. Firstly, 1367THX is consumed by *Hs*PT8PX to form the mono-prenylated derivative and then 8PX is used as a substrate for the subsequent prenylation on the same carbon atom (C-8) to yield the di-prenylated derivative patulone **(Figure 63)**. Further confirmation of this successive prenylation pattern was achieved by real-time gene expression analysis of the two *Hs*PTanalogues, i.e. the xanthone PTs identified in the cell culture of *H. calycinum*. After applying yeast extract as elicitor, the gene for the 1,3,6,7-tetrahydroxy-8-prenylxanthone-forming enzyme, *Hc*PT8PX, exhibited the maximum expression level eight hours post-elicitation and the gene for the patulone-forming enzyme, *Hc*PTpat, showed the highest expression level twelve hours post-elicitation

(Biedermann, 2017; Nagia et al., submitted). So far, nothing is recorded about gem-diprenylation of the xanthone skeleton, except for a single report about similar reactions on acylphloroglucinols. Thus, this one is the first concerning with the successive prenylation of xanthones (Tsurumaru et al., 2012; Li et al., 2015).

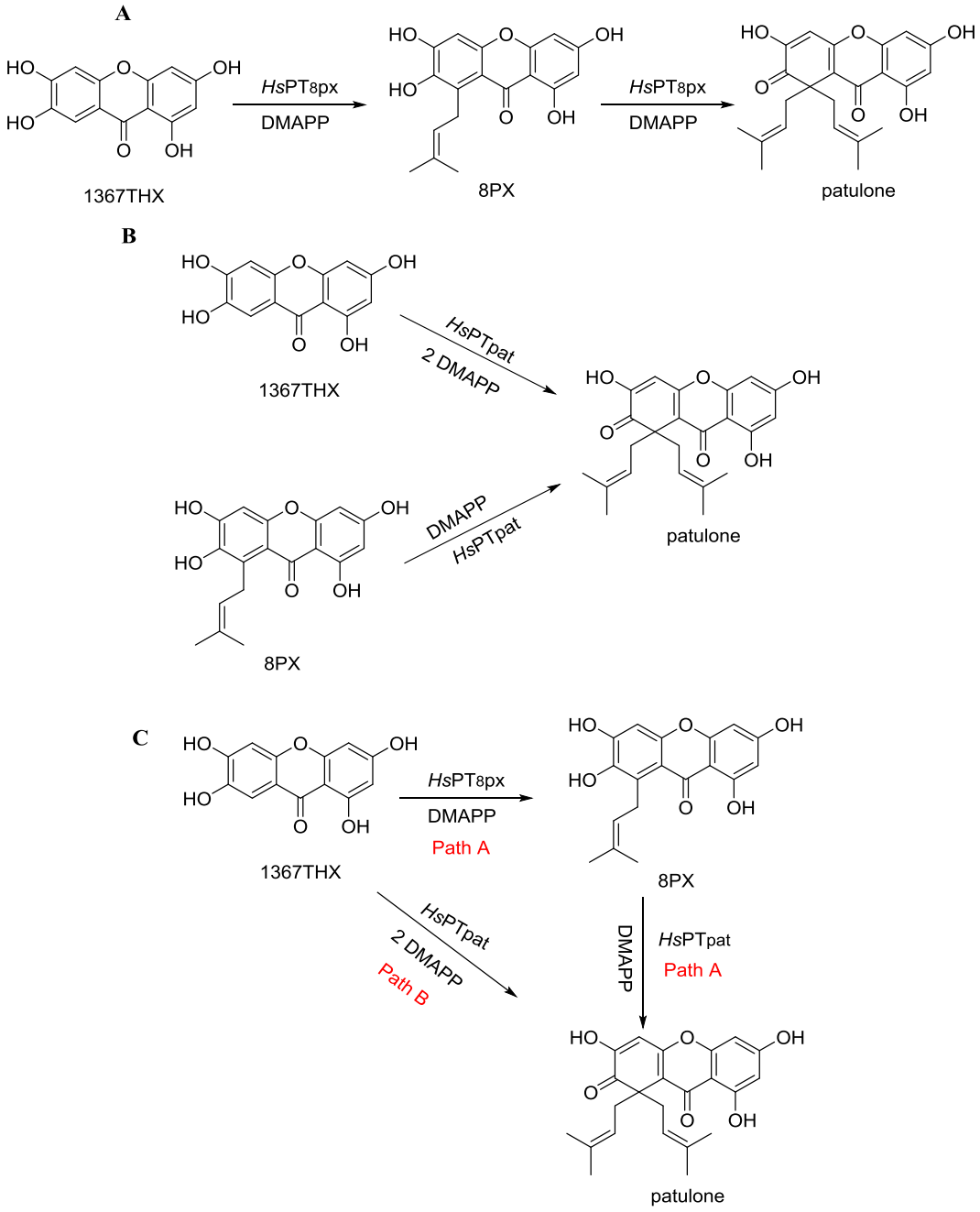

Figure 63: Enzymatic activities of xanthone *Hs*PTs. A) The catalytic activity of *Hs*PT8PX. B) The catalytic activity of *Hs*PTpat. C) Alternative biosynthetic pathways converting 1367THX to patulone. Based on the kinetic measurements, path A is the preferred one.

5.5.1.2 Proposed biosynthetic pathway of pharmacologically active plant constituents bearing a xanthone skeleton

The above results led us to the assumption of a biosynthetic pathway for a series of xanthone derivatives reported for *H. sampsonii*. 8PX, the anti-inflammatory patulone (Li et al., 2004; Yamakuni et al., 2006) and its structurally related antibacterial compound hyperixanthone A (Xiao et al., 2008) are derived from 1367THX as a core xanthone skeleton through the formation of the di-prenylated xanthone derivative patulone as an intermediate. The biosynthesis of this special type of PPAPs is achieved in two stages: first the formation of the tetrahydroxyxanthone nucleus and then the decoration by addition of side chains. The 1,3,6,7-tetrahydroxyxanthone nucleus is biosynthesized through the BPS-catalyzed condensation of three molecules of malonyl-CoA and one molecule of benzoyl-CoA originating from phenylalanine (Gaid et al., 2012) to form 2,4,6-trihydroxybenzophenone (Liu et al., 2003). Subsequently, the latter intermediate undergoes a regioselective *para*-phenol coupling and intramolecular cyclization to produce 1,3,7-trihydroxyxanthone. Recently, a bifunctional cytochrome P450, namely CYP81AA1, was capable of both hydroxylation and subsequent cyclization (El-Awaad et al., 2016). Finally, an enzyme called xanthone 6-hydroxylase serves to add a hydroxyl group to C-6 on the xanthone skeleton to form the 1,3,6,7-tetrahydroxyxanthone scaffold (Schmidt et al., 2000). Subsequently, *Hs*PT8PX and *Hs*PTpat catalyze the consecutive attachment of prenyl side chains on the formed tetrahydroxyxanthone nucleus and form the anti-inflammatory patulone. An antimicrobial agent, namely hyperixanthone A, is formed by the following step, a reverse prenylation. To date, however, no plant reverse prenyltransferase was reported. Reverse prenylation has been described for dimethylallyl tryptophan synthases (DMATS) on the nitrogen atom of the tryptophan moiety by an enzyme called CymD (Qian et al., 2012) or on C3 position of an indol system using the enzymes CdpNPT, AnaPT, or CdpC3PT (Yin et al., 2009; Yin et al., 2010; Tanner, 2015). The assumption of the participation of both *Hs* enzymes in the same biosynthetic pathway is boosted by the results of localization studies, where both proteins were targeted to the plastids.

The formed prenylated tetrahydroxyxanthone skeleton can undergo downstream modifications, which justify the biosynthesis of related xanthone metabolites in other species of the genus *Hypericum* or other genera within the family Hypericaceae. An example is the pyranoxanthone phytoalexin metabolite hyperxanthone E, identified previously in *H. calycinum* cell cultures (Gaid et al., 2012) as well as *H. scabrum* and *Garcinia esculenta* (Tanaka et al., 2004; Zhang et al., 2014). The formation of a 2,2-dimethylbenzopyran ring could be accomplished spontaneously through the intramolecular cyclization of the γ-carbon atom of the prenyl group attached to the xanthone skeleton with the *o*-hydroxy group. This reaction is feasible under the biosynthetic conditions inside plant cells (Molyneux and Jurd, 1970). Alternatively, the ring closure is catalyzed by a cyclase, as described by Batista et al. (2017) for *o*-prenylated phenyl compounds. This intramolecular cyclization could be catalyzed regardless of the electronic environment of substituents on the ring, to which the prenyl and hydroxyl groups are connected (Nicolaou et al., 2000) **(Figure 64)**.

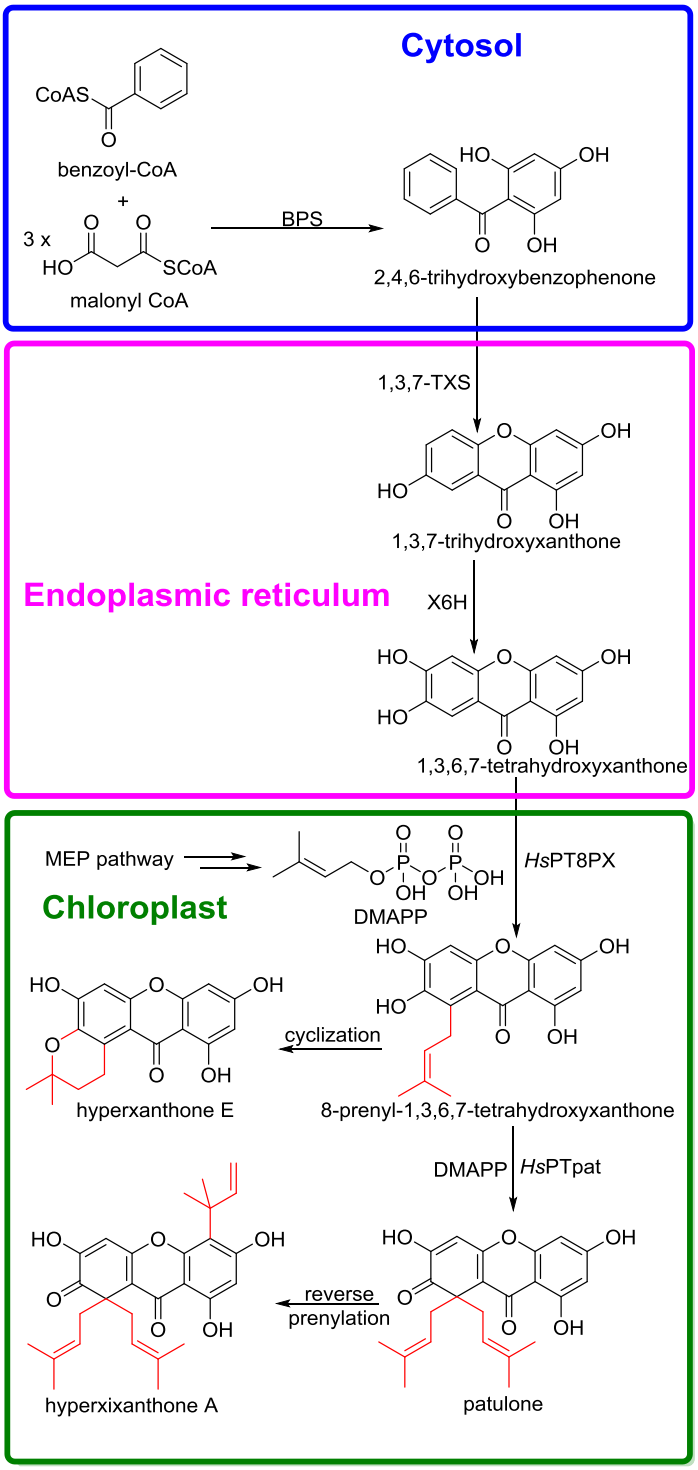

Figure 64: Proposed biosynthesis of patulone and hyperixanthone A in *H. sampsonii* as well as other related xanthone derivatives identified in members of the family Hypericaceae. BPS, benzophenone synthase; 1,3,7-TXS, 1,3,7-trihydroxyxanthone synthase; X6H, xanthone 6-hydroxylase.

Despite the potential pharmacological activities of *H. sampsonii* chemical constituents including prenylated xanthone derivatives, their limited isolation yields (0.0015-0.000026% w/w from plant material for hypersampsone G and sampsonion B, respectively) and the lack of a convenient regioselective synthetic scheme restrict their use in clinical trials or even in exploring their pharmacological activities. The cytotoxic prenylated xanthone derivative elliptoxanthone A (8-prenyl-1,4,7-trihydroxyxanthone) was isolated from *H. ellipticum* in a yield ≈ 0.005% from the starting plant material (Manning et al., 2011). Its total synthesis was accomplished in 2016, which comprises 12 steps with an overall yield of only 28% *via* anion-accelerated aromatic oxy-Cope rearrangement (Fujimoto et al., 2016). Through the reaction of different tri- or tetra-hydroxylated xanthone derivatives with prenyl bromide, a non-selective mixture of *O*- and *C*-prenylated synthetic products could be formed with yields ranging from 1% to 5% (Lim et al., 2011; Lim et al., 2012; Yen et al., 2012). An additional challenge is the formation of undesired artifacts, mostly the production of pyranoxanthone derivatives which form through the intramolecular cyclization between the prenyl group and the adjacent hydroxyl group. A good illustration was shown for the synthesis of the anti-inflammatory *γ*-mangostine (1,3,6,7-tetrahydroxy-2,8-bis(3-methyl-2-butenyl)-9H-xanthen-9-one) by demethylation of *α*-mangostin, when the desired product was formed only at a yield of 3% while the benzopyran derivative was produced as a major product at 40% (Gokaraju et al., 2009).

The utilization of structurally related xanthone derivatives (**Figure 39**) as aromatic substrates for *Hs*PT8PX and *Hs*PTpat revealed the strict structural selectivity of *H. sampsonii* xanthone-PTs. Considering the accepted substrates, only 1367THX and its monoprenylated derivative could be prenylated specifically at position C-8. However, the closely related compound 137TrHX showed only trace activity, being prenylated to form a trace product, which may be according to the retention time and the UV spectrum the mono-prenylated 137TrHX. On the other hand, no prenylated products were detected when closely related tetrahydroxyxanthone (1356THX) or its trihydroxylated analog (135TrHX) were used as substrates under the utilized test conditions. Furthermore, when C-8 in the xanthone skeleton is blocked or no longer available for a reaction like in hyperxanthone E and patulone, respectively, no products were formed. These results, together with the high and specific conversion yield within 90 min (≈ 60%) upon upscaling the 8PX-producing enzymatic reaction (3.2.6), acknowledge the utilization of enzymatic bio-catalysis to overcome the problems of conventional chemical synthesis of PPAPs.

5.5.2 Acylphloroglucinol-related *Hs*PT

5.5.2.1 Enzymatic activity screening

An acylphloroglucinol alkylating enzyme was detected during activity screening of *Hs*PTs. *Hs*PTAPG catalyzes the conversion of some of the tested acylphloroglucinols to their corresponding 3-monogeranylated derivatives. Significant geranyltransferase activity was observed for 246trHiBP, 2MBP, and 246TrHBP, whereas other accepted aromatic substrates from the same chemical group showed only trace activity and even no products were detected when prenylated benzoylphloroglucinol and pentahydroxylated benzophenone (maclurin) were

employed as geranyl acceptors. On the other hand, the narrow substrate utility window of this enzyme was further confirmed when no xanthones or flavonoids were accepted (Heide, 2009; Yazaki et al., 2009). *Hs*PTAPG showed the highest affinity, in terms of nmol product formation and Michaelis-Menten kinetics, for 2-methyl-2`,4`,6`-trihydroxybutyrophenone (2MBP) among the acylphloroglucinol family. This affirms the first report of an acylphloroglucinol PT not only from the plant *H. sampsonii* but also from the genus *Hypericum*. Currently, all reported plant acylphloroglucinol-active PTs are from the family Cannabinaceae. The geranylating enzyme *Cs*PT1, identified in *Cannabis sativa*, adds a geranyl moiety to olivetolic acid (Page and Boubakir, 2014). For another plant belonging to the same family, *Humulus lupulus*, a heteromeric prenyltransferase complex of two prenyltransferases, namely *Hl*PT-1 and *Hl*PT-2, was reported and had a more flexible substrate spectrum extended to chalcones and prenylated acylphloroglucinols (Tsurumaru et al., 2012; Li et al., 2015). Acyl- and benzoylphloroglucinol dimethylallylation was also reported for two fungal aPTs with wide substrate acceptance. AnaPT and AtaPT, apart from their main tryptophan-related substrates (Liu and Walsh, 2009; Chen et al., 2017), also catalyzed the formation of monoprenylated 246TrHiBP, 246TrHVP, and 246TrHBP. Furthermore, AtaPT can even use the formed product for additional prenylation steps and it also has an extended prenyl donor promiscuity for DMAPP, GPP, and FPP (Zhou et al., 2015; Zhou et al., 2017), which may be attributed to the *β*-barrel structure of fungal PTs in the DMATS superfamily, as discussed before (see 5.3).

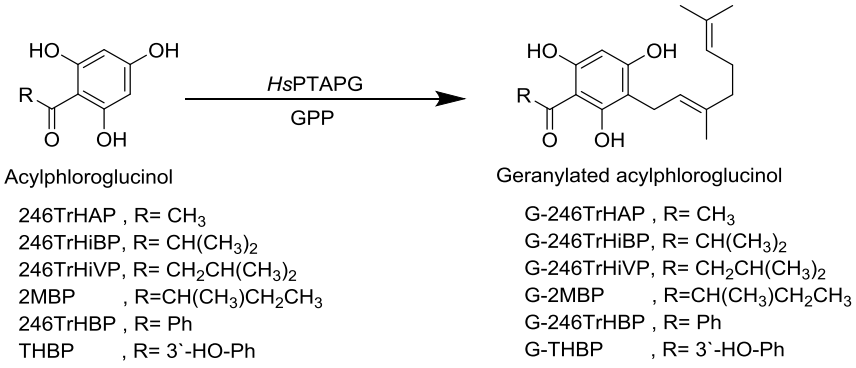

Figure 65: Catalytic activities of *Hs*PTAPG.

5.5.2.2 First-step geranylation in the biosynthesis of PPAPs

H. sampsonii is a rich source of type A and to a lesser extent type B PPAPs developed from small different acyl- and benzoylphloroglucinol scaffolds, for example the phlorbenzophenone derivatives sampsoniones and hyperisampsins, the phlorisobutyrophenone derivatives hypersampsones, and the phlorisovalerophenone building block in sampsonol F (Hu and Sim, 2000; Xiao et al., 2007; Xin et al., 2012; Chen et al., 2014; Zhu et al., 2015; Tian et al., 2016) (1.2.2.2.2). To date, no reports about PPAPs bearing the 2-methylbutyrophenone nucleus could be traced for *H. sampsonii*, which, according to the present results, offers the chance that *in vitro* cultivated plants form a novel PPAP bearing this scaffold similar to adhyperforin in *H. perforatum* (Klingauf et al., 2005).

The first section of the biosynthesis of the above-mentioned *Hs*-PPAPs should be the formation of acylphloroglucinol starter units through the condensation of 3 molecules of malonyl CoA with isobutyryl-, 2-methylbutyryl-, isovaleryl- and benzoyl-CoAs to form 246TrHiBP, 2-MBP, 246TrHVP, and 246TrHBP, respectively. These condensation reactions are done by IBS or VPS for the aliphatic building blocks and by BPS for the aromatic moiety (Okada and Ito, 2001; Beerhues and Liu, 2009; Beerhues, 2011). *Hs*PTAPG is supposed to catalyze the first step of C-geranylation in the biosynthesis cascade of the above-mentioned caged pharmacologically active metabolites descending from different lead acylphloroglucinols. The suggested biosynthetic pathways mimic that proposed for the model PPAP hyperforin (Adam et al., 2002; Beerhues, 2006, 2011), where the construction of a monocyclic polyprenylated acylphloroglucinol (MPAP) intermediate is achieved through the addition of one GPP and two DMAPP molecules to form an intermediate comparable to α- and β-bitter acids in hop cones originating from 246TrHiVP (Okada and Ito, 2001; Li et al., 2015) **(Figure 66)**. Afterward, the formed MPAP undergo intramolecular cyclization at different positions on the carbon skeleton of the starter molecule, followed by different cascades of hydroxylation or further prenylation reactions to give rise to the caged molecules **(Figure 7; Figure 9)** (Cuesta-Rubio et al., 2001)

*Hs*PTAPG accepts multiple substrates, which encourages its future adaptation to the production of PPAPs identified not only in *H. sampsonii* but also in other related plants, such as hyperforin and garsubellin A, whose pharmacological activities are well established but their syntheses are still challenging due to the complex substitution patterns and the presence of multiple chiral centers (Cuesta-Rubio et al., 2001; Adam et al., 2002; Ciochina and Grossman, 2006). The first total synthesis of a PPAP was achieved in 2005 for garsubellin A (Kuramochi et al., 2005; Siegel and Danishefsky, 2006), a neurotropic isobutyrophenone-PPAP identified in the wood of *Garcinia subelliptica* (Fukuyama et al., 1997; Fukuyama et al., 1998). Subsequently, many approaches were introduced to enhance the prenylation, cyclization, and stereochemistry, hence the yield of the chemical synthesis of this type A PPAP (Ciochina and Grossman, 2006). Numerous trials were also approached towards the total synthesis of hyperforin. However, the first success was accomplished in 2010 for the synthesis of *ent*-hyperforin, the antipode of hyperforin, which comprised 51 steps including Diels–Alder reaction augmented by a chiral cationic iron, a diastereoselective Claisen rearrangement, an intramolecular aldol condensation, and a vinylogous Pummerer rearrangement (Shimizu et al., 2010). Since then, many trials to simplify the synthetic scheme of hyperforin were attempted. Through an 18-step scheme, the enantioselective synthesis of hyperforin was totally attained in 2013 (Sparling et al., 2013). Later in 2016, the synthetic pathway of this important PPAP was shortened to 10 steps but the low yield and selectivity (Ting and Maimone, 2016) were the marked disadvantages.

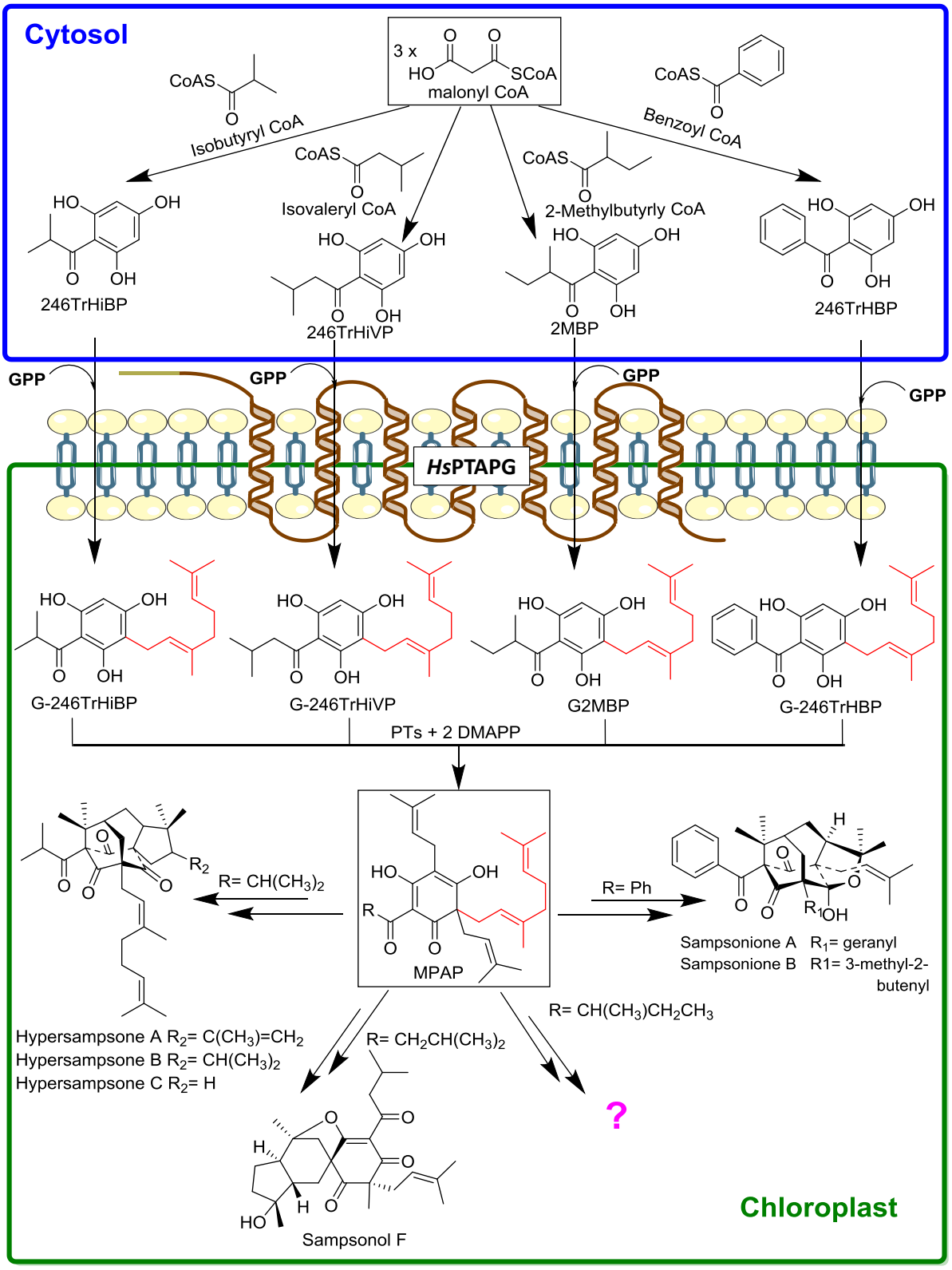

Figure 66: Involvement of *Hs*PTAPG in the proposed biosynthesis of various PPAP series in *H. sampsonii*.

Attempts for the synthesis of type B PPAPs were succeeded first in 2011 (Biber et al., 2011) introducing a simplified scheme for the synthesis of three benzoyl phloroglucinols, namely oblongifolin A (Hamed et al., 2006), hyperibone L (Tanaka et al., 2004), and *epi*-clusianone (Piccinelli et al., 2005; Santos et al., 2007) and one phlorisobutyrophenone derivative, hyperpapuanone (Winkelmann et al., 2001). These compounds were isolated previously from different members of the *Hypericum* and *Garcinia* genera and have verified antimicrobial and anticancer activities. The main problem with the introduced synthetic scheme is the low yield ranging from 6- 22% and the formation of non-natural products due to the difficult configuration of the asymmetric quaternary carbons (Biber et al., 2011). Sampsonione P, a caged phlorbenzophenone isolated from *H. sampsonii* (Xiao et al., 2007), together with hyperibone I from *H. scabrum* (Matsuhisa et al., 2002) were fully synthesized in 2013 applying a regioselective bidirectional prenylation synthetic approach from a common core (Lindermayr and Plietker, 2013). Another disadvantage of the chemical synthesis of prenylated PPAPs was practically touched during the present study by the formation of the benzopyran derivative while attempting the synthesis of mono- and diprenylated 246TrHBP (4.5.1).

5.6 The proposed catalytic mechanism of prenylation

Biochemical reactions catalyzed by aromatic prenyltransferases involve the C-C coupling between isoprenyl diphosphate units of different lengths and an aromatic substrate, which is usually a phenol (Bräuer et al., 2008; Wessjohann et al., 2009). This carbon-carbon, or even carbon-oxygen bond formation is mediated by two defined catalytic mechanisms (Kuzuyama et al., 2005; Luk and Tanner, 2009), namely dissociative and associative mechanisms.

5.6.1 Dissociative mechanism S_N1

This S_N1 or dissociative route invokes an initial ionization of the alkyl donor with the diphosphate as a leaving group to form an allyl cation/pyrophosphate ion pair. The activated carbon on the skeleton of the prenyl acceptor then adds to the formed carbocation and an arenium ion intermediate is generated. Finally, a step of deprotonation explains the re-aromatization of the aromatic substrates **(Figure 67)**. Terpene cyclases as an example of aPTs involved in secondary metabolism (Cane, 1999), FPP synthase from primary metabolism (Tarshis et al., 1994) and fungal aPTs from the DMATS family (Luk and Tanner, 2009) follow this prenylation mechanism.

5.6.2 Associative mechanism S_N2

A second, associative mechanistic pathway involves the nucleophilic attack of the aromatic ring onto C-1 on the prenyl pyrophosphate with a simultaneous displacement of the diphosphate group and direct formation of the arenium ion intermediate (**Figure 67**). This S_N2 pathway was previously reported for protein farnesyltransferase (Long et al., 2002; Luk and Tanner, 2009). A protein farnesyltransferase catalyzes the attachment of a farnesyl group to nucleophilic cysteines on the substrate protein with a direct separation of pyrophosphate by a thiolate (Long et al., 2002).

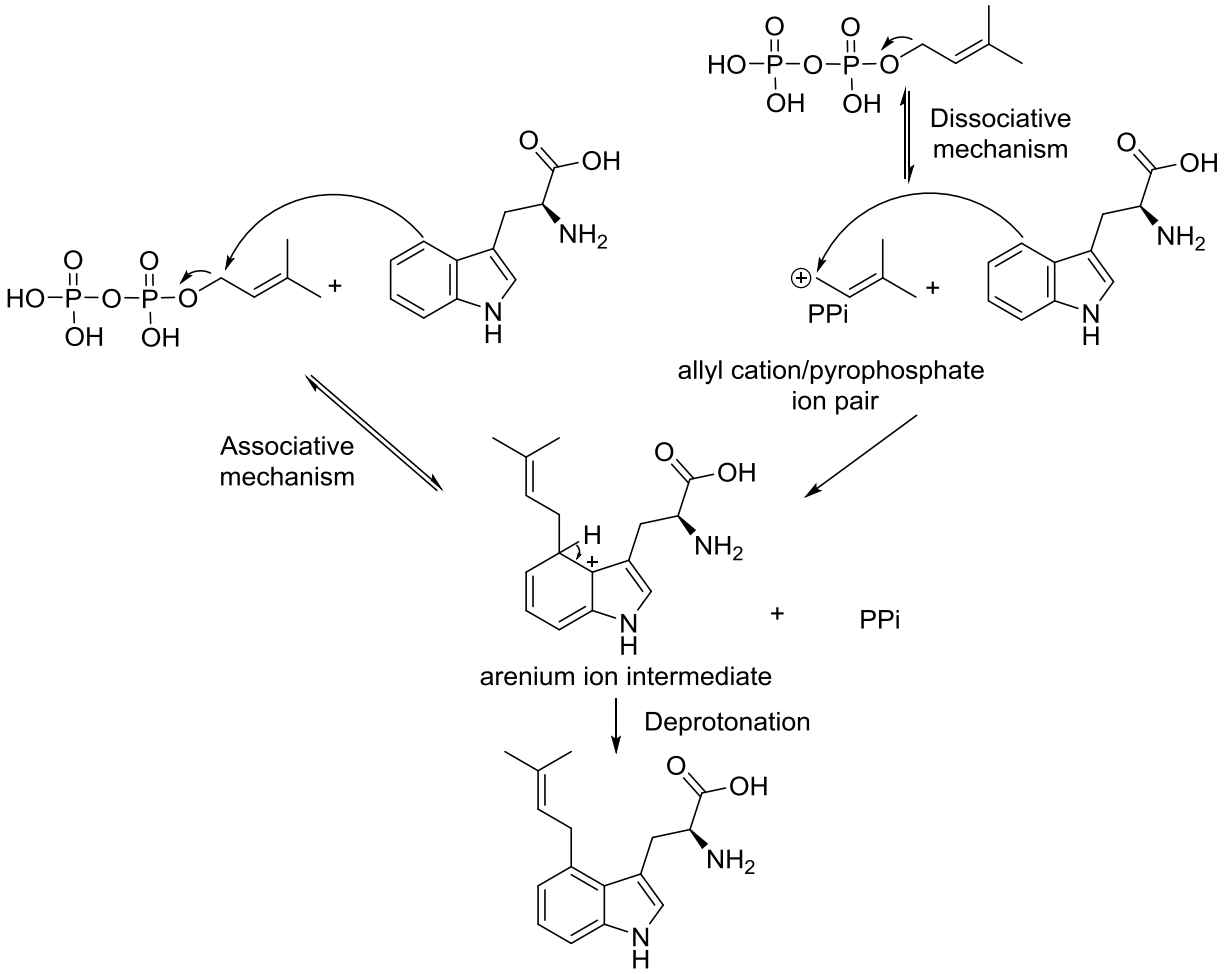

Figure 67: Postulated catalytic mechanisms of tryptophan prenylation by DMATS. Adapted from Luk and Tanner (2009).

5.6.3 Mechanism of *Hs*PTs

The family UbiA was named after the prototype enzyme *Ec*UbiA, identified for the first time from *E. coli*. The enzyme catalyzes the condensation of isoprenyl units of different lengths with p-hydroxybenzoic acid (PHB) for the formation of the electron carrier ubiquinone (Young et al., 1972). UbiA is a membrane-integrated protein that contains two shorter conserved Asp-rich motifs with the amino acid sequence DXXXD and depends on magnesium cation for its catalytic activity (Melzer and Heide, 1994). The reaction mechanism catalyzed by UbiA was confirmed to follow the dissociative (S_N1) pathway through several pieces of evidence. First is the calculations of reaction enthalpies for several steps of the catalytic action through the models provided for UbiA (Bräuer et al., 2004; Bräuer et al., 2008), where the cleavage of the C-O bond of the oligoprenyl diphosphate and the consecutive protonation of the pyrophosphate anion by proton transfer from a protonated neighboring lysine or arginine moiety was energetically favored (Brandt et al., 2009). Furthermore, the existence of a dimethylallyl carbocation intermediate in the prenylation of tryptophan was evidenced by the usage of ^{18}O radio labeled DMAPP (Luk and Tanner, 2009).

In a trial to understand catalytic mechanisms and substrate recognition for UbiA, Bräuer et al. (2008) introduced a model based on five single mutations D71A, D75A, R137A, D191A, and D195A. All mutants lost the activity, except only 5% activity for the mutant R137A, which indicates the participation of the two Asp-rich motifs in one active site (Bräuer et al., 2008). These results were confirmed by the first X-ray crystal for an *Ec*UbiA homolog from the bacterium *Aeropyrum pernix* (*Ap*UbiA) in Apo- and substrate-bound forms using non-cleavable geranyl thiolopyrophosphate (GSPP). Conserved sequences of *Ap*UbiA $D_{54}XXXD_{58}$ and $D_{182}XXXD_{186}$ constituted one active site that accommodates both the prenyl donor (GSPP) and acceptor (PHB) (Cheng and Li, 2014). As a conclusion by combining the modelling and thermodynamic results (Bräuer et al., 2008; Brandt et al., 2009) with the crystal structure of *Ap*UbiA (Cheng and Li, 2014), the 2 D-residues in the first motif of UbiA-father aPT (D_{71} and D_{75}) are responsible for the fixation of one magnesium ion, which coordinates simultaneously with the oxygen atoms of diphosphate, thus, the activation of the pyrophosphate leaving group. The aromatic acceptor (PHB) binds directly to one aspartate moiety (D_{191}) through which the phenolate ion is stabilized. Asp195 has an indirect effect by stabilization of the side chain of Arg137 to form a salt bridge with the diphosphate and grants the recognition and correct positioning of the prenyl substrate relative to 4-hydroxybenzoate. The condensation of the prenyl group at the *ortho*-position of a hydroxyl group is favored as indicated by characterization studies involving electron donating/withdrawing groups (Brandt et al., 2009; Luk and Tanner, 2009). A model for the plant UbiA homolog *Le*PGT (Ohara et al., 2009) revealed that the same mechanism applies for this enzyme and supports a similar catalytic mechanism of other phylogenetically-related UbiA family members.

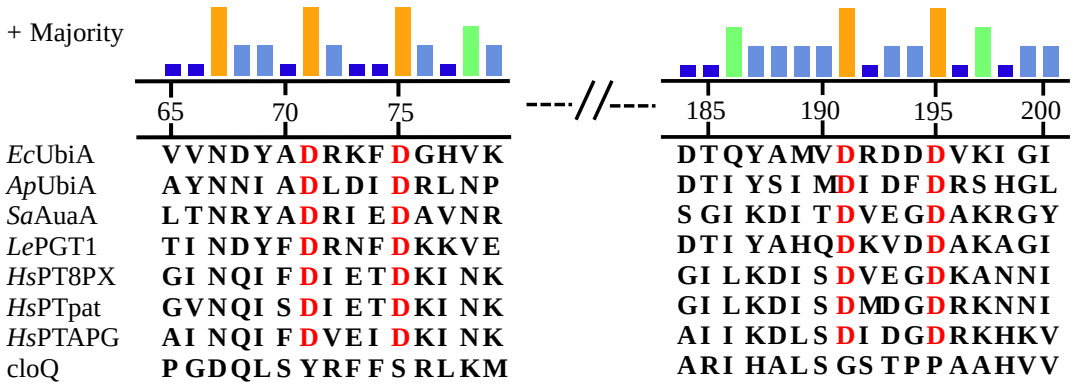

Figure 68: Multiple amino acid sequence alignment of active *Hs*PTs with previously studied aPTs belonging to the UbiA superfamily and soluble bacterial aPTs. The highly conserved aspartate residues in the two motifs of the membrane-bound aPTs are in red. They are absent from soluble aPTs. Three bacterial Mg^{+2}-dependant membrane-bound aPTs are *E.coli* UbiA (*Ec*UbiA; ANK04607), *Aeropyrum pernix* UbiA (*Ap*UbiA; BAA80570.1), and *Stigmatella aurantiaca* AuaA (*Sa*AuaA; AM404078). The plant UbiA homolog from *Lithospermum erythrorhizon* (*Le*PGT1; AB055078), and one soluble bacterial aPT from *Streptomyces roseochromogenes* (cloQ; AF329398). The ruler displays sequence numbering of *Ec*UbiA.

Active aromatic prenyltransferases identified from *H. sampsonii* were aligned with *Le*PGT, three bacterial Mg^{+2}-dependant membrane-bound aPTs, namely *Ec*UbiA, *Ap*UbiA, and *Sa*AuaA (Stec and Li, 2012) and one soluble bacterial aPT that lacks the conserved motifs (cloQ) **(Figure 68)**. Multiple sequence alignment (MSA) confirmed the conservation of D-residues in the motifs of *Ec*UbiA and *Ap*UbiA in all UbiA superfamily members. The same was true for PTs described in the course of this study **(Figure 61)**, which collects evidence to follow the same electrophilic aromatic substitution mechanism described above.

5.6.3.1 Successive prenylation catalyzed by xanthone prenyltransferases

First, the aspartate residues D_{161} and D_{165} of *Hs*PT8PX coordinate with Mg^{+2}, which itself fixes the pyrophosphate group of DMAPP, and D_{291} activates the hydroxyl group at C-7 of the skeleton of 1367THX. Finally, a proton is abstracted for the rebuild of the aromatic structure of the product 8PX. The second round of prenylation is started by *Hs*PTpat as exactly described for *Hs*PT8PX involving the corresponding aspartate moieties D_{149}, $D_{153,}$ and D_{279}. The last aspartate, D_{295} or D_{283} in the second conserved motif of *Hs*PT8PX and *Hs*PTpat, respectively, might be indirectly involved in right positioning of both substrates for the regiospecific prenylation at C-8 on the xanthone skeleton, as indicated by crystal study of the role model UbiA (Cheng and Li, 2014). This indirect arrangement through arginine or lysine residues together with the proton transfer to the diphosphate group may offer a function to the amino acid rests (NKP; **Figure 61**) in the extended conserved regions of plant aPTs (5.3). The stepwise prenylation of 1367THX for the production of patulone is graphically represented in **Figure 69**.

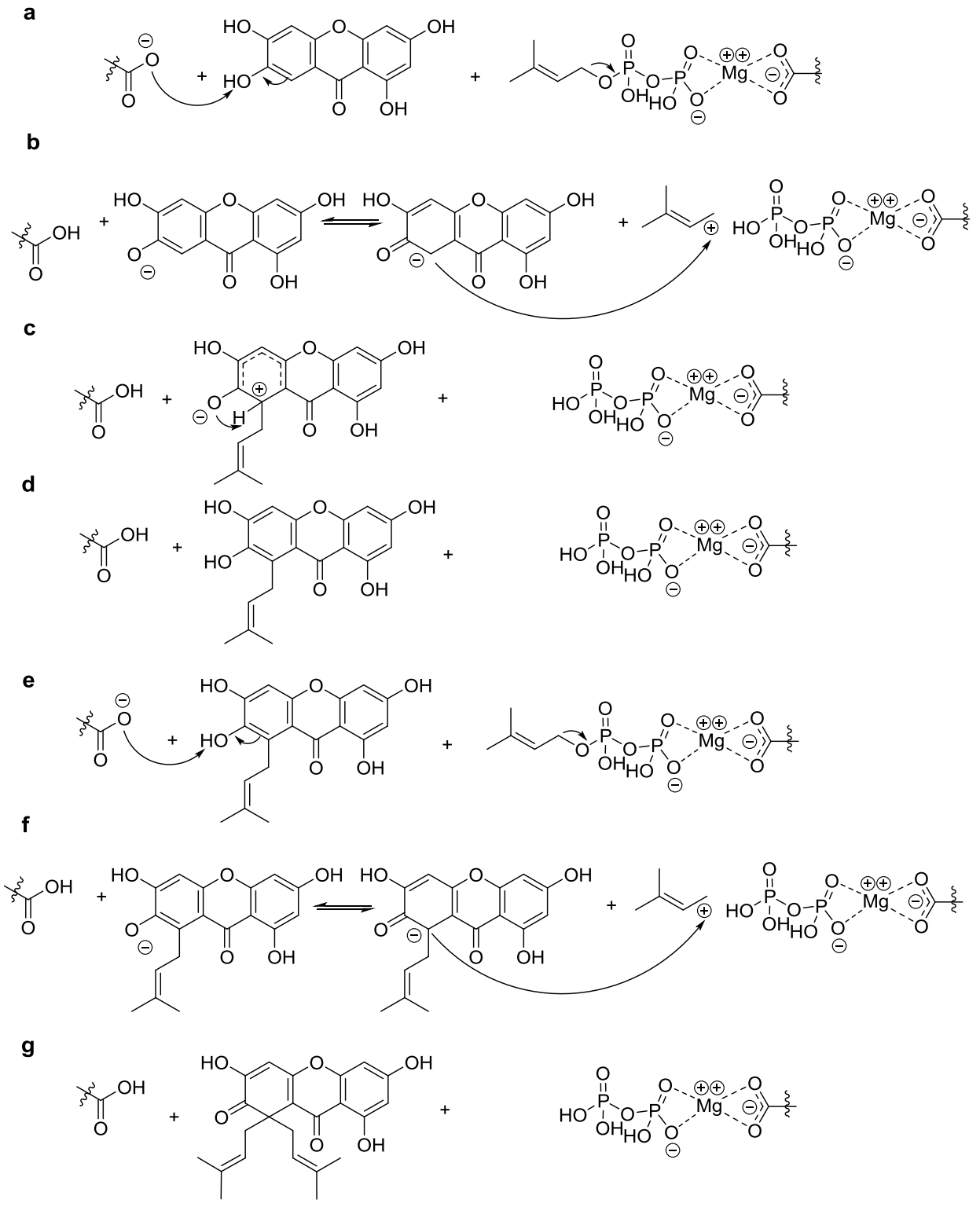

Figure 69: Stepwise electrophilic aromatic substitution on the tetrahydroxyxanthone skeleton catalyzed successively by *Hs*PT8PX and *Hs*PTpat.

5.6.3.2 First step geranylation catalyzed by acyl- and benzoylphloroglucinol *Hs*PT

Likely, the geranylation of acylphloroglucinols by *Hs*PTAPG involves the magnesium-mediated stabilization of the leaving diphosphate group from the alkyl donor to form a geranyl carbocation by D_{160} and D_{164}. The aromatic alkyl acceptor is then hooked by the residue D_{290} and the regioselective geranylation is pursued by the virtue of D_{294} with a final abstraction of hydrogen for reconstruction of the aromaticity of the formed product.

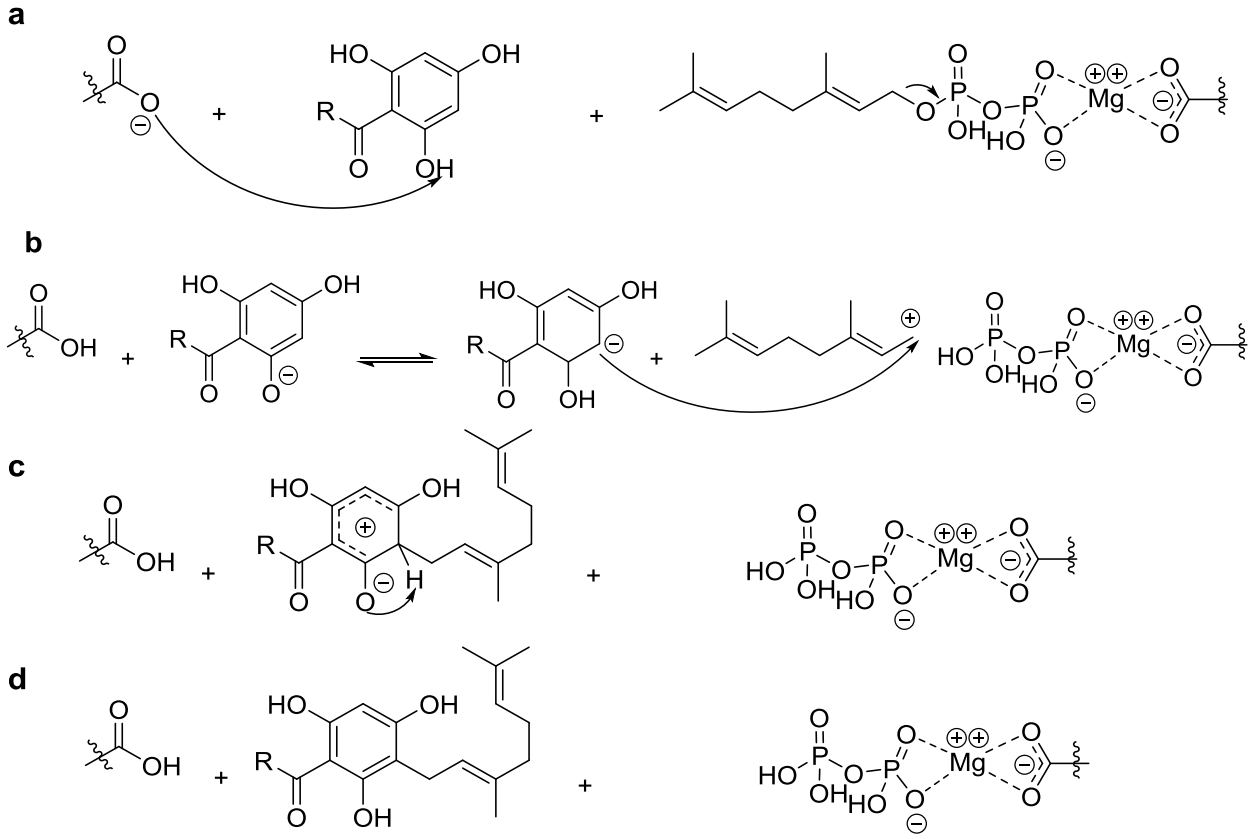

Figure 70: Stepwise electrophilic aromatic substitution on the acylphloroglucinol skeleton catalyzed by *Hs*PTAPG.

5.7 Viewpoint

Hypericum-PPAPs possess a complex caged system arising from multiple isoprene units attached to the core structure, giving them a distinctive property among plant natural products. A long biogenetic cascade passing by polyketide, phenylpropanoid, and methylerythritol phosphate pathways along with post modification processes, which occur in different cellular compartments, give PPAPs their unique structural and biological diversity. The bottle-neck reactions leading to the formation of these complex skeletons are the prenylation steps catalyzed by aromatic prenyltransferases. Despite the intriguing biological activities of PPAPs, they did not find their way to clinical studies, except for the well-known hyperforin. The scarce occurrence inside plants, which results in low isolation yields (section 5.5.1.2), as well as the challenging chemical synthesis because of the multichiral centers and multi-ring system, are the obstacles hindering their use as drug leads. These reasons necessitate the discovery of an alternative production system to provide a continuous supply of these natural products.

Hypericum sampsonii is the richest source of caged PPAPs with diamond-like skeletons (Yang et al., 2018), Unfortunately, there is no report about molecular or transcriptomic data. Therefore, this study started with the approach of homology-based cloning of aPTs and applying degenerate primers to fish a number of aPTs. After activity testing and characterization, *Hs*-identified aPTs can be positioned as biocatalysts in chemoenzymatic synthesis or pave the way, together with the already known steps, for future engineering of the whole pathway for biotechnological and de novo production of pharmacologically active PPAPs in microbes. These alternative ways mimic the biosynthetic pathways of PPAPs in the plant and overcome the disadvantage of conventional chemical synthesis. Long and tedious synthetic schemes, low specificity, the formation of artifacts and the questionable regioselectivity that can affect the bioactivity of the resulting compounds and result in low yield are the main drawbacks. The produced compounds (i.e. 8PX, patulone, and geranylated acylphloroglucinols) may be used as starting nuclei for an in depth-research of the downstream reactions, i.e. more prenylation and caging steps. Further, upscaling of the enzymatic production of 8PX gives insight into the explicit positional bio-catalysis for producing compounds with high yield and purity.

Additionally, *Hs*PTs are hits that facilitate the isolation and identification of aPTs from related plant species, whose transcriptomic data are yet unexplored, or offer a possibility to discover metabolons, gene clusters, and catalytic complexes (Li et al., 2015). Bioinformatics-based phylogeny can suggest functions for the inactive aPTs. A future perspective that will allow more understanding of the underlying mechanism of the here-identified aPTs is the combined modeling and site-directed mutagenesis to define precisely the amino acids that are responsible for the activity. This will enable the design and expression of manipulated proteins with higher activity, altered regiospecificity, and the ability to produce new scaffolds.

6 Summary

- Polycyclic polyprenylated acylphloroglucinol derivatives (PPAPs) are a group of compounds with fascinating structures and affluent biological activities. They are widely distributed in the genera of Hypericaceae and Clusiaceae.
- Biosynthesis of PPAPs is achieved in two stages. First, the formation of the aromatic acylphloroglucinol skeleton, followed by the attachment of prenyl moieties. The latter step is catalyzed by a group of enzymes, assigned the name aromatic prenyltransferases.
- Aromatic prenyltransferases are distributed among plants, bacteria, and fungi. They are subgrouped in two superfamilies, the UBiA, and ABBA superfamilies. The members of the former one are membrane-bound enzymes with two aspartate-rich conserved motifs and their activities are dependant on the presence of divalent cations as a co-factor, whereas the ABBA family members are soluble proteins and do not depend on cations for the activity. All plant aPTs belong to the UBiA superfamily.
- One member of the genus *Hypericum*, namely *H. sampsonii*, was identified as a rich source of caged PPAPs. Thus, the plant was the main focus of the present study. Metabolic profiling of *in vitro H. sampsonii* seedlings aimed at the detection of aromatic acylphloroglucinol cores that can be prenylated in later biosynthetic steps. 246TrHiBP, 246TrHBP, 2MBP, 1367THX, 8PX, patulone, G-246TrHBP, and pseudohypericin were detected and identified in the methanolic extract of *H. sampsonii*.
- Ten aPT cDNAs of the plant were identified, based on publicly and internally available transcriptomes for the related species *H. perforatum* and *H. calycinum*, respectively, together with the use of degenerate primers designed according to the sequence of conserved motifs of aPTs, which was an additional strategy to glean the target sequences. The cDNAs were expressed in yeast and insect cell (*Sf9*) expression systems.
- Potentially accepted substrates, prenyl donors, and prenylated intermediates were chemically synthesized, namely 246TrHiBP, GPP, DMAPP, 3-prenyl-2,4,6-trihydroxybenzophenone, and 3,5-diprenyl-2,4,6-trihydroxybenzophenone.
- Yeast or insect microsomes containing the recombinant proteins were individually tested for prenyl- and/or geranyltransferase activities against a number of aromatic substrates belonging to different chemical nuclei, namely acyl- and benzoylphloroglucinols, xanthones, and flavonoids. Three recombinant enzymes showed activity.
- The enzyme *Hs*PT8PX (*Hs*PT2) expressed in yeast was able to convert 1367THX to 8PX, which then was further converted to the diprenylated xanthone patulone, i.e. geminal addition of a prenyl group to C-8 of 8PX.
- Another xanthone PT, namely *Hs*PTpat (*Hs*PT5), accepted both 1367THX and 8PX, resulting only in a single product, which was patulone. The enzyme catalyzed either parallel addition of two prenyl residues to 1367THX or addition of a *gem*-prenyl group to 8PX.

- A third enzyme assigned as *Hs*PTAPG (*Hs*PT7) adds a geranyl residue to acyl phloroglucinols, producing the corresponding 3-monogeranyl derivatives. A substrate specificity test revealed that the two most preferred substrates are 2MBP and 246TrHiBP. Since 246TrHBP is a potential physiological substrate, it was also considered for further kinetic studies, regardless of its poor acceptance by *Hs*PTAPG (13% relative to 2MBP).
- All active enzymes and catalysed reactions were characterised with respect to biochemical (pH, incubation temperature, incubation time, protein amount, preferred co-factor) and kinetic parameters (K_m and V_{max}).
- Xanthone-related *Hs*PTs preferred neutral pH and Mg^{2+} as a co-factor, except for the patulone-producing reaction (1367THX + *Hs*PTpat + DMAPP) that preferred slightly basic pH (Tris-HCl pH 7.5) and Mn^{2+}. The main substrates for *Hs*PT8PX and *Hs*PTpat were 1367THX and 8PX, respectively, as indicated by the kinetic parameters. This result confirms the successive catalytic activities of these enzymes, as the product of the first enzyme is accepted by the second one. Hence, patulone is formed by sequential regiospecific prenylation of 1367THX. Subcellular localization of xanthone-related *Hs*PTs was confirmed to be plastidial, which augments the assumption of the contribution of these enzymes to the same biosynthetic pathway. Patulone may be an intermediate of the structurally related antibacterial agent hyperxanthone A, which is formed in a further step through the reverse prenylation at position C-4.
- *Hs*PTAPG preferred basic pH and Mg^{2+} for the incubation medium and cofactor, respectively. The K_m and V_{max} values confirmed the order of catalytic preference of the enzyme for 2MBP and 246TrHiBP, followed by 246TrHBP, which agrees with the substrate specificity results. The enzyme is supposed to catalyze the first prenylation step in the biosynthetic cascade of *Hs*-PPAPs, such as hypersampsones and sampsoniones/hypersampsins, by addition of a geranyl moiety to 246TrHiB and 246TrHBP, respectively. The results also suggested the possibility of isolating new, 2MBP-derived PPAPs from *in vitro*-cultivated *H. sampsonii*.
- Phylogenetic reconstruction positioned all *Hs*PTs in a single clade. Xanthone *Hs*PTs were closest to the already known xanthone-specific aPTs (Fiesel et al., 2015; Nagia et al., 2017; Nagia et al., submitted), whereas *Hs*PTAPG did not group with the known acylphloroglucinol aPTs (Page and Boubakir 2014; Li et al 2015).
- Prenyl moieties are attached to the aromatic substrates *via* electrophilic substitution. The underlying stepwise mechanism of action is described.

7 References

Abd El-Mawla, A.M., and Beerhues, L. (2002). Benzoic acid biosynthesis in cell cultures of *Hypericum androsaemum*. Planta **214,** 727-733.

Adam, P., Arigoni, D., Bacher, A., and Eisenreich, W. (2002). Biosynthesis of Hyperforin in *Hypericum perforatum*. Journal of Medicinal Chemistry **45,** 4786-4793.

Akashi, T., Sasaki, K., Aoki, T., Ayabe, S.-i., and Yazaki, K. (2009). Molecular cloning and characterization of a cDNA for pterocarpan 4-dimethylallyltransferase catalyzing the key prenylation step in the biosynthesis of glyceollin, a soybean phytoalexin. Plant Physiology **149,** 683-693.

Alhassan, l.M., Abdullahi, M.I., Uba, A., and Umar, A. (2014). Prenylation of aromatic secondary metabolites: A new frontier for development of novel drugs. Tropical Journal of Pharmaceutical Research **13,** 307- 314.

Almeida, L.S.B., Murata, R.M., Yatsuda, R., Dos Santos, M.H., Nagem, T.J., Alencar, S.M., Koo, H., and Rosalen, P.L. (2008). Antimicrobial activity of *Rheedia brasiliensis* and 7-epiclusianone against *Streptococcus* mutans. Phytomedicine **15,** 886-891.

Anna, R.-P., Stacie, B., and Joanna, M.L. (2005). A Historical overview of the heterologous expression of mammalian UDP-glucuronosyltransferase isoforms over the past twenty years. Current Drug Metabolism **6,** 141-160.

Baliga, M.S., Bhat, H.P., Pai, R.J., Boloor, R., and Palatty, P.L. (2011). The chemistry and medicinal uses of the underutilized Indian fruit tree *Garcinia indica* Choisy (kokum): A review. Food Research International **44,** 1790-1799.

Banthorpe, D.V., Charlwood, B.V., and Francis, M.J.O. (1972). The biosynthesis of monoterpenes. Chemical Reviews **72,** 115-155.

Banthorpe, D.V., Long, D.R.S., and Pink, C.R. (1983). Biosynthesis of geraniol and related monoterpenes in *Pelargonium graveolens*. Phytochemistry **22,** 2459-2463.

Batista, A.N.L., dos Santos-Pinto, J.R.A., Batista, J.M., Jr., Souza-Moreira, T.M., Santoni, M.M., Zanelli, C.F., Kato, M.J., Lopez, S.N., Palma, M.S., and Furlan, M. (2017). The combined use of proteomics and transcriptomics reveals a complex secondary metabolite network in *Peperomia obtusifolia*. Journal of Natural Products **80,** 1275-1286.

Baureithel, K.H., Berger Bueter, K., Engesser, A., Burkard, W., and Schaffner, W. (1997). Inhibition of benzodiazepine binding in vitro by amentoflavone, a constituent of various species of *Hypericum*. Pharmaceutica Acta Helvetiae **72,** 153-157.

Becker, D.M., and Lundblad, V. (2001). Introduction of DNA into yeast cells. In Current Protocols in Molecular Biology (John Wiley & Sons, Inc.

Beerhues, L. (2006). Hyperforin. Phytochemistry **67,** 2201-2207.

Beerhues, L. (2011). Biosynthesis of the active *Hypericum perforatum* constituents. In *Hypericum*. Medicinal and Aromatic Plant Science and Biotechnology Special Issue 1, M.S. Odabas and C. Çirak, eds, pp. 70–77.

Beerhues, L., and Liu, B. (2009). Biosynthesis of biphenyls and benzophenones – Evolution of benzoic acid-specific type III polyketide synthases in plants. Phytochemistry **70,** 1719-1727.

Behera, A.K., Swamy, M.M., Natesh, N., and Kundu, T.K. (2016). Garcinol and its role in chronic diseases. In Anti-inflammatory Nutraceuticals and Chronic Diseases, S.C. Gupta, S. Prasad, and B.B. Aggarwal, eds (Cham: Springer International Publishing), pp. 435-452.

Bencúrová, M., Rendić, D., Fabini, G., Kopecky, E.-M., Altmann, F., and Wilson, I.B.H. (2003). Expression of eukaryotic glycosyltransferases in the yeast *Pichia pastoris*. Biochimie **85,** 413-422.

Biber, N., Möws, K., and Plietker, B. (2011). The total synthesis of hyperpapuanone, hyperibone L, epi-clusianone and oblongifolin A. Nature Chemistry **3,** 938.

Biedermann, E. (2017). Untersuchungen zur Charakterisierung von Prenyltransferasen aus *Hypericum*-Arten nach Expression in *Nicotiana benthamiana*. Dissertation. Pharmaceutical Biology. (Technische Universität Braunschweig).

Birnboim, H.C., and Doly, J. (1979). A rapid alkaline extraction procedure for screening recombinant plasmid DNA. Nucleic Acids Research **7,** 1513-1523.

Biswas, T., Sen, A., Roy, R., Maji, S., and Maji, H.S. (2015). Isolation of mangiferin from flowering buds of *Mangifera indica* L and its evaluation of in vitro antibacterial activity. Res. Rev.: J. Pharm. Anal. **4,** 49-56.

Booth, P.J., and Curran, A.R. (1999). Membrane protein folding. Current Opinion in Structural Biology **9,** 115-121.

Bouron, A., and Lorrain, E. (2014). Cellular and molecular effects of the antidepressant hyperforin on brain cells: Review of the literature. L'Encephale **40,** 108-113.

Bouvier, F., Rahier, A., and Camara, B. (2005). Biogenesis, molecular regulation and function of plant isoprenoids. Progress in Lipid Research **44,** 357-429.

Bradford, M.M. (1976). A rapid and sensitive method for the quantitation of microgram quantities of protein utilizing the principle of protein-dye binding. Analytical Biochemistry **72,** 248-254.

Branco-de-Almeida, L.S., Murata, R.M., Franco, E.M., dos Santos, M.H., de Alencar, S.M., Koo, H., and Rosalen, P.L. (2011). Effects of 7-epiclusianone on *Streptococcus mutans* and caries development in rats. Planta Medica **77,** 40-45.

Brandt, W., Bräuer, L., Günnewich, N., Kufka, J., Rausch, F., Schulze, D., Schulze, E., Weber, R., Zakharova, S., and Wessjohann, L. (2009). Molecular and structural basis of metabolic diversity mediated by prenyldiphosphate converting enzymes. Phytochemistry **70,** 1758-1775.

Bräuer, L., Brandt, W., and Wessjohann, L.A. (2004). Modeling the E. coli 4-hydroxybenzoic acid oligoprenyltransferase (UBiA transferase) and characterization of potential active sites. Journal of Molecular Modeling **10,** 317-327.

Bräuer, L., Brandt, W., Schulze, D., Zakharova, S., and Wessjohann, L. (2008). A Structural model of the membrane-bound aromatic Prenyltransferase UbiA from *E. coli*. ChemBioChem **9,** 982-992.

Buchanan, S.K. (1999). *β*-Barrel proteins from bacterial outer membranes: structure, function and refolding. Current Opinion in Structural Biology **9,** 455-461.

Cane, D.E. (1999). 2.01 - Isoprenoid Biosynthesis: Overview A2 - Barton, Sir Derek. In Comprehensive Natural Products Chemistry, K. Nakanishi and O. Meth-Cohn, eds (Oxford: Pergamon), pp. 1-13.

Chen, J.-J., Chen, H.-J., and Lin, Y.-L. (2014). Novel polyprenylated phloroglucinols from *Hypericum sampsonii*. Molecules **19,** 19836.

Chen, M.-T., and Chen, C.-M. (1985). Xanthones from *Hypericum sampsonii*. Heterocycles **23,** 2543-2548.

Chen, R., Gao, B., Liu, X., Ruan, F., Zhang, Y., Lou, J., Feng, K., Wunsch, C., Li, S.-M., Dai, J., and Sun, F. (2017). Molecular insights into the enzyme promiscuity of an aromatic prenyltransferase. Nature Chemical Biology **13,** 226-234.

Chenchik, A., Zhu, Y., Diatchenko, L., Li, R., Hill, J., Siebert, P., Chenchik, A., and Zhu, Y. (1998). Generation and use of high-quality cDNA from small amounts of total RNA by SMART PCR. In Gene cloning and analysis by RT-PCR, P.D. Siebert and J.W. Larrick, eds (BioTechniques Books), pp. 305–319.

Cheng, W., and Li, W. (2014). Structural insights into ubiquinone biosynthesis in membranes. Science **343,** 878-881.

Christenhusz, M.J.M., and Byng, J.W. (2016). The number of known plants species in the world and its annual increase. Phytotaxa **261,** 201.

Ciochina, R., and Grossman, R.B. (2006). Polycyclic polyprenylated acylphloroglucinols. Chemical Reviews **106,** 3963-3986.

Coelho, L.P., Serra, M.F., de Aguiar Pires, A.L., Cordeiro, R.S.B., e Silva, P.M.R., dos Santos, M.H., and Martins, M.A. (2008). 7-Epiclusianone, a tetraprenylated benzophenone, relaxes airway smooth muscle through activation of the nitric oxide-cGMP pathway. Journal of Pharmacology and Experimental Therapeutics **327,** 206-214.

Cornforth, J.W., Cornforth, R.H., Popják, G., and Yengoyan, L. (1966). Studies on the Biosynthesis of Cholesterol: XX. Steric course of decarboxylation of 5-pyrophosphomevalonate and of the carbon to carbon bond formation in the biosynthesis of farnesyl pyrophosphate. Journal of Biological Chemistry **241,** 3970-3987.

Cottet, K., Neudörffer, A., Kritsanida, M., Michel, S., Lallemand, M.-C., and Largeron, M. (2015). Polycyclic polyprenylated xanthones from *Symphonia globulifera*: Isolation and biomimetic electrosynthesis. Journal of Natural Products **78,** 2136-2140.

Crockett, S.L., and Robson, N.K.B. (2011). Taxonomy and chemotaxonomy of the genus *Hypericum*. Medicinal and aromatic plant science and biotechnology **5,** 1-13.

Cuesta-Rubio, O., Velez-Castro, H., Frontana-Uribe, B.A., and Cárdenas, J. (2001). Nemorosone, the major constituent of floral resins of *Clusia rosea*. Phytochemistry **57,** 279-283.

Demirkiran, O. (2007). Xanthones in *Hypericum*: Synthesis and biological activities. In Bioactive Heterocycles III, M.T.H. Khan, ed (Berlin, Heidelberg: Springer Berlin Heidelberg), pp. 139-178.

Dohmen, R.J., Strasser, A.W.M., Höner, C.B., and Hollenberg, C.P. (1991). An efficient transformation procedure enabling long-term storage of competent cells of various yeast genera. Yeast **7,** 691-692.

Don, M.-J., Huang, Y.-J., Huang, R.-L., and Lin, Y.-L. (2004). New phenolic principles from *Hypericum sampsonii*. Chemical and Pharmaceutical Bulletin **52,** 866-869.

Dreßen, A., Hilberath, T., Mackfeld, U., Billmeier, A., Rudat, J., and Pohl, M. (2017). Phenylalanine ammonia lyase from *Arabidopsis thaliana* (AtPAL2): A potent MIO-enzyme for the synthesis of non-canonical aromatic alpha-amino acids: Part I: Comparative characterization to the enzymes *from Petroselinum crispum* (PcPAL1) and *Rhodosporidium toruloides* (RtPAL). Journal of Biotechnology **258,** 148-157.

Drew, D., Fröderberg, L., Baars, L., and de Gier, J.-W.L. (2003). Assembly and overexpression of membrane proteins in *Escherichia coli*. Biochimica et Biophysica Acta (BBA) - Biomembranes **1610,** 3-10.

Dumelin, C.E., Chen, Y., Leconte, A.M., Chen, Y.G., and Liu, D.R. (2012). Discovery and biological characterization of geranylated RNA in bacteria. Nature Chemical Biology **8,** 913-919.

Eisenreich, W., Bacher, A., Arigoni, D., and Rohdich, F. (2004). Biosynthesis of isoprenoids via the non-mevalonate pathway. Cellular and Molecular Life Sciences CMLS **61,** 1401-1426.

El-Awaad, I., Bocola, M., Beuerle, T., Liu, B., and Beerhues, L. (2016). Bifunctional CYP81AA proteins catalyse identical hydroxylations but alternative regioselective phenol couplings in plant xanthone biosynthesis. Nature Communications **7,** 11472.

Eppens, E.F., Nouwen, N., and Tommassen, J. (1997). Folding of a bacterial outer membrane protein during passage through the periplasm. The EMBO Journal **16,** 4295-4301.

Fan, A., Chen, H., Wu, R., Xu, H., and Li, S.-M. (2014). A new member of the DMATS superfamily from *Aspergillus niger* catalyzes prenylations of both tyrosine and tryptophan derivatives. Applied Microbiology and Biotechnology **98,** 10119-10129.

Farrokhi, N., Firouzabadi, M.B., and Gholani, A. (2013). Functional genomics of plant cell wall biosynthetic Enzymes: type-II membrane-bound glycosyltransferases. International Journal of Botany **9,** 1-17.

Ferrer, J.L., Austin, M.B., Stewart, C., and Noel, J.P. (2008). Structure and function of enzymes involved in the biosynthesis of phenylpropanoids. Plant physiology and biochemistry : PPB / Societe francaise de physiologie vegetale **46,** 356-370.

Fiesel, T. (2016). Aromatische Prenyltransferasen aus *Hypericum*-Arten: Biosynthese (poly)prenylierter Acylphloroglucin-Derivate im Johanniskraut. Dissertation. Pharmazeutische Biologie. (Technische Universität Braunschweig).

Fiesel, T., Gaid, M., Müller, A., Bartels, J., El-Awaad, I., Beuerle, T., Ernst, L., Behrends, S., and Beerhues, L. (2015). Molecular cloning and characterization of a xanthone prenyltransferase from *Hypericum calycinum* Cell Cultures. Molecules **20,** 15616-15630.

Forssten, S.D., Björklund, M., and Ouwehand, A.C. (2010). *Streptococcus* mutans, caries and simulation models. Nutrients **2,** 290-298.

Friedland, K., and Harteneck, C. (2015). Hyperforin: To be or not to be an Activator of TRPC(6). In Reviews of Physiology, Biochemistry and Pharmacology Vol. 169, B. Nilius, T. Gudermann, R. Jahn, R. Lill, O.H. Petersen, and P.P. de Tombe, eds (Cham: Springer International Publishing), pp. 1-24.

Frohman, M.A., Dush, M.K., and Martin, G.R. (1988). Rapid production of full-length cDNAs from rare transcripts: amplification using a single gene-specific oligonucleotide primer. Proceedings of the National Academy of Sciences **85,** 8998-9002.

Fu, W., Wu, M., Zhu, L., Lao, Y., Wang, L., Tan, H., Yuan, Q., and Xu, H. (2015). Prenylated benzoylphloroglucinols and biphenyl derivatives from the leaves of *Garcinia multiflora* Champ. RSC Advances **5,** 78259-78267.

Fujimoto, Y., Yanai, H., and Matsumoto, T. (2016). Concise total synthesis of elliptoxanthone A by utilizing aromatic oxy-cope rearrangement for efficient C-isoprenylation of xanthone Skeleton. Synlett **27,** 2229-2232.

Fukuyama, Y., Kuwayama, A., and Minami, H. (1997). Garsubellin A, a novel polyprenylated phloroglucin derivative, increasing choline acetyltransferase (ChAT) activity in postnatal rat septal neuron cultures. Chemical and Pharmaceutical Bulletin **45,** 947-949.

Fukuyama, Y., Minami, H., and Kuwayama, A. (1998). Garsubellins, polyisoprenylated phloroglucinol derivatives from *Garcinia subelliptica*. Phytochemistry **49,** 853-857.

Gadzovska, S., Maury, S., Ounnar, S., Righezza, M., Kascakova, S., Refregiers, M., Spasenoski, M., Joseph, C., and Hagège, D. (2005). Identification and quantification of hypericin and pseudohypericin in different *Hypericum perforatum* L. *in vitro* cultures. Plant Physiology and Biochemistry **43,** 591-601.

Gaid, M., Haas, P., Beuerle, T., Scholl, S., and Beerhues, L. (2016). Hyperforin production in *Hypericum perforatum* root cultures. Journal of Biotechnology **222,** 47-55.

Gaid, M., Biedermann, E., Füller, J., Haas, P., Behrends, S., Krull, R., Scholl, S., Wittstock, U., Müller-Goymann, C., and Beerhues, L. (2018). Biotechnological production of hyperforin for pharmaceutical formulation. European Journal of Pharmaceutics and Biopharmaceutics **126,** 10-26.

Gaid, M.M., Scharnhop, H., Ramadan, H., Beuerle, T., and Beerhues, L. (2011). 4-Coumarate:CoA ligase family members from elicitor-treated *Sorbus aucuparia* cell cultures. Journal of Plant Physiology **168,** 944-951.

Gaid, M.M., Sircar, D., Müller, A., Beuerle, T., Liu, B., Ernst, L., Hänsch, R., and Beerhues, L. (2012). Cinnamate: CoA Ligase initiates the biosynthesis of a benzoate-derived xanthone phytoalexin in *Hypericum calycinum* Cell Cultures. Plant Physiology **160,** 1267-1280.

Garnsey, M.R., Matous, J.A., Kwiek, J.J., and Coltart, D.M. (2011). Asymmetric total synthesis of (+)- and (−)-clusianone and (+)- and (−)clusianone methyl enol ether via ACC alkylation and evaluation of their anti-HIV activity. Bioorganic & Medicinal Chemistry Letters **21,** 2406-2409.

Gebler, J.C., and Poulter, C.D. (1992). Purification and characterization of dimethylallyl tryptophan synthase from *Claviceps purpurea*. Archives of Biochemistry and Biophysics **296,** 308-313.

Gehl, C., Waadt, R., Kudla, J., Mendel, R.-R., and Hänsch, R. (2009). New GATEWAY vectors for high throughput analyses of protein-protein interactions by bimolecular fluorescence complementation. Molecular Plant **2,** 1051-1058.

Gelb, M.H., Brunsveld, L., Hrycyna, C.A., Michaelis, S., Tamanoi, F., Van Voorhis, W.C., and Waldmann, H. (2006). Therapeutic intervention based on protein prenylation and associated modifications. Nature Chemical Biology **2,** 518.

Goese, M., Kammhuber, K., Bacher, A., Zenk Meinhart, H., and Eisenreich, W. (1999). Biosynthesis of bitter acids in hops. European Journal of Biochemistry **263,** 447-454.

Gokaraju, G.R., Gokaraju, R.R., Golakoti, T., Somepalli, V., and Bhupathiraju, K. (2009). A process for producing γ-mangostin and its use as an anti-inflammatory (India .), pp. 44 pp.

Goldstein, J.L., and Brown, M.S. (1990). Regulation of the mevalonate pathway. Nature **343,** 425.

Griffith, T.N., Varela-Nallar, L., Dinamarca, M.C., and Inestrosa, N.C. (2010). Neurobiological effects of hyperforin and its potential in Alzheimer's disease therapy. Current Medicinal Chemistry **17,** 391-406.

Grossman, R.B. (2018). Table of Naturally Occurring PPAPs (University of Kentucky).

Guedes, A.P., Franklin, G., and Fernandes-Ferreira, M. (2012). *Hypericum* sp.: essential oil composition and biological activities. Phytochemistry Reviews **11,** 127-152.

Guo, J., Xu, C., Xue, R., Jiang, W., Wu, B., and Huang, C. (2015). Cytotoxic activities of chemical constituents from rhizomes of *Anemarrhena asphodeloides* and their analogues. Archives of Pharmacal Research **38,** 598-603.

Guo, R.-T., Ko, T.-P., Chen, A.P.-C., Kuo, C.-J., Wang, A.H.-J., and Liang, P.-H. (2005). Crystal structures of undecaprenyl pyrophosphate synthase in complex with magnesium, isopentenyl pyrophosphate, and farnesyl thiopyrophosphate: Roles of the metal ion and conserved residues in catalysis. The Journal of Biological Chemistry **280,** 20762–20774.

Guo, Z., Wu, Y.-W., Das, D., Delon, C., Cramer, J., Yu, S., Thuns, S., Lupilova, N., Waldmann, H., Brunsveld, L., Goody, R.S., Alexandrov, K., and Blankenfeldt, W. (2008). Structures of RabGGTase–substrate/product complexes provide insights into the evolution of protein prenylation. The EMBO Journal **27,** 2444-2456.

Gurevich, A.I., Dobrynin, V.N., Kolosov, M.N., Popravko, S.A., Ryabova, I.D., Chernov, B.K., Derbentseva, N.A., Aizenman, B.E., and Garagulya, A.D. (1971). Hyperforin, an antibiotic from *Hypericum perforatum*. Antibiotiki (Moscow) **16,** 510-513.

Hamed, W., Brajeul, S., Mahuteau-Betzer, F., Thoison, O., Mons, S., Delpech, B., Hung, N.V., Sévenet, T., and Marazano, C. (2006). Oblongifolins A−D, polyprenylated benzoylphloroglucinol derivatives from *Garcinia oblongifolia*. Journal of Natural Products **69,** 774-777.

Heide, L. (2009). Prenyl transfer to aromatic substrates: genetics and enzymology. Current Opinion in Chemical Biology **13,** 171-179.

Henry, G.E., Jacobs, H., Carrington, C.M.S., McLean, S., and Reynolds, W.F. (1996). Plukenetione A. An unusual adamantyl ketone from *Clusia plukenetii* (guttiferae). Tetrahedron Letters **37,** 8663-8666.

Hernandez-Lopez, J., Crockett, S., Kunert, O., Hammer, E., Schuehly, W., Bauer, R., Crailsheim, K., and Riessberger-Galle, U. (2014). *In vitro* growth inhibition by *Hypericum* extracts and isolated pure compounds of *Paenibacillus larvae*, a lethal disease affecting honeybees worldwide. Chemistry & Biodiversity **11,** 695-708.

Hernández, I.M., Fernandez, M.C., Cuesta-Rubio, O., Piccinelli, A.L., and Rastrelli, L. (2005). Polyprenylated benzophenone derivatives from cuban propolis. Journal of Natural Products **68,** 931-934.

Hill, C.B., and Roessner, U. (2013). Metabolic profiling of plants by GC–MS. In The Handbook of Plant Metabolomics, W. Weckwerth and G. Kahl, eds (Wiley-Blackwell), pp. 3- 23.

Hoffman, C.S., and Winston, F. (1987). A ten-minute DNA preparation from yeast efficiently releases autonomous plasmids for transformation of *Escherichia coli*. Gene **57,** 267-272.

Hong, D., Yin, F., Hu, L.-H., and Lu, P. (2004). Sulfonated xanthones from *Hypericum sampsonii*. Phytochemistry **65,** 2595-2598.

Hu, L.-H., and Sim, K.-Y. (2000). Sampsoniones A–M, a Unique Family of Caged Polyprenylated Benzoylphloroglucinol Derivatives, from *Hypericum sampsonii*. Tetrahedron **56,** 1379-1386.

Huang, L., Wang, H., Yea, H., Dua, Z., Zhang, Y., Beerhues, L., and Liu, B. (2012). Differential expression of benzophenone synthase and chalcone synthase in *Hypericum sampsonii*. Natural Product Communications **7,** 1615-1618.

Iranshahi, M., Shahverdi, A.R., Mirjani, R., Amin, G., and Shafiee, A. (2004). Umbelliprenin from Ferula persica roots inhibits the red pigment production in *Serratia marcescens*. Zeitschrift für Naturforschung. Teil C: Biochemie, Biophysik, Biologie, Virologie **59,** 506-508.

Iranshahi, M., Jabbari, A., Orafaie, A., Mehri, R., Zeraatkar, S., Ahmadi, T., Alimardani, M., and Sadeghian, H. (2012). Synthesis and SAR studies of mono O-prenylated

coumarins as potent 15-lipoxygenase inhibitors. European Journal of Medicinal Chemistry **57,** 134-142.

Ishiguro, K., Nagareya, N., Suitani, A., and Fukumoto, H. (1997). A prenylated xanthone from cell suspension cultures of *Hypericum patulum*. Phytochemistry **44,** 1065-1066.

Itoigawa, M., Ito, C., Wu, T.-S., Enjo, F., Tokuda, H., Nishino, H., and Furukawa, H. (2003). Cancer chemopreventive activity of acridone alkaloids on Epstein–Barr virus activation and two-stage mouse skin carcinogenesis. Cancer Letters **193,** 133-138.

Jaakola, L., Pirttilä, A.M., Halonen, M., and Hohtola, A. (2001). Isolation of high quality RNA from bilberry (*Vaccinium myrtillus* L.) fruit. Molecular Biotechnology **19,** 201-203.

Jackson, D.N., Yang, L., Wu, S., Kennelly, E.J., and Lipke, P.N. (2015). Garcinia xanthochymus benzophenones promote hyphal apoptosis and potentiate activity of fluconazole against *Candida albicans* biofilms. Antimicrobial Agents and Chemotherapy **59,** 6032-6038.

Jauhiainen, M., Mönkkönen, H., Räikkönen, J., Mönkkönen, J., and Auriola, S. (2009). Analysis of endogenous ATP analogs and mevalonate pathway metabolites in cancer cell cultures using liquid chromatography–electrospray ionization mass spectrometry. Journal of Chromatography B **877,** 2967-2975.

Jez, J.M., Bowman, M.E., Dixon, R.A., and Noel, J.P. (2000). Structure and mechanism of the evolutionarily unique plant enzyme chalcone isomerase. Nature Structural Biology **7,** 786.

Jing-Ru, W., Chun-Nan, L., Lo-Ti, T., and Jih-Pyang, W. (2003). Terpenoids with a new skeleton and novel triterpenoids with anti-inflammatory effects from *Garcinia subelliptica*. Chemistry – A European Journal **9,** 5520-5527.

Karamat, F., Olry, A., Munakata, R., Koeduka, T., Sugiyama, A., Paris, C., Hehn, A., Bourgaud, F., and Yazaki, K. (2014). A coumarin-specific prenyltransferase catalyzes the crucial biosynthetic reaction for furanocoumarin formation in parsley. The Plant Journal **77,** 627-638.

Karioti, A., and Bilia, A.R. (2010). Hypericins as potential leads for new therapeutics. International Journal of Molecular Sciences **11,** 562-594.

Karppinen, K., Hokkanen, J., Tolonen, A., Mattila, S., and Hohtola, A. (2007). Biosynthesis of hyperforin and adhyperforin from amino acid precursors in shoot cultures of *Hypericum perforatum*. Phytochemistry **68,** 1038-1045.

Kasper, S., Anghelescu, I.-G., Szegedi, A., Dienel, A., and Kieser, M. (2006). Superior efficacy of St John's wort extract WS 5570 compared to placebo in patients with major depression: a randomized, double-blind, placebo-controlled, multi-center trial [ISRCTN77277298]. BMC Medicine **4,** 14-14.

Khaghanzadeh, N., Samiei, A., Mojtahedi, Z., Ramezani, M., Hosseinzadeh, M., and Ghaderi, A. (2017). Umbelliprenin induced both anti-inflammatory and regulatory cytokines in C57/BL6 mice. Iranian Journal of Basic Medical Sciences **20,** 829-834.

Klingauf, P., Beuerle, T., Mellenthin, A., El-Moghazy, S.A.M., Boubakir, Z., and Beerhues, L. (2005). Biosynthesis of the hyperforin skeleton in *Hypericum calycinum* cell cultures. Phytochemistry **66,** 139-145.

Koeberle, A., Rossi, A., Bauer, J., Dehm, F., Verotta, L., Northoff, H., Sautebin, L., and Werz, O. (2011). Hyperforin, an anti-inflammatory constituent from St. John's wort, inhibits microsomal prostaglandin E2 synthase-1 and suppresses prostaglandin E2 formation in vivo. Front. Inflammation Pharmacol. **2,** 7.

Kumar, S., Stecher, G., and Tamura, K. (2016). MEGA7: Molecular evolutionary genetics analysis version 7.0 for bigger datasets. Molecular Biology and Evolution **33,** 1870-1874.

Kuramochi, A., Usuda, H., Yamatsugu, K., Kanai, M., and Shibasaki, M. (2005). Total Synthesis of (±)-Garsubellin A. Journal of the American Chemical Society **127,** 14200-14201.

Kuzuyama, T., Noel, J.P., and Richard, S.B. (2005). Structural basis for the promiscuous biosynthetic prenylation of aromatic natural products. Nature **435,** 983-987.

Kwon, J., Oh, K.S., Cho, S.-Y., Bang, M.A., Kim, H.S., Vaidya, B., and Kim, D. (2016). Estrogenic activity of hyperforin in MCF-7 human breast cancer cells transfected with estrogen receptor. Planta Medica **82,** 1425-1430.

Lam, H.C., Spence, J.T.J., and George, J.H. (2016). Biomimetic total synthesis of hyperjapones A-E and hyperjaponols A and C. Angewandte Chemie International Edition **55,** 10368-10371.

Lech, K., and Brent, R. (2001). Growing Bacteria in Liquid Media. In Current Protocols in Cytometry (John Wiley & Sons, Inc.

Li, H., Ban, Z., Qin, H., Ma, L., King, A.J., and Wang, G. (2015). A heteromeric membrane-bound prenyltransferase complex from Hop Catalyzes three sequential aromatic prenylations in the bitter acid pathway. Plant Physiology **167,** 650.

Li, Z., Luo, L., Ma, G., Huang, R., and Hu, Z. (2004). Sampsoniones and xanthones of *Hypericum sampsonii* from Yunnan Province. Zhongcaoyao **35,** 131-134.

Liao, Y., Liu, X., Yang, J., Lao, Y.-Z., Yang, X.-W., Li, X.-N., Zhang, J.-J., Ding, Z.-j., Xu, H.-X., and Xu, G. (2015). Hypersubones A and B, new polycyclic acylphloroglucinols with intriguing adamantane type cores from *Hypericum subsessile*. Organic Letters **17,** 1172-1175.

Lim, C.K., Tho, L.-Y., Lim, Y.M., Shah, S.A.A., and Weber, J.-F.F. (2012). Synthesis of 1,3,6-trioxygenated prenylated xanthone derivatives as potential antitumor agents. Letters in Organic Chemistry **9,** 549-555.

Lim, C.K., Tho, L.-Y., Lim, C.H., Lim, Y.M., Shah, S.A.A., and Weber, J.-F.F. (2011). Synthesis and SAR study of prenylated xanthone analogues as HeLa and MDA-MB-231 cancer cell inhibitors. Letters in Drug Design & Discovery **8,** 523-528.

Lin, Y.-L., and Wu, Y.-S. (2003). Polyprenylated phloroglucinol derivatives from *Hypericum sampsonii*. Helvetica Chimica Acta **86,** 2156-2163.

Lindermayr, K., and Plietker, B. (2013). The bidirectional total synthesis of sampsonione P and hyperibone I. Angewandte Chemie International Edition **52,** 12183-12186.

Liu, B., Falkenstein-Paul, H., Schmidt, W., and Beerhues, L. (2003). Benzophenone synthase and chalcone synthase from *Hypericum androsaemum* cell cultures: cDNA cloning, functional expression, and site-directed mutagenesis of two polyketide synthases. The Plant Journal **34,** 847-855.

Liu, C., Sun, Z., Shen, S., Lin, L., Li, T., Tian, B., and Hua, Y. (2013a). Identification and characterization of the geranylgeranyl diphosphate synthase in *Deinococcus radiodurans*. Letters in Applied Microbiology **58,** 219-224.

Liu, R., Su, Y., Yang, J., and Wang, A. (2017). Polyprenylated acylphloroglucinols from *Hypericum scabrum*. Phytochemistry **142,** 38-50.

Liu, X.-N., Zhang, X.-Q., and Sun, J.-S. (2007). Effects of cytokinins and elicitors on the production of hypericins and hyperforin metabolites in *Hypericum sampsonii* and *Hypericum perforatum*. Plant Growth Regulation **53,** 207-214.

Liu, X., and Walsh, C.T. (2009). Characterization of cyclo-acetoacetyl-L-tryptophan dimethylallyltransferase in cyclopiazonic acid biosynthesis: Substrate promiscuity and site directed mutagenesis studies. Biochemistry **48,** 11032-11044.

Liu, X., Yang, X.-W., Chen, C.-Q., Wu, C.-Y., Zhang, J.-J., Ma, J.-Z., Wang, H., Yang, L.-X., and Xu, G. (2013b). Bioactive polyprenylated acylphloroglucinol derivatives from *Hypericum cohaerens*. Journal of Natural Products **76,** 1612-1618.

Long, S.B., Casey, P.J., and Beese, L.S. (2002). Reaction path of protein farnesyltransferase at atomic resolution. Nature **419,** 645.

Luckow, V.A., Lee, S.C., Barry, G.F., and Olins, P.O. (1993). Efficient generation of infectious recombinant baculoviruses by site-specific transposon-mediated insertion of foreign genes into a baculovirus genome propagated in *Escherichia coli*. Journal of Virology **67,** 4566-4579.

Luk, L.Y.P., and Tanner, M.E. (2009). Mechanism of dimethylallyltryptophan synthase: Evidence for a dimethylallyl cation intermediate in an aromatic prenyltransferase reaction. Journal of the American Chemical Society **131,** 13932-13933.

Madhuri, K., and Naik, P.R. (2017). Modulatory effect of garcinol in streptozotocin-induced diabetic Wistar rats. Archives of Physiology and Biochemistry **123,** 322-329.

Mali, K.K., Dias, R.J., Havaldar, V.D., and Yadav, S.J. (2017). Antidiabetic effect of garcinol on streptozotocin-induced diabetic rats. Indian Journal of Pharmaceutical Sciences **79,** 463-468.

Mandel, M., and Higa, A. (1970). Calcium-dependent bacteriophage DNA infection. Journal of Molecular Biology **53,** 159-162.

Manning, K., Petrunak, E., Lebo, M., González-Sarrías, A., Seeram, N.P., and Henry, G.E. (2011). Acylphloroglucinol and xanthones from *Hypericum ellipticum*. Phytochemistry **72,** 662-667.

Marrelli, M., Statti, G., Conforti, F., and Menichini, F. (2016). New potential pharmaceutical applications of *Hypericum* species. Mini Reviews in Medicinal Chemistry **16,** 710-720.

Martinez-Poveda, B., Verotta, L., Bombardelli, E., Quesada, A.R., and Medina, M.A. (2010). Tetrahydrohyperforin and octahydrohyperforin are two new potent inhibitors of angiogenesis. PloS One **5,** No pp. given.

Matsuhisa, M., Shikishima, Y., Takaishi, Y., Honda, G., Ito, M., Takeda, Y., Shibata, H., Higuti, T., Kodzhimatov, O.K., and Ashurmetov, O. (2002). Benzoylphloroglucinol Derivatives from *Hypericum scabrum*. Journal of Natural Products **65,** 290-294.

McCormac, A.C., Elliott, M.C., and Chen, D.F. (1998). A simple method for the production of highly competent cells of *Agrobacterium* for transformation via electroporation. Molecular Biotechnology **9,** 155-159.

McIntosh, J.A., Donia, M.S., Nair, S.K., and Schmidt, E.W. (2011). Enzymatic basis of ribosomal peptide prenylation in cyanobacteria. Journal of the American Chemical Society **133,** 13698-13705.

Medina, M.A., Martinez-Poveda, B., Amores-Sanchez, M.I., and Quesada, A.R. (2006). Hyperforin: More than an antidepressant bioactive compound? Life Sciences **79,** 105-111.

Meinke, M.C., Schanzer, S., Haag, S.F., Casetti, F., Mueller, M.L., Woelfle, U., Kleemann, A., Lademann, J., and Schempp, C.M. (2012). *In vivo* photoprotective and anti-inflammatory effect of hyperforin is associated with high antioxidant activity *in vitro* and *ex vivo*. European Journal of Pharmaceutics and Biopharmaceutics **81,** 346-350.

Melzer, M., and Heide, L. (1994). Characterization of polyprenyldiphosphate: 4-hydroxybenzoate polyprenyltransferase from *Escherichia coli*. Biochimica et Biophysica Acta (BBA) - Lipids and Lipid Metabolism **1212,** 93-102.

Miller, A.L. (1998). St. John's Wort (*Hypericum perforatum*): clinical effects on depression and other conditions. Alternative Medicine Review **3,** 18-26.

Miranda, C.L., Stevens, J.F., Ivanov, V., McCall, M., Frei, B., Deinzer, M.L., and Buhler, D.R. (2000). Antioxidant and prooxidant actions of prenylated and nonprenylated chalcones and flavanones *in vitro*. Journal of Agricultural and Food Chemistry **48,** 3876-3884.

Mitsopoulou, K.P., Vidali, V.P., Koliopoulos, G., Couladouros, E.A., and Michaelakis, A. (2014). Hyperforin and deoxycohumulone as a larvicidal agent against *Culex pipiens* (Diptera: Culicidae). Chemosphere **100,** 124-129.

Molyneux, R.J., and Jurd, L. (1970). Isoprenylation of polyphenols in aqueous acid solutions. Tetrahedron **26,** 4743-4751.

Müller, A. (2013). Molekulare Analyse von Prenyltransferasen aus *Hypericum*-Arten. Pharmazeutische Biologie. (Technische Universität Braunschweig).

Mullis, K.B. (1994). The Polymerase Chain Reaction (Nobel Lecture). Angewandte Chemie International Edition in English **33,** 1209-1213.

Munakata, R., Olry, A., Karamat, F., Courdavault, V., Sugiyama, A., Date, Y., Krieger, C., Silie, P., Foureau, E., Papon, N., Grosjean, J., Yazaki, K., Bourgaud, F., and Hehn, A. (2016). Molecular evolution of parsnip (*Pastinaca sativa*) membrane-bound prenyltransferases for linear and/or angular furanocoumarin biosynthesis. New Phytologist **211,** 332-344.

Munakata, R., Inoue, T., Koeduka, T., Karamat, F., Olry, A., Sugiyama, A., Takanashi, K., Dugrand, A., Froelicher, Y., Tanaka, R., Uto, Y., Hori, H., Azuma, J.-I., Hehn, A., Bourgaud, F., and Yazaki, K. (2014). Molecular cloning and characterization of a geranyl diphosphate-specific aromatic prenyltransferase from Lemon. Plant Physiology **166,** 80.

Murashige, T., and Skoog, F. (1962). A revised medium for rapid growth and bio-assays with tobacco tissue cultures. Physiologia Plantarum **15,** 473-497.

Nagia, M., Gaid, M., Beuerle, T., and Beerhues, L. (2017). Successive xanthone prenylation in *Hypericum sampsonii*. Planta Medica International Open **4,** Tu-SL-01.

Nagia, M., Gaid, M., Biedermann, E., Fiesel, T., El-Awaad, I., Haensch, R., Wittstock, U., and Beerhues, L. (submitted). Sequential regiospecific *gem*-diprenylation of tetrahydroxyxanthone by prenyltransferases from *Hypericum* sp.

Nicolaou, K.C., Pfefferkorn, J.A., and Cao, G.Q. (2000). Selenium-based solid-phase synthesis of benzopyrans I: Applications to combinatorial synthesis of natural products. Angewandte Chemie International Edition **39,** 734-739.

Noldner, M., and Schotz, K. (2002). Rutin is essential for the antidepressant activity of *Hypericum perforatum* extracts in the forced swimming test. Planta Medica **68,** 577-580.

Nour-Eldin, H.H., Hansen, B.G., Nørholm, M.H.H., Jensen, J.K., and Halkier, B.A. (2006). Advancing uracil-excision based cloning towards an ideal technique for cloning PCR fragments. Nucleic Acids Research **34,** e122-e122.

Nürk, N.M. (2011). Phylogenetic analyses in St. John's wort (*Hypericum*). (Free University of Berlin, Berlin, Germany).

Ohara, K., Mito, K., and Yazaki, K. (2013). Homogeneous purification and characterization of LePGT1 – a membrane-bound aromatic substrate prenyltransferase involved in secondary metabolism of *Lithospermum erythrorhizon*. FEBS Journal **280,** 2572-2580.

Ohara, K., Muroya, A., Fukushima, N., and Yazaki, K. (2009). Functional characterization of LePGT1, a membrane-bound prenyltransferase involved in the geranylation of p-hydroxybenzoic acid. Biochemical Journal **421,** 231.

Okada, Y., and Ito, K. (2001). Cloning and analysis of valerophenone synthase gene expressed specifically in lupulin gland of Hop (*Humulus lupulus* L.). Bioscience, Biotechnology, and Biochemistry **65,** 150-155.

Oku, H., Ueda, Y., Iinuma, M., and Ishiguro, K. (2005). Inhibitory effects of xanthones from Guttiferae plants on PAF-induced hypotension in mice. Planta Medica **71,** 90-92.

Padhye, S., Ahmad, A., Oswal, N., and Sarkar, F.H. (2009). Emerging role of Garcinol, the antioxidant chalcone from *Garcinia indica* Choisy and its synthetic analogs. Journal of Hematology & Oncology **2,** 38-38.

Page, J.E., and Boubakir, Z. (2014). Aromatic prenyltransferase from cannabis (National Research Council of Canada, Can.; University of Saskatchewan .), pp. No pp. given.

Pagny, S., Bouissonnie, F., Sarkar, M., Follet-Gueye, M.L., Driouich, A., Schachter, H., Faye, L., and Gomord, V. (2003). Structural requirements for *Arabidopsis β*1,2-xylosyltransferase activity and targeting to the Golgi. The Plant Journal **33,** 189-203.

Palsuledesai, C.C., and Distefano, M.D. (2015). Protein prenylation: Enzymes, therapeutics, and biotechnology applications. ACS Chemical Biology **10,** 51-62.

Pan, Z., Baerson, S.R., Wang, M., Bajsa-Hirschel, J., Rimando, A.M., Wang, X., Nanayakkara, N.P.D., Noonan, B.P., Fromm, M.E., Dayan, F.E., Khan, I.A., and Duke, S.O. (2018). A cytochrome P450 CYP71 enzyme expressed in *Sorghum bicolor* root hair cells participates in the biosynthesis of the benzoquinone allelochemical sorgoleone. New Phytologist**,** n/a-n/a.

Pepper, H.P., Tulip, S.J., Nakano, Y., and George, J.H. (2014). Biomimetic total synthesis of (±)-doitunggarcinone A and (+)-garcibracteatone. The Journal of Organic Chemistry **79,** 2564-2573.

Piccinelli, A.L., Cuesta-Rubio, O., Chica, M.B., Mahmood, N., Pagano, B., Pavone, M., Barone, V., and Rastrelli, L. (2005). Structural revision of clusianone and 7-epi-clusianone and anti-HIV activity of polyisoprenylated benzophenones. Tetrahedron **61,** 8206-8211.

Ploss, O., Petereit, F., and Nahrstedt, A. (2001). Procyanidins from the herb of *Hypericum perforatum*. Pharmazie **56,** 509-511.

Pojer, F., Wemakor, E., Kammerer, B., Chen, H., Walsh, C.T., Li, S.-M., and Heide, L. (2003). CloQ, a prenyltransferase involved in clorobiocin biosynthesis. Proceedings of the National Academy of Sciences **100,** 2316-2321.

Pompon, D., Louerat, B., Bronine, A., and Urban, P. (1996). Yeast expression of animal and plant P450s in optimized redox environments. In Methods in Enzymology, F.J. Eric and R.W. Michael, eds (Academic Press), pp. 51-64.

Poulter, C.D. (2006). Farnesyl diphosphate synthase. A paradigm for understanding structure and function relationships in E-polyprenyl diphosphate synthases. Phytochemistry Reviews **5,** 17-26.

Qian, Q., Schultz, A.W., Moore, B.S., and Tanner, M.E. (2012). Mechanistic studies on CymD: A tryptophan reverse N-prenyltransferase. Biochemistry **51,** 7733-7739.

Quiney, C., Billard, C., Faussat, A.M., Salanoubat, C., Ensaf, A., Nait-Si, Y., Fourneron, J.D., and Kolb, J.P. (2006). Pro-apoptotic properties of hyperforin in leukemic cells from patients with B-cell chronic lymphocytic leukemia. Leukemia **20,** 491-497.

Reis, F.H.Z., Pardo-Andreu, G.L., Nuñez-Figueredo, Y., Cuesta-Rubio, O., Marín-Prida, J., Uyemura, S.A., Curti, C., and Alberici, L.C. (2014). Clusianone, a naturally occurring nemorosone regioisomer, uncouples rat liver mitochondria and induces HepG2 cell death. Chemico-Biological Interactions **212,** 20-29.

Ritter, H., and Schulz, G.E. (2004). Structural Basis for the Entrance into the Phenylpropanoid Metabolism Catalyzed by Phenylalanine Ammonia-Lyase. The Plant Cell **16,** 3426.

Robinson, A.R., Gheneim, R., Kozak, R.A., Ellis, D.D., and Mansfield, S.D. (2005). The potential of metabolite profiling as a selection tool for genotype discrimination in *Populus*. Journal of Experimental Botany **56,** 2807-2819.

Robson, N.K.B. (2001). Studies in the genus *Hypericum* L. (Guttiferae) 4(1). Section 7. Roscyna to 9. *Hypericum* sensu lato (part 1). Bull. Nat. Hist. Mus. (London), Bot. **31**.

Robson, N.K.B. (2016). And then came molecular phylogenetics—Reactions to a monographic study of *Hypericum* (Hypericaceae). Phytotaxa **255,** 18.

Rohmer, M. (1999). The discovery of a mevalonate-independent pathway for isoprenoid biosynthesis in bacteria, algae and higher plants. Natural Product Reports **16,** 565-574.

Russo, E., Scicchitano, F., Whalley Benjamin, J., Mazzitello, C., Ciriaco, M., Esposito, S., Patanè, M., Upton, R., Pugliese, M., Chimirri, S., Mammì, M., Palleria, C., and De Sarro, G. (2013). *Hypericum perforatum*: Pharmacokinetic, mechanism of action, tolerability, and clinical drug–drug interactions. Phytotherapy Research **28,** 643-655.

Saadat, N., and Gupta, S.V. (2012). Potential role of garcinol as an anticancer agent. Journal of Oncology **2012,** 8.

Sachelaru, I., Winter, L., Knyazev, D.G., Zimmermann, M., Vogt, A., Kuttner, R., Ollinger, N., Siligan, C., Pohl, P., and Koch, H.-G. (2017). YidC and SecYEG form a heterotetrameric protein translocation channel. Scientific Reports **7,** 101.

Saleh, O., Haagen, Y., Seeger, K., and Heide, L. (2009). Prenyl transfer to aromatic substrates in the biosynthesis of aminocoumarins, meroterpenoids and phenazines: The ABBA prenyltransferase family. Phytochemistry **70,** 1728-1738.

Samuelson, J.C., Chen, M., Jiang, F., Möller, I., Wiedmann, M., Kuhn, A., Phillips, G.J., and Dalbey, R.E. (2000). YidC mediates membrane protein insertion in bacteria. Nature **406,** 637.

Santos, M.H., Speziali, N.L., Nagem, T.J., and Oliveira, T.T. (2007). Epiclusianone: a new natural product derivative of bicyclo[3.3.1]nonane-2,4,9-trione. Acta Crystallographica Section C **54,** 1990-1992.

Sasaki, K., Mito, K., Ohara, K., Yamamoto, H., and Yazaki, K. (2008). Cloning and characterization of naringenin 8-prenyltransferase, a flavonoid-specific prenyltransferase of *Sophora flavescens*. Plant Physiology **146,** 1075-1084.

Sato, A., Fujiwara, H., Oku, H., Ishiguro, K., and Ohizumi, Y. (2004). *α*-Mangostin induces Ca^{2}+-ATPase-dependent apoptosis via mitochondrial pathway in PC12 cells. J. Pharmacol. Sci. (Tokyo, Jpn.) **95,** 33-40.

Schiavone, B.I.P., Rosato, A., Marilena, M., Gibbons, S., Bombardelli, E., Verotta, L., Franchini, C., and Corbo, F. (2013). Biological evaluation of hyperforin and its hydrogenated analogue on bacterial growth and biofilm production. Journal of Natural Products **76,** 1819-1823.

Schiller, H., Forster, A., Vonhoff, C., Hegger, M., Biller, A., and Winterhoff, H. (2006). Sedating effects of *Humulus lupulus* L. extracts. Phytomedicine **13,** 535-541.

Schmidt, W., Peters, S., and Beerhues, L. (2000). Xanthone 6-hydroxylase from cell cultures of *Centaurium erythraea* RAFN and *Hypericum androsaemum* L. Phytochemistry **53,** 427-431.

Schneider, E.H., and Seifert, R. (2010). Sf9 cells: A versatile model system to investigate the pharmacological properties of G protein-coupled receptors. Pharmacology & Therapeutics **128,** 387-418.

Schuller, J.M., Zocher, G., Liebhold, M., Xie, X., Stahl, M., Li, S.-M., and Stehle, T. (2012). Structure and catalytic mechanism of a cyclic dipeptide prenyltransferase with broad substrate promiscuity. Journal of Molecular Biology **422,** 87-99.

Seabra, R.M., and Correia Alves, A. (1989). Mangiferin and chlorogenic acid from *Hypericum* species. Planta Medica **55,** 404.

Shen, G., Huhman, D., Lei, Z., Snyder, J., Sumner, L.W., and Dixon, R.A. (2012). Characterization of an isoflavonoid-specific prenyltransferase from *Lupinus albus*. Plant Physiology **159,** 70-80.

Shimizu, Y., Shi, S.L., Usuda, H., Kanai, M., and Shibasaki, M. (2010). Catalytic asymmetric total synthesis of ent-Hyperforin. Angewandte Chemie International Edition **49,** 1103-1106.

Siegel, D.R., and Danishefsky, S.J. (2006). Total synthesis of garsubellin A. Journal of the American Chemical Society **128,** 1048-1049.

Sosa, S., Pace, R., Bornancin, A., Morazzoni, P., Riva, A., Tubaro, A., and Della Loggia, R. (2007). Topical anti-inflammatory activity of extracts and compounds from *Hypericum perforatum* L. Journal of Pharmacy and Pharmacology **59,** 703-709.

Sparling, B.A., Moebius, D.C., and Shair, M.D. (2013). Enantioselective total synthesis of hyperforin. Journal of the American Chemical Society **135,** 644-647.

Stec, E., and Li, S.-M. (2012). Mutagenesis and biochemical studies on AuaA confirmed the importance of the two conserved aspartate-rich motifs and suggested difference in the amino acids for substrate binding in membrane-bound prenyltransferases. Archives of Microbiology **194,** 589-595.

Steffan, B., Wätjen, W., Michels, G., Niering, P., Wray, V., Ebel, R., Edrada, R., Kahl, R., and Proksch, P. (2010). Polyphenols from plants used in traditional Indonesian medicine (Jamu): uptake and antioxidative effects in rat H4IIE hepatoma cells. Journal of Pharmacy and Pharmacology **57,** 233-240.

Stojanovic, G., Dordevic, A., and Smelcerovic, A. (2013). Do other *Hypericum* species have medical potential as St. John's Wort (*Hypericum perforatum*)? Current Medicinal Chemistry **20,** 2273-2295.

Strickland, C.L., Windsor, W.T., Syto, R., Wang, L., Bond, R., Wu, Z., Schwartz, J., Le, H.V., Beese, L.S., and Weber, P.C. (1998). Crystal structure of farnesyl protein transferase complexed with a CaaX peptide and farnesyl diphosphate analogue. Biochemistry **37,** 16601-16611.

Tanaka, N., Mamemura, T., Abe, S., Imabayashi, K., Kashiwada, Y., Takaishi, Y., Suzuki, T., Takebe, Y., Kubota, T., and Kobayashi, J.i. (2010). Biyouxanthones A - D, prenylated xanthones from roots of *Hypericum chinense*. Heterocycles **80,** 613-621.

Tanaka, N., Takaishi, Y., Shikishima, Y., Nakanishi, Y., Bastow, K., Lee, K.-H., Honda, G., Ito, M., Takeda, Y., Kodzhimatov, O.K., and Ashurmetov, O. (2004). Prenylated

benzophenones and xanthones from *Hypericum scabrum*. Journal of Natural Products **67,** 1870-1875.

Tanner, M.E. (2015). Mechanistic studies on the indole prenyltransferases. Natural Product Reports **32,** 88-101.

Tarshis, L.C., Yan, M., Poulter, C.D., and Sacchettini, J.C. (1994). Crystal structure of recombinant farnesyl diphosphate synthase at 2.6-.ANG. Resolution. Biochemistry **33,** 10871-10877.

Tello, M., Kuzuyama, T., Heide, L., Noel, J.P., and Richard, S.B. (2008). The ABBA family of aromatic prenyltransferases: broadening natural product diversity. Cellular and molecular life sciences : CMLS **65,** 1459-1463.

Tian, W.-J., Qiu, Y.-Q., Yao, X.-J., Chen, H.-F., Dai, Y., Zhang, X.-K., and Yao, X.-S. (2014). Dioxasampsones A and B, two polycyclic polyprenylated acylphloroglucinols with unusual epoxy-ring-fused skeleton from *Hypericum sampsonii*. Organic Letters **16,** 6346-6349.

Tian, W.-J., Qiu, Y.-Q., Jin, X.-J., Chen, H.-F., Yao, X.-J., Dai, Y., and Yao, X.-S. (2016). Hypersampsones S-W, new polycyclic polyprenylated acylphloroglucinols from *Hypericum sampsonii*. RSC Advances **6,** 50887-50894.

Tian, W.-J., Qiu, Y.-Q., Chen, J.-J., Yao, X.-J., Wang, G.-H., Dai, Y., Chen, H.-F., and Yao, X.-S. (2017). Norsampsone E, an unprecedented decarbonyl polycyclic polyprenylated acylphloroglucinol with a homoadamantyl core from *Hypericum sampsonii*. RSC Advances **7,** 33113-33119.

Ting, C.P., and Maimone, T.J. (2016). The total synthesis of hyperforin. Synlett **27,** 1443-1449.

Tocci, N., D'Auria, F.D., Simonetti, G., Panella, S., Palamara, A.T., Debrassi, A., Rodrigues, C.A., Filho, V.C., Sciubba, F., and Pasqua, G. (2013). Bioassay-guided fractionation of extracts from *Hypericum perforatum* in vitro roots treated with carboxymethylchitosans and determination of antifungal activity against human fungal pathogens. Plant Physiology and Biochemistry **70,** 342-347.

Tocci, N., Gaid, M., Kaftan, F., Belkheir Asma, K., Belhadj, I., Liu, B., Svatoš, A., Hänsch, R., Pasqua, G., and Beerhues, L. (2017). Exodermis and endodermis are the sites of xanthone biosynthesis in *Hypericum perforatum* roots. New Phytologist **217,** 1099-1112.

Treco, D.A., and Winston, F. (2001). Growth and manipulation of yeast. In Current Protocols in Molecular Biology (John Wiley & Sons, Inc.

Tsai, H.F., Wang, H., Gebler, J.C., Poulter, C.D., and Schardl, C.L. (1995). The *Claviceps purpurea* gene encoding dimethylallyltryptophan synthase, the committed step for ergot alkaloid biosynthesis. Biochemical and Biophysical Research Communications **216,** 119-125.

Tsurumaru, Y., Sasaki, K., Miyawaki, T., Momma, T., Umemoto, N., and Yazaki, K. (2010). An aromatic prenyltransferase-like gene HlPT-1 preferentially expressed in lupulin glands of hop. Plant Biotechnology **27,** 199-204.

Tsurumaru, Y., Sasaki, K., Miyawaki, T., Uto, Y., Momma, T., Umemoto, N., Momose, M., and Yazaki, K. (2012). HlPT-1, a membrane-bound prenyltransferase responsible for the biosynthesis of bitter acids in hops. Biochemical and Biophysical Research Communications **417,** 393-398.

Van Cleemput, M., Cattoor, K., De Bosscher, K., Haegeman, G., De Keukeleire, D., and Heyerick, A. (2009). Hop (*Humulus lupulus*)-derived bitter acids as multipotent bioactive compounds. Journal of Natural Products **72,** 1220-1230.

van Klink, J.W., Brophy, J.J., Perry, N.B., and Weavers, R.T. (1999). *β*-Triketones from Myrtaceae: Isoleptospermone from *Leptospermum scoparium* and Papuanone from *Corymbia dallachiana*. Journal of Natural Products **62,** 487-489.

Venkatesh, T.V., Karunanandaa, B., Free, D.L., Rottnek, J.M., Baszis, S.R., and Valentin, H.E. (2006). Identification and characterization of an *Arabidopsis* homogentisate phytyltransferase paralog. Planta **223,** 1134-1144.

Verotta, L., Appendino, G., Bombardelli, E., and Brun, R. (2007). *In vitro* antimalarial activity of hyperforin, a prenylated acylphloroglucinol. A structure-activity study. Bioorganic & Medicinal Chemistry Letters **17,** 1544-1548.

Vickery, C.R., La Clair, J.J., Burkart, M.D., and Noel, J.P. (2016). Harvesting the biosynthetic machineries that cultivate a variety of indispensable plant natural products. Current Opinion in Chemical Biology **31,** 66-73.

Wagner, S., Bader, M.L., Drew, D., and de Gier, J.-W. (2006). Rationalizing membrane protein overexpression. Trends in Biotechnology **24,** 364-371.

Wagner, S., Baars, L., Ytterberg, A.J., Klussmeier, A., Wagner, C.S., Nord, O., Nygren, P.-Å., van Wijk, K.J., and de Gier, J.-W. (2007). Consequences of membrane protein overexpression in *Escherichia coli*. Molecular & Cellular Proteomics **6,** 1527-1550.

Wagner, S., Klepsch, M.M., Schlegel, S., Appel, A., Draheim, R., Tarry, M., Högbom, M., van Wijk, K.J., Slotboom, D.J., Persson, J.O., and de Gier, J.-W. (2008). Tuning *Escherichia coli* for membrane protein overexpression. Proceedings of the National Academy of Sciences **105,** 14371-14376.

Wang, J., Chu, S., Zhu, Y., Cheng, H., and Yu, D. (2015a). Positive selection drives neofunctionalization of the UbiA prenyltransferase gene family. Plant Molecular Biology **87,** 383-394.

Wang, R., Chen, R., Li, J., Liu, X., Xie, K., Chen, D., Peng, Y., and Dai, J. (2016). Regiospecific prenylation of hydroxyxanthones by a plant flavonoid prenyltransferase. Journal of Natural Products **79,** 2143-2147.

Wang, R., Chen, R., Li, J., Liu, X., Xie, K., Chen, D., Yin, Y., Tao, X., Xie, D., Zou, J., Yang, L., and Dai, J. (2014). Molecular characterization and phylogenetic analysis of two novel regio-specific flavonoid prenyltransferases from *Morus alba* and *Cudrania tricuspidata*. The Journal of Biological Chemistry **289,** 35815-35825.

Wang, Y., Tsai, M.-L., Chiou, L.-Y., Ho, C.-T., and Pan, M.-H. (2015b). Antitumor activity of garcinol in human prostate cancer cells and xenograft mice. Journal of Agricultural and Food Chemistry **63,** 9047-9052.

Wang, Y., Xia, Z., Xu, J.-R., Wang, Y.-X., Hou, L.-N., Qiu, Y., and Chen, H.-Z. (2012). *α*-Mangostin, a polyphenolic xanthone derivative from mangosteen, attenuates *β*-amyloid oligomers-induced neurotoxicity by inhibiting amyloid aggregation. Neuropharmacology **62,** 871-881.

Weng, J.-R., Tsao, L.-T., Wang, J.-P., Wu, R.-R., and Lin, C.-N. (2004). Anti-inflammatory phloroglucinols and terpenoids from *Garcinia subelliptica*. Journal of Natural Products **67,** 1796-1799.

Wessjohann, L., Zakharova, S., Schulze, D., Kufka, J., Weber, R., Bräuer, L., and Brandt, W. (2009). Enzymatic C–C-coupling prenylation, bioinformatics – modelling – mechanism– protein-redesign – biocatalytic application. CHIMIA International Journal for Chemistry **63,** 340-344.

Winkelblech, J., and Li, S.M. (2014). Biochemical investigations of two 6-DMATS enzymes from *Streptomyces* reveal new features of L-tryptophan prenyltransferases. ChemBioChem **15,** 1030-1039.

Winkelblech, J., Fan, A., and Li, S.-M. (2015). Prenyltransferases as key enzymes in primary and secondary metabolism. Applied Microbiology and Biotechnology **99,** 7379-7397.

Winkelmann, K., Heilmann, J., Zerbe, O., Rali, T., and Sticher, O. (2001). New prenylated bi- and tricyclic phloroglucinol derivatives from *Hypericum papuanum*. Journal of Natural Products **64,** 701-706.

Woelfle, U., Seelinger, G., and Schempp, C.M. (2014). Topical application of St. John's Wort (*Hypericum perforatum*). Planta Medica **80,** 109-120.

Woodside, A.B., Huang, Z., and Poulter, C.D. (1988). Trisammonium Geranyl Diphosphate. Organic Syntheses **66,** 211-215.

Wu, S.-B., Long, C., and Kennelly, E.J. (2014). Structural diversity and bioactivities of natural benzophenones. Natural Product Reports **31,** 1158-1174.

Xiao, Z.Y., Mu, Q., Shiu, W.K.P., Zeng, Y.H., and Gibbons, S. (2007). Polyisoprenylated benzoylphloroglucinol derivatives from *Hypericum sampsonii*. Journal of Natural Products **70,** 1779-1782.

Xiao, Z.Y., Shiu, W.K.P., Zeng, Y.H., Mu, Q., and Gibbons, S. (2008). A naturally occurring inhibitory agent from *Hypericum sampsonii* with activity against multidrug-resistant *Staphylococcus aureus*. Pharmaceutical Biology **46,** 250-253.

Xiao, Z.Y., Zeng, Y.H., Mu, Q., Shiu, W.K.P., and Gibbons, S. (2010). Prenylated benzophenone peroxide derivatives from *Hypericum sampsonii*. Chemistry & Biodiversity **7,** 953-958.

Xin, W.-B., Mao, Z.-J., Jin, G.-L., and Qin, L.-P. (2011a). Two new xanthones from *Hypericum sampsonii* and biological activity of the isolated compounds. Phytotherapy Research **25,** 536-539.

Xin, W.-b., Man, X.-h., Zheng, C.-j., Jia, M., Jiang, Y.-p., Zhao, X.-x., Jin, G.-l., Mao, Z.-j., Huang, H.-q., and Qin, L.-p. (2012). Prenylated phloroglucinol derivatives from *Hypericum sampsonii*. Fitoterapia **83,** 1540-1547.

Xin, W.B., Jin, G.L., Mao, Z.J., and Qin, L.P. (2011b). Two unusual phenolic substances and one new xanthone from *Hypericum sampsonii*. Helvetica Chimica Acta **94,** 686-692.

Xu, H., Zhang, F., Liu, B., Huhman, D.V., Sumner, L.W., Dixon, R.A., and Wang, G. (2013). Characterization of the formation of branched short-chain fatty acid:CoAs for bitter acid biosynthesis in hop glandular trichomes. Molecular Plant **6,** 1301-1317.

Yamakuni, T., Aoki, K., Nakatani, K., Kondo, N., Oku, H., Ishiguro, K., and Ohizumi, Y. (2006). Garcinone B reduces prostaglandin E2 release and NF-κB-mediated transcription in C6 rat glioma cells. Neuroscience Letters **394,** 206-210.

Yang, X.-W., Yang, J., and Xu, G. (2017a). Skeleton reassignment of type C polycyclic polyprenylated acylphloroglucinols. Journal of Natural Products **80,** 108-113.

Yang, X.-W., Grossman, R.B., and Xu, G. (2018). Research progress of polycyclic polyprenylated acylphloroglucinols. Chemical Reviews **118,** 3508-3558.

Yang, X.-W., Wang, H., Ma, W.-G., Xia, F., and Xu, G. (2017b). Homo-adamantane type polyprenylated acylphloroglucinols from *Hypericum pseudohenryi*. Tetrahedron **73,** 566-570.

Yang, X.-W., Li, M.-M., Liu, X., Ferreira, D., Ding, Y., Zhang, J.-J., Liao, Y., Qin, H.-B., and Xu, G. (2015). Polycyclic polyprenylated acylphloroglucinol congeners possessing diverse structures from *Hypericum henryi*. Journal of Natural Products **78,** 885-895.

Yazaki, K., Sasaki, K., and Tsurumaru, Y. (2009). Prenylation of aromatic compounds, a key diversification of plant secondary metabolites. Phytochemistry **70,** 1739-1745.

Yazaki, K., Kunihisa, M., Fujisaki, T., and Sato, F. (2002). Geranyl diphosphate:4-hydroxybenzoate geranyltransferase from *Lithospermum erythrorhizon*. Cloning and characterization of a key enzyme in shikonin biosynthesis. The Journal of Biological Chemistry **277,** 6240-6246.

Yen, C.-T., Nakagawa-Goto, K., Hwang, T.-L., Morris-Natschke, S.L., Bastow, K.F., Wu, Y.-C., and Lee, K.-H. (2012). Design and synthesis of gambogic acid analogs as potent cytotoxic and anti-inflammatory agents. Bioorganic & Medicinal Chemistry Letters **22,** 4018-4022.

Yin, W.-B., Grundmann, A., Cheng, J., and Li, S.-M. (2009). Acetylaszonalenin biosynthesis in *Neosartorya fischeri*: Identification of the biosynthetic gene cluster by genomic mining and functional proof of the genes by biochemical investigation. Journal of Biological Chemistry **284,** 100-109.

Yin, W.-B., Yu, X., Xie, X.-L., and Li, S.-M. (2010). Preparation of pyrrolo[2,3-b]indoles carrying a *β*-configured reverse C3-dimethylallyl moiety by using a recombinant prenyltransferase CdpC3PT. Organic & Biomolecular Chemistry **8,** 2430-2438.

Young, I.G., Leppik, R.A., Hamilton, J.A., and Gibson, F. (1972). Biochemical and genetic studies on ubiquinone biosynthesis in Escherichia coli K-12. 4-Hydroxybenzoate octaprenyltransferase. Journal of Bacteriology **110,** 18-25.

Yu, X., and Li, S.-M. (2012). Chapter Thirteen - Prenyltransferases of the dimethylallyltryptophan synthase superfamily. In Methods in Enzymology, D.A. Hopwood, ed (Academic Press), pp. 259-278.

Zeng, Y.-H., Osman, K., Xiao, Z.-Y., Gibbons, S., and Mu, Q. (2012). Four geranyl-bearing polyisoprenylated benzoylphloroglucinol derivatives from *Hypericum sampsonii*. Phytochemistry Letters **5,** 200-205.

Zeng, Y.H., Mu, Q., Xiao, Z.Y., Xu, Y., Rahman, M.M., and Gibbons, S. (2009). Geranyl bearing polyisoprenylated benzoylphloroglucinol derivatives from *Hypericum sampsonii*. Chemistry Letters **38,** 440-441.

Zeyhle, P., Bauer, J.S., Kalinowski, J., Shin-ya, K., Gross, H., and Heide, L. (2014). Genome-based discovery of a novel membrane-bound 1,6-dihydroxyphenazine prenyltransferase from a marine Actinomycete. PloS One **9,** e99122.

Zhang, H., Zhang, D.-D., Lao, Y.-Z., Fu, W.-W., Liang, S., Yuan, Q.-H., Yang, L., and Xu, H.-X. (2014). Cytotoxic and anti-inflammatory prenylated benzoylphloroglucinols and xanthones from the twigs of *Garcinia esculenta*. Journal of Natural Products **77,** 1700-1707.

Zhang, J.-S., Zou, Y.-H., Guo, Y.-Q., Li, Z.-Z., Tang, G.-H., and Yin, S. (2016). Polycyclic polyprenylated acylphloroglucinols: natural phosphodiesterase-4 inhibitors from *Hypericum sampsonii*. RSC Advances **6,** 53469-53476.

Zhang, K.Y.J., Ibrahim, P.N., Gillette, S., and Bollag, G. (2005). Phosphodiesterase-4 as a potential drug target. Expert Opinion on Therapeutic Targets **9,** 1283-1305.

Zhao, J., Liu, W., and Wang, J.-C. (2015). Recent advances regarding constituents and bioactivities of plants from the genus *Hypericum*. Chemistry & Biodiversity **12,** 309-349.

Zhou, K., Ludwig, L., and Li, S.-M. (2015). Friedel–Crafts alkylation of acylphloroglucinols catalyzed by a fungal indole prenyltransferase. Journal of Natural Products **78,** 929-933.

Zhou, K., Wunsch, C., Dai, J., and Li, S.-M. (2017). *gem*-Diprenylation of acylphloroglucinols by a fungal prenyltransferase of the dimethylallyltryptophan synthase superfamily. Organic Letters **19,** 388-391.

Zhu, H., Chen, C., Tan, D., Li, D., Guo, Y., Wei, G., Zhang, J., Wang, J., Luo, Z., Xue, Y., and Zhang, Y. (2016). Sampbenzophenones A-G, prenylated benzoylphloroglucinol derivatives from *Hypericum sampsonii*. RSC Advances **6,** 86710-86716.

Zhu, H., Chen, C.-M., Zhang, J.-W., Guo, Y., Tan, D.-D., Wei, G.-Z., Yang, J., Wang, J.-P., Luo, Z.-W., Xue, Y.-B., and Zhang, Y.-H. (2017). Hyperisampsins N and O, two new benzoylated phloroglucinol derivatives from *Hypericum sampsonii*. Chinese Chemical Letters **28,** 986-990.

Zhu, H., Chen, C., Tong, Q., Chen, X., Yang, J., Liu, J., Sun, B., Wang, J., Yao, G., Luo, Z., Xue, Y., and Zhang, Y. (2015). Hyperisampsins H–M, cytotoxic polycyclic polyprenylated acylphloroglucinols from *Hypericum sampsonii*. Scientific Reports **5,** 14772.

Zhu, H., Chen, C., Yang, J., Li, X.-N., Liu, J., Sun, B., Huang, S.-X., Li, D., Yao, G., Luo, Z., Li, Y., Zhang, J., Xue, Y., and Zhang, Y. (2014). Bioactive acylphloroglucinols with adamantyl skeleton from *Hypericum sampsonii*. Organic Letters **16,** 6322-6325.

Zuckerkandl, E., and Pauling, L. (1965). Evolutionary divergence and convergence in proteins. Edited in Evolving Genes and Proteins by V. Bryson and H.J. Vogel **Academic Press, New York,** 97- 166.

Zuurbier, K.W.M., Fung, S.-Y., Scheffer, J.J.C., and Verpoorte, R. (1998). *In-vitro* prenylation of aromatic intermediates in the biosynthesis of bitter acids in *Humulus lupulus*. Phytochemistry **49,** 2315-2322.

8 Appendix

8.1 Accession numbers of aPTs used for reconstruction of phylogenetic analysis

Sequence name\	Accession no.	Species	Family
ApUbiA [a]	BAA80570.1	*Aeropyrum pernix*	Desulfurococcaceae
ApVTE2-1	DQ231057	*Allium ampeloprasum*	Amaryllidaceae
AtaPT [b]	KP893683	*Aspergillus terreus*	Trichocomaceae
AtPPT1	NP_567688.1	*Arabidopsis thaliana*	Brassicaceae
AtVTE2-1	AY089963	*Arabidopsis thaliana*	Brassicaceae
AtVTE2-2	DQ231060	*Arabidopsis thaliana*	Brassicaceae
Cl-PT1a	AB813876	*Citrus limon*	Rutaceae
CpVTE2-1	DQ231058	*Cuphea pulcherrima*	Lythraceae
CsPT-1	WO 2011017798 A1 [c]	*Cannabis sativa*	Cannabaceae
GmG4DT	AB434690	*Glycine max*	Fabaceae
GmVTE2-1	DQ231059	*Glycine max*	Fabaceae
GmVTE2-2	DQ231061	*Glycine max*	Fabaceae
GuA6DT	KJ123716	*Glycyrrhiza uralensis*	Fabaceae
HcPT	KT325851	*Hypericum calycinum*	Hypericaceae
HcPT8PX	MH461102	*Hypericum calycinum*	Hypericaceae
HcPTpat	MH461103	*Hypericum calycinum*	Hypericaceae
HIPT-1	AB543053	*Humulus lupulus*	Cannabaceae
HIPT-2	KM222442	*Humulus lupulus*	Cannabaceae
HvHGGT	AY222860	*Hordeum vulgare*	Poaceae
LaPT1	JN228254	*Lupinus albus*	Fabaceae
LePGT1	AB055078	*Lithospermum erythrorhizon*	Boraginaceae
LePGT2	AB055079	*Lithospermum erythrorhizon*	Boraginaceae
OsHGGT	AY222862	*Oryza sativa*	Poaceae
OsPPT1	AB263291	*Oryza sativa*	Poaceae
OsVTE2-2	XP_015646905.1	*Oryza sativa*	Poaceae
PcPT	AB825956	*Petroselinum crispum*	Apiaceae
PsPT1	KM017083	*Pastinaca sativa*	Apiaceae
PsPT2	KM017084	*Pastinaca sativa*	Apiaceae
SfFPT	KC513505	*Sophora flavescens*	Fabaceae
SfG6DT	AB604224	*Sophora flavescens*	Fabaceae
SfiLDT	AB604223	*Sophora flavescens*	Fabaceae
SfN8DT-1	AB325579	*Sophora flavescens*	Fabaceae
SfN8DT-2	AB370330	*Sophora flavescens*	Fabaceae
SfN8DT-3	AB604222	*Sophora flavescens*	Fabaceae
TaHGGT	AY222861	*Triticum aestivum*	Poaceae
TaVTE2-1	DQ231056	*Triticum aestivum*	Poaceae

ZmVTE2-1	DQ231055	*Zea mays*	Poaceae

[a] bacterial sequence, [b] fungal sequence, [c] patent number.

8.2 List of tables

8.3 List of figures

8.4 NMR spectra

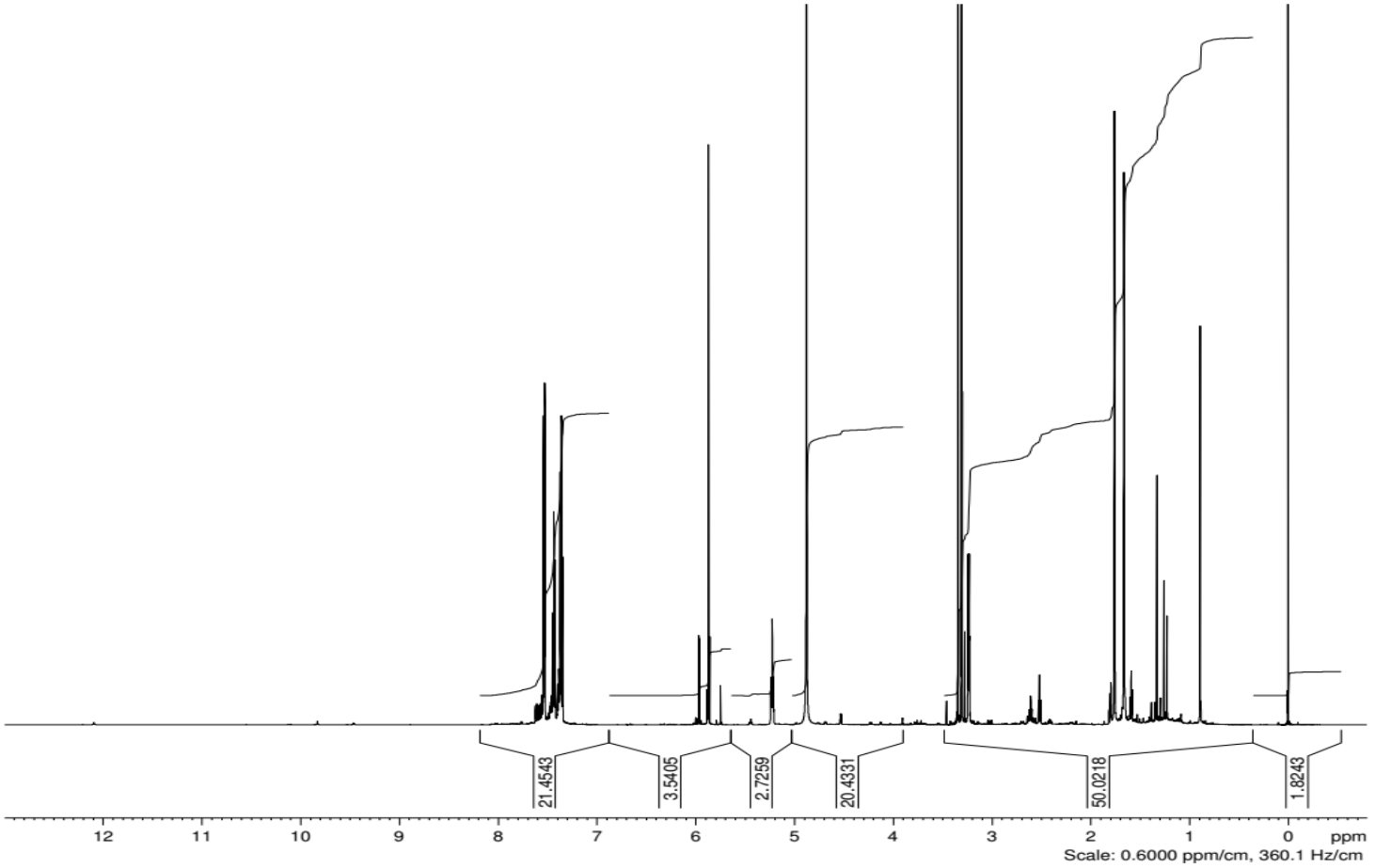

^{1}H NMR spectrum of 3-prenyl-2,4,6-trihydroxybenzophenone (MPPBP).

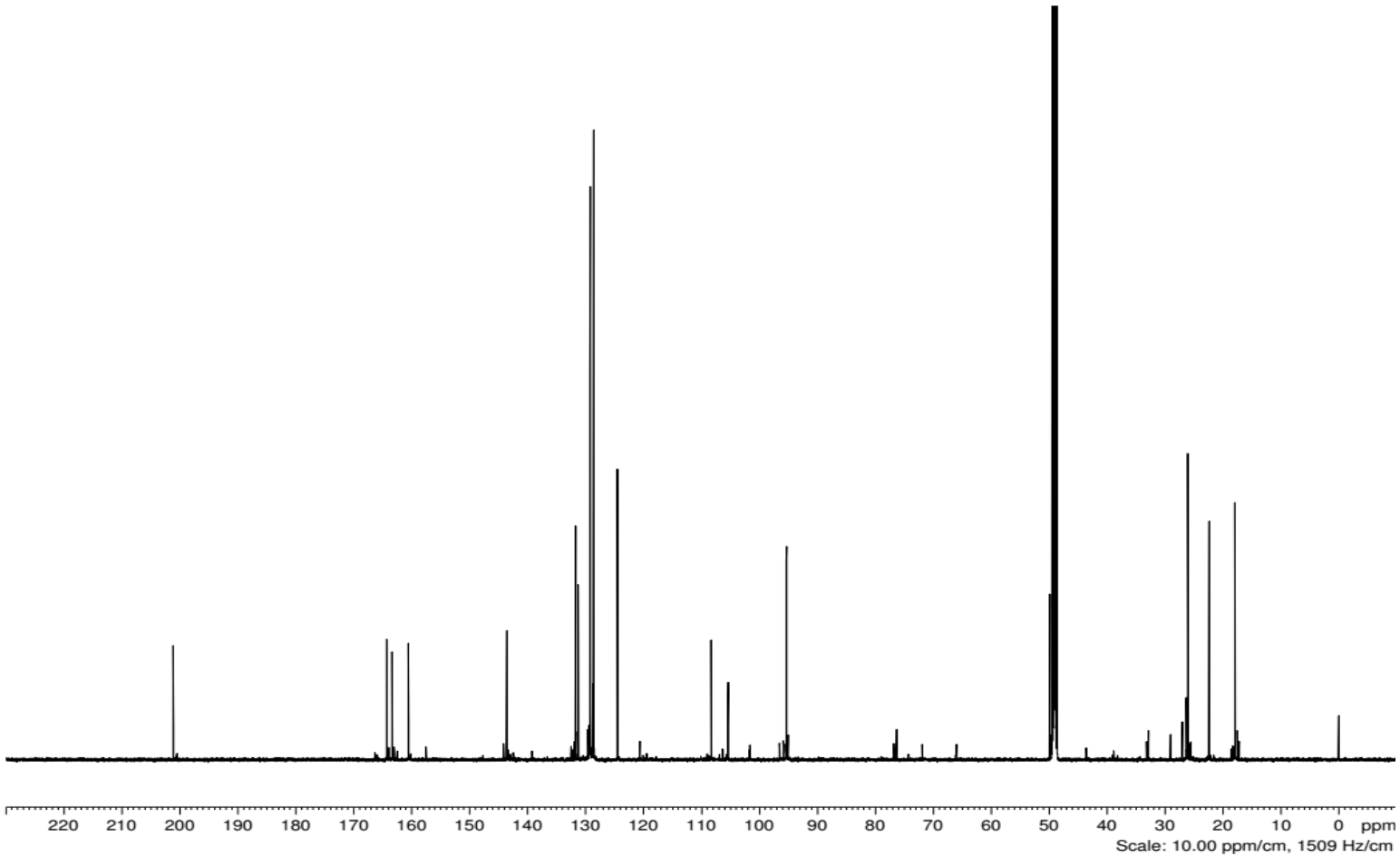

^{13}C NMR spectrum of 3-prenyl-2,4,6-trihydroxybenzophenone (MPPBP).

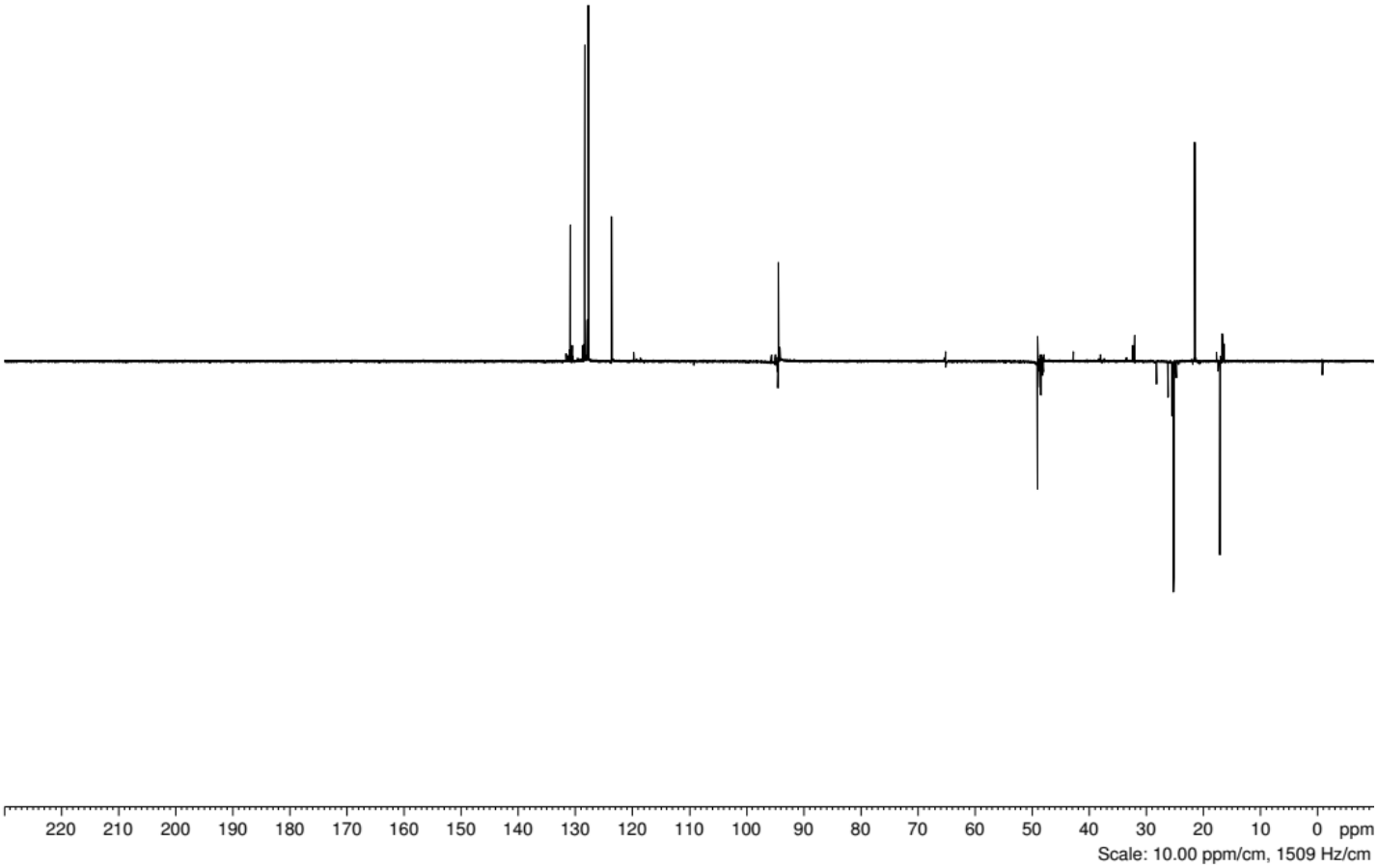

^{13}C-Dept NMR spectrum of 3-prenyl-2,4,6-trihydroxybenzophenone (MPPBP).

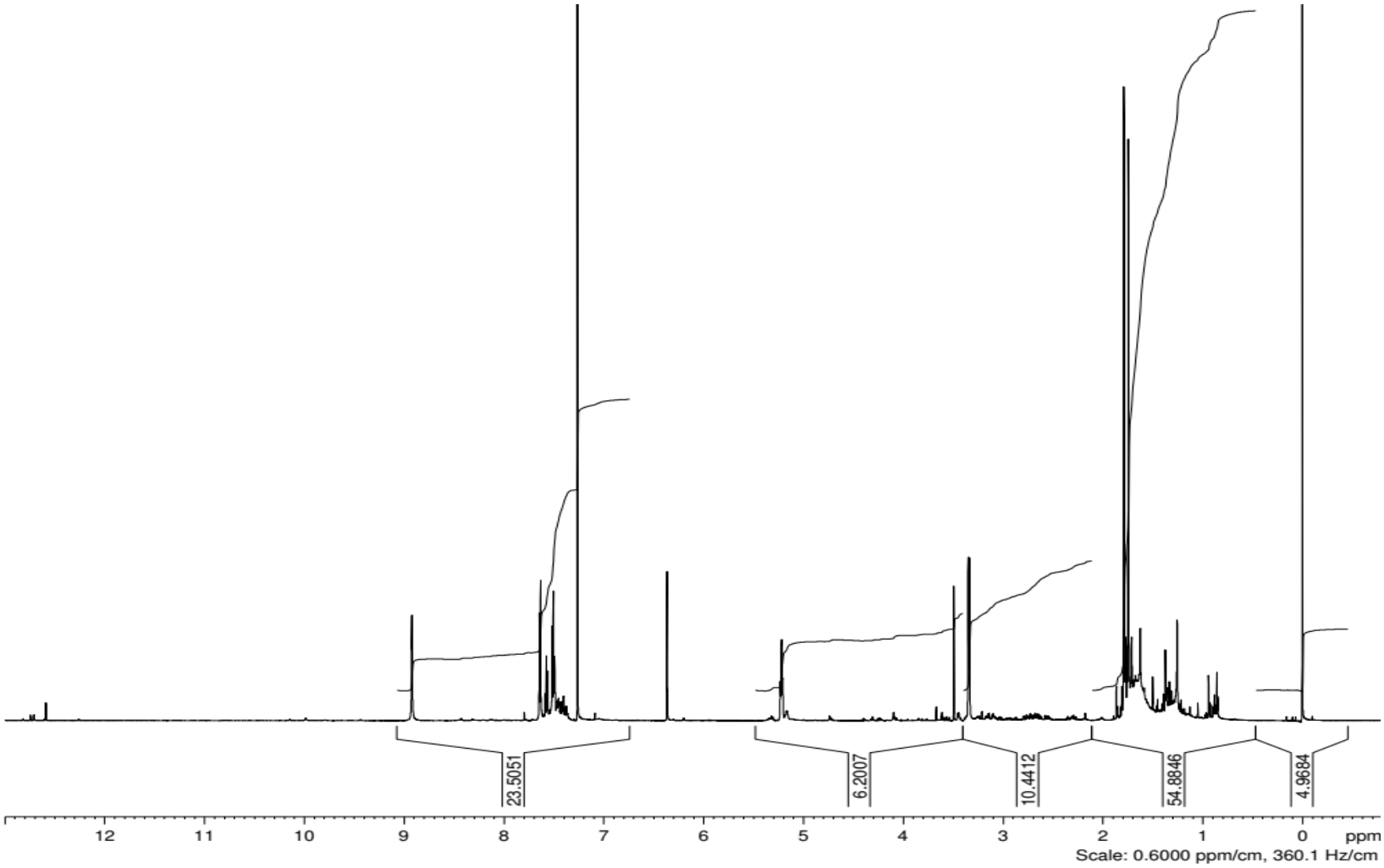

^{1}H NMR spectrum of 3,5-diprenyl-2,4,6-trihydroxybenzophenone (DPPBP).

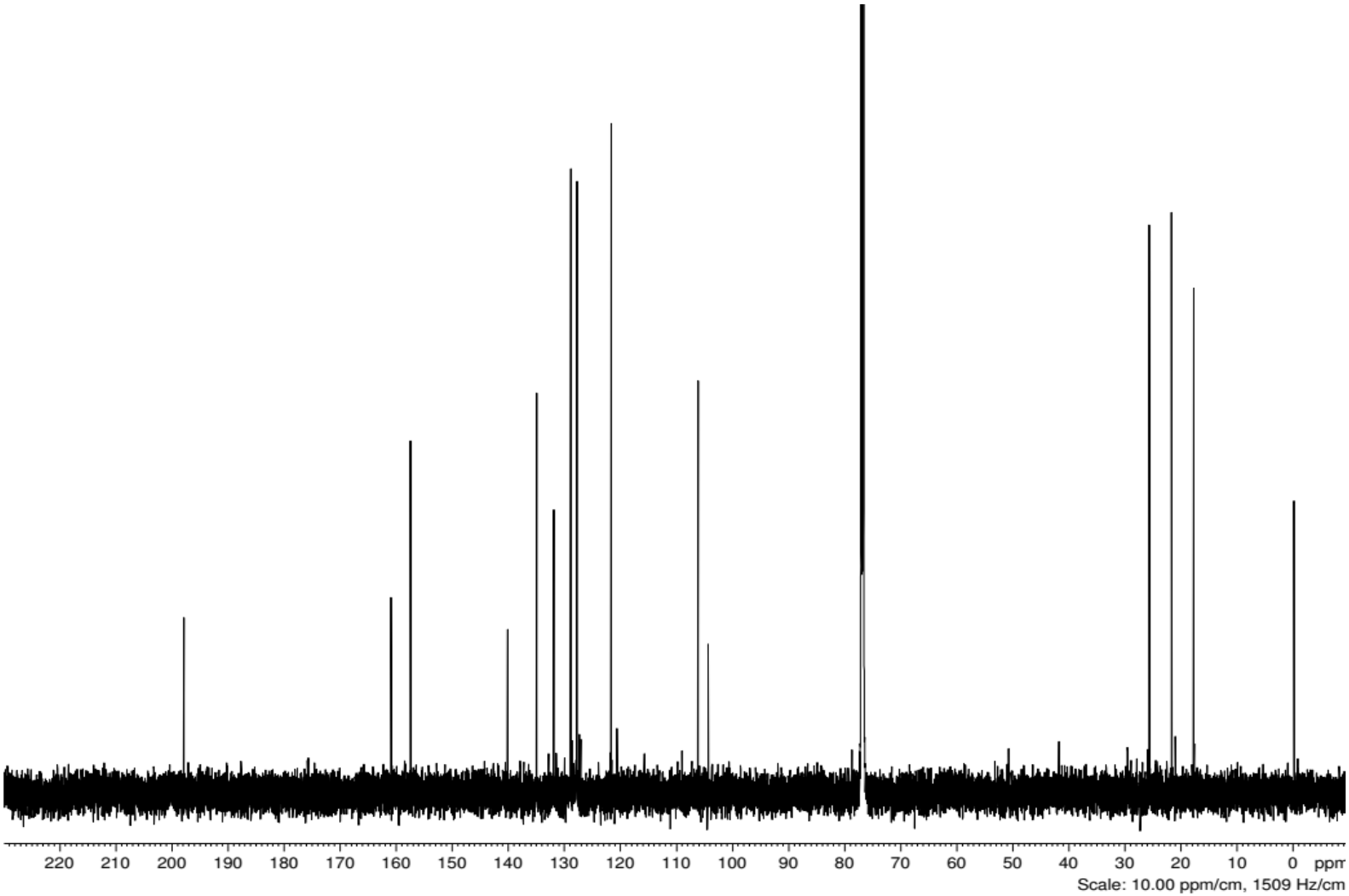

^{13}C NMR spectrum of 3,5-diprenyl-2,4,6-trihydroxybenzophenone (DPPBP).

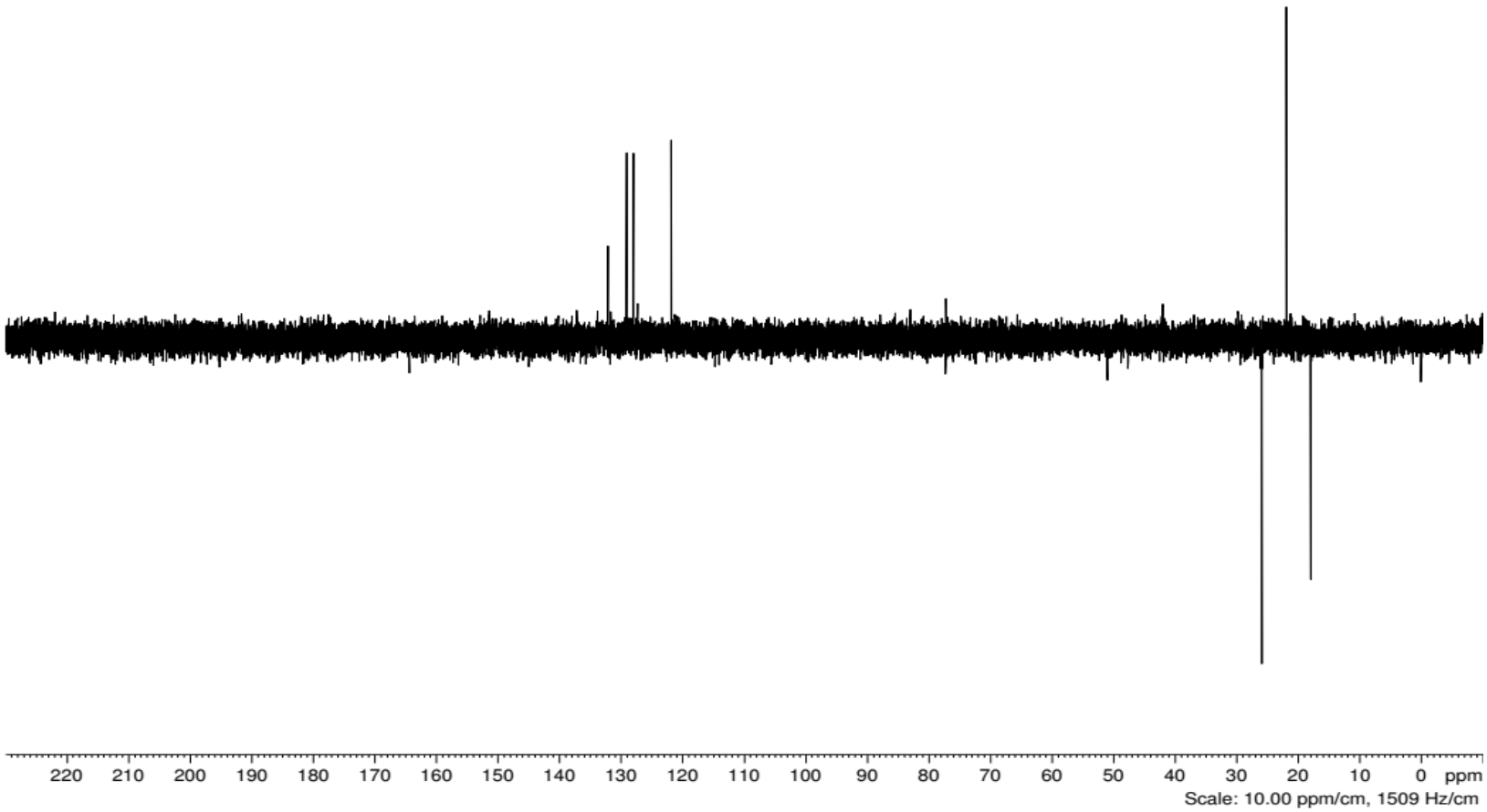

^{13}C-Dept NMR spectrum of 3,5-diprenyl-2,4,6-trihydroxybenzophenone (DPPBP).

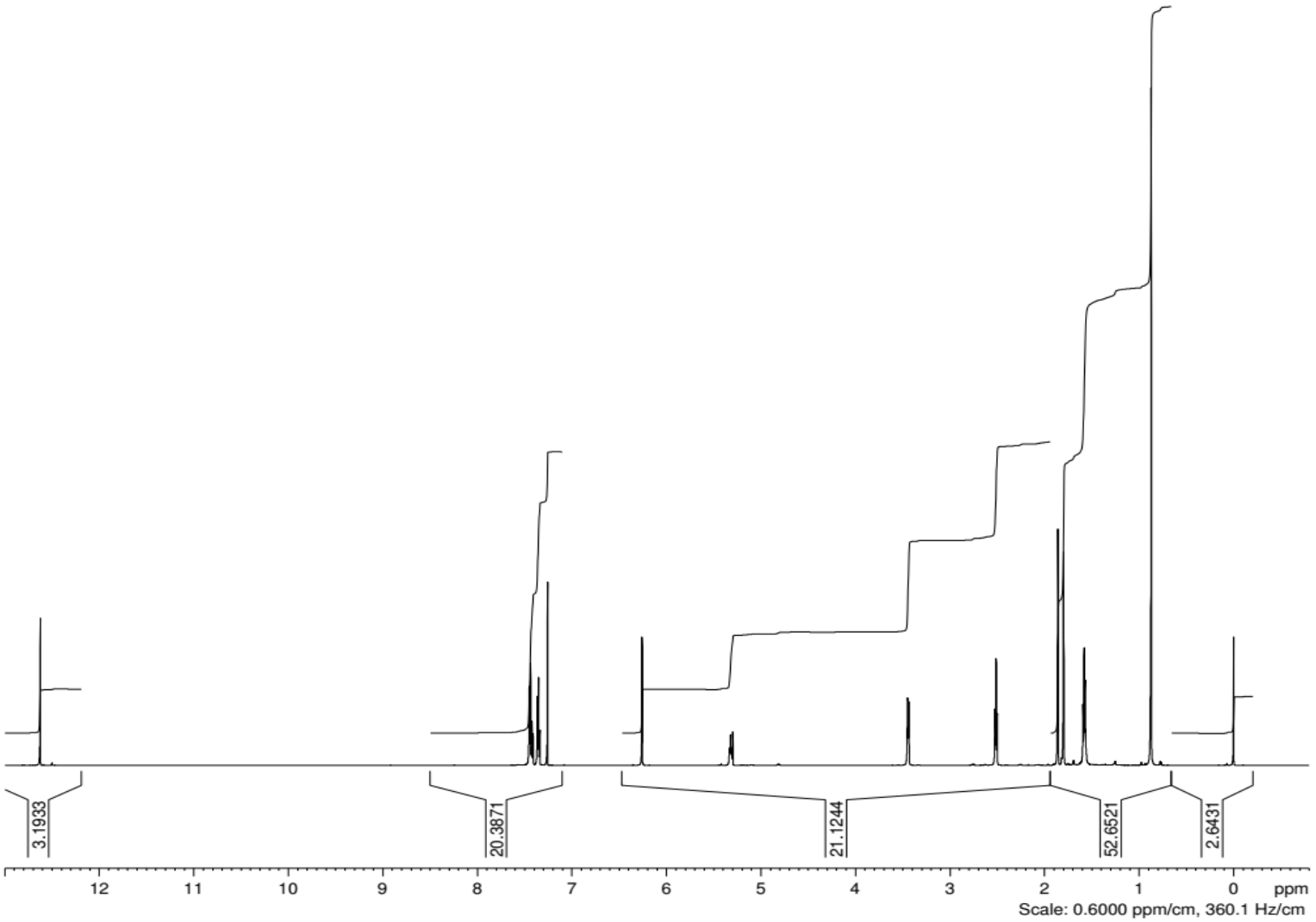

^{1}H NMR spectrum of (5,7-dihydroxy-2,2-dimethyl-6-(3-methylbut-2-en-1-yl)chroman-8-yl)(phenyl)methanone.

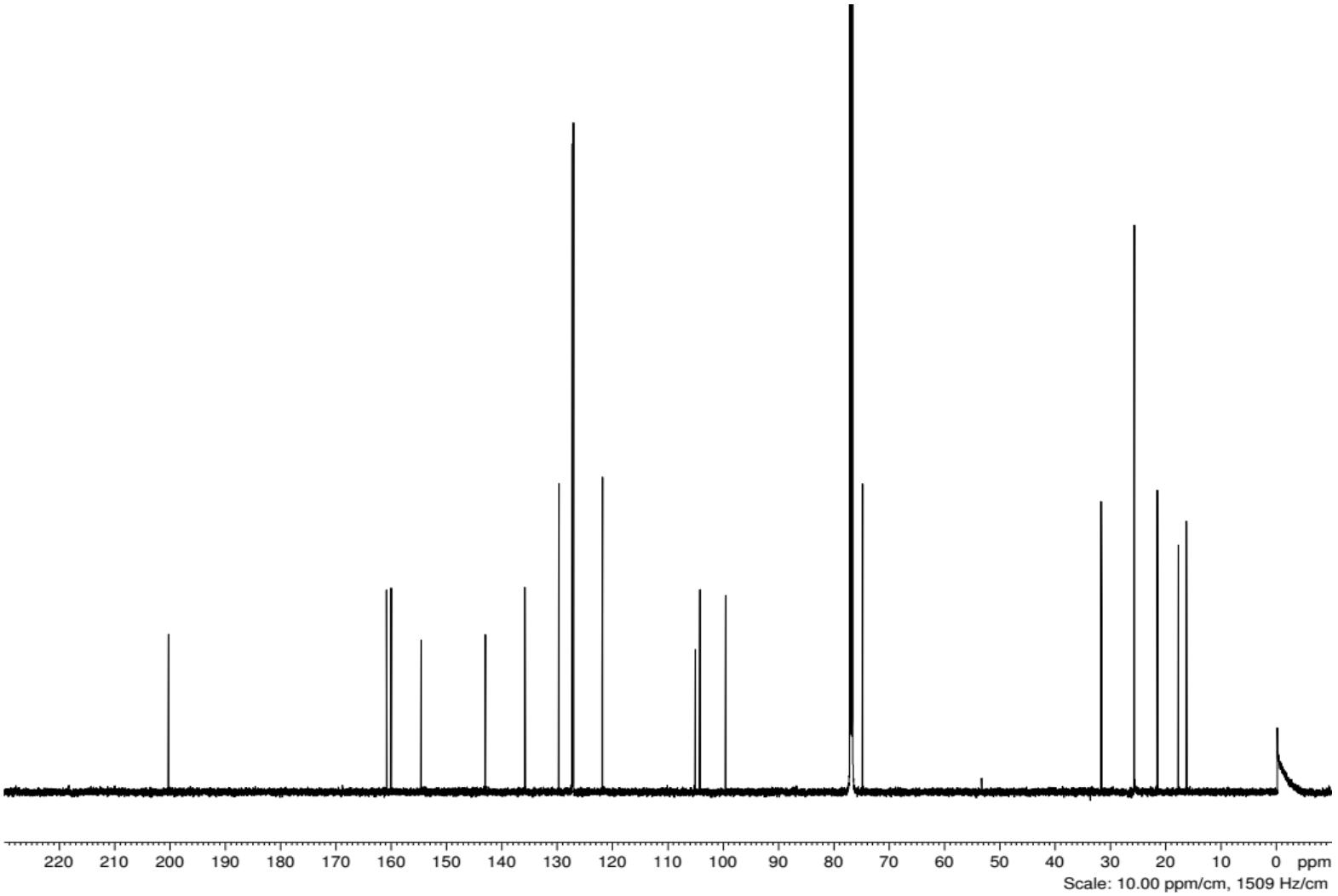

^{13}C NMR spectrum of (5,7-dihydroxy-2,2-dimethyl-6-(3-methylbut-2-en-1-yl)chroman-8-yl)(phenyl)methanone.

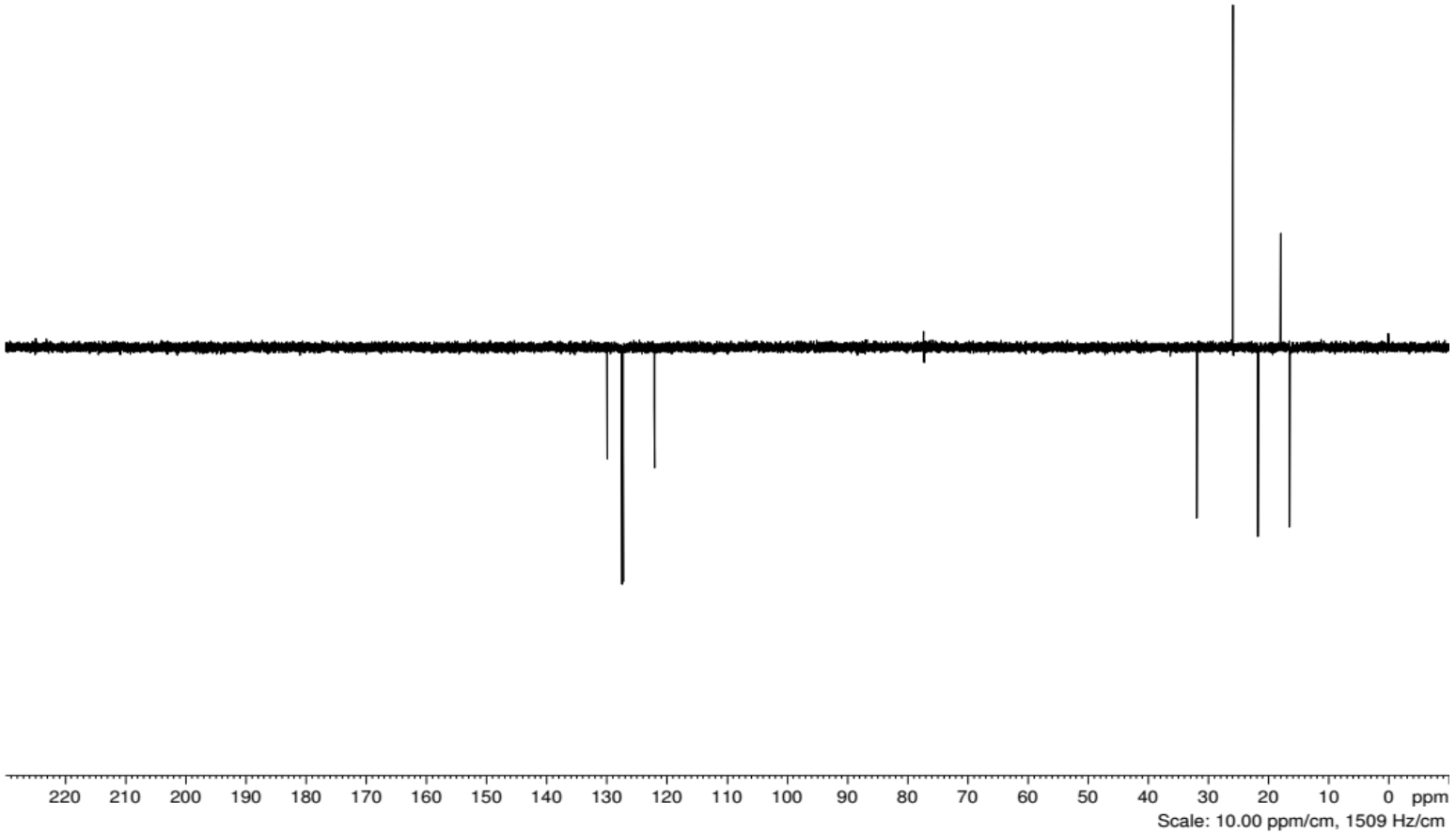

^{13}C-Dept NMR spectrum of (5,7-dihydroxy-2,2-dimethyl-6-(3-methylbut-2-en-1-yl)chroman-8-yl)(phenyl)methanone.